Identification of CUL9-related signaling pathways in human pluripotent stem cells and cortical precursors

By

Natalya Anne Ortolano

Dissertation

Submitted to the Faculty of the

Graduate School of Vanderbilt University

in partial fulfillment of the requirements

for the degree of

DOCTOR OF PHILOSOPHY

in

Cell and Developmental Biology

May 31, 2021

Nashville, Tennessee

Approved:

Vivian Gama, Ph.D., Advisor

William Tansey, Ph.D. , Committee Chair

Jason MacGurn, Ph.D.

Kevin Ess, Ph.D.

Aaron Bowman, Ph.D.

Dedication

I dedicate this thesis to my momma,

Tanya Anticich.

Without her love, support,

And occasional kick in the butt

I most certainly would have mastered out,

Or gone insane.

Acknowledgements

I don't know where to start. Graduate school was a challenging time professionally, but also personally. I lost loved ones, struggled with my mental health, and recovered from a tornado. In the last year of graduate school, I rebuilt my life from the ground up after a combination of personal losses and gains. I don't think I would have had the strength to do this and finish graduate school without the support of my mentors, family, and friends from all stages of life. I feel humbled to have so many important people in my life that I worry this acknowledgements section will rival the other sections of my thesis. But this is my manifesto, and I'll do what I want.

First and foremost, I'd like to thank my mom. We are arguably too close, but I wouldn't have it any other way. I've learned so much from you, thanking you for everything I appreciate about you would require me to write yet another thesis, but I only have the stamina and patience to write one, so I'll keep it short. You taught me to not only value myself, but to be as authentic as possible. Not everyone will always like you, but it's more important that you like yourself. I worry more about others than myself sometimes, and this can hold me back. I will let other's judgements and comments bring me down or change my path. You taught me to stand my ground. Push forward. Because of you, I chose to surround myself with people who valued me and supported me, and that made all the difference. Now, I value myself. The most important thing you taught me though, is that growing up doesn't mean you have to be lame. Thanks for showing me that prioritizing fun and happiness is probably the most important thing. I hope I can be as cool as you when I grow up.

I'd also like to thank my dad. Our relationship has never been easy. But during graduate school, I feel like we moved forward, were able to meet each other as adults, and really connect. I'm glad you've been there to support me through the hardships of the past few years and celebrate my successes. I've learned a lot about myself because of our strengthened bond. I'd also like to thank my step-mom Kelly. We've grown closer in the past few years as well, and I really value our relationship. Kelly and my step-grandmother Ms. Pat treat me the same as any other family member, and that means more to me than they know. I also want to thank my brother Noah. I've loved watching him grow from an annoying teenage boy to a somewhat put together 20 something in the army. I enjoy our rare, but memorable conversations and holiday meet-ups. I'm also glad I was the first person to take you around New Orleans at night during Mardi Gras because otherwise you only would have gone to Bourbon Street, and that would hurt my heart.

I want to thank the rest of my family as well. They've supported me throughout my life, and my visits home helped me get through graduate school. I'd especially like to thank my cousin Andrea, her daughter Stella, my Aunt Janis, and my Uncle Henry. Despite some challenging times in our family, we've been able to maintain strong relationships. Stella especially made my time in grad school easier. She's growing up to be a goofy, but smart woman and I can't wait to see who she becomes. I especially want to thank family members who are no longer with us. I was incredibly close with my grandmother who passed away during my second year of graduate school. I wish she were still here to share this accomplishment because without her it would not have been possible. I also want to thank my grandfather. He was a chemical engineer and strongly encouraged me to develop my skills in science. He absolutely loved his job and he inspired me to choose a career I wanted to wake up and do everyday. I think I've found that.

I also want to thank my pre-grad school friends. You guys will never read this, and my acknowledgements section is going to be long, so I'll give you the shortest acknowledgements. This is not a reflection of your value. Thank you to my childhood friend Suzanne Coco. I'm so thankful we've been able to maintain a relationship for so long. I value your friendship so much, and though we don't see each other often, when we do it feels like no time has passed (terrible cliché but very true). Stefanie Hummel has been an incredible friend to me in the past ten years. During my first two years of graduate school she helped take care of my sick grandmother when I could not, even staying with my grandmother at the hospital overnight when no one else in my family could. You made my time in graduate school easier. Thank you to my friends from undergraduate, Abbie Cathcart, Will Simmons, Hannah Roberts, Drew Legget, Rakeem Daniels and Quinn Mackey. I've only seen you all sporadically, but I know if I need to I can call or text you any time I need, no matter the time. I'm glad I've been able to stay friends with you all, and hope (expect) we will keep it up as we get older.

I truly do not know who I would be without Vivian Gama. Let me start by saying that Vivian is a fantastic scientist. She absolutely loves what she does and any professional hardship she has encountered, she overcame it because of her pure, unwavering passion for research. Vivian's dedication to her student's and the pursuit of scientific knowledge are inspiring. Seeing Vivian's eyes light up when she asked a question in lab meeting, or saw an exciting new piece of data motivated me to keep working. It also made me realize that scientific research was not my passion. During challenges with my research, it was not my undying love that pushed me through, but rather the knowledge that I could use my PhD knowledge to pursue other things. Vivian never tried to push me into research, rather, she helped me identify my strengths and weaknesses, my

likes and dislikes, and identify the best career path for me. She let me take time from my research, while she was a new professor under pressure to publish and get funding, to explore opportunities in outreach and writing. She didn't have to do that. She wanted to do that.

And that is the most important lesson Vivian taught me. In all your pursuits, personal or professional, use your power to lift others up. If you see potential in someone. If you see someone struggling. Helping them is never to your detriment. If you invest your time and energy into helping people you know personally or professionally, it will almost always pay off. Vivian is smart and driven enough to win a Nobel prize, but I think her legacy will be her students. Not because I think I'm great, but because I think Vivian's true gift and passion is people. There isn't enough of that in science, and I'm glad Vivian will change that (even if only in a small way) by training others to prioritize lifting others up when possible.

I had more mentors than just Vivian during graduate school as well. Chris Wright's unwavering support throughout my graduate studies kept me going. He's not only supported my science, but my transition into science writing, and that means a lot. I enjoy talking to Chris not just about data, but about the philosophy behind science, which isn't discussed enough. He also throws quite a party…I mean retreat. Steve Hann was an incredible DGS. His support and feedback during my first year in CDB were instrumental to my success as a graduate student. He is dearly missed. My committee has helped guide my research project from its inception, giving me critical feedback and suggestions. They too were extremely supportive of my transition into science writing. I especially want to thank Bill Tansey for being such an incredibly helpful and supportive chair. He always went the extra mile to help me succeed and feel confident in my abilities. Few chairs sit with a student to look over their qualifying exam presentation before the exam to give them feedback and guidance.

Acting as a mentor to undergraduate students was one of my favorite parts of graduate school. But it also felt like a huge responsibility. The relationships I had with graduate students I worked with as an undergraduate like William (Bill) D'Angelo and Manisha Shrestha were so important not just for my development as a scientist, but as a person. It's hard to be in your early 20s, and it's even harder to figure out what you want to do. Bill and Manisha were so open about their paths to science, the obstacles they faced, and the challenges they still had. They were mentors, but they were also friends. I hope my mentees feel the same. Not because I think every mentor should be your friend, but because I hope they felt I cared about them as people and not just how well they ran a Western blot.

Everyone I mentored was different, but so talented and engaging. Leigh Anne Kline, my first mentee and the only other student in the lab when I rotated, taught me so much. Neither of us knew how to do a Western blot when I rotated. We figured out so many things together. She was such a ray of light, and I'm sure she will make a brilliant doctor. Sarah Byun was a tough egg to crack. She was quiet, but always thinking. She'd always impress me with her knowledge – it was clear she was reading papers about my project all the time. I hope she keeps being curious and learning everything she can. I have no doubt she will do great things as a doctor as well. I'd also like to thank Dylan Holzgruber. Dylan was such a talented researcher and an incredible communicator. I loved reading his reports – they were so easy to edit. I'm sure Dylan will make an excellent doctor. I hope he approaches medicine with the same passion and humor as he did everything else. I also want to thank Mary Chalkley. Mary is the only undergraduate I mentored that went to graduate school, and I love that our mentor-mentee relationship has blossomed into a friendship. Mary has been there for me whenever I needed it. I enjoy our shared love of trash TV and Pizza Perfect lasagna. But most importantly, I appreciate your support and humor.

I also want to thank the Gama lab. There is something incredibly special about watching a lab grow from the start and I think this has bonded everyone who has worked in our lab more than usual. I'm so glad that Megan Rasmussen joined the lab with me. I really can't imagine my time as a graduate student without her. Megan is incredibly kind, talented, and fun. I wish Megan could see herself the way others do because she's truly an incredible human and I'm proud to call her a friend. She fed my cells when she didn't have to, cleaned up after me without complaining, and supported me when I was struggling with my mental health. I often approach things with humor to deflect, but Megan was always there to help me realize that sometimes things are hard, and admitting they are is okay. She's a strong person, and I'm excited to see the amazing person and scientist she will become. Alejandra Romero Morales is a force of nature. She's passionate and unapologetic and working with her has been amazing. I can remember the first time I decided I wanted to Ale to join our lab while she was rotating. We were walking from lab, and she said she enjoyed the finale of How I Met Your Mother, an uncommon opinion I share. We talked outside in the parking lot of my apartment complex for a couple hours after. I'm excited to see her take the neuroscience field by storm.

Although he left us, I want to thank Anuj Rastoji for his time in the lab. I'm not sure anyone can really describe AJ – he's one of those people you just have to meet. I loved our strange philosophical discussions, even if they annoyed me at first. Most of all, I appreciate how aware you were of when I was struggling while you were in the lab. You always checked in on me, and

gave me strange pep talks when I needed them. Helpful or not, your advice always made me laugh.

I'd like to give a shout out to the Gama lab "next gen." You guys are incredible, and I have no doubt you will take the research to the next level. Gabriella Robertson is an extremely passionate, intelligent, and hardworking scientist. She seems infinitely wiser than I ever was in graduate school, and she's only in her third year. I also appreciate her love for Lil' Wayne. Caroline Bodnya is probably the hardest working person I've ever known. Although she is leaving our lab as lab manager to start graduate school, I still consider her part of "next gen." Caroline can handle an infinite number of experiments at once, and produce beautiful results. I look forward to reading her *Science* paper, which she'll probably publish six months into graduate school. Tierney Baum joined our lab during COVID, so we haven't worked together a lot, but she has a great attitude and was easy to work with, even just by slack. She also approaches things with humor and positivity, which I think will make graduate school infinitely more enjoyable for her. I wish the two newest members of the lab, Melanie Gill and Marina Hanna the best of luck. Keep the lab cool and productive.

I have to thank the friends I've made during graduate school outside of the lab. Although we've hung out in waves, I appreciate all the hangs and support. Michael Yarboro is an incredibly strong person. His perseverance and kindness inspire me. Eric Figueroa is one of the purest souls I've ever known. He doesn't just find the good in people, he manages to bring it out in them. He just generally taught me to be a little nicer. Kevin Childress is an enigma, but an incredibly dedicated friend. You can call him anytime, and he will be there with whatever you need: beer, conversation, or someone to carry an extremely heavy box of textbooks. Marc Wozniac is one of the most unique people I've ever met. I wasn't sure if Marc liked me until he started bringing me random, niche textbooks he though I may like. Michael, Ale, Megan, and I tried to develop a cell biology board game with him back in the day, but we were scooped. I'm excited to keep hanging out and playing board games together.

If I missed anyone in these acknowledgements, I'm sorry. We had countless other undergraduates in the lab like Stellan Riffle and Stephen Russel who I didn't directly mentor, but developed friendships with. I made so many friendships with other students, post-docs, and staff. If I could give anyone starting graduate school a piece of advice, I would remind them that what gets most of us through graduate school isn't groundbreaking research or a passion for science, its other people. Choosing people who support you will not only help you survive challenging times, but teach you new things about yourself. Help you recognize your own strengths and

weaknesses. And ultimately help you not only become the person you want to be, but embrace and accept it. Surround yourself with people who build you up, not break you down – it takes a village. That's really what I learned from graduate school.

Table of Contents

List of Figures

List of Tables

Abbreviations

AMP: Adenosine monosphate

APAF1: Apoptotic protease activating factor 1

APC/C: Anaphase Promoting Complex or Cyclosome

Apcin: Inhibitor of the anaphase-promoting complex/cyclosome

ASD: Autism Spectrum Disorder

ATP: Adenosine triphosphate

BAX: Bcl-2-associated X protein

BioID: Proximity-dependent biotin identification

BTB: Broad-complex, tramtrack, and bric-a-brac

CAND1: Cullin-associated NEDD8-dissociated protein 1

CAS9: CRISPR associated protein 9

CCDC8: Coiled-Coil Domain Containing 8

CDC20: Cell Division Cycle 20

CDK: Cyclin dependent kinase

CDK: Cyclin-dependent Kinase

CDK5RAP2: CDK5 Regulatory Subunit Associated Protein 2

ChIPSeq: Chromatin immunoprecipitation sequencing

CKI: Cyclin-dependent Kinase Inhibitor

COP9: Constitutive photomorphogenesis 9

CPH: Conserved domain within Cul7, PARC, and HERC2 proteins

CRISPR: Clustered regularly interspaced short palindromic repeats

CRL: Cullin RING Ligase

CSN: Constitutive photomorphogenesis 9 signalosome

CTD: C-terminal Domain

CUL-1, -2, -3, -4A, -4B, -5, -7, -9: Cullin-1, -2, -3, -4A, -4B, -5, -7, -9

CUX1: Cut Like Homeobox 1

DAB1: Disabled-1

DAVID: Database for Annotation, Visualization, and Integrated Discovery

DDB: DNA damage-binding protein

DDB1: DNA damage-binding protein 1

DDX39A: DExD-Box Helicase 39A

DDX3X: DEAD-Box Helicase 3 X-Linked

DEAD: Asp-Glu-Ala-Asp

DHX9: DExH-Box Helicase 9

diGLY: di-glycine

DNA: Deoxyribonucleic acid

EIF4G1: Eukaryotic translation initiation factor 4 gamma 1

EMX2: Empty Spiracles Homeobox 2

ESC: Embryonic Stem Cell

FADS2: Fatty Acid Desaturase 2

FASN: Fatty acid synthase

FBXW: F-box/WD repeat-containing protein

FMRP: Fragile X mental retardation protein 1

FUCCI: Fluorescence Ubiquitination Cell Cycle Indicator

FZR1: Fizzy And Cell Division Cycle 20 Related 1

GFAP: Glial fibrillary acidic protein

GLRX: Glutaredoxin

GO: Gene ontology

HECT: Homologous to E6AP C-Terminus

HERC: HECT And RLD Domain Containing E3 Ubiquitin Protein Ligase

HHARI: Human Homolog of Ariadne

ID2: Inhibitor Of DNA Binding 2

IDI1: Isopentenyl-Diphosphate Delta Isomerase 1

IKK: IκB kinase

iPSC: Induced pluripotent stem cell

iTRAQ: Isobaric tags for relative and absolute quantitation

IκBα: NF-κB inhibitor, alpha

JAMM: JAB1/MPN/Mov34 metalloenzyme

KD: Knockdown

KO: Knockout

LC-MS/MS: Liquid chromatography tandem mass spectrometry

MAP2: Microtubule-associated protein 2

MEF: Mouse Embryonic Fibroblasts

MOMP: Mitochondrial outer membrane permeabilization

mRNA: Messenger RNA

MSI1: Musashi RNA Binding Protein 1

NANOG: Homeobox protein NANOG

NEDD8: Neuronal precursor cell-expressed developmentally down-regulated protein 8

NF-κB: Nuclear Factor of kappa light polypeptide gene enhancer in B-cells

NGS: Next Generation Sequencing

NPC: Neural progenitor/precursor cells

NSC: Neural Stem Cells

NTD: N-terminal Domain

OBSL1: Obscurin Like Cytoskeletal Adaptor 1

OCT4: Octamer-binding transcription factor 4

OTUD7B: OTU Deubiquitinase 7B

PARC: p53-associated Parkin-like cytoplasmic protein

PAX6: Paired box protein 6

PCID2: Proteasome, COP9, Initiation factor 3 Domain Containing 2

Pro-TAME: Pro-N-4-tosyl-L-arginine methyl ester

PSC: Pluripotent stem cell [denotes both iPSCs and ESCs]

PSD-95: Postsynaptic density protein 95

PTM: Post-translational modification

RBP: RNA binding proteins

RBR: RING-Between-RING

RBX1: RING-box 1

RING: Really Interesting New Gene

RNA: Ribonucleic acid

ROC1: Regulation of Cullins-1

RPN: Regulatory particle of non-ATPase

RT-qPCR: Real-time quantitative polymerase chain reaction

SCD1: Stearoyl co-A desaturase

SCF: Skp, Cullin, F-box containing complex

shRNA: Short hairpin RNA

SILAC: Stable Isotope Labeling by/with Amino acids in Cell culture

siRNA: Small interfering RNA

SMAD: Small Mothers Against Decapentaplegic

snRNP: Small nuclear ribonucleoproteins

SNRNP200: Small Nuclear Ribonucleoprotein U5 Subunit 200

SOCS: Suppressor of cytokine signaling

SOX-2, -3: SRY-related HMG-box-2, -3

STRING: Search Tool for the Retrieval of Interacting Genes/Proteins

TBR1: T-Box Brain Transcription Factor 1

TM7SF2: Transmembrane 7 Superfamily Member 2 or delta(14) stearoyl reductase

TMEM167A: Transmembrane Protein 167A or Protein Kish-A precursor

TRIAD1: Two RING [really interesting new gene] fingers and DRIL [double RING finger linked] 1

TRP: Tetratricopeptide repeat

TUBA: Tubulin alpha chain

TUBB3: Tubulin Beta 3 Class III

UBD: Ubiquitin Binding Domain

UBE2D: UbcH5 Ubiquitin-Conjugating enzymes

WT: Wild-type

XLMR: X-linked mental retardation

ZO-1: Zonula occludens-1

Chapter 1

INTRODUCTION

Regulation of protein stability and function by ubiquitin modification

Throughout the life span of the cell, billions of proteins are dynamically synthesized and degraded. Inefficient proteolysis can result in protein aggregation and subsequent toxicity as seen in severe neurodegenerative disorders like Alzheimer's and Parkinson's disease (Ciechanover and Kwon, 2015). One important cellular defense against misfolded proteins involves degradation by the proteasome, a complex molecular machine that can unfold proteins and process them to short peptide fragments (Hershko and Ciechanover, 1998). Classically, proteins are modified by ubiquitin to be targeted by the proteasome for ubiquitin-mediated degradation through the action of 3 enzymes: E1 (activating), E2 (conjugating), and E3 (ligase). E3 ubiquitin ligases modify target proteins with ubiquitin moieties not only for proteasomal degradation, but also changes in protein function, subcellular localization, or protein interactions (Akutsu et al., 2016). The outcome of ubiquitination is dictated by the type of linkages between the moieties or length of the ubiquitin chain (French et al., 2021). We've translated part of this complex code, but we've only scratched the surface of the role of ubiquitin mediated regulation in cellular processes.

Ubiquitination is mediated by an enzyme cascade

Ubiquitin is an 8.5 kDa protein that acts as a post-translational modification generally signaling for proteasomal degradation of proteins (Ciechanover and Kwon, 2015). In fact, ubiquitination accounts for 80% of all protein degradation in cells. Ubiquitin was first identified by Gideon Goldstein as a polypeptide that induced differentiation of T and B cells (Goldstein et al., 1975). He found that the protein was highly conserved, found in every organism he tested including guinea pigs, squids, and celery. Additionally, he discovered that it was expressed in every tissue he tested from the salivary gland to the brain. Based on his findings, he dubbed the newly discovered protein "ubiquitous immunoprotein polypeptide," which was eventually shortened to ubiquitin. Two years later, Goldberg created a cell-free system to test ATP-dependent proteolysis of abnormal hemoglobin protein from reticulocyte lysates (Etlinger and Goldberg, 1977). Aaron Ciechanover and Avram Hershko analyzed this cell-free system by biochemical fractionation and reconstitution (Ciechanover et al., 1980; Hershko et al., 1979, 1980, 1983). Briefly, they separated the lysate into three fractions (Fraction 1-3). Fraction 2, though it

contained all the hemoglobin protein, was unable to perform ATP dependent proteolysis. When Fraction 1 was added, ATP dependent proteolysis was restored. They discovered that ubiquitin was present in this fraction through protein purification, with the assistance of Irwin Rose, ultimately uncovering its role in protein degradation. In 2004, Hershko, Ciechanover, and Irwin Rose shared the Nobel prize “for discovery of ubiquitin-mediated protein degradation.” Two decades after their initial groundbreaking studies, our understanding of ubiquitin protein regulation has exponentially increased and continues to expand every day.

Ubiquitin modification of a given substrate is catalyzed by an enzymatic cascade involving three key proteins: E1 (activating), E2 (conjugating), and E3 (ligase) (**Figure 1-1**). Each enzyme provides an increasing level of ubiquitin substrate specificity – this is best represented by how many of each enzyme humans express. Humans express 2 E1s, at least 38 E2s, and about 600 E3s, each with increasing specificity (Stewart et al., 2016; Ye and Rape, 2009). The activating enzyme, E1, catalyzes the first reaction, adenylating ubiquitin. The E1 bound to ATP-Mg^{2+} form a phosphodiester bond between AMP and the hydroxyl group at the C-terminus of ubiquitin. The catalytic cysteine within the E1’s active site attacks the high energy bond between ubiquitin and AMP creating a thioester bond between the catalytic cysteine and the carboxyl group at the terminal end of ubiquitin (Schulman and Wade Harper, 2009). Once an E1 is bound to ubiquitin, it undergoes structural changes that expose its ubiquitin fold domain (Huang et al., 2007; Ye and Rape, 2009). The E2 interacts with this domain via two conserved lysine residues and ubiquitin is ultimately transferred to the E2’s catalytic cysteine via a thioester transfer (Pickart and Rose, 1985; Stewart et al., 2016; Ye and Rape, 2009). The association between an E2 and an E3 is unstable, so as soon as the transfer is complete, the E2 dissociates freeing the E3 enzyme to associate with another E2 and elongate the ubiquitin chain on the targeted substrate (Ye and Rape, 2009).

The ligase, or the E3 enzyme, facilitates the final attachment of ubiquitin to its substrate through the formation of an isopeptide bond between the C-terminus of ubiquitin and a specific ε-amino group of the targeted substrate. However, there are three families of E3 enzymes, each with its own distinct ubiquitination mechanism (**Figure 1-1**). RING ubiquitin ligases act as a scaffold. They bring the E2 and the substrate together, and facilitate ubiquitin transfer directly from the active site of the E2 enzyme (Liu et al., 2018). HECT E3 ubiquitin ligases, however, directly transfer ubiquitin to the substrate, first forming a thioester intermediate. HECT E3s have a conserved catalytic cysteine at their C-terminus; ubiquitin moves from the E2 to this catalytic cysteine via a thioester transfer (Wang et al., 2020). RBR ubiquitination mechanism is a

combination between the two. The RBR consists of three subdomains: RING1, In Between RING (IBR), and RING2. First, the E2 is recruited to the RING1 domain, just like in a RING E3 ligase. Then, the ubiquitin is transferred to an active cysteine on the RING2 via thioester transfer forming a thioester intermediate, like a HECT E3 ligase, before finally transferring ubiquitin to its substrate (Smit and Sixma, 2014) (**Figure 1-1**). Additionally, this conjugation is reversible – all ubiquitination can be reversed by a group of enzymes known as deubiquitinases that cleave ubiquitin from its substrate by breaking the isopeptide or peptide bond connecting them (Mevissen and Komander, 2017).

The growing complexity of the ubiquitin code

Ubiquitin can signal for more than proteasomal degradation, depending on the number of ubiquitin moieties added to a substrate and the type of linkages within a polyubiquitin chain (Rajalingam and Dikic, 2016; Ye and Rape, 2009). Another ubiquitin moiety can be added to any of ubiquitin's seven lysine residues (K6, K11, K27, K29, K33, K48, or K63) or the methionine at its N-terminus forming a polyubiquitin chain (Swatek and Komander, 2016). The fate of a ubiquitinated protein is determined by recognition of the unique structure of a ubiquitin chain by the ubiquitin-binding domain (UBD) of an effector protein (Beal et al., 1996; French et al., 2021). Substrates can be either monoubiquitinated or polyubiquitinated (French et al., 2021). Monoubiquitinated substrates can have a single ubiquitin moiety on one residue or multiple sites of monoubiquitination. Polyubiquitinated substrates are modified with a chain of conjugated ubiquitin moieties. Homotypic chains are comprised of a single type of linkage. Heterotypic chains can be mixed, meaning they contain more than one type of ubiquitin linkage. Branch heterotypic chains contain ubiquitin moieties that are modified on multiple lysine residues forming branches in the chain. K48 and K63 homotypic chains are considered the canonical linkages and thus the best characterized, but our understanding of the remaining linkages, and even the more complex branched chains has grown substantially in the past decade (French et al., 2021).

K48 is the canonical linkage signaling for proteasomal degradation of a conjugated protein. The 750 kDa proteasome complex is composed of more than thirty subsets of proteins and is considered the cells catalytic trash can. Proteasome subunits Rpn1, Rpn10, and Rpn13 contain UBDs that recognize and recruit K48 polyubiquitin chains subjecting the ubiquitinated protein to proteasomal degradation (Deveraux et al., 1994; Husnjak et al., 2008; Shi et al., 2016). K11 linkages have slowly emerged as a linkage key for signaling proteasomal degradation, and branched chains – chains containing moieties with more than one lysine conjugated to a second

moiety – consisting of K48/K11 linkages seem to enhance proteasomal degradation of targeted proteins (Boughton et al., 2020; French et al., 2021; Jin et al., 2008; Meyer and Rape, 2014). In yeast cells, a majority of ubiquitin linkages are K11 or K48, each making up about 30% of all seven linkages (Xu et al., 2009). K11-linked ubiquitin chains seem to be a key signal for proteasomal degradation during cell cycle progression. They have become a hallmark of ubiquitination by the major cell cycle regulator the anaphase-promoting complex/cyclosome (APC/C).

The anaphase-promoting complex/cyclosome (APC/C) is a 1.5mDa multi-subunit E3 ubiquitin ligase complex that regulates cell cycle progression primarily during the mitotic and G1 phases of cell cycle through the precisely timed proteasomal degradation of key cell cycle regulatory proteins like G1 cyclins (Pines, 2011). Rather than K48-linked ubiquitin chains, APC/C conjugates K11-linked ubiquitin chains on targeted proteins to mark them for proteasomal degradation (Jin et al., 2008; Matsumoto et al., 2010). APC/C also forms branched chains composed of K11/K48-linkages enhancing substrate proteasomal degradation (Meyer and Rape, 2014; Rana et al., 2017). A recent study demonstrated the proteasomal subunit Rpn1 has an increased affinity for K11/K48-linkages, explaining the observed enhancement in proteasomal degradation (Boughton et al., 2020).

Similarly, branched variants of the well-characterized K63-linked ubiquitin chains seem to enhance its known effects on protein function. K63-linked ubiquitin chains were the first identified linkage that did not promote proteasomal degradation; Cecile Pickart, who was trained in Irwin Rose's lab, first reported they signaled for DNA repair (Hofmann and Pickart, 1999). In the two decades since, K63-linked ubiquitin chains have been shown to promote the formation of signaling complexes that control processes like DNA repair, mitophagy, spliceosome assembly, and activation of transcription factor NF-κB (French et al., 2021; Yau and Rape, 2016). NF-κB promotes the innate immune response by inducing transcription of pro-inflammatory proteins like cytokines (Liu et al., 2017c). NF-κB activity is inhibited by its association with the IκBα which localizes it to the cytoplasm preventing its nuclear translocation. Proteasomal degradation of IκBα requires phosphorylation by IκBα kinase (IKK). The E3 ubiquitin ligase TRAF6 modifies IKK with K63-linked ubiquitin chains promoting its activity, and subsequently NF-κB mediated transcription (Deng et al., 2000; Wang et al., 2001). Research shows that K48/K63 branched chains protect K63-linkages conjugated to IKK from deubiquitination stabilizing its ubiquitin modification (Ohtake et al., 2016). In fact, K48/K63 branched chains account for 20% of all K63-linked ubiquitin chains in U2OS osteosarcoma cells (Ohtake et al., 2016). Another study even demonstrated that these

branched chains can signal for the canonical function of ubiquitination – proteasomal degradation (Ohtake et al., 2018). Characterization of the understudied ubiquitin linkages alone and in combination will provide further insight into the complex regulation of cellular processes by post-translational modifications.

The Cullin RING Ligase (CRL) family of ubiquitin ligases are defined by key structural features

CRLs are the largest family of E3 ubiquitin ligases and account for 20% of all protein degradation. There are only eight cullin scaffolds – the main component of a CRL – but these can recruit countless adapter proteins required for interaction with specific substrates, each forming a distinct CRL complex (Petroski and Deshaies, 2005). There are an estimated 500 CRL complexes comprising an expansive repertoire of functions (Zimmerman et al., 2010). Through association with adapters, one cullin scaffold can respond to diverse cellular signals and can adapt to any cellular stress. Despite their unique ability to adapt to the everchanging needs of the cell, all members of the family share common structural features, and are regulated by a common post-translational modification (Duda et al., 2011; Zimmerman et al., 2010). However, one non-canonical cullin, CUL9, does not fit the classical definition of a CRL (Skaar et al., 2007). Its function and structural assembly remain poorly characterized.

Cullin scaffolds were first identified as key cell cycle regulators

The first cullin was discovered when two groups of researchers sought to determine why a set of proteins containing an uncharacterized domain were required for cell cycle progression. Cullin domain containing proteins were first discovered to be required for cell cycle progression in S*accharomyces cerevisiae* (Mathias et al., 1996) and *Caenorhabditis elegans* (Kipreos et al., 1996). Together, these landmark studies determined that mutation of Cullin-1 (CUL1) resulted in tissue hyperplasia and inhibited progression through the G1 phase. Both provided evidence that CUL1 somehow negatively regulated the levels of cyclins required for mitotic exit (Cyclin B) and S-phase entry (Cyclin E). Both papers boasted the exciting discovery of an entire new family of proteins: the cullins. They determined cullin containing proteins were present in yeast, nematodes, and humans – at the time they predicted there were at least six cullin proteins in humans. Work began to characterize the function of this new family of proteins with suspected ubiquitination activity.

One year later, Raymond J. Deshaies and J. Wade Harper published landmark findings on the same day in *Cell* 1997 detailing the discovery of the first class of CUL1 complexes: the Skp, Cullin, F-box containing complex (SCF) (Feldman et al., 1997; Skowyra et al., 1997). They specifically discovered the SCF complex containing the F-box adapter protein Cdc4. Deshaies' group demonstrated that SCF^{CDC4} promotes progression from G1 phase to S phase in cell cycle in *S. cerevisiae* by targeted degradation of cyclin dependent kinase inhibitors (CKI) Sic1 and Far1 (Feldman et al., 1997). Cell cycle is propelled forward by a tightly orchestrated oscillation of proteins known as cyclins. Each cyclin peaks at a particular cell cycle phase, complexing with a particular cyclin dependent kinase (CDK). The resulting complex phosphorylates substrates generally promoting their degradation by a specific E3 ubiquitin ligase. They demonstrated that phosphorylation at multiple sites on Sic1 and Far1 were required for targeted ubiquitination by SCF and activation of the S-phase CDK (Feldman et al., 1997).

Harper's group built on this discovery. They determined that this SCF complex was not limited to incorporating one F-box protein (Skowyra et al., 1997). In addition to SCF^{CDC4}, they identified SCF^{Grr1}. SCF^{Grr1} targets the G1-cyclins Cln1 and Cln2 for ubiquitination – they were only able to postulate this at the time as their data only demonstrated that Grr1 recruited these cyclins to SCF *in vitro*. This key study found that SCF could form multiple complexes, each with unique substrate specificity determined by the incorporated F-box protein (Skowyra et al., 1997). 68 F-box proteins have been identified since, and more are predicted to exist (Jin et al., 2005).

Both Deshaies and Harper suggested that newly discovered SCF complexes SCF^{Cdc4} and SCF^{Grr1} would act as a model for other SCF complexes – they were correct. SCF complexes have been heavily studied in the past two decades, most following a similar structural and mechanistic model as the originals. For example, all require phosphodegrons for substrate recognition by F-box adapter proteins (Cardozo and Pagano, 2004). However, SCF complexes act as base models for nearly all CRL structural assemblies and act as a blueprint for the general ubiquitination mechanisms employed by other CRLs.

Canonical CRLs share common structural features

Despite the ever-expanding diversity of CRL substrates and functions, most of these multisubunit ligases share common structural features (**Figure 1-2**). The SCF complex exemplifies these key commonalities. The first insight into CRL structure came from visualization of the SCF^{SKP2} complex (Schulman et al., 2000; Zheng et al., 2002b). Prior to this study, researchers had a basic understanding of the composition of the complex. The RBX1 RING

subunit associates with the CUL1 scaffold to form the catalytic core complex that recruits the E2 enzyme bound to a ubiquitin chain (Kamura et al., 1999; Ohta et al., 1999; Seol et al., 1999; Skowyra et al., 1999). The adapter protein SKP1 recruits the F-box domain containing protein SKP2, which ultimately acts as the substrate receptor (Bai et al., 1996; Feldman et al., 1997; Skowyra et al., 1997). However, exactly how these proteins worked together to position the substrate for ubiquitin transfer was not known.

The initial crystal structure of SCF^{SKP2} revealed that CUL1 has an elongated, crescent like shape with a notably rigid structure – this rigidity is required for CRL ubiquitination activity (Schulman et al., 2000; Zheng et al., 2002b; Zimmerman et al., 2010). CUL1, like other cullins, has structurally distinctive C-terminal (CTD) and N-terminal domains (NTD). (Schulman et al., 2000; Zheng et al., 2002b). The N-terminal domain was “stalk-like” composed of alpha helices that were unique from other known helical domains that acted as the site of protein-protein interactions like the tetratricopeptide repeat domain (TRP) (Zheng et al., 2002b). The SKP1-SKP2 proteins bind to the tip of the NTD domain on a solvent exposed, a structural motif composed of helical bundles known as a cullin repeat, well-conserved across other cullin scaffolds. The NTD forms a narrow, string like linker connecting the NTD to the CTD. This linker is more flexible than the rest of the protein essentially allowing it to fold in on itself to connect the substrate bound to the substrate receptor on the NTD to the RING binding protein on the CTD to facilitate ubiquitination (Zheng et al., 2002b).

The CTD is more globular and contains the hallmark of cullin scaffolds: the cullin homology domain common amongst canonical and non-canonical cullins alike. The most important and well conserved motif in the CTD is a hydrophobic groove where the zinc binding RING domain portion of the RING binding protein, RBX1 in the case of SCF^{SKP2}, binds (Schulman et al., 2000; Zheng et al., 2002b; Zimmerman et al., 2010). A similar hydrophobic groove in the RING protein recruits the E2 ubiquitin ligase bound to ubiquitin – this hydrophobic groove is well-conserved across all RING proteins. Once the SCF^{SKP2} complex is fully formed, the cullin essentially folds in on itself. A leucine-rich repeat domain of SKP2 moves near the active site of the E2 leaving a small space between them allowing the flexibility needed to promote ubiquitination. Interestingly, the well-characterized APC/C subunit APC2 contains a cullin-homology domain as well that interacts with the APC11 domain, the RING subunit of the APC/C – these two proteins interact in a similar manner to CRLs, though APC/C is still considered a non-canonical CRL (Zheng et al., 2002b).

Although complexes formed by CUL1, CUL2, CUL3, CUL4A, CUL4B, CUL5, and CUL7 share strikingly similar structures, there are some notable differences (Petroski and Deshaies, 2005; Zimmerman et al., 2010). Each cullin essentially has its own set of adapter proteins with common binding domains, like the F-BOX motif in SCF adapter proteins. For example, CUL2 and CUL5 recruit adapter proteins called BC-box containing proteins like the supressor of cytokine signaling proteins (SOCS) containing a Broad complex, Tramtrack, Bric-a-bric (BTB) fold – this fold is also present in SKP1 (Bullock et al., 2006; Cardote et al., 2017; Mahrour et al., 2008; Schulman et al., 2000). There are other, larger structural differences that suggest altered ubiquitination mechanisms between cullin scaffolds (Petroski and Deshaies, 2005). CUL4A, for example, has a unique cullin repeat sequence where adapter proteins bind in other cullins (Zheng et al., 2002b).

Mutations in conserved domains amongst cullins often lead to severe disease. CUL7 mutations are thought to account for over 80% of all cases of a the rare but debilitating autosomal recessive disorder known as 3-M syndrome (Huber et al., 2005, 2009). Those afflicted with 3-M syndrome have delayed bone maturation ultimately causing facial deformities and short stature. Many of the mutations resulted in truncated CUL7 protein (Huber et al., 2005, 2009). Other point mutations commonly seen were present in the cullin domain itself, ultimately preventing ROC1, a specific RING protein, binding (Huber et al., 2005, 2009).

Another study suggests that dysfunctional regulation of non-canonical cullin CUL9 by CUL7 and other commonly mutated proteins obscurin-like cytoskeletal adapter 1 (OBSL1) and coiled-coil domain containing 8 (CCDC8) is a driving mechanism behind 3-M syndrome as well (Glotzer, 2009; Li et al., 2014). This study concluded that CUL7, OBSL1, and CCDC8 form a complex that modulates microtubule stability at the centrosomes ultimately protecting genome integrity (Li et al., 2014; Yan et al., 2014). The group initially reported that CUL9 KO mice were extremely tumor prone, with tumors in nearly every organ in the body – this led them to believe that CUL9 was a tumor suppressor (Pei et al., 2011). In fact, a p53/CUL9 double knockout mouse had more tumors than either single knockout (Li et al., 2014).

When the group noticed that CUL9 protein levels were increased in CUL7 KO mouse cells, they suspected CUL7 may negatively regulate CUL9 protein (Li et al., 2014). They showed some evidence, including decreased levels of ubiquitinated CUL9 protein, in CUL7 KO and KD mouse cells that implies CUL9 is a substrate of CUL7. However, deletion of OBSL1 also resulted in increased CUL9 levels, indicating the entire “3M complex” composed of CUL7, OBSL1, and CCDC8 is required for CUL9 regulation. Depletion of any of the three complex components

resulted in cytokinetic failure leading to high levels of aneuploidy and polyploidy, but co-depletion of CUL9 rescued these phenotypes. Ultimately, the authors determined that SURVIVIN, an inhibitor of apoptosis thought to regulate the mitotic spindle checkpoint, protein levels were regulated by CUL9 through ubiquitin mediated proteasome degradation (Altieri, 2006; Li et al., 2014). Increased levels of SURVIVIN were present when any of the four proteins were depleted or deleted in mouse cells and U2OS cancer cells resulting in inactivation of the mitotic spindle checkpoint resulting in missegregation of the chromosomes, resulting in genomic instability (Li et al., 2014).

This study suggested that CUL9 and CUL7 heterodimerize to inhibit CUL9 function in a ubiquitin independent manner (Li et al., 2014). However, others have reported that CUL9 and CUL7 heterodimerized, but provided evidence that they do not regulate one another, nor is the dimerization necessary for the ligase activity of either cullin (Skaar et al., 2005, 2007). Conflicting findings on CUL9 and CUL7 interaction and cross-regulation need to be clarified. CRL and cell cycle regulators APC/C and an SCF complex also antagonize one another during the G1 stage of the cell cycle (Margottin-Goguet et al., 2003; Vodermaier, 2004; Wei et al., 2004). This cross-regulation could inform future studies about CUL9 and CUL7 cross-regulation and ultimately provide insight into other potential cullin heterodimerizations.

CRL activity is regulated by post-translational modification by NEDD8

In addition to common structural features, CRLs are also regulated by similar mechanisms (**Figure 1-3**) CRL ubiquitin ligase activity requires modification on conserved residue in the cullin domain by ubiquitin-like protein NEDD8 (neural precursor cell-expressed developmentally downregulated gene 8), a protein whose sequence and structure is over 75% homologous to ubiquitin (Whitby et al., 1998). The original crystal structure of SCF^{SKP2} did not capture the complex in its active form. A key piece of the picture was missing: exactly how does the E2 active site transfer ubiquitin to the substrate or extend a ubiquitin chain when the E2 is localized on the CTD and the substrate on the NTD?

Researchers caught their first glimpse of two neddylated CRLs in 2008. They compared crystal structures of NEDD8 modified and unmodified versions of the CTD of Cul5-Rbx1 and Cul1-Rbx1 using small angle X-ray scattering – the complexes had nearly identical active and inactive confirmations (Duda et al., 2008, 2011). In the inactive, closed confirmation, the RBX1 RING domain is tightly bound to a hydrophobic portion of the cullin domain. Neddylation of a conserved lysine within the “WHB” subdomain in both cullins dissociated RBX1 from the cullin allowing it to

reorient to position the RING-E2~ub adjacent to the substrate promoting ubiquitin transfer to the substrate bound to the substrate receptor at the NTD (Duda et al., 2008; Saha and Deshaies, 2008). Others have introduced mutations that inhibit the dissociation of the RING- binding protein RBX1 from the CTD and determined this prevents polyubiquitination of substrates (Yamoah et al., 2008).

However, all CRL structures always had a curious 50Å gap between the E2~ubiq and the substrate(Duda et al., 2008; Saha and Deshaies, 2008; Yamoah et al., 2008). The complex had to be “caught in action” to understand how CRLs ultimately bridge the gap and transfer ubiquitin from the E2 to their substrates. A group of researchers recently visualized a chemically trapped crystal structure of SKP1/B-TRCP actively transferring ubiquitin to its substrate phosphorylated IκBα and beta-catenin bound to its F-box containing substrate receptor, finally bridging the gap (Baek et al., 2020b, 2020a). Briefly, the new structure demonstrated that NEDD8 crosslinked the phosphodegron of the substrate attached to the substrate receptor of the CRL and the E2 enzyme UBE2D. NEDD8 itself is bound not only to the cullin at the conserved residue, but also to the backside of the RBX1 bound UBE2D, optimally position the substrate and E2~ubiquitin for transfer (Baek et al., 2020b, 2020a).

NEDD8 modification can be reversed by the COP9 (Constitutive photomorphogenesis 9) signalosome (CSN) providing another level of CRL regulation (Cope et al., 2002; Wei et al., 2008). The CSN is a large multi-subunit protease containing eight subunits. Four subunits contain a non-catalytic proteasome-COP9 signalosome-initiation factor 3 domain (PCI) that acts as a scaffolding domain that stabilizes protein-protein interactions within the complex (Lydeard et al., 2013; Wei et al., 2008). The two catalytic subunits, CSN5 and CSN6, are metalloenzymes with isopeptidase activity meaning they can cleave ubiquitin-like proteins from their substrates – proteasome components have homologous domains with the same enzymatic activity allowing for cleavage of conjugated ubiquitin. CSN5 is the main effector of NEDD8 cleavage (Lydeard et al., 2013; Wei et al., 2008). CSN5 contains a Jab1/MPN domain metalloenzyme motif (JAMM) required for its isopeptidase activity (Cope et al., 2002). Even in assembled COP9 signalasomes, if point mutations are introduced in the JAMM motif rendering CSN5 catalytically inactive, CRLs are hyperneddylated causing increased CRL component ubiquitin mediated degradation due to unregulated autoubiquitination (Cope and Deshaies, 2006; Denti et al., 2006; Peth et al., 2007; Wu et al., 2003). However, mutations in other CSN subunits still decrease or obliterate CSN catalytic activity (Gusmaroli et al., 2007; Peth et al., 2007) Mutation or antibody neutralization of the CSN2 subunit inhibit deneddylation (Yang et al., 2002).

Beyond preventing autoubiquitination of CRLs, deneddylation of cullin scaffolds by the CSN promotes disassembly of CRL complexes to allow for assembly of a new complex ready to ubiquitinate a new set of substrates in response to the cell's changing needs (Lydeard et al., 2013; Wei et al., 2008). Although exactly how the CSN dynamically regulates assembly and disassembly in response to cellular stress is an open are of research, some research has shed light on mechanisms of CSN regulation. For example, a group of researchers demonstrated that DNA damage induced by UV irradiation resulted in translocation of the CSN from the cytoplasmic CUL4A-DDB1^{DDB2} to CUL4A-DDB1^{CSA} complex in the nucleus which is then recruited to a subunit of RNA polymerase II (Groisman et al., 2003). Interestingly, another group showed that CSN subunits are phosphorylated (Füzesi-Levi et al., 2014,). Following DNA damage, CSN1, CSN3, and CSN8 are phosphorylated promoting translocation of the CSN from the cytoplasm to the nucleus where the CSN associates with chromatin (Füzesi-Levi et al., 2014). The authors of this study suggest that phosphorylation of the CSN could affect its association with CRLs themselves as phosphorylation does often affect protein structure and binding (Barford et al., 1991).

Assembly of unneddylated CRLs is further inhibited through binding of the cellular inhibitor CAND1 (Cullin-Associated and Neddylation-Dissociated 1) (Duda et al., 2011). CAND1 binds to unneddylated cullin-RBX complexes and inhibits binding of adapter proteins and neddylation machinery (Duda et al., 2011; Goldenberg et al., 2004; Liu et al., 2002; Zheng et al., 2002a). CAND1 wraps around cullin-RBX complexes like a snake, forming a solenoid structure – just like tightly packed chromatin – with its CTD bound to the NTD of the cullin and vice versa (Goldenberg et al., 2004). When bound to the cullin-RBX complexes NTD, the motif where the adapter protein is recruited forming the substrate receptor is blocked. At the CTD, CAND1 binds directly to the lysine modified by NEDD8 essentially "locking" the cullin-RBX complex in a closed, inactive conformation. When the cullin-RBX complex is neddylated, CAND1 binding sites are inaccessible allowing for full assembly and activation of the complex (Duda et al., 2008; Goldenberg et al., 2004).

Non-canonical CUL9 structure and regulation remains poorly characterized

CUL9 (formerly PARC) is considered non-canonical because it has a variant structure and evidence of its regulation and function are limited – we don't have the information to know if CUL9 shares some of the key features of other cullins (**Figure 1-4**). There are 21 papers to date on CUL9 according to a PubMed search of "CUL9", and their findings often contradict one another.

Although there are no current crystal structures of full length CUL9, we do understand its domains and their predicted functions based on their homology to other proteins.

CUL9 shares 60% sequence identity to CUL7 – nearly the first 1700 amino acids of the 2517 amino acids CUL9 is composed of are almost identical to full-length CUL7 (Kaustov et al., 2007; Nikolaev et al., 2003) (**Figure 1-4**). These two proteins share three key domains: CPH (Cullin-7, PARC, and HERC2 proteins), DOC, and the cullin homology domain. The CPH domain, as its name suggests, is also present in the E3 ubiquitin ligase HERC2 (HECT and RLD Domain Containing E3 Ubiquitin Protein Ligase 2). In fact, the CPH domain of CUL9 and CUL7 share 40% sequence identity with that of HERC2 (Kaustov et al., 2007). All proteins bind the p53 tetramerization domain via their CPH domain, though evidence indicates none directly ubiquitinate p53 (Andrews et al., 2006; Cubillos-Rojas et al., 2014; Kaustov et al., 2007). One study, however, did show that CUL7 can mono-ubiquitinate p53 *in vitro* (Andrews et al., 2006)

The first published study about CUL9, originally dubbed PARC (p53-associated, Parkin-like cytoplasmic protein), showed that CUL9 bound to the tumor suppressor p53 and sequestered it in the cytoplasm in unstressed cells (Nikolaev et al., 2003). When DNA is damaged, p53 translocates to the nucleus to promote transcription of pro-apoptotic proteins ultimately resulting in apoptosis of damaged cells (Vousden and Lane, 2007). Mutations in p53 result in uncontrolled proliferation and are commonly seen in cancer (Vousden and Lane, 2007). Cytoplasmic p53 is observed in neuroblastoma cells (Nikolaev et al., 2003). This study demonstrated that depletion of CUL9 induced nuclear localization of p53 in response to DNA damage, making it an attractive target for cancer therapeutics (Nikolaev and Gu, 2003; Nikolaev et al., 2003). Later studies demonstrated that mutations in conserved residues in the CPH domain of CUL7 and CUL9 prevented their association with p53 at its tetramerization domain (Andrews et al., 2006; Dias et al., 2002; Kaustov et al., 2007).

The DOC domain is also present in HERC2, CUL7, and CUL9, but it's exact function in these proteins remains unclear. The DOC domain was originally identified in a subunit of the key cell cycle regulator E3 ubiquitin ligase complex APC/C, APC10 (Kominami et al., 1998; Kurasawa and Todokoro, 1999). The APC/C is a multisubunit E3 ubiquitin ligase that promotes cell cycle progression through the targeted ubiquitination and subsequent degradation of key cell cycle regulatory proteins. Its substrate specificity is dependent on which adapter proteins, cell division control protein 20 (CDC20) or Fizzy-related (FZR1, also known as CDH1), it is associated with. APC/C-CDC20 promotes progression of the mitotic phase of cell cycle and APC/C-FZR1 promotes progression of the G1 phase. The complex is highly spatiotemporally regulated to

ensure proper progression of cell cycle. APC10 is a core component of this complex and functions, in part, as a substrate receptor within the complex (Carroll and Morgan, 2002; Carroll et al., 2005; Passmore et al., 2003). Specifically, the DOC domain within APC10 directly interact with substrate degrons. Mutations in the DOC domain prevent substrate recognition and result in delayed mitosis (Carroll et al., 2005). Similarly, a point mutation in the DOC domain of CUL7 caused high levels of tetraploidy and aneuploidy in 293T cells (Yan et al., 2014). These studies suggest that the DOC domain could play a role in supporting the assembly of the CRL substrate receptor of CUL9 and/or CUL7.

Even with a basic understanding of CUL9's NTDs based on function in homologous proteins, there are still no identified adapter proteins or substrate receptors associated with CUL9. However, it does have two known substrates: SURVIVIN (Li et al., 2014) and cytochrome c (cyt c) (Gama et al., 2014). As referenced above, a group of researchers demonstrated that CUL9 deletion in mice results in tumor formation in nearly every organ of the body (Pei et al., 2011). They determined that CUL9 deletion results in increased levels of aneuploidy and DNA damage, however, there were no known substrates of CUL9 at the time (Li et al., 2014). They, and many others investigating CUL9, sought to identify CUL9 substrates via unbiased mass spectrometry of the CUL9 immunoprecipitates but were unsuccessful. Through screening mitotic proteins, they determined that survivin, an inhibitor of apoptosis implicated in mitotic regulation, co-immunoprecipitated with CUL9. Additionally, CUL9 KO mice had significantly increased levels of survivin protein in tissues obtained from several organs. Using *in vivo* and *in vitro* ubiquitination assays, the authors were able to show that CUL9 ubiquitinates survivin. Although they were able to show that CUL9 ubiquitylation of survivin was dependent on its interaction with RBX1, confirming previous reports (Skaar et al., 2007), they were not able to identify a substrate receptor (Li et al., 2014).

CUL9 also targets cytosolic cyt c in sympathetic neurons and neuroblastoma cells preventing initiation of apoptosis ultimately promoting cell survival (Gama et al., 2014). Following DNA damage, cells undergo mitochondrial outer membrane permeabilization (MOMP) which results in the release of cytochrome c (Singh et al., 2019). Cytosolic cyt c complexes with the apoptotic protease activating factor 1 (APAF1) to form the apoptosome that ultimately initiates the caspase cascade (Singh et al., 2019). Previously, release of cyt c was considered the point of no return. However, neurons and cancer cells can survive after MOMP (Vaughn and Deshmukh, 2008). Prior to the study identifying cyt c as a CUL9 substrate, a few mechanisms of apoptotic resistance have been described for sympathetic neurons, describing that these cells could avoid cell death

after the release of cytochrome c. This study showed that cyt c accumulated in these cells following DNA damage when treated with a proteasome inhibitor, indicating it is ubiquitinated for proteasomal degradation (Gama et al., 2014). The group did an unbiased siRNA screen of many E3 ubiquitin ligases and determined that KD of CUL9 resulted in increased levels of cytosolic cyt c after DNA damage. The group showed CUL9 ubiquitinated cyt c via *in vitro* ubiquitination assay using immunoprecipitated FLAG-CUL9. Interestingly, both sympathetic neurons and neuroblastoma cells express low levels of APAF1 and high levels of CUL9, suggesting that any cell with this combined expression pattern could have the same apoptotic resistance (Gama et al., 2014).

The mechanism used by CUL9 to ubiquitinate any of its substrates is not known. Insight into CUL9 ubiquitination mechanism may even provide insight into additional substrates that may be modified by CUL9. Although RBX1 seems to associate with its cullin domain, we cannot rule out that its RBR domain plays a critical role in ubiquitination of CUL9 substrates or that each may have different substrate specificities. Its RBR domain is homologous to that of Parkin, another protein with a critical role in neuronal cell survival via mitophagy (Marín et al., 2004). CUL9 could be a fusion between CUL7 and Parkin, but further characterization of its structural assembly and regulation should be pursued to gain a better appreciation of CUL9 structure, regulation, and function.

CUL9's C-terminus has another motif found in other RBR ligases that may provide critical insight into its mechanism of ubiquitination: an Ariadne domain (Dove and Klevit, 2017; Marín and Ferrús, 2002). Several other RBR E3s contain this domain including Human Homolog of Drosophila Ariadne-1 (HHARI) and TRIAD1 (Dove and Klevit, 2017; Kelsall et al., 2013). The Ariadne domain inhibits ubiquitin conjugation of these ligases. The active cysteine on RING2 is blocked by its interaction with the Ariadne domain and this interaction is not affected by E2~Ub binding; a structural change must occur to activate ubiquitin ligase activity. CRLs appear to play a major role in regulating these ligases. HHARI and TRIAD1 are activated when complexed with specific neddylated cullins (Kelsall et al., 2013). TRIAD1 is activated by CUL5, while HHARI is activated by CUL1, -2, -3, and -4A (Dove and Klevit, 2017). Interestingly, only neddylated CUL4B and CUL7 do not associate with any Ariadne containing ligases (Kelsall et al., 2013). CUL7 and CUL9 may complex at the Ariadne domain – though CUL9 heterodimerization with CUL7 does not appear to be required for its activity (Gama et al., 2014; Skaar et al., 2005, 2007). It would also be exciting to explore if neddylated CUL9 can activate its own RBR domain through either

homodimerization or a structural confirmation allowing interaction between CUL9's own cullin and Ariadne domains.

CRLs play a critical role in early developmental processes

Most cullins are required for normal development. Deletion of six cullin scaffolds results in embryonic lethality in mice largely due to the result of cell cycle abnormalities during embryonic development. Research has revealed that CRLs play a particularly important role in mammalian nervous system development. Several CRLs have been implicated in neurodevelopmental disorders like schizophrenia and autism spectrum disorder. However, the role of the non-canonical cullin CUL9 in early development remains elusive as *Cul9* KO mice are viable and studies exploring its role in neurodevelopment are not available. The growing foundation of research characterizing the role of canonical cullins in early developmental processes could inform future studies characterizing novel roles of understudied ligases like CUL9. Additionally, using a human-derived model like human pluripotent stem cells could provide needed insight into human specific roles of CRLs in neuronal differentiation and beyond.

CRLs are required for normal embryonic development

CRLs are critical in normal embryonic development, largely due to their pivotal roles in cell cycle regulation. *Cul1* KO mice don't survive past E6.5 and have significantly elevated protein levels of its substrate Cyclin E (Dealy et al., 1999; Wang et al., 1999). Dysregulation of Cyclin E often results in arrest at the late stage of the G1 phase (Craney and Rape, 2013). Trophoblast giant cells in *Cul1* KO mice are abnormally large due to unregulated endocycling – the cells have 10 times higher DNA content than their WT counterparts (Wang et al., 1999). Deletion of *Cul-3*, *-4b*, and *-5* are also embryonic lethal and result in notable cell cycle defects during embryo development (Liu et al., 2012; Singer et al., 1999; Zhu et al., 2016). Like *Cul1*, *Cul3* deletion resulted in significantly increased levels specifically in Cyclin E – levels of other cyclins like Cyclin A and Cyclin B were not increased. Cells in the extraembryonic endoderm were stalled in S-phase. In fact, gastrulation was so abnormal there did not appear to be formation of the mesoderm and endoderm (Singer et al., 1999). Total KO of *Cul4b* results in loss of proliferating cells at E7.5 and a G2/M arrest. The primitive streak was absent and embryonic endoderm tissues were highly disordered within the *Cul4b* KO embryos (Liu et al., 2012). Deletion of *Cul5* in mice only produced heterozygote pups; detailed examination of the KO embryos was not performed (Zhu et al., 2016).

A mouse KO model of *Cul2* has yet to be developed so its role in early development remains elusive.

Loss of CRL regulation is lethal, further highlighting the importance of CRLs in early development. NEDD8 is expressed at a relatively similar level in all tissues (Hori et al., 1999). Its expression has been demonstrated to be critical in normal embryonic development of *Caenorhabditis elegans* (Jones and Candido, 2000), *Drosophila melanogaster* (Ou et al., 2002), and the mice (Tateishi et al., 2001). Specifically, deletion of *Ubc12*, the E1 activating enzyme specific to NEDD8, resulted in lethality at the peri-implantation stage in mice. This embryonic lethality appeared to be due to ineffective function of its CRL substrates resulting aberrant cell cycle progression (Tateishi et al., 2001). Deletion of the *Csn2*, *Csn3*, *Csn5*, and *Csn8* also results in early embryonic lethality in mice, again, majorly due to dysregulation of cell cycle progression caused by aberrant regulation of CRL substrates like Cyclin E (Lykke-Andersen et al., 2003; Menon et al., 2007; Tomoda et al., 2004; Wei et al., 2008; Yan et al., 2003). Notably, massive cell death was observed in *Csn5* KO mice, likely attributed to its complex independent regulation of apoptotic proteins like the pro-apoptotic protein BCL-2-associated X protein (BAX) (Tomoda et al., 2004). The lethal effects of CRL dysregulation further highlights not only the importance of CRL function for development, but the unique ability of the complexes to adapt their substrate specificity to the changing needs of the cell in various cellular environments and in response stress through its disassembly and reassembly with a seemingly infinite number of adapter proteins. However, not all CRLs are required for embryonic development. *Cul9* KO embryos are viable (Arai et al., 2003; Gama et al., 2014; Hollville et al., 2020; Pei et al., 2011; Skaar et al., 2005). *Cul7* KO mice die immediately after birth due to respiratory distress or between E10.5-E12.5. The embryo is smaller at all stages of development, the placenta is smaller, and severe vascular issues are observed (Arai et al., 2003).

Mice that do not express the *Cul4a* gene are viable. An initial study reported that *Cul4a* KO mice did not develop past 7.5 days postcoitum (Li et al., 2002). However, a later study demonstrated that *Cul4a* KO mice were viable with no developmental abnormalities, though they were more susceptible to UV-damage, especially in skin specific deletions (Liu et al., 2009). The authors showed that the embryonic lethality reported in the first paper was not due to *Cul4a* deletion, but rather deletion of PCI domain containing protein 2 (PCID2); the original construct deleted a 529 bp region upstream of the first exon of the *Pcid2* gene. PCID2 is critical for mRNA transport from the nucleus, and has been shown to be localized to the centrosomes where it contributes to regulation of cell cycle progression (Cunningham et al., 2014). The authors also

point out that the PCI domain is present in components of the CSN and the 26S proteasome, implicating PCI domain containing proteins in ubiquitin regulation of protein turnover (Hofmann and Bucher, 1998; Liu et al., 2009). They demonstrated that lentiviral mediated knockdown of PCI inhibited proliferation in mouse embryonic fibroblasts (MEFs) ultimately resulting in cell death. However, Cul4a knockdown MEFS were viable (Liu et al., 2009). CUL4B may compensate for loss of CUL4A, but further studies must be done to test this.

Cul9 KO mice are also viable, but different phenotypes have been reported. Most studies have reported that deletion of the *Cul9* gene causes no apparent phenotype (Gama et al., 2014; Hollville et al., 2020; Skaar et al., 2005, 2007). One group reports that *Cul9* KO mice develop tumors throughout the body; they provide evidence that this phenotype is a result of the loss of Cul9 regulation of the tumor suppressor p53 (Li and Xiong, 2017a; Li et al., 2014; Pei et al., 2011). However, they were unable to replicate the initial report that CUL9 sequesters p53 in the cytoplasm (Nikolaev et al., 2003; Pei et al., 2011). They do show that *Cul9* KO phenotype can be rescued via overexpression of full-length Cul9 protein, but not Cul9 protein with a point mutation in its p53 binding domain (CPH) indicating the Cul9-p53 interaction must play some role in tumor suppression (Pei et al., 2011). Although CUL9 did not appear to ubiquitinate or alter the localization of p53, they suggest that the CUL9-p53 interaction promotes p53 activity (Li and Xiong, 2017a). CUL9 deletion in U2OS osteosarcoma cells caused increased levels of the CDK inhibitor p21, which is targeted by transcription factor p53 to initiate the DNA damage response. Additionally, a mutation in the Cul9 CPH domain in MEFs results in increased DNA damage, but decreased apoptosis when treated with DNA damaging agents indicating that the p53 mediated DNA damage response is non-functional (Li and Xiong, 2017a). Validation of these results in non-carcinogenic human cell lines is key to seeing if this CUL9 function is relevant to humans. Additionally, further investigation into the distinction between CUL9 KO mice reported phenotypes is needed to truly understand CUL9 function in early development.

CRLs critically regulate neurodevelopment

Over the past decade, researchers have developed a greater appreciation for the role of CRLs in nearly every part of neurodevelopment (Rape, 2018). APC/C, CUL3, and CUL4B have been implicated in neurodevelopmental disorders like autism, schizophrenia, intellectual disabilities, and anxiety disorders (De Rubeis et al., 2014; Dong et al., 2020; Ripke et al., 2014; Tarpey et al., 2007). Other cullins, like CUL5, CUL3, and CUL7 play critical roles in neuronal migration and dendrite morphogenesis. NEDD8 even plays a role in spinal development

potentially independent of its role in regulating CRLs (Vogl et al., 2015). A key role of CRLs in neurodevelopment is the coordinated regulation of cell cycle and differentiation.

Cell cycle length is dynamically regulated during differentiation. G1 length is critical to a cell's decision to self-renew or differentiate (Calder et al., 2013; Filipczyk et al., 2007; Liu et al., 2017b; Patmanidi et al., 2017). For example, lengthening of G1 phase in neural stem cells is required for their differentiation to neurons (Lange et al., 2009; Lukaszewicz et al., 2005, 2005; Pilaz et al., 2009; Salomoni and Calegari, 2010). Cell cycle duration *in vivo* grows from 8 hours to 18 hours within the ventricular zone of the developing mouse cortex (Ponti et al., 2013). This drastic increase in cell cycle length is the result of rapid expansion of the G1 phase, which lengthens from 3 to 13 hours (Ponti et al., 2013; Takahashi et al., 1995).

Neural stem cells (NSCs) exhibit a shortened G1 phase compared to their more differentiated counterparts and G1 regulation impacts their differentiation decisions. Several *in vivo* studies demonstrated that lengthening of G1 is not only a result of differentiation, but a key factor promoting differentiation of NSCs (Delgado-Esteban et al., 2013; Lange et al., 2009; Pilaz et al., 2009; Roccio et al., 2013). Lengthening of G1 phase in NSCs within the developing mouse cortex by inhibition of Cdk4 using inhibitors and RNAi was sufficient to promote neurogenesis. In contrast, shortening of G1 phase by overexpression of Cdk4 inhibited neurogenesis, promoted self-renewal of NSCs within the sub-ventricular zone (Roccio et al., 2013). These studies suggest that lengthening of the G1 phase may be the primary cause of the observed differentiation. One study focused on confirming these observations *in vitro* to understand the underlying molecular mechanisms. Using FUCCI at the single cell level in mouse embryonic stem cells (mESCs) and mNSCs, researchers discovered that G1 phase was longer in mESCs and mNSCs grown under differentiating conditions in vitro. Inhibition of Cdk4 was sufficient to induce differentiation in both cell types as well (Roccio et al., 2013). It will be exciting in the future to use these tools to examine if G1 phase lengthening is sufficient to promote differentiation in human NSCs and ESCs.

G1 phase regulator APC/C-FZR1 activity increases during hESC differentiation, and its function is required for neurogenesis in mice (Bar-On et al., 2010; Delgado-Esteban et al., 2013). One group showed *in vitro* and *in vivo* that CUL9 deletion in the mouse cortex prevents differentiation of post-mitotic cortical neurons, reducing the number of neurons, ultimately resulting in microcephaly (Delgado-Esteban et al., 2013). Cortical development is a delicate balancing act between proliferation of the neural progenitor pool and differentiation of mature cortical neurons (Baum and Gama, 2021). The neural progenitor pool must expand in early cortical development to produce enough precursors for differentiation. Then, progenitors undergo

asymmetric division where they both self-renew and produce a differentiated cortical neuron. Finally, the neural progenitor pool is depleted with cells undergoing symmetric differentiating divisions (Baum and Gama, 2021). If the pool over proliferates or differentiates too early, this leads to disorganization of the cortical layers and altered brain size (Hong et al., 2017). Inhibition of APC/C-FZR1 activity or deletion of *Fzr1* in the mouse cortex increased the number of neural progenitors in S-phase preventing production of differentiated neurons (Delgado-Esteban et al., 2013). Since DNA synthesis was stalled in the progenitors, they underwent p53-mediated apoptosis depleting the progenitor pool. Ultimately, inhibition of neuronal differentiation resulted in reduced brain size or microcephaly (Delgado-Esteban et al., 2013). One study demonstrated that ID2, a protein that regulates progenitor proliferation and differentiation, is a substrate of APC/C-FZR1 in cortical neurons and neuroblastoma cells providing further insight into the role APC/C-FZR1 in regulation of cortical differentiation (Lasorella et al., 2006; Sullivan et al., 2016).

However, APC/C-FZR1 also appears to have cell cycle independent functions in neurodevelopment. FZR1, but not the other APC/C co-factor CDC20, are widely expressed in the adult mouse brain in nearly every neuron even though neurons are post-mitotic (Gieffers et al., 1999; Li et al., 2008). APC/C-FZR1 has been implicated in axonal growth and patterning, glial migration, and neuronal metabolism (Almeida et al., 2005; Herrero-Mendez et al., 2009; Juo and Kaplan, 2004; Kannan et al., 2012; Konishi, 2004; van Roessel et al., 2004; Silies and Klämbt, 2010; Stegmüller et al., 2006). Most striking, it seems to play a critical role in synaptic plasticity and cognitive disorders. Synaptic plasticity is the brain's ability to respond to experiences by rewiring neural circuits through modification of synaptic signaling (Citri and Malenka, 2008). Synaptic transmission between neurons can strengthen through long-term potentiation or weaken through long-term depression. Synaptic signaling is thought to correlate with certain cognitive functions like learning and memory. Ubiquitin mediated degradation of synaptic signaling proteins is a main method of controlling synaptic signaling (Citri and Malenka, 2008). APC/C-FZR1 appears to be one of the ligases regulating synaptic signaling through degradation of key synaptic signaling proteins.

Deletion of the *Fzr1* gene in mice is embryonic lethal, but heterozygotes display deficiencies in learning and memory (Li et al., 2008). *Fzr1* heterozygous KO mice had no visible abnormalities in brain organization, but neurons in the hippocampus had abnormal long-term potentiation. The researchers performed standard fear conditioning behavioral tests to determine if the mice had cognitive deficits often observed from hippocampal dysfunction (Li et al., 2008; Paylor et al., 1994). First, mice were trained in a chamber where they were shocked, then exposed

to a specific noise for thirty seconds. One day later, the mice were placed back in the chamber and their behavior was analyzed with and without the auditory stimulus. *Fzr1* heterozygous KO mice exhibited fear response behavior (i.e. freezing) in the chamber, but this behavior was not exacerbated by the auditory stimuli like in the wild-type mice, a phenotype observed in known hippocampal defective mouse models (Li et al., 2008; Paylor et al., 1994). Similarly, another group reports that deletion of the cullin subunit *Apc2* in forebrain neurons of mice worsens fear response compared to wild-type mice, a common phenotype in models of anxiety disorders like phobias or post-traumatic stress disorder (Kuczera et al., 2011). Moreover, these mice were resistant to exposure therapy also known as “fear extinction.” Aberrant degradation of proteins at synapses of neurons in the hippocampus contributes to fear extinction, so further understanding of APC/C function at synapses could provide insight into the mechanisms of not only anxiety disorders, but their treatments (Kuczera et al., 2011; Lee et al., 2008). One group of researchers determined that APC/C-FZR1 targets the protein Fmrp for proteasomal degradation in the mouse hippocampus (Huang et al., 2015). FMRP regulates synaptic transmission by modulating the translation of synaptic signaling proteins – loss of FMRP function contributes to fragile X syndrome which causes intellectual disabilities and autism spectrum disorder (Sidorov et al., 2013).

Other CRLs also play cell-cycle independent roles in neuronal development, particularly in cortical development. CUL5 and CUL3 are required for normal neuronal migration and cortical layer formation in the cortex (Courtheoux et al., 2016; Feng et al., 2007; Simó and Cooper, 2013; Simó et al., 2010). The cortex is composed of six layers that form in an “inside-out” fashion meaning that the inner most layer is formed before the outer most layers (Buchsbaum and Cappello, 2019). This mechanism requires neurons to migrate out from the ventricular zone following differentiation from neuronal progenitors and neurons of the outermost layer must “crawl” over formed inner layers. Improper migration can cause incomplete layer formation or mispositioning of neurons, meaning the neurons are present in the wrong layers – this is commonly seen in neurodevelopmental disorders like intellectual disability and epilepsy (Buchsbaum and Cappello, 2019). Cul5 knockdown cortical neurons in mice were unable to properly migrate causing differentiated neurons meant for the outer most layers to remain in the superficial layers (Feng et al., 2007). Cul5 bound to its substrate receptor Socs (suppressor of cytokine signaling) targets Dab1 (disabled-1), a pro-migratory protein, for degradation (Feng et al., 2007; Simó and Cooper, 2013; Simó et al., 2010). DAB1 is a receptor for the secreted protein REELIN which promotes proper neuronal migration and positioning (Honda et al., 2011).

Disruption of the DAB1-REELIN pathway causes brains to develop in an “outside-in fashion” resulting in the cortical neurons generally comprising the innermost layer 6 to form the outermost layer and vice versa (Caviness and Sidman, 1973; Honda et al., 2011). Cul5 seems to prevent excessive neuronal migration through targeted degradation of DAB1 as deletion or depletion of *Cul5* in mouse cortical neurons causes them to aggregate at the superficial cortical layer (Feng et al., 2007). Cul3 also regulates neuronal migration in the cortex, but rather through modulation of the microtubule and actin network that directs migrating neurons (Courtheoux et al., 2016).

Cul7 and Obsl1 of the 3M complex also regulate the formation of dendrites, filamentous neuronal extensions that receive signals from axons by modulating Golgi morphology (Litterman et al., 2011). Golgi secretory trafficking plays a key role in the growth and branching of dendrites (Horton et al., 2005; Litterman et al., 2011). Cul7 in complex with its adapter protein Fbxw8 is recruited to the Golgi in granule mouse neurons by Obsl1 (Litterman et al., 2011). Depletion of Cul7 and Fbxw8 resulted in diffuse localization of Golgi and increased dendrite length due to decreased secretory trafficking. The researchers discovered that Cul7-Fbxw8 targets the Golgi protein Grasp65 for proteasomal degradation – depletion of Grasp65 results in increased secretory vesicle trafficking from the Golgi. Cul7-Fbxw8 regulates Grasp65 to balance Golgi morphogenesis during neuronal maturation and signaling, ultimately controlling dendrite length (Litterman et al., 2011).

CRLs are even implicated in dynamic regulation of transcription factors during differentiation. For example, CUL4 regulates protein levels of the transcription factor SOX2 during *in vitro* differentiation of ESCs to neural progenitor cells (Cui et al., 2018; Zhang et al., 2019). SOX2 is one of the main pluripotency factors in embryonic stem cells, promoting a transcriptional program that supports their self-renewal capacity of pluripotent differentiation potential (Masui et al., 2007; Sarkar and Hochedlinger, 2013; Takahashi and Yamanaka, 2006). Although its expression decreases during differentiation, it is still expressed in neural progenitor cells at the ventricular zone of the cortex in the early stages of development (Graham et al., 2003; Masui et al., 2007). SOX2 deletion or depletion causes decreased production of mature neurons and prolonged maintenance of the neural progenitor pool (Cavallaro et al., 2008; Ferri et al., 2004). Interestingly, constitutively elevated SOX2 levels cause a 32% increase in neuronal cell density in the cerebral cortex (Fero et al., 1996; Li et al., 2012). Fine-tuning of SOX2 protein levels is critical for proper neurogenesis, but most studies have focused on its transcriptional regulation. This recent study reports that CUL4A-Det1-COP1 complex ubiquitinates SOX2 for proteasomal degradation during neuronal differentiation of neural progenitor cells, while the deubiquitinase

OTUD7B stabilizes SOX2 protein levels in neural progenitor cells promoting their self-renewal (Cui et al., 2018). This study provides needed insight into dynamic post-translational regulation of transcription factor levels during differentiation.

CRL regulation by neddylation is critical to proper neurodevelopment as well. Nedd8 was originally identified in the embryonic mouse brain and was shown to be downregulated in expression over the course of mouse embryonic development (Kumar et al., 1992, 1993). Although one group was unable to replicate decreased expression of Nedd8 over the course of neuronal development, they did observe increased levels of neddylated substrates during postnatal brain development (Vogl et al., 2015). Downregulation of the Nedd8 protein and its E1 activating enzyme Ubc12 prevented dendritic spine maturation in a CRL independent manner, indicating this novel role was mediated through a previously unidentified substrate. Further investigation identified PSD-95, a scaffolding protein critical for organization of the post-synaptic density, as a target of neddylation. Neddylation of PDS-95 negatively affected its function, causing synapse instability, decreased synaptic transmission, and spinal loss. These neurodevelopmental defects resulted in major cognition deficits, mostly involving impairment in learning and memory (Fu and Ip, 2015; Vogl et al., 2015). A recent study determined that actin regulator COFILIN is modified by NEDD8 in developing neurons and that chemical inhibition of neddylation in neurons causes severe cytoskeletal defects providing greater insight into non-CRL dependent functions of neddylation in neurodevelopment and synaptic signaling (Vogl et al., 2020).

Mutations in some cullins contribute to neurodevelopmental disorders

Emerging studies are slowly revealing how mutations in *CUL3* and *CUL4B* contribute to autism spectrum disorders (ASDs) and X-linked mental retardation syndrome (XLMR), respectively (De Rubeis et al., 2014; Dong et al., 2020; Kong et al., 2012; Ly et al., 2019; O'Roak et al., 2012; Tarpey et al., 2007; Zhao and Sun, 2012). ASD is classically considered the result of increased activity of excitatory (glutamatergic) neurons and decreased activity of inhibitory (GABAergic) (Coghlan et al., 2012; Dong et al., 2020). Patients with ASD have symptoms like intellectual deficiencies, increased anxiety, display repetitive behaviors, and verbal and non-verbal communication issues (Bryson et al., 2003; Gillott et al., 2001; Lever and Geurts, 2016). *CUL3* mutations have been identified in ASD patients and as an ASD risk gene in a genome-wide association study (De Rubeis et al., 2014; Kong et al., 2012; O'Roak et al., 2012). A group recently used a neuron specific *Cul3* KO heterozygote mouse model to characterize its cognitive abilities

and identify CUL3 substrates relevant to its potential role in neurodevelopment (Dong et al., 2020).

Deletion of *Cul3* in GFAP-expressing cells (neural progenitors, neurons, and astrocytes) of mice resulted in death around postnatal day 17 – the mice had decreased brain size and the cortex had reduced thickness and disorganized layers (Dong et al., 2020). This phenotype mirrors previous reports of altered brain size and cortex organization in ASD patients (Carper et al., 2002; Hazlett et al., 2017; Schumann et al., 2010; Wegiel et al., 2014). Heterozygote KO mice, however, did not display obvious, visible abnormalities in the brain (Dong et al., 2020). The mice did have behavioral abnormalities akin to those described in established mouse models of ASD including increased anxiety and impaired social interactions. They also had altered dendritic spine morphology, synaptic signaling, and overly active glutamatergic neurons. Using a quantitative proteomics approach, they identified proteins that were differentially expressed in *Cul3* heterozygote KO mice and identified Eif4g1 (Eukaryotic translation initiation factor 4 gamma 1) as a potential Cul3 substrate. This was particularly interesting as protein translation was increased in neurons in the *Cul3* heterozygote KO mouse. In fact, inhibition of Eif4g1 rescued the observed behavioral phenotypes implying that Cul3 regulation of Eif4g1 is key for proper neurodevelopment and its disruption could contribute to ASD (Dong et al., 2020).

Several mutations in *CUL4B* that result in translation of non-functional protein have been reported in patients with XLMR (Badura-Stronka et al., 2010; Isidor et al., 2010; Tarpey et al., 2007). XLMR is a broad category of intellectual disabilities all resulting from a mutation in a gene found on the X-chromosome (Ropers and Hamel, 2005). Those with *CUL4B* mutations have symptoms in addition to intellectual disability like seizures, aggression, megalencephaly, cortical malformations, and delayed puberty (Badura-Stronka et al., 2010; Isidor et al., 2010; Tarpey et al., 2007; Vulto-van Silfhout et al., 2015). Interestingly, unlike humans, *Cul4b* deletion in mice results in death at E7.5, making them an imperfect model for its role in XLMR (Liu et al., 2012). Although characterization of CUL4B in other animal models like *D. melanogaster* and zebrafish have provided some insight into CUL4B function during neurodevelopment, a better understanding of its function in human brain development is needed (Ando et al., 2019; Ly et al., 2019). Pluripotent stem cells may provide an advantageous model for analyzing the mechanism of CUL4B in neurodevelopment.

Two groups of researchers developed induced pluripotent stem cell lines to analyze the molecular mechanisms of CUL3 and CUL4B function in neuronal differentiation (Fischer et al., 2020; Liu et al., 2020). One group developed a heterozygous *CUL3* KO iPSC line and

demonstrated that the neuronal differentiation was delayed and the neurons that were produced had abnormal activity (Fischer et al., 2020). The other group reprogrammed fibroblasts obtained from a patient with XLMR with a specific mutation in *CUL4B* – they demonstrated that the iPSCs produced were capable of self-renewal and trilineage differentiation (Liu et al., 2020). These human-cell derived models open the door to exploring the role of these ligases in neuronal differentiation at the cellular level providing insight into the underlying molecular mechanisms of their contribution to these neurodevelopmental disorders. These iPSCs can be used to model human brain development as well using the advent of brain organoids which could reveal human specific functions of these ligases. iPSC models of other CRLs can also be developed to identify any neuronal differentiation deficits that may have been overlooked in the mouse models.

The role of the non-canonical CRL CUL9 in neurodevelopment remains virtually unexplored. Our laboratory previously reported that CUL9 levels increase during neuronal differentiation, but we only reported CUL9's function in post-mitotic neurons (Gama et al., 2014). Additionally, the cognitive effects of *Cul9* deletion in mice have not been tested since there are no obvious brain abnormalities in the mice (Gama et al., 2014; Hollville et al., 2020; Pei et al., 2011; Skaar et al., 2007). However, mice with cognitive defects do not always present visible phenotypes as previously reported in brain specific deletion of *Fzr1* and *Cul3* (Dong et al., 2020; Kuczera et al., 2011; Li et al., 2008). These tests should be performed and complemented with studies using *CUL9* KO iPSCs. We developed the first *CUL9* KO iPSC model and detail its characterization in this dissertation.

Summary of thesis

The body of work presented in this dissertation details the characterization of a novel human-cell derived model of the understudied, non-canonical cullin scaffold CUL9. Unlike other cullins, previous efforts to characterize CUL9 function during the early stages of development using mouse KO models have been unsuccessful (Gama et al., 2014; Pei et al., 2011; Skaar et al., 2005, 2007). In **Chapter 2**, the development of a CUL9 KO hiPSC cell line using CRISPR-Cas9 is outlined. The line has normal expression of key pluripotent markers and is capable of neuronal differentiation, though there are abnormalities. With the advent of this new model, we sought to identify new CUL9 interacting proteins including substrates, regulators, and adapters that could provide insight into the aberrant neuronal differentiation observed through the experiments described in **Chapter 3** and **Chapter 4**. The application of mass spectrometry based proteomic approaches to characterize CUL9 have also been unsuccessful in the past by our group and others (Gama et al., 2014; Li et al., 2014), however, we were able to successfully identify the APC/C subunit APC7 as a possible CUL9 regulating protein through LC-MS/MS analysis of immunoprecipitation of endogenous CUL9 protein in hiPSCs – this finding is detailed in **Chapter 3**. However, we were unable to fully elucidate the function or biochemical properties of this interaction leaving the question of CUL9's function during neuronal differentiation unanswered. We attempted to remedy this in the study described in **Chapter 4** though quantitative analysis of the proteome in CUL9 KO hiPSCs and differentiated neural precursors to identify proteins differentially expressed in KO cells compared to WT cells. We identified proteins involved in fatty acid metabolism and neuronal transcription but were unable to confirm their functional interaction with CUL9. However, we identified over 100 proteins differentially expressed in CUL9 KO cells which can be studied in the future to analyze the dynamic function of CUL9 during neuronal differentiation. In **Chapter 5**, I critically discuss the data presented and provide insight into the potential function of CUL9 in neuronal differentiation and how future studies can finally reveal the function of this mysterious and elusive enzyme.

Figures

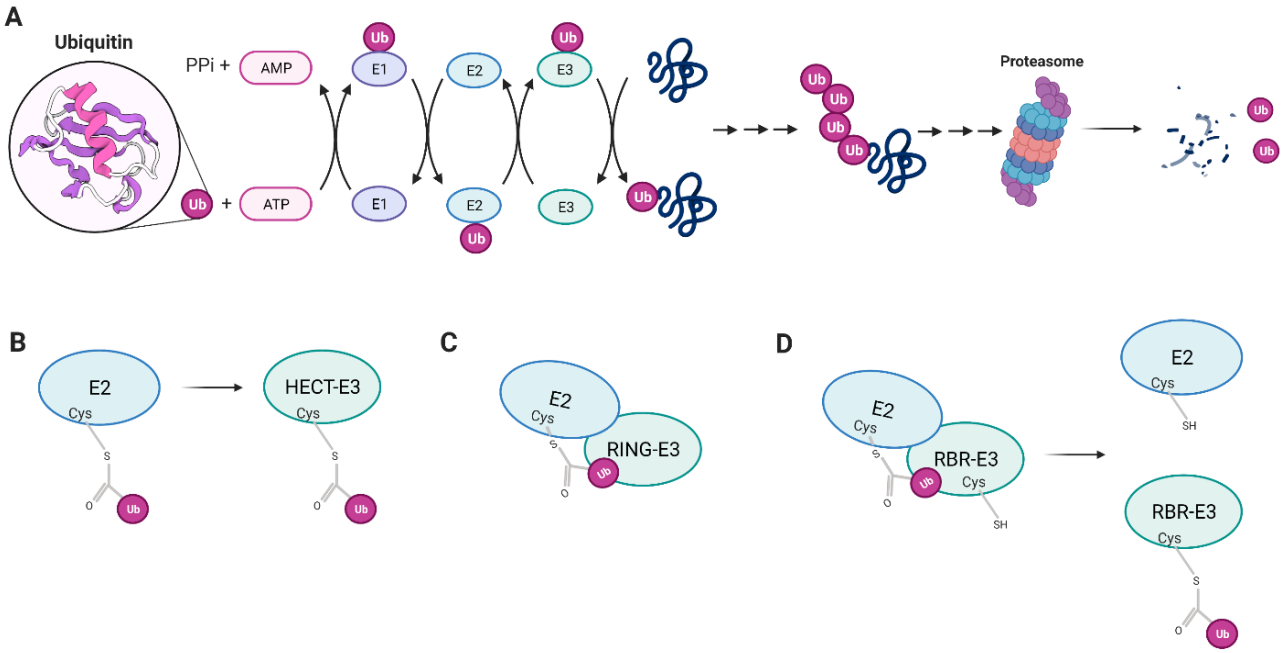

Figure 1-1. Ubiquitin is added to proteins via an enzyme cascade.

(**A**) Schematic depicts a general overview of the process of ubiquitination. A cartoon representation of ubiquitin structure is shown. Ubiquitin is first activated in an ATP-dependent manner by E1, then conjugated to the E2 which transfers ubiquitin to the E3 ligase which catalyzes the final transfer of ubiquitin to its targeted substrate which canonically marks the target for proteasomal degradation. Three families of E3 ligases exist, each with their own unique mechanism of ubiquitin transfer (**B**) Ubiquitin is directly transferred to a conserved lysine residue on the HECT E3 ligase, which then directly transfers the moiety to the targeted substrate. (**C**) RING-E3 ligases form a transient structure e where the E2 and E3 are bound, but the ubiquitin moiety remains bonded to the E2 prior to transfer. (**D**) RBR-E3 ligases use an approach that marries the HECT and RING mechanisms. The E2 first forms a transient structure as observed in the HECT ligase where the E2 is bound to the RING1 domain. Then, ubiquitin is transferred to a conserved cysteine in the RING2 domain where ubiquitin is finally transferred to the substrate. Created with BioRender.com

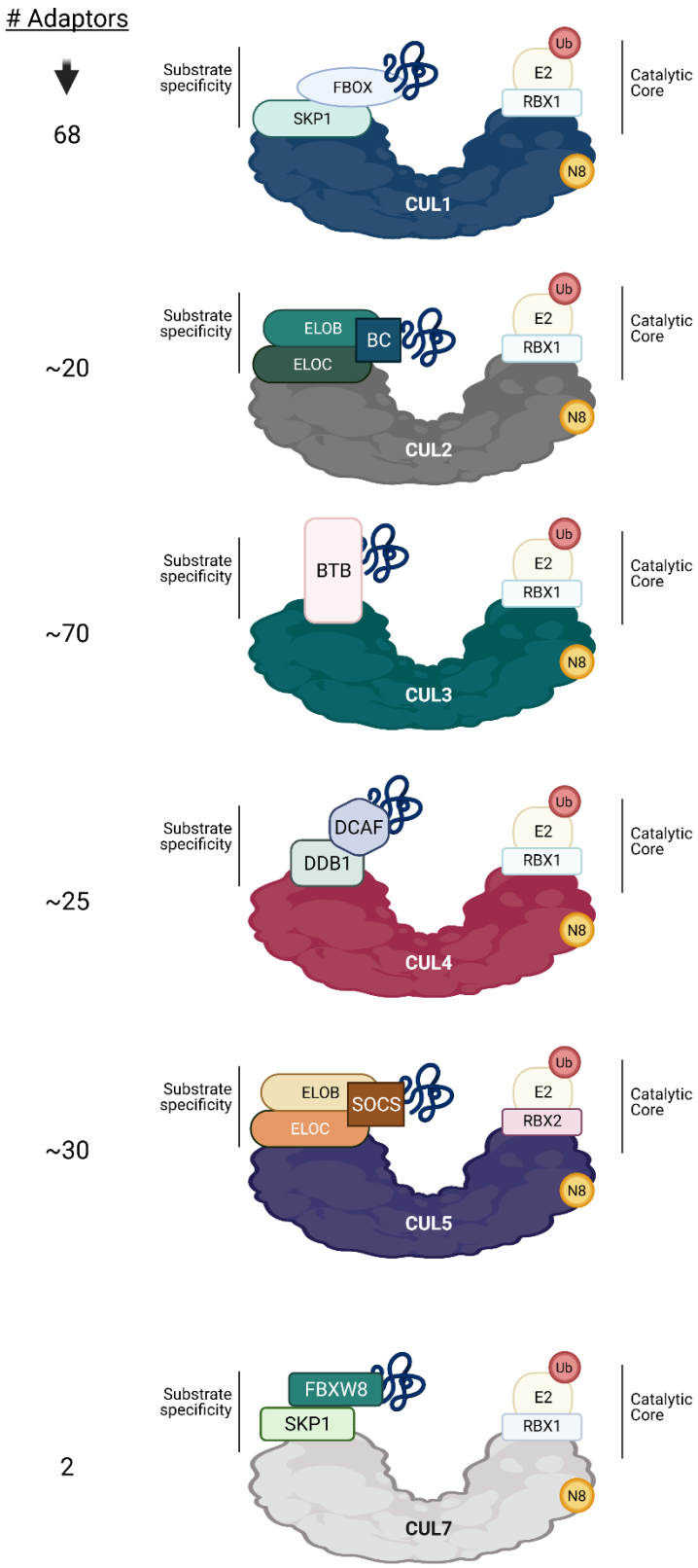
Adaptors
68
Substrate specificity
FBOX
SKP1
Ub
E2
RBX1
N8
CUL1
Catalytic Core
~20
Substrate specificity
ELOB
BC
ELOC
Ub
E2
RBX1
N8
CUL2
Catalytic Core
~70
Substrate specificity
BTB
Ub
E2
RBX1
N8
CUL3
Catalytic Core
~25
Substrate specificity
DCAF
DDB1
Ub
E2
RBX1
N8
CUL4
Catalytic Core
~30
Substrate specificity
ELOB
SOCS
ELOC
Ub
E2
RBX2
N8
CUL5
Catalytic Core
2
Substrate specificity
FBXW8
SKP1
Ub
E2
RBX1
N8
CUL7
Catalytic Core

Figure 1-2. Key structural elements are conserved across the eight canonical members of the CRL family.

Visual representations of the eight canonical CRLs are depicted. Note that CRL4A and -4B are represented together as, simply, CRL4. The notable commonalities are the binding of an adapter and substrate receptor at the N-terminus of each cullin scaffold, the binding of a RING binding protein (RBX1 and RBX2) and E2 carrying ubiquitin at the C-terminus, modification by NEDD8 (N8), and the elongated crescent shape of the cullin scaffold. The number of known adapter proteins for each corresponding cullin are listed on the left. Design was based on figure from (Lydeard et al., 2013). Created with BioRender.com.

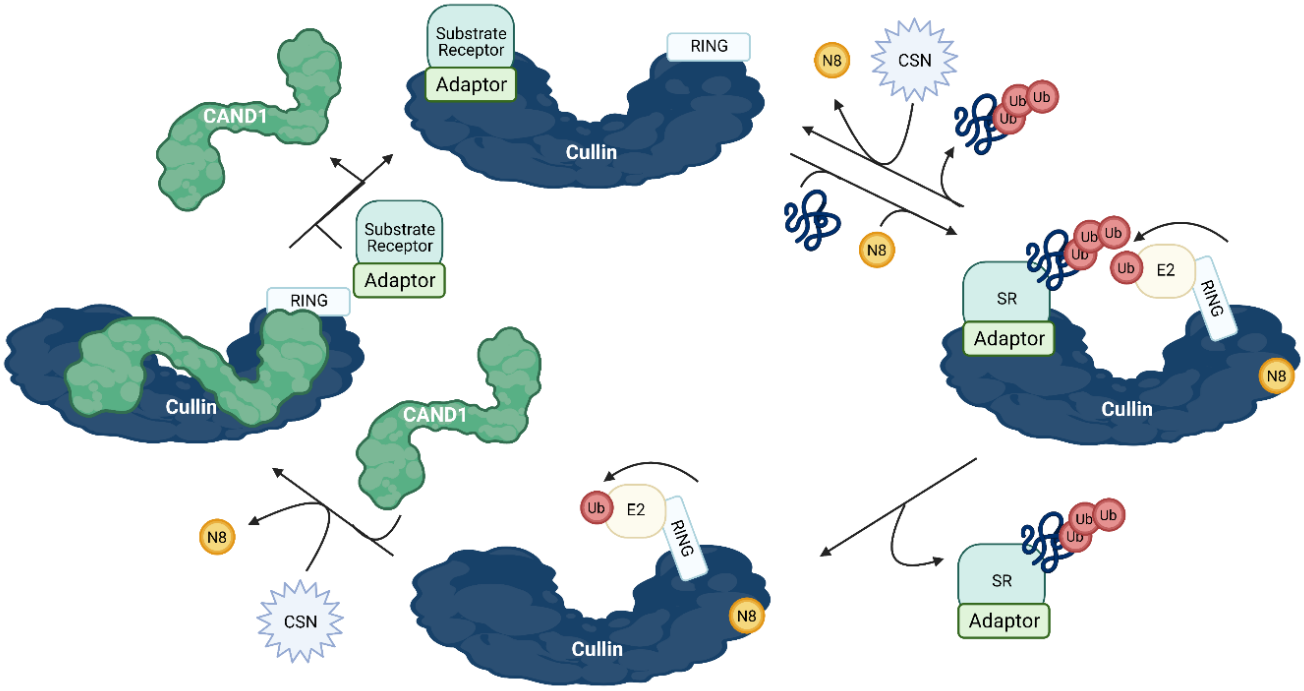

Figure 1-3. CRLs are primarily regulated by NEDD8 modification.

The schematic depicts the canonical regulatory cycle of CRL complex formation and activity. Modification by NEDD8 (N8) promotes E2~ub binding and structural changes allowing the N- and C-terminus to position the substrate and E2~ub complex in close proximity to promote ubiquitin transfer. After ubiquitin transfer, the ubiquitinated substrate and adapter and substrate receptor dissociate from the cullin scaffold. NEDD8 is removed by the COP9 signalosome (CSN) and CAND1 binds to the complex blocking the neddylation site, preventing complex formation. Created with BioRender.com

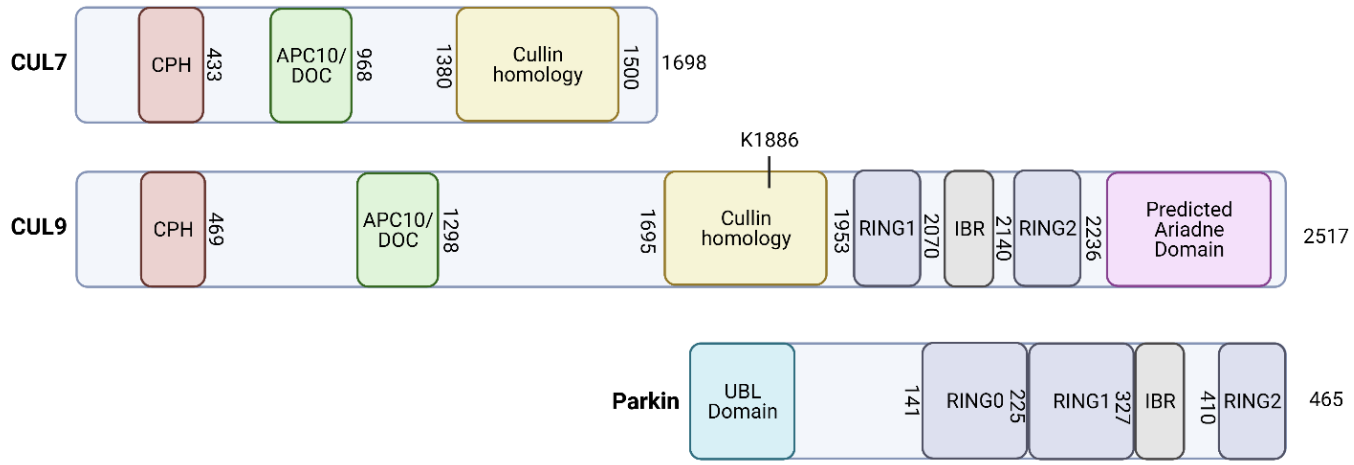

Figure 1-4. CUL9 shares significant homology with CUL7 and PARKIN.

CUL9 shares significant homology with CUL7 and PARKIN. Additionally, CUL9 has a conserved lysine in its cullin homology domain that aligns with the signature of other neddylation domains (K1886). Created with Biorender.com

Tables

Deletion	Reported phenotype (s) in mice	References
CUL1	Embryonic lethality at E6.5; Arrest in late G1-phase; Enlarged trophoblast giant cells with increased DNA content	Dealy et al., 1999; Wang et al., 1999
CUL2	No mouse model available	---
CUL3	Embryonic lethality at BLAH; Extraembryonic endoderm stalled in S-phase; Mesodern and endoderm don't form	Singer et al., 1999
CUL4A	Viable; Increased susceptibility to UV damage	Li et al., 2002; Liu et al., 2009
CUL4B	Embryonic lethality at E7.5; G2/M arrest; Primitive streak does not develop; Disorganized endoderm	Liu et al., 2012
CUL5	Embryonic lethal; detailed characterization of embryos not performed	Zhu et al., 2016
CUL7	Die immediately after birth; major vascular defects; decreased embryo and placenta size	Aria et al., 2003
CUL9	Viable; No phenotype; Widespread tumor development	Gama et al., 2014; Hollville et al., 2020; Skaar et al., 2005, 2007

Table 1-1. Phenotypes of cullin scaffold deletions in mice

Deletion of cullin scaffolds generally results in embryonic lethality, but some are not required for development and have multiple reported phenotypes.

Chapter 2

DEVELOPMENT OF A CUL9 CRISPR KO STEM CELL LINE TO CHARACTERIZE CUL9 FUNCTION DURING NEURAL DIFFERENTIATION

Parts of Chapter 2 have been adapted with permission from Ortolano, N.A., Romero-Morales, A.I., Rasmussen M.L., Bodnya, C., Kline, L.A., Joshi, P., Connelly, J.P., Rose K.L., Pruett-Miller, S., and Gama V. (2021). A proteomics approach for the identification of cullin-9 (CUL9) related signaling pathways in induced pluripotent stem cell models. PLoS One.

Summary

CUL9 is a non-canonical and poorly characterized member of the largest family of E3 ubiquitin ligases known as the Cullin RING ligases (CRLs). Most CRLs play a critical role in developmental processes, however, the role of CUL9 in early development remains elusive. We developed a CUL9 KO hiPSC line to provide a new tool for ourselves and the larger research community to identify CUL9 substrates and functions that may have been overlooked in CUL9 KO mouse models and transformed cell lines. CUL9 KO hiPSCs have a normal karyotype, express key pluripotent factors at normal levels, and maintain a cell death response. However, deletion of CUL9 protein causes aberrant formation of neural rosettes, an *in vitro* model of early neuralization. The results of our study build on current evidence that CUL9 may have unique functions in different cell types. Our CUL9 KO hiPSC line can be used to characterize CUL9 function in a variety of stem, progenitor, and specialized cell types to reveal cell-specific CUL9 functions.

Introduction

Post-translational modifications are critical to the regulation of protein function, subcellular localization, structure, and turnover. Ubiquitin is a post-translational modification that primarily signals for protein turnover (Ciechanover and Kwon, 2015). In fact, ubiquitination accounts for 80% of all protein degradation in cells. However, ubiquitin can signal for more than proteasomal degradation, depending on the type of linkages within a polyubiquitin chain (Rajalingam and Dikic, 2016; Ye and Rape, 2009). Ubiquitin modification of a given substrate is catalyzed by three enzymes: E1 (activating enzyme), E2 (conjugating enzyme), and E3 (ubiquitin ligase). The E1 activates ubiquitin in an ATP dependent manner. Adenylated ubiquitin forms a thioester bond with the catalytic cysteine in the E1 active site and is then moved to the E2 via a thioester transfer. The E2-ubiquitin conjugate is recruited to an E3 ubiquitin ligase which aids or directly catalyzes ubiquitin thioester transfer to a specific residue, often a lysine, on the targeted substrate. The largest family of E3 ubiquitin ligases is the Cullin Ring Ligase (CRL) family.

CRLs function as multi-subunit complexes ubiquitinating a variety of substrates. The central part of CRLs is the cullin protein, a hydrophobic scaffolding protein that recruits a RING binding protein (Rbx1 or Rbx2) through their homologous cullin domain. CRL function also requires a covalent modification by NEDD8 at a conserved lysine residue within the cullin scaffold. Each cullin contains a unique set of domains at their N-terminal that mediate substrate adapter binding. While there are only eight cullins, there are numerous possible CRLs based on the recruited adapter proteins. For example, the E3 ubiquitin ligase Cullin-1 (CUL1) complexes with adapter proteins known as FBOX proteins which determine CUL1's protein specificity. There are 68 FBOX proteins that have been identified, meaning that CUL1 could form up to 68 complexes, each with its own individual set of specific substrates (Nalepa et al., 2006). Considering the ubiquitous nature of CRLs, they contribute to the regulation of nearly every cellular process. In fact, mouse knockout models of most members of the CRL family result in embryonic or neonatal lethality often as a result of aberrant cell cycle progression (Arai et al., 2003; Dealy et al., 1999; Li et al., 2002; Singer et al., 1999; Wang et al., 1999). CUL9 KO mice, however, are viable and most report no apparent phenotype (Gama et al., 2014; Hollville et al., 2020; Li et al., 2014; Skaar et al., 2007). Due to its elusive function and variant structure, CUL9 is considered a non-canonical CRL.

CUL9 contains an additional RING between RING (RBR) domain at its C-terminus and has no identified adapter proteins (Gama et al., 2014; Li et al., 2014; Yan et al., 2014). CUL9 KO mice are viable, and only a few phenotypes have been reported, providing limited insight into its function (Nikolaev and Gu, 2003; Pei et al., 2011; Skaar et al., 2005). Studies at the cellular level,

including our own, identified a role for CUL9 in promoting survival in post-mitotic neurons and various cancer cell lines. CUL9 promotes ubiquitin mediated proteasomal degradation of cytochrome *c* in neurons and human brain tumor cell lines, and survivin in human cancer cells (Gama et al., 2014; Li et al., 2014). With only two identified substrates, the mechanism of CUL9 ubiquitination is not known. Considering CUL9 has two potential ubiquitin catalytic domains, further characterization of CUL9 function and regulation is needed.

Our laboratory and others report that CUL9 is highly expressed in the brain, particularly the cortex, and that its levels increase over the course of neuronal differentiation (Gama et al., 2014; Hollville et al., 2020). However, studies have focused on its role in post-mitotic neurons and aging neurons in relationship to neurodegenerative diseases like Parkinson's disease, largely due to it's homology with the E3 ubiquitin ligase PARKIN (Gama et al., 2014; Hollville et al., 2020). The role of CUL9 in neurodevelopment is virtually unexplored, despite the prevalent role of CRLs in neurodevelopment and its related diseases like ASD and XLMS (Badura-Stronka et al., 2010; Dong et al., 2020; Isidor et al., 2010; Tarpey et al., 2007). Recent studies using iPSC models of CRL dysfunction in neurodevelopmental disorders from patient derived lines and CRISPR directed mutations have provided insight into CRL regulation of early neuronal differentiation (Fischer et al., 2020; Liu et al., 2020).

Here, we report the first CUL9 KO hiPSC line that can be leveraged to identify new CUL9 interactions leading to discovery of adapters, substrates, and regulators during differentiation. We characterized the ability of CUL9 KO hiPSCs to differentiate to cortical neural precursor cells considering the high expression of CUL9 in the murine cortex (Gama et al., 2014; Hollville et al., 2020). While the CUL9 KO hiPSCs can produced neural stem and progenitor cells, the KO cells form abnormal neural rosettes, an *in vitro* model of the neurulation. The data presented in this chapter establish our CUL9 KO hiPSC as an effective model for characterizing CUL9 function and interactions during human neuronal differentiation. Analysis of the cognitive state in CUL9 KO mice would complement our studies and provide insight into the potential functional consequences of these subtle differences in neuronal differentiation observed in our CUL9 KO hiPSC model.

Results

CRISPR/Cas9 CUL9 KO iPSC clones are pluripotent

To explore the role of CUL9, we used hPSCs as a model. We first generated a CUL9 knockout cell line in human induced pluripotent stem cells (hiPSCs) using the CRISPR/Cas9 system. We designed several guide RNAs directed to an early, conserved exon within *CUL9*, exon 9 (**Figure 2-1A**). Previous guide RNAs designed were directed towards exon 1 and 2, but these were ineffective. The selected guide RNA had an editing efficiency of 92% and zero potential off-target sites including up to three base pair mismatches. Single-cell clones were isolated from cells electroporated with guide RNA and recombinant CAS9 by flow activated cell sorting. Individual clones were sequenced by next generation sequencing (NGS) and analyzed for insertions/deletions (indels) resulting in frameshift mutations at the guide RNA target site using CRIS.py (Connelly and Pruett-Miller, 2019). Two clones containing a single base pair insertion were selected for downstream analysis. More than 99% of the genomic DNA analyzed in each of these clones contained an indel resulting in a frameshift mutation (**Figure 2-1B**). Most importantly, these clones only contained a single type of indel, with both having a single base pair insertion in >99% of the genomic DNA analyzed. An unedited clone was also identified and used downstream as a control (isogenic WT). Western blotting was used to validate the loss of CUL9 protein expression in both knockout clones (**Figure 2-1C**). Metaphase spread analysis was used to validate that all isogenic clones had a normal karyotype (**Supplemental Figure 2-1**). Previous studies demonstrate that CUL9 heterodimerizes with another CRL known as CUL7 (Li et al., 2014; Skaar et al., 2007). Although CUL9 function does not require heterodimerization with CUL7, the two are highly homologous, and we wanted to ensure CUL7 protein levels would not increase to compensate for loss of CUL9. We determined by Western blotting analysis that CUL7 levels are not significantly changed in CUL9 KO iPSCs (**Figure 2-1C**).

Next, we assessed the effects of CUL9 deletion on the pluripotency of hiPSCs. We initially tested this using a global gene expression profile assay known as the PluriTest Assay (Müller et al., 2011). Briefly, the gene expression profile of each clone was compared to a reference data set containing over 450 genome wide transcriptional profiles of validated pluripotent cells. The pluripotency score (y-axis) quantifies the presence of metagenes within the data set that separate pluripotent cells from non-pluripotent cells. The novelty score (x-axis) measures how well the gene expression pattern of the cell in question matches the expected profile. Compared to a non-iPSC control, our parental wild-type, isogenic wild-type, and CUL9 KO iPSCs have the expected transcriptional profile of a pluripotent cell (**Figure 2-2A**). To complement the PluriTest assay, we

examined the mRNA and protein level expression of key pluripotency factors OCT4 and NANOG. In both CUL9 KO clones, there were no significant changes in expression levels of OCT4 or NANOG as determined by RT-qPCR and Western blotting (**Figure 2-2B-C**). Additionally, confocal microscopy analysis of immunostained hiPSCs showed that OCT4 and NANOG localized to the nucleus in all cell types and are expressed at similar levels (**Figure 2-2D**). Based on our results, we concluded that the CUL9 KO clones remain pluripotent and are an appropriate tool for analyzing the downstream effects of CUL9 deletion on differentiation.

CUL9 does not target cytochrome c for degradation

We previously reported that CUL9 promotes survival in post-mitotic neurons and neuroblastoma cells (Gama et al., 2014). During apoptosis, cytochrome c is released from mitochondria, initiating the caspase cascade. Although this was previously considered the "point of no return" in apoptosis, we showed that CUL9 targets cytochrome c for ubiquitin mediated degradation following its release from the mitochondria in sympathetic neurons and neuroblastoma cells. Post-mitotic neurons and cancer cells are resistant to apoptosis and this mechanism is one mechanism contributing to this increased resistance (Gama et al., 2014; Vaughn and Deshmukh, 2008). We hypothesized that cytochrome c would not be a CUL9 substrate in hPSCs since our laboratory previously demonstrated that hPSCs are highly sensitive to apoptosis (Dumitru et al., 2012). To test our hypothesis, we treated control and CUL9 KO cells with 1μM of the DNA damaging agent etoposide for 3 hours; then, we measured cell survival by examining caspase activity. CUL9 KO cells did not show differences in caspase 3/7 activity compared to control cells (**Supplemental Figure 2-2**).

We further validated that CUL9 does not directly target cytosolic cytochrome c for degradation by examining cytochrome c release from mitochondria following a four-hour treatment with 1μM etoposide in the presence of pan-caspase inhibitor QVD-OPh in control and CUL9 KO cells (**Figure 2-3**). In both the control and KO cells, cytochrome c was released from the mitochondria into the cytosol after four hours of treatment at the same level. These data indicate that cytochrome c is not directly degraded by CUL9 in hPSCs, and that these cells rapidly initiate apoptosis in response to double stranded breaks as previously shown (Dumitru et al., 2012). Additionally, we show that cytochrome c is likely targeted for proteasomal degradation in hPSCs as reported in neuronal cells (Gama et al., 2014) as cytochrome c levels increase with

additional treatment of proteasome inhibitor bortezomib in both cell lines, though at lower levels in CUL9 KO cells (**Figure 2-3B**).

CUL9 KO iPSC clones differentiate to hNSCs and hNPCs.

We validated previous studies showing that CUL9 protein and mRNA levels increase over the course of human cortical differentiation particularly during the neural induction phase when neural precursors form (**Figure 2-4A-B**). Based on this, we focused our study on characterizing the effects of CUL9 deletion in the first 25 days of cortical differentiation of hiPSCs (**Figure 2-4A**). During the first ten days of cortical differentiation, N2 media is gradually increased during dual SMAD inhibition; this phase is known as neuralization. At this phase, neuroepithelial-like cells (which we have termed human Neural Stem Cells (hNSCs)) expressing neural stem cell markers like PAX6 and NESTIN begin to form. After day ten, N2/B27 media is used to maintain the cells, and over time the cells differentiate further (Shi et al., 2012). Around day 25, the cells are a mixture of intermediate progenitor cells and immature cortical neurons (which we have termed human Neural Progenitor Cells (hNPCs)). These cells are highly migratory permitting them to form the cortical layers in an inside outside fashion. Cells at this phase express neuron specific microtubules and associated proteins including microtubule associated protein (MAP2) and beta-3 tubulin (TUBB3) (Poirier et al., 2010; Teng et al., 2001). They also express transcription factors present in radial glia cells and intermediate progenitor cells like Empty Spiracles Homeobox 2 (EMX2), and those present in early born neurons like T-box brain 1 (TBR1) (Englund, 2005; Hamasaki et al., 2004). Beyond day 25, the cells will form neurons in the expected order starting with deep-layer neuron populations followed by upper-layer neuron populations and astrocytes.

Both CUL9 KO iPSC clones successfully differentiated to hNSCs expressing neural stem cell transcription factor PAX6 and microtubule associated protein NESTIN (**Figure 2-4D; Supplemental Figure 2-3**). The clones further differentiated to hNPCs at day 25 and expressed microtubule markers TUBB3 and MAP2 as well as transcription factors EMX2 and TBR1 (**Figure 2-4E; Figure 2-5**). Although there are little significant changes in protein or mRNA expression of neuronal markers at day seven or day 25 of CUL9 KO differentiated cells, substantial variability in expression is observed between replicates (**Figure 2-5 and Supplemental Figure 2-3**). This clonal variability could indicate that CUL9 deficiency generates genomically unstable cell lines. A confounding factor is the variability between cortical differentiations using this method as previously reported (Volpato et al., 2018). To delineate if the observed variability in expression is a phenotype or a result of the differentiation method used, we employed 3D differentiation

methods which have been demonstrated to be highly reproducible at differentiating neural cell populations (Chandrasekaran et al., 2017).

Deletion of CUL9 results in abnormal embryoid body and neural rosette formation

Neural rosettes serve as an *in vitro* model for neurulation, the early stages of neural tube formation (Elkabetz et al., 2008; Wilson and Stice, 2006) (**Figure 2-6A-B**). Neural rosettes have a distinctive apical-basal polarity and can be easily identified by marker localization. ZO-1 (tight junction marker) and CDK5RAP2 (centrosome marker) localize apically, marking the central lumen. Cells extend radially from the lumen, as demonstrated by TUBA (alpha tubulin) staining (**Figure 2-6A**). Previous data demonstrate that the cells surrounding the lumen have a similar expression profile to the cells within the neural epithelium layer of the neural tube (Elkabetz et al., 2008; Haremaki et al., 2019) (**Figure 2-6B**).

To determine the effect of CUL9 deletion on neural rosette formation, we first grew CUL9 KO clones in suspension with dual SMAD inhibitors to form EBs (**Figure 2-6A**). EB diameter was measured five days after initial seeding. EBs derived from CUL9 KO clones have a significantly reduced diameter (**Figure 2-6C**). Neural rosettes formed from these EBs have the expected morphology based on marker localization (**Figure 2-6D**). To quantify neural rosette morphology, ZO1 staining was used to quantify the number of rosettes formed per EB, as well as the area of the lumen. While we saw no significant differences in the number of neural rosettes per EB, we observed significant differences in lumen size in both clones despite clonal variability (**Figure 2-6E-F**). We corroborated this result in CUL9 KD rosettes as well. Both shRNAs used resulted in decreased lumen size indicating (**Supplemental Figure 2-4**). The corroboration of our results in CUL9 depleted cells indicates that the altered lumen size observed in CUL9 KO cells, despite differing between the two clones, is likely not the result of an off-target effect of CRISPR editing.

Discussion

Previous studies characterizing CUL9 demonstrated that it promotes cell survival through ubiquitin-mediated degradation of its two known substrates, cytochrome c and SURVIVIN (Gama et al., 2014; Li et al., 2014). However, our study shows that this CUL9 function seems specific to post-mitotic neurons and cancer cell lines, highlighting the cell specific functions CUL9 may have and emphasizing the need to characterize its role in various cell types at various stages of life. We determined that CUL9 deletion in hiPSCs caused abnormal formation of neural rosettes and variable expression of stage-specific neuronal markers during cortical differentiation. These findings indicate that CUL9 may play a role in early neurodevelopment as reported in other cullins (Badura-Stronka et al., 2010; Dong et al., 2020; Isidor et al., 2010; Tarpey et al., 2007). Characterization of CUL9 in the newly developed human-derived cell system described here may provide needed insight into CUL9 function is as it is a late evolutionary gene present only in vertebrates. We and others have hypothesized that CUL9 is a duplicate of the highly homologous CUL7, which is also present only in vertebrates (Gama et al., 2014; Skaar et al., 2005, 2007). This indicates that CUL9 may have a highly specified role in vertebrates, which may provide a plausible explanation for why CUL9 substrates have been so challenging to identify.

In our hiPSC CUL9 KO cell line, we first sought to determine if CUL9 deletion affects iPSC cell survival. Using a caspase assay, we determined that CUL9 KO cells were no more susceptible to apoptosis than WT cells, however, we did observe some interesting differences in cytochrome c release in CUL9 KO cells. Unexpectedly, when the WT cells were treated with the DNA damaging agent etoposide and proteasome inhibitor bortezomib, some cytochrome c was released into the cytosol, but the amount of mitochondrial localized cytochrome c seemed higher compared to treatment with only etoposide. This result suggests that ubiquitin mediated degradation of cytochrome c may occur at the mitochondria rather than in the cytosol in – the ubiquitination of cytochrome c in hiPSCs has not been examined, so further investigation is needed. In CUL9 KO cells treated with etoposide and bortezomib, the levels of cytosolic cytochrome c were decreased. However, there was significantly less cytochrome c still localized to the mitochondria, indicating that CUL9 may play a role in cytochrome c release from the mitochondria or degradation at the organelle. It will be interesting to investigate how mitochondrial release of cytochrome c following DNA damage is regulated in hiPSCs and how CUL9 may be involved in this process. Considering that CUL9 is highly homologous to PARKIN, it could collaborate with PARKIN to degrade proteins at the outer and inner mitochondrial membranes to

regulate mitochondrial release of cytochrome c. Alternatively, it could regulate PARKIN activity itself.

Despite the prevalent role of most CRLs in development, mouse knockout models of CUL9 are viable and do not present a consistent phenotype (Pei et al., 2011). In this study, we developed a human cell-derived model to characterize CUL9 in human neuronal development. Our data indicate that CUL9 does not affect hPSC pluripotency or regulate apoptotic execution as previously described in other cell types. CUL9 mouse KO models have no apparent phenotypes in neuronal development (Pei et al., 2011; Skaar et al., 2005). While we did not observe any affects in hPSCs or differentiated NSCs and NPCs, we did observe defects in neural rosette formation. Abnormal lumen size can be the result of asymmetric division of R-NPCs or dysregulation of apical membrane size which affects the apical-basal polarity of rosettes (Elkabetz et al., 2008; Medelnik et al., 2018). Further investigation into the mechanism behind altered lumen size in CUL9 KO and KD neural rosettes is needed.

Our results also suggest that further characterization of the CUL9 KO mouse model may be beneficial. Mice with phenotypes indicative of neurodevelopmental disorders like ASD, schizophrenia, generalized anxiety, and XLMS do not always present observable, physical phenotypes (Badura-Stronka et al., 2010; Dong et al., 2020; Isidor et al., 2010; Kuczera et al., 2011; Tarpey et al., 2007). Experiments directly testing cognitive attributes like anxiety levels, fear extinction, and obsessive behaviors could provide insight into the potential roles of CUL9 in neurodevelopment and direct future molecular cell-based studies. Additionally, brain specific deletion of CUL9 in mice could limit confounding, unobserved phenotypes in the CUL9 total KO mouse. Alternatively, this finding could indicate a distinction between CUL9 function in mouse and human neurodevelopment. It would be exciting to examine the role of primate specific neuronal cell populations such as outer radial glia cells using a single-cell approach to clarify if this function is species specific (Pollen et al., 2015).

In summary, CUL9 has an elusive developmental function compared to other CRLs, and it does not appear to have a common function amongst different cell types. In our own data, we see variable expression of key PSC, NSC and NPC markers and abnormal formation of neural rosettes. If CUL9's primary function in early development is involved in regulating cells undergoing countless dynamic changes during differentiation, characterization of its function will be challenging as it will require catching a cell in a transitional state. Future studies should investigate the role of CUL9 during the dynamic state of cell differentiation. Trilineage differentiation of the CUL9 KO hPSCs would reveal if other tissue specific transcription factors have variable

expression as we observed in NSCs and NPCs. CUL9 function may be just as, if not more, relevant to other lineages. Protein levels of key transcription factors of other mature, specialized cell types like astrocytes or cardiomyocytes should also be examined. The variable levels of protein, but not mRNA levels of key pluripotency and neuronal markers could indicate CUL9 deletion results in dysregulation of protein translation. Mass spectrometric analysis of the proteome of the CUL9 KO iPSCs could reveal any dysregulation present in these cells and direct future studies using this new human cell-derived model for studying CUL9.

Figures

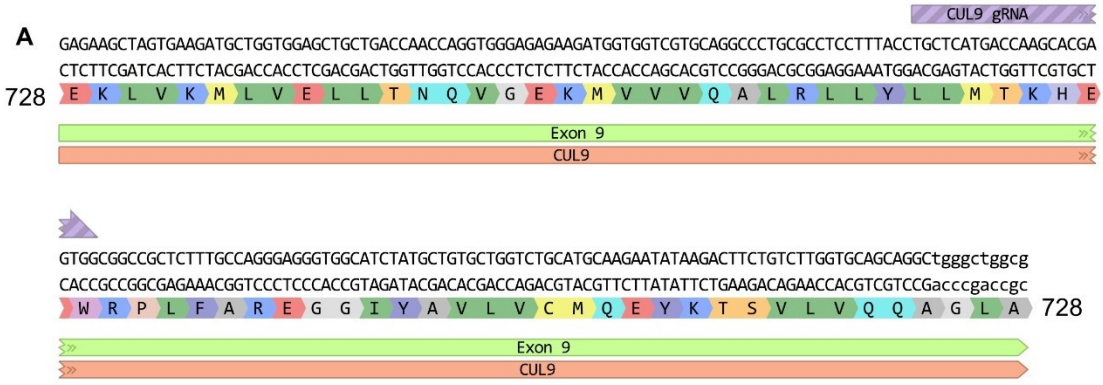

B

Sample	Total % Indels	Top Indel	# Reads (%)
Parental WT	0.30%	0	310 (99.7%)
Isogenic WT	0.50%	0	397 (99.5%)
CUL9 KO #1	99.6%	+1	227 (100%)
CUL9 KO #2	100%	+1	512 (99.6%)

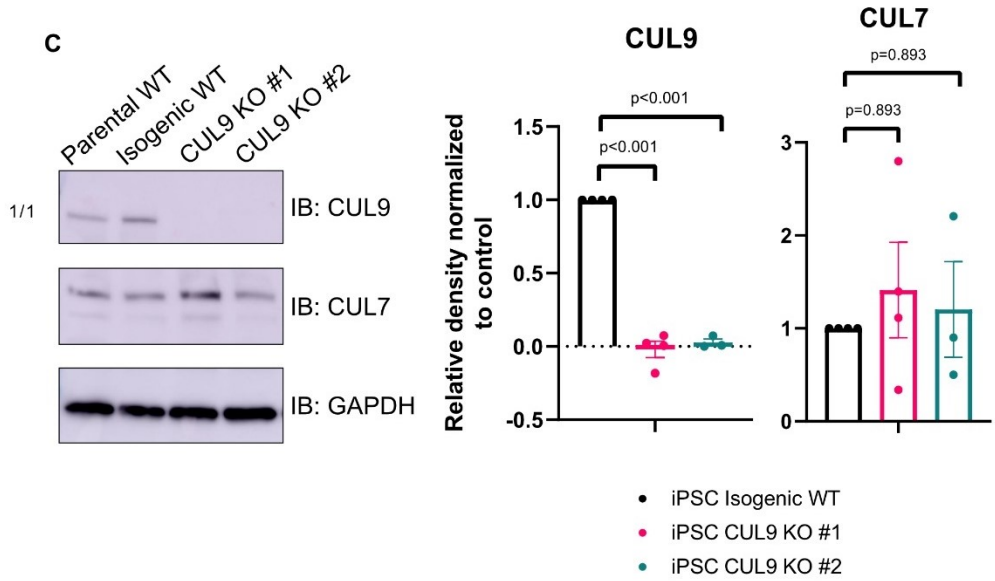

Figure 2-1: Design and analysis of CUL9 KO hPSC clones.

(**A**) Sequence CUL9 exon 9 with antisense gRNA aligned to target sequence. Figure made using Benchling (**B**) CUL9 KO clones have single nucleotide insertions resulting in a frameshift mutation. Table summarizing the results of Next Generation Sequencing (NGS) analysis of control and CUL9 KO lines used for downstream experiments. Segment of CUL9 exon 9 sequenced for analysis by NGS are shown below table for each cell line. gRNA targeted sequence is highlighted in yellow, and single nucleotide insertions are highlighted in green. (**C**) CUL9 KO cells do not express CUL9 protein or increased levels of homologue CUL7. Western blot of analysis of control and CUL9 KO clones to analyze CUL9 and CUL7 protein levels. Isogenic WT and Clone #1 n=4; Clone #2 n=3; mean +/- SEM; Analysis done using student's t-test, α=0.05.

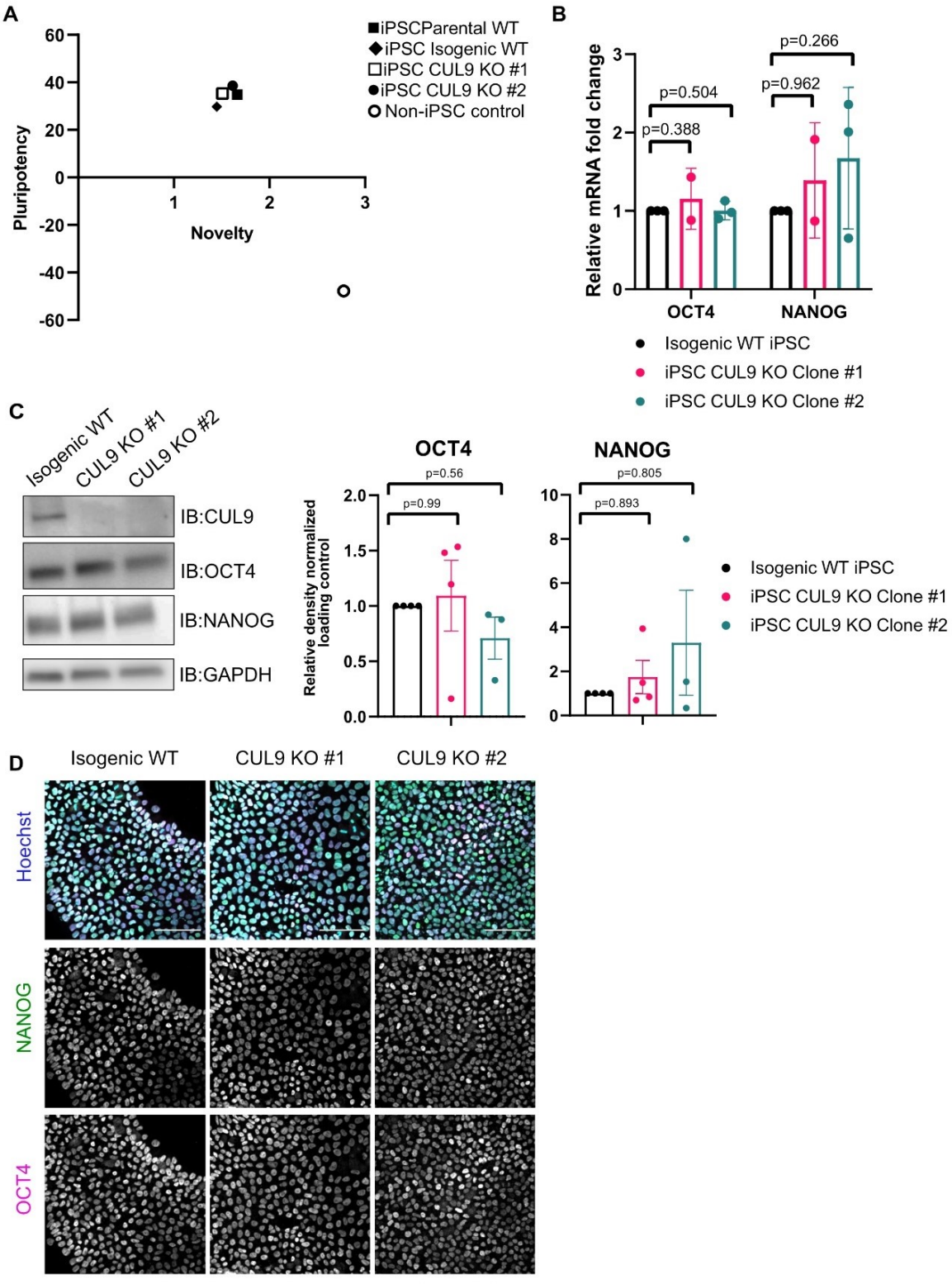
A
Pluripotency
Novelty
iPSCParental WT
iPSC Isogenic WT
iPSC CUL9 KO #1
iPSC CUL9 KO #2
Non-iPSC control
B
Relative mRNA fold change
p=0.388
p=0.504
p=0.962
p=0.266
OCT4
NANOG
Isogenic WT iPSC
iPSC CUL9 KO Clone #1
iPSC CUL9 KO Clone #2
C
Isogenic WT
CUL9 KO #1
CUL9 KO #2
IB:CUL9
IB:OCT4
IB:NANOG
IB:GAPDH
OCT4
NANOG
Relative density normalized loading control
p=0.56
p=0.99
p=0.805
p=0.893
Isogenic WT iPSC
iPSC CUL9 KO Clone #1
iPSC CUL9 KO Clone #2
D
Isogenic WT
CUL9 KO #1
CUL9 KO #2
Hoechst
NANOG
OCT4

Figure 2-2: CUL9 KO hPSCs normally express key pluripotent genes.

(**A**) CUL9 KO clones have expected global gene expression profile of pluripotent cell lines. Pluritest (Thermo) is a gene expression profile assay. Pluripotency score measures the presence of metagenes within the data set that separate pluripotent samples from non-pluripotent samples. Novelty score measures how well the gene expression pattern of samples fits expected profile. (**B**) RNA isolated from WT and CUL9 KO iPSCs were analyzed by RT-qPCR. Error bars +/- SD. iPSC. n=3. (**C**) CUL9 KO cells express normal protein levels of key pluripotency markers as determined by Western Blotting. Isogenic WT and Clone #1 n=4; Clone #2 n=3; mean +/- SEM; Analysis done using student's t-test, α=0.05. (**D**) Key pluripotency markers are appropriately localized and expressed in CUL9 KO cells. hPSCs were fixed with 4% PFA and stained with key transcription factors NANOG (red, Alexa 546) and OCT4 (purple, Alexa 647), and Hoechst, marking nuclei (blue). Images acquired on Nikon Spinning Disk; 20X objective; scale bar=100 μm.

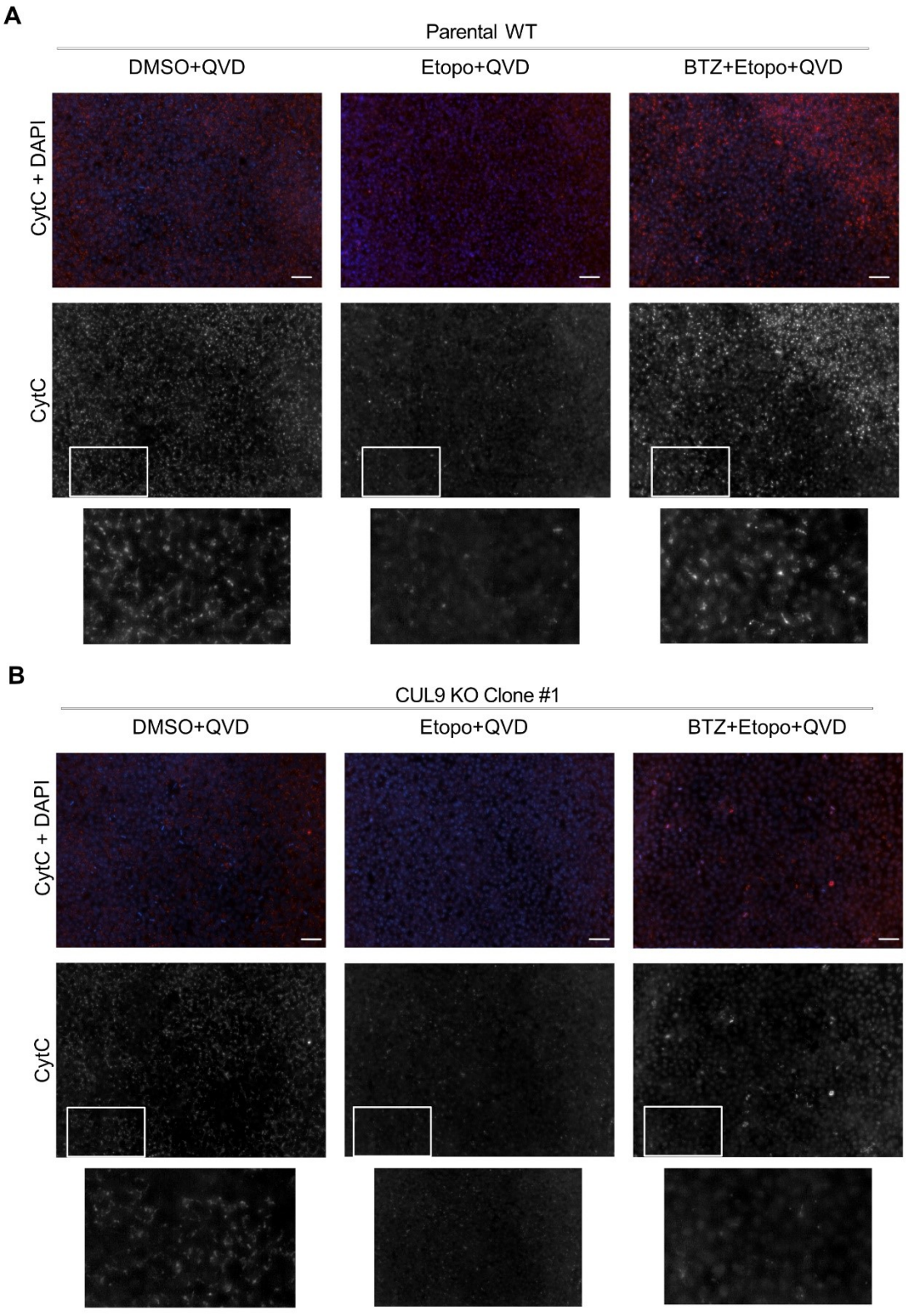
A
Parental WT
DMSO+QVD
Etopo+QVD
BTZ+Etopo+QVD
CytC + DAPI
CytC
B
CUL9 KO Clone #1
DMSO+QVD
Etopo+QVD
BTZ+Etopo+QVD
CytC + DAPI
CytC

Figure 2-3: Deletion of CUL9 does not affect cytochrome c levels after its release from mitochondria during apoptosis.

Isogenic WT (**A**) and CUL9 KO Clone #1 (**B**) were treated with the pan-caspase inhibitor Q-VD-OPh (25μM), the DNA damaging agent etoposide (3 mM), and proteasome inhibitor bortezomib (1mM) or DMSO and collected for analysis at four hours after treatment. Cells were stained with cytochrome c (cyt c) and Hoechst. In DMSO +QVD samples, cyt c is localized to the mitochondria (First panel). Following treatment with etoposide, cyt c is released into the mitochondria (Second panel). Treatment with bortezomib results in accumulation of cyt c (Third panel). levels Boxed areas are enlarged below images, demonstrating the change in cyt c localization. Scale bars=100 mm.

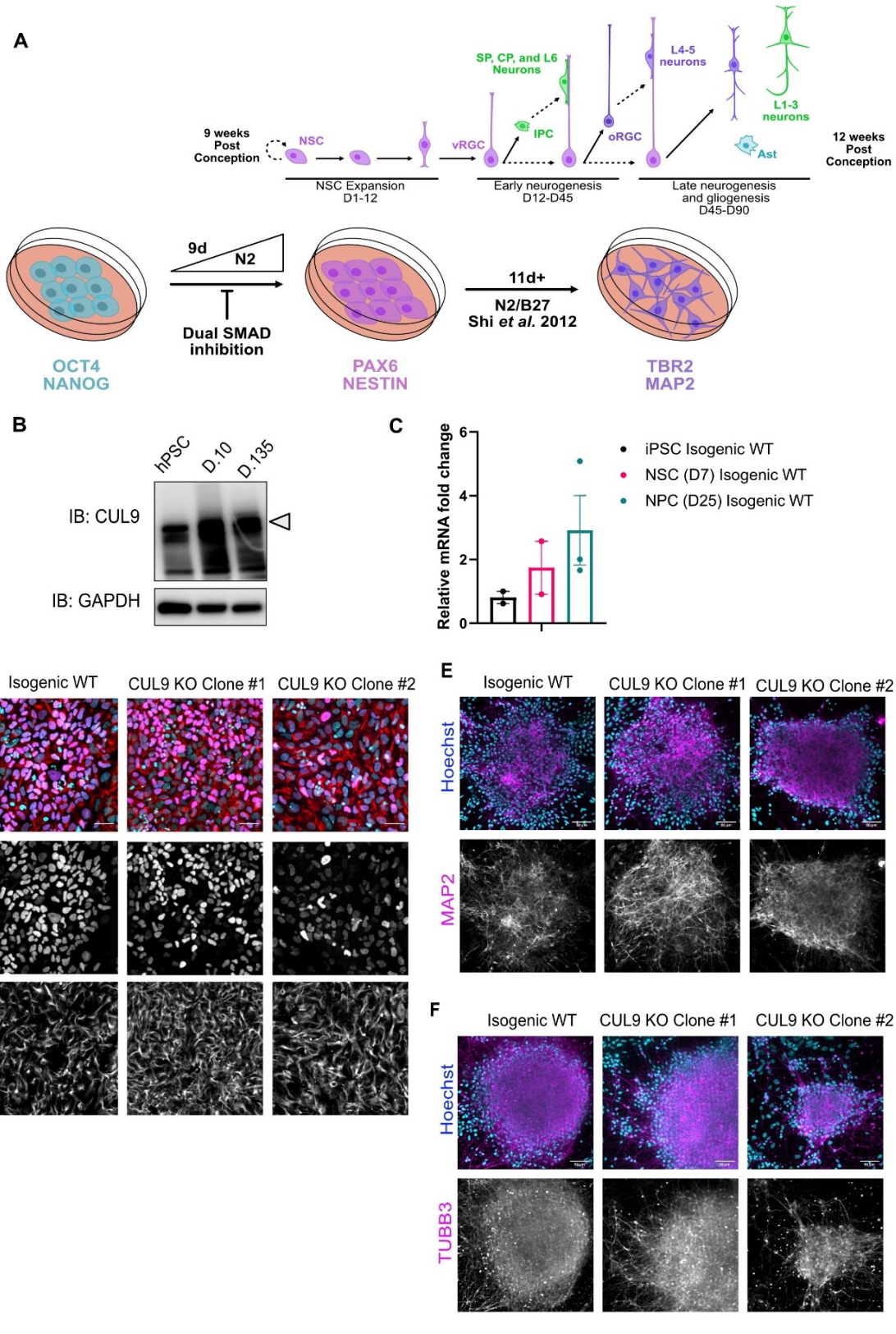
A
9 weeks Post Conception
NSC
vRGC
SP, CP, and L6 Neurons
IPC
oRGC
L4-5 neurons
L1-3 neurons
Ast
12 weeks Post Conception
NSC Expansion D1-12
Early neurogenesis D12-D45
Late neurogenesis and gliogenesis D45-D90
9d
N2
Dual SMAD inhibition
11d+
N2/B27
Shi et al. 2012
OCT4
NANOG
PAX6
NESTIN
TBR2
MAP2
B
hPSC
D.10
D.135
IB: CUL9
IB: GAPDH
C
Relative mRNA fold change
iPSC Isogenic WT
NSC (D7) Isogenic WT
NPC (D25) Isogenic WT
D
Isogenic WT
CUL9 KO Clone #1
CUL9 KO Clone #2
Hoechst
PAX6
NES
E
Isogenic WT
CUL9 KO Clone #1
CUL9 KO Clone #2
Hoechst
MAP2
F
Isogenic WT
CUL9 KO Clone #1
CUL9 KO Clone #2
Hoechst
TUBB3

Figure 2-4: CUL9 KO clones differentiate to hNPCs and early born cortical neurons.
(**A**) Protocol for neuronal differentiation of hPSCs. Diagram above in vitro differentiation roughly correlates in vivo corticogenesis with differentiation protocol. Exact cell population at stages of differentiation often varies between differentiations. NPC=neuroepithelial progenitor cells; PP=preplate; vRGC=ventricular radial glia cells; IPC=intermediate progenitor cells; SP=subplate; CP=cortical plate; oRGC=outer radial glia cells; Ast=astrocyte (**B**) CUL9 protein levels increase over the course of cortical neuron differentiation. Western blot analysis of lysates obtained from WT neurons differentiated for ten days and 135 days show gradual increase in CUL9 protein levels compared to WT hPSCs. APC7 levels increase during initial neuronal induction but remain relatively stable. n=3. (**C**) CUL9 mRNA levels increase over the course of cortical differentiation. RNA isolated from iPSCs, D7 cortical differentiation, and D25 cortical differentiation were analyzed by RT-qPCR. Error bars +/- SD. iPSC and D7 n=2. D25 n=3. Key hNPC (**D**) and neuronal markers (E) are appropriately localized and expressed in CUL9 KO cells. hPSCs were fixed with 4% PFA and stained with key transcription factors NANOG (red, Alexa 546) and OCT4 (purple, Alexa 647), and Hoechst, marking nuclei (blue). Images acquired on Nikon Spinning Disk; 20X objective; scale bar=50 μM. NES=Nestin; TUBB3=Beta-3-tubulin.

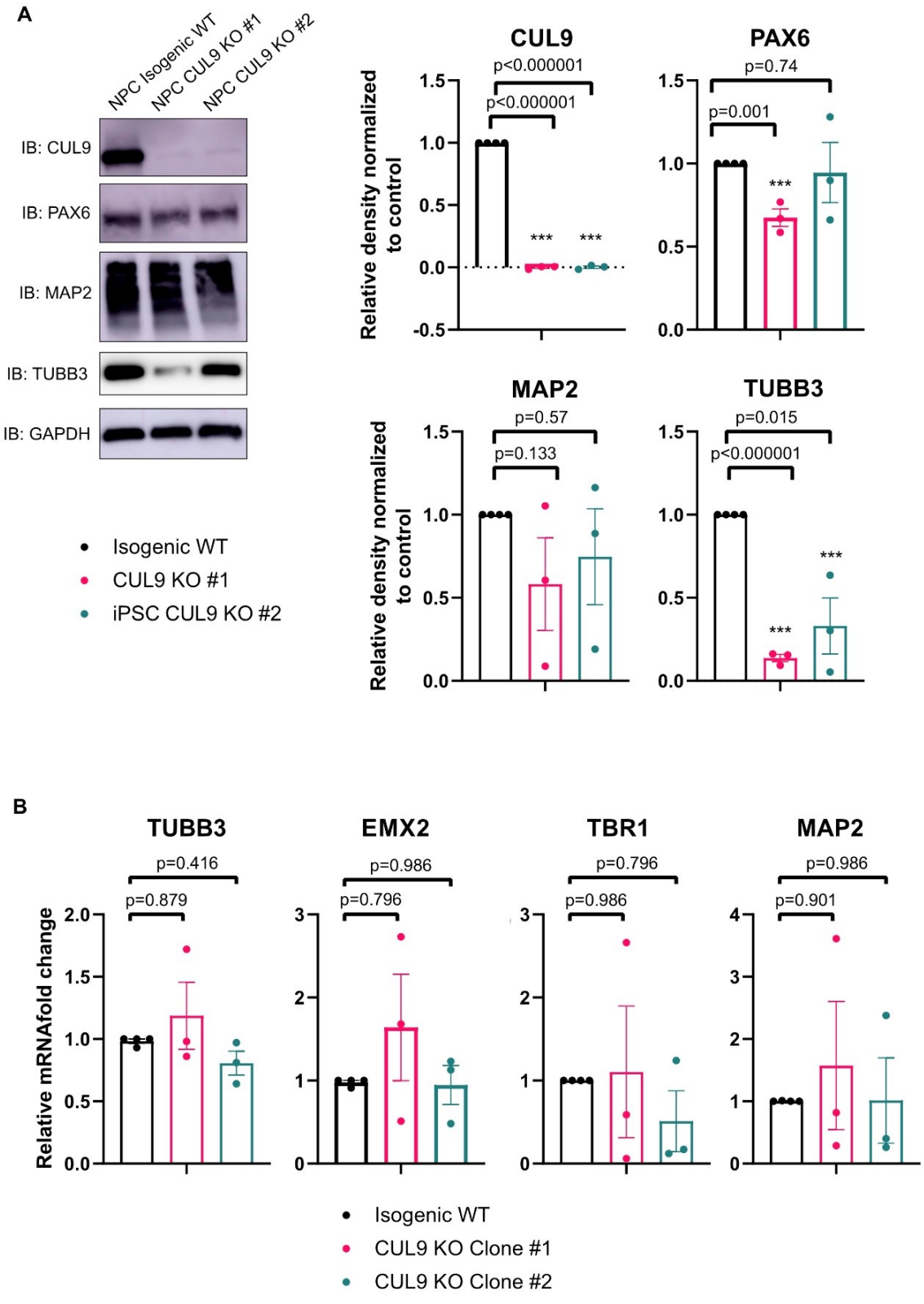
A
NPC Isogenic WT
NPC CUL9 KO #1
NPC CUL9 KO #2
IB: CUL9
IB: PAX6
IB: MAP2
IB: TUBB3
IB: GAPDH
Isogenic WT
CUL9 KO #1
iPSC CUL9 KO #2
CUL9
PAX6
MAP2
TUBB3
Relative density normalized to control
p<0.000001
p<0.000001
p=0.74
p=0.001
p=0.57
p=0.133
p=0.015
p<0.000001
***
B
TUBB3
EMX2
TBR1
MAP2
Relative mRNAfold change
p=0.416
p=0.879
p=0.986
p=0.796
p=0.796
p=0.986
p=0.986
p=0.901
Isogenic WT
CUL9 KO Clone #1
CUL9 KO Clone #2

Figure 2-5: NPCs derived from CUL9 KO NSCs express key markers of neuronal differentiation.

CUL9 KO NPCs were derived by standardized neuronal differentiation methods. NPCs were produced twenty-five days after neuronal differentiation initiated. (**A**) CUL9 KO NPCs do not express CUL9 protein or increased levels of homologue CUL7. Differentiation of hPSCs for 25 days results in increased expression of MAP2 and TUBB3; TUBB3 protein levels are significantly decreased in both clones as determined by Western blotting. Mean +/- SEM; Analysis done using student's t-test, α=0.05. n=3. (**B**) Despite differences in TUBB3 at the protein level, RNA expression of B3TU (TUBB3) is unchanged. Analysis of RNA expression of markers EMX2, TBR1, and MAP2. RNA isolated from WT and CUL9 KO NPCs were analyzed by RT-qPCR. Error bars +/- SEM. iPSC. n=3

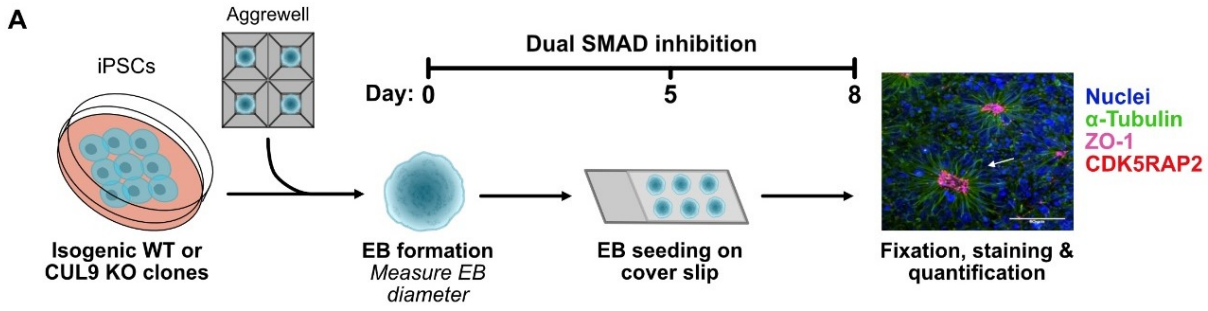
A
Aggrewell
iPSCs
Dual SMAD inhibition
Day: 0
5
8
Nuclei
α-Tubulin
ZO-1
CDK5RAP2
Isogenic WT or CUL9 KO clones
EB formation
Measure EB diameter
EB seeding on cover slip
Fixation, staining & quantification

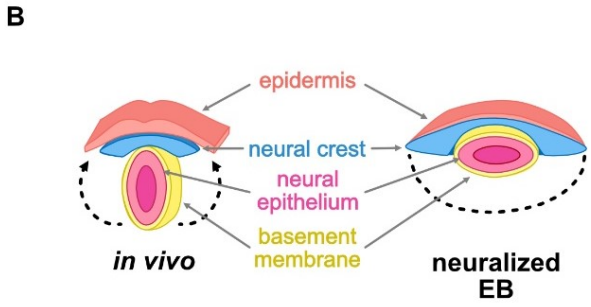
B
epidermis
neural crest
neural epithelium
basement membrane
in vivo
neuralized EB

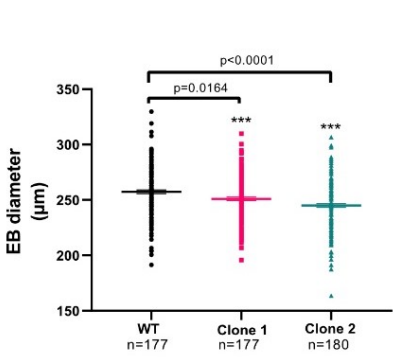
C
p<0.0001
p=0.0164
***
***
EB diameter (µm)
350
300
250
200
150
WT n=177
Clone 1 n=177
Clone 2 n=180

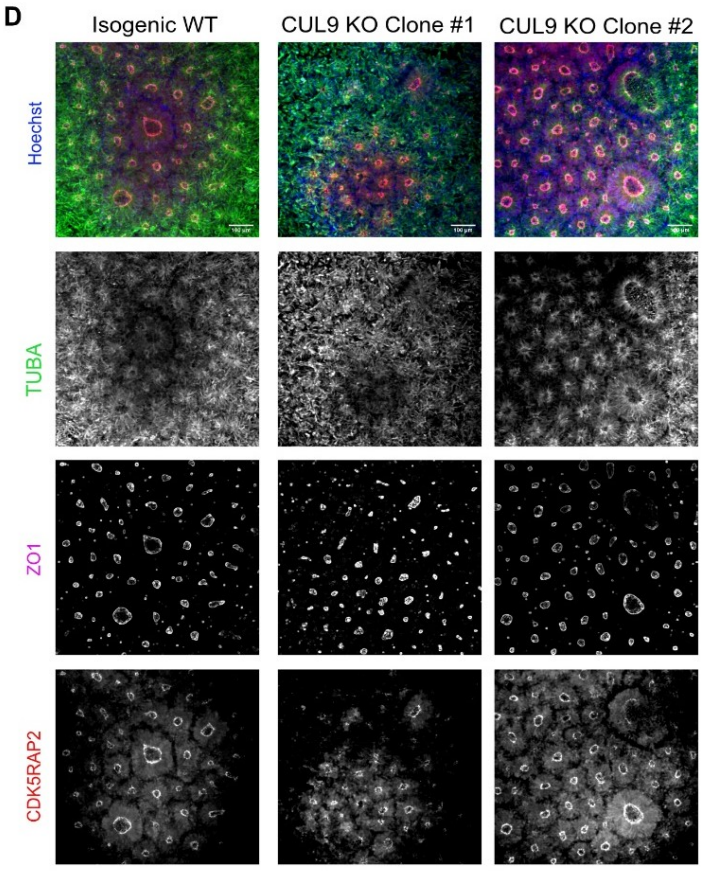
D
Isogenic WT
CUL9 KO Clone #1
CUL9 KO Clone #2
Hoechst
TUBA
ZO1
CDK5RAP2

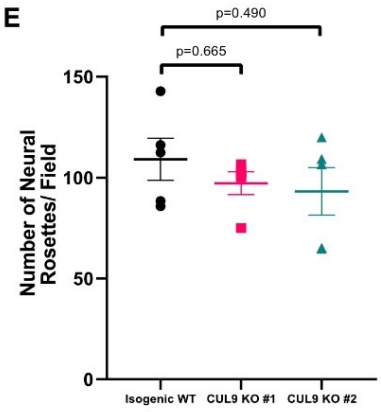
E
p=0.490
p=0.665
Number of Neural Rosettes/ Field
150
100
50
0
Isogenic WT
CUL9 KO #1
CUL9 KO #2

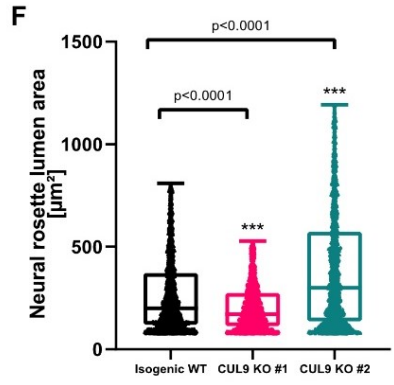
F
p<0.0001
p<0.0001
***
***
Neural rosette lumen area [µm²]
1500
1000
500
0
Isogenic WT
CUL9 KO #1
CUL9 KO #2

Figure 2-6: EBs and neural rosettes derived from CUL9 KO clones display abnormalities. (**A**) Protocol for EB and neural rosette differentiation. (**B**) Comparison of in vivo neural tube and in vitro neural rosette structure. Adapted from Haremaki et al., 2019 (**C**) The diameter of EBs derived from isogenic WT and CUL9 KO hPSCs derived EBs were imaged using an EVOS Inverted Fluorescent Microscope and the diameter of EBs was quantified using ImageJ. Mean and SEM were quantified. n=3, number of EBs quantified in each biological replicated shown. (**D**) Isogenic WT and CUL9 KO EBs derived from hPSCs were differentiated by dual SMAD inhibition. Cells were fixed on day 8 of differentiation and stained for CDK5RAP2 (red), ZO1 (magenta), alpha-tubulin (TUBA, green) and Hoechst (blue). Scale bar=100 μm. 10X objective. (**E**) Graph representing the average number of neural rosettes (NR) formed from a single EB (assumed to be a single field of view). 5 ROI per sample. Mean +/- SEM. P-value determined by one-way ANOVA. n=3. (**F**) Graph representing the average size lumens within NRs rosettes. Thresholding ZO1 staining was used to count number of objects given set parameters. Area of ZO1 was calculated for each object, all lumenal areas per biological replicate were included individually in graph. 5 ROI per sample. P-values determined by one-way ANOVA; outliers removed using ROUT. Median with min to max displayed. n=3.

Supplemental Figures

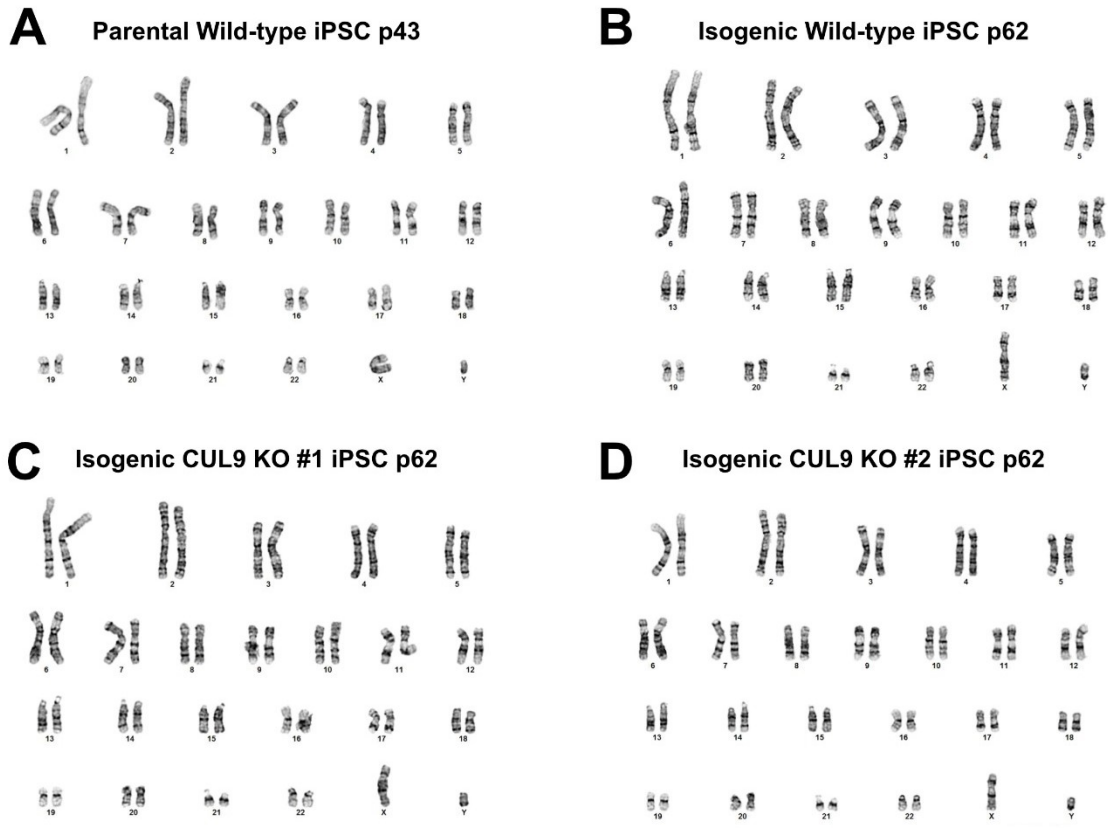

Supplemental Figure 2-1: All cell lines used in this study have normal karyotypes.
Metaphase spread of indicated cell line at indicated passage number displayed. Karyotype analysis was performed by Genomic Associates, Nashville, TN.

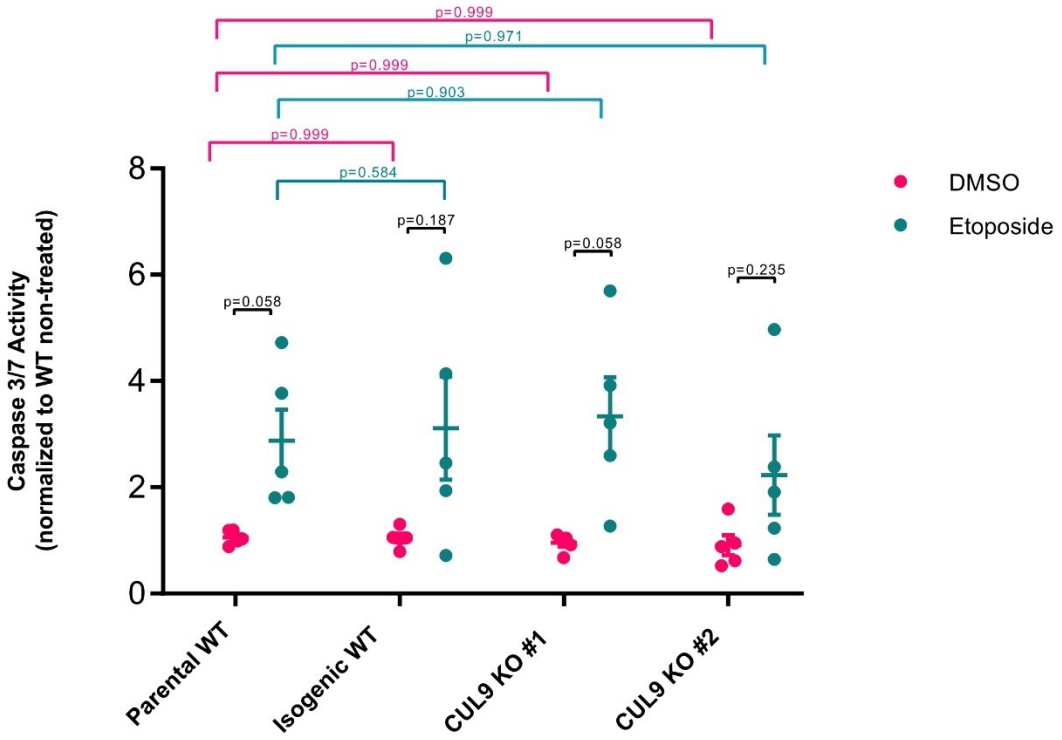

Supplemental Figure 2-2: CUL9 KO and CUL9 depleted cell lines have varied apoptotic resistance at exposure to low levels of DNA damaging agent etoposide.

CUL9 KO cells and control cells were treated with 1 mM etoposide for 3 hours, and caspase 3/7 activity was measured using a CaspaseGlo assay. n=5; +/- SEM; data analyzed using multiple t-tests, α=0.05.

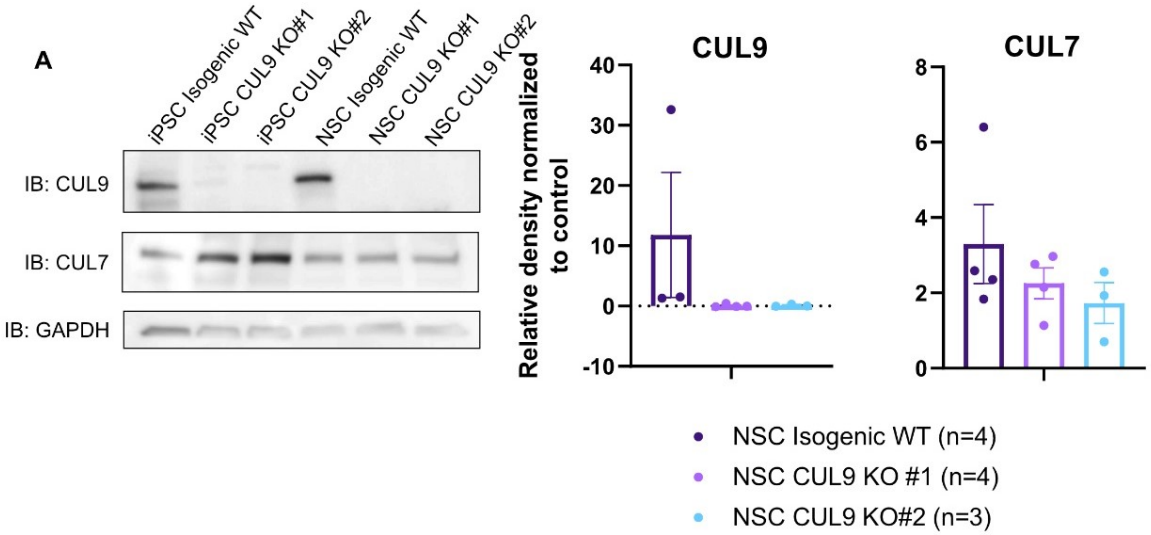
A
iPSC Isogenic WT
iPSC CUL9 KO#1
iPSC CUL9 KO#2
NSC Isogenic WT
NSC CUL9 KO#1
NSC CUL9 KO#2
IB: CUL9
IB: CUL7
IB: GAPDH
CUL9
CUL7
Relative density normalized to control
NSC Isogenic WT (n=4)
NSC CUL9 KO #1 (n=4)
NSC CUL9 KO#2 (n=3)

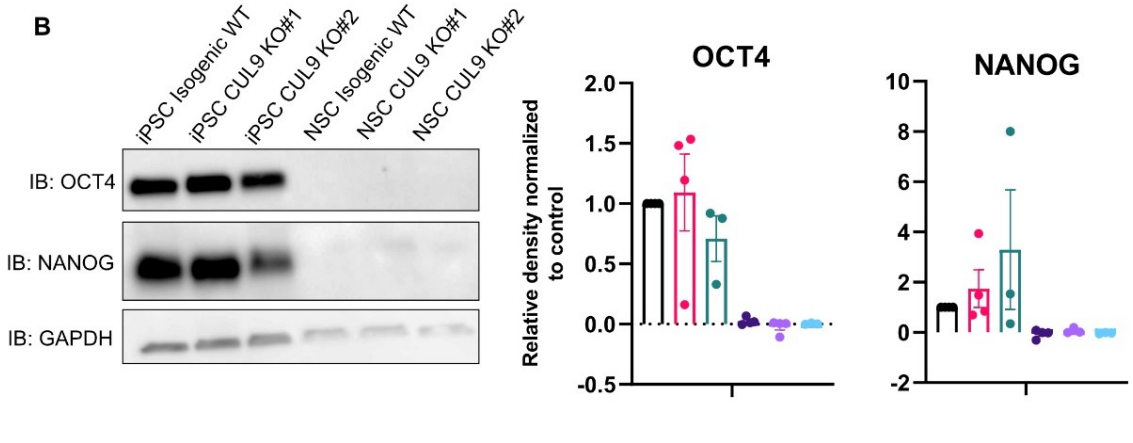
B
iPSC Isogenic WT
iPSC CUL9 KO#1
iPSC CUL9 KO#2
NSC Isogenic WT
NSC CUL9 KO#1
NSC CUL9 KO#2
IB: OCT4
IB: NANOG
IB: GAPDH
OCT4
NANOG
Relative density normalized to control
iPSC Isogenic WT (n=4)
iPSC CUL9 KO Clone #1 (n=4)
iPSC CUL9 KO Clone #2 (n=3)
NSC Isogenic WT (n=4)
NSC CUL9 KO Clone #1 (n=4)
NSC CUL9 KO Clone #2 (n=3)

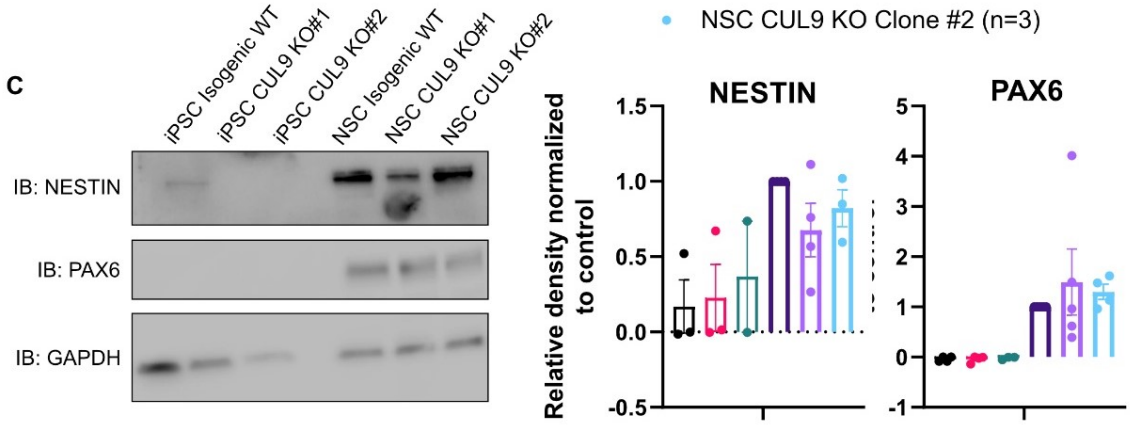
C
iPSC Isogenic WT
iPSC CUL9 KO#1
iPSC CUL9 KO#2
NSC Isogenic WT
NSC CUL9 KO#1
NSC CUL9 KO#2
IB: NESTIN
IB: PAX6
IB: GAPDH
NESTIN
PAX6
Relative density normalized to control

Supplemental Figure 2-3: CUL9 KO cells can differentiate to NSCs.

CUL9 KO NSCs were derived by standardized neuronal differentiation methods. NSCs produced seven days after neuronal differentiation initiated. (**A**) CUL9 KO NSCs do not express CUL9 protein or increased levels of homologue CUL7. Differentiation of CUL9 KO hPSCs for seven days results in loss of pluripotency markers OCT4 and NANOG expression (**B**) as well as increased expression of NSC markers PAX6 and NESTIN (**C**). Isogenic WT and Clone #1 n=4; Clone #2 n=3; mean +/- SEM; Analysis done using student's t-test, α=0.05.

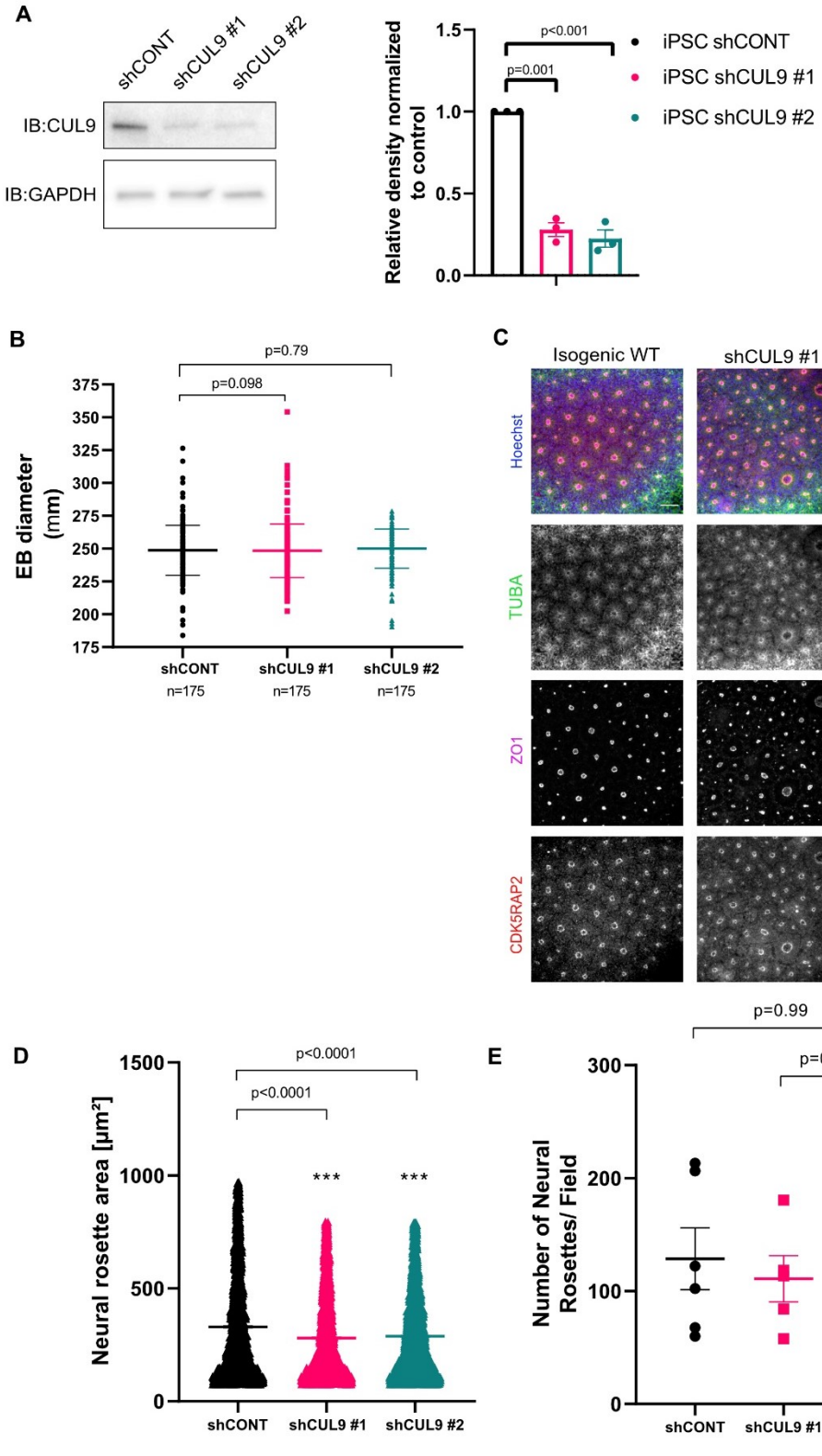
A
shCONT
shCUL9 #1
shCUL9 #2
IB:CUL9
IB:GAPDH
Relative density normalized to control
p<0.001
p=0.001
iPSC shCONT
iPSC shCUL9 #1
iPSC shCUL9 #2
B
EB diameter (mm)
p=0.79
p=0.098
shCONT
shCUL9 #1
shCUL9 #2
n=175
n=175
n=175
C
Isogenic WT
shCUL9 #1
shCUL9 #2
Hoechst
TUBA
ZO1
CDK5RAP2
D
Neural rosette area [µm²]
p<0.0001
p<0.0001
***
***
shCONT
shCUL9 #1
shCUL9 #2
E
Number of Neural Rosettes/ Field
p=0.99
p=0.88
shCONT
shCUL9 #1
shCUL9 #2

Supplemental Figure 2-4: EBs and neural rosettes derived from CUL9 KD clones display abnormalities.

(**A**) CUL9 KO cells express significantly decreased levels of CUL9 protein. Western blot of analysis of control and CUL9 KD clones to analyze CUL9 and CUL7 protein levels. n=3; mean +/- SEM; Analysis done using student's t-test, α=0.05. (**B**) The diameter of EBs derived from isogenic shCONT and shCUL9 hPSC derived EBs were imaged using an EVOS Inverted Fluorescent Microscope and the diameter of EBs was quantified using ImageJ. Mean and SEM were quantified. n=3, number of EBs quantified in each biological replicated shown. (**C**) shCONT and shCUL9 EBs derived from hPSCs were differentiated by dual SMAD inhibition. Cells were fixed on day 8 of differentiation and stained for CDK5RAP2 (red), ZO1 (magenta), alpha-tubulin (TUBA, green) and Hoechst (blue). Scale bar=100 µm. 10X objective. (**D**) Graph representing the average number of neural rosettes (NR) formed from a single EB (assumed to be a single field of view). 5 ROI per sample. Mean +/- SEM. P-value determined by one-way ANOVA. n=3. (**E**) Graph representing the average size lumens within NRs rosettes. Thresholding ZO1 staining was used to count number of objects given set parameters. Area of ZO1 was calculated for each object, all lumenal areas per biological replicate were included individually in graph. 5 ROI per sample. P-values determined by one-way ANOVA; outliers removed using ROUT. Median with min to max displayed. n=3.

Chapter 3

IDENTIFICATION OF A CUL9-APC/C INTERACTION USING LC-MS/MS ANALYSIS

Parts of Chapter 3 have been adapted with permission from Ortolano, N.A., Romero-Morales, A.I., Rasmussen M.L., Bodnya, C., Kline, L.A., Joshi, P., Connelly, J.P., Rose K.L., Pruett-Miller, S., and Gama V. (2021). A proteomics approach for the identification of cullin-9 (CUL9) related signaling pathways in induced pluripotent stem cell models. PLoS One.

Summary

The largest family of E3 ubiquitin ligases, the Cullin RING ligase (CRL) family, are well studied cell cycle regulators. Arguably, one of the best characterized cell cycle regulatory ligases is the non-canonical CRL the anaphase promoting complex/cyclosome (APC/C). However, the other non-canonical CRL, CUL9 remains poorly characterized. In this study, we use hPSCs to identify CUL9 interacting proteins to screen as potential substrates and regulators in pluripotency and neuronal differentiation by LC-MS/MS analysis of CUL9 immunoprecipitation. We demonstrate that CUL9 interacts with subunits of the anaphase promoting complex/cyclosome (APC/C), but CUL9 deletion does not affect protein levels of APC/C subunits or progression of the cell cycle. However, knockdown of APC7 or FZR1 result in a moderate increase in CUL9 protein levels. Further characterization of the biochemical nature and function of this interaction is needed to understand its importance in hPSC pluripotency and differentiation.

Introduction

The cell cycle consists of gap phases separating the S phase, where chromosomes are replicated, and the M phase, where chromosomes are separated and two identical daughter cells are produced by cytokinesis. Cell cycle regulation in somatic cells is well characterized, but investigation of novel mechanisms of modulation in pluripotent stem cells (PSCs) remains an active area of research. PSC cycle length is shorter than that of somatic cells, and the G1 phase is abbreviated (Becker et al., 2006; Boward et al., 2017; Calder et al., 2013; Filipczyk et al., 2007). As PSCs differentiate, the G1 phase gradually lengthens, increasing cell cycle duration (Ponti et al., 2013; Salomoni and Calegari, 2010; Takahashi et al., 1995). While novel cell cycle control mechanisms have been identified in mouse PSCs (Ballabeni et al., 2011; Faast et al., 2004; Li and Kirschner, 2014; Liu et al., 2017b; White et al., 2005; Yang et al., 2011; Zhao et al., 2014), the elucidation of regulatory mechanisms in the hPSC division cycle has been less successful (Neganova et al., 2009; Zhang et al., 2009). Characterization of the novel hPSC cycle and its regulatory mechanisms is necessary, especially due to growing evidence that self-renewal, differentiation, and cell cycle progression are closely tied (Li and Kirschner, 2014; Liu et al., 2017b; Vallier, 2015). However, there has been little insight into the exact signaling events underlying the link between cell cycle progression and pluripotency in hPSCs and NSCs.

Ubiquitination of key substrates is the main driving force of cell cycle. One of the most well characterized E3 ubiquitin ligases propelling cell cycle forward is the APC/C. The APC/C is a 1.6 Mda E3 ubiquitin ligase complex consisting of nineteen subunits composed of fourteen unique proteins. The primary role of the APC/C is to promote progression through G1 and M phases of the cell cycle by targeted ubiquitination and subsequent degradation of cell cycle regulatory proteins known as cyclins (Peters, 2006). APC/C substrate specificity is mediated by its association with two adapter proteins: CDC20 and FZR1 (also known as CDH1). The APC/C targets mitotic cyclins when associated with CDC20, promoting mitotic progression, and G1-cyclins when associated with FZR1, promoting G1 progression. However, the APC/C has also been implicated in coordinating dynamic cell cycle changes, particularly regarding G1 phase, during differentiation (Almeida et al., 2005; Delgado-Esteban et al., 2013; Konishi, 2004; Silies and Klämbt, 2010; Stegmüller et al., 2006). Specifically, APC/C-FZR1 is required for neurogenesis, normal cortical development, and hypothalmus function; aberrant function of APC/C-FZR1 in the brain results in memory and learning deficits (Delgado-Esteban et al., 2013; Li et al., 2008).

The APC/C is composed of several sub-complexes each consisting of a set of subunits with a common function or homology (Sivakumar and Gorbsky, 2015). The catalytic core of the APC/C is composed of the main subunits that recruit required ubiquitination machinery and adapter proteins for substrate recruitment. One member of this complex is APC2, a cullin-like subunit containing a domain with high similarity to the cullin homology domain within CRLs, a family of E3 ubiquitin ligases involved in regulating several key phases of cell cycle (Petroski and Deshaies, 2005; Yu et al., 1998). The “arc-lamp” of the APC/C is the only subcomplex of the APC/C containing subunits with a common domain, the tetratricopeptide repeat (TPR) domain (Chang et al., 2015, 2014). This is the only APC/C sub-complex whose composition is not conserved from yeast. TPR subunit APC7 is only found in vertebrates and thought to be a gene duplication of the TPR subunit APC3 (known as CDC27 in yeast) as their amino acid sequences are highly similar (Thornton et al., 2006).

Recent studies have provided insight into the function of the vertebrate specific APC7 subunit. Knocking out APC7 in human cells is not lethal, and has no affect on mitotic progression, but slightly decreases APC/C ubiquitination efficiency (Wild et al., 2018). Structural and biochemical studies indicate the TPR domain within APC/C subunits interacts with the “IR (isoleucine and arginine) tail” of the FZR1 and CDC20 adapter proteins (Chang et al., 2015; Vodermaier et al., 2003). Research indicates that APC7 preferentially interacts with the IR tail of FZR1, emphasizing its importance in substrate specificity and APC/C ubiquitination activity (Wild et al., 2018). Despite recent progress in characterizing TPR subunits, further characterization of their function, and specifically that of APC7, is needed.

Our results indicate that the poorly characterized CRL family member Cullin-9 (CUL9) interacts with APC7 in hPSCs. Like APC/C, CUL9 is considered a non-canonical CRL since its structure and regulation differ from that of other family members. Interaction and cross regulation between two CRLs is relatively common. In fact, CUL9 dimerizes with another CRL, CUL7. Although the dimerization is not necessary for its function, one study demonstrates CUL7 regulates CUL9 protein levels (Pei et al., 2011; Skaar et al., 2007). Additionally, CUL1 and APC/C regulate one another to promote G1 progression and entry into the S-phase (Vodermaier, 2004). We show evidence that the APC/C and CUL9 may interact to regulate CUL9 protein stability in hPSCs. However, this interaction does not seem to regulate cell cycle as deletion or overexpression of CUL9 in hPSCs does not affect cell cycle progression. Future studies should biochemically validate this interaction and examine how its disruption affects the role of CUL9 and APC/C-FZR1 in neuronal differentiation.

Results

CUL9 interacts with several subunits of the APC/C.

Previous data from our laboratory demonstrated that CUL9 deletion results in aberrant neuronal differentiation (**Chapter 2**). To identify a potential CUL9 function during neuronal differentiation, we set out to identify CUL9 interacting proteins in hPSCs and hNSCs. We performed liquid chromatography tandem mass spectrometry (LC-MS/MS) in cells treated with a proteasome inhibitor (bortezomib) to enrich for potential CUL9 substrates (Figure 4A; Supplementary Figure 8). We identified 24 proteins significantly (1% FDR; Fisher's exact p-value of <0.05) enriched in the hPSC CUL9 immunoprecipitation with a protein probability of 95% or higher in our initial LC-MS/MS analysis (**Table 1**; **Figure 3-1**). We analyzed the direct and indirect interactions amongst our proteins of interest using the Search Tool for the Retrieval of Interacting Genes/Proteins (STRING) (Franceschini et al., 2012, 2016; Jensen et al., 2009; von Mering, 2004; Snel, 2000; Szklarczyk et al., 2011, 2015, 2017, 2019). STRING is a database containing protein-protein interactions. These include direct binding as well as indirect interactions including shared functions or common signaling pathways. Analysis of our dataset showed a group of protein interactions involved in transcriptional regulation and cell cycle regulation (**Figure 3-1B**). Considering the prevalent role of other CRLs in cell cycle regulation, we took a closer look at the interacting proteins involved in cell cycle progression (Craney and Rape, 2013). All the interacting proteins involved in cell cycle regulation, barring CUL7, were subunits of the APC/C. These were the only identified proteins in the CUL9 immunoprecipitation from hNPC lysates (**Table 2**). A majority of the most enriched subunits in both hPSCs and hNSCs contained the tetratricopeptide repeat (TPR) domain, the only domain shared by multiple subunits within the APC/C (**Tables 1 and 2**; **Figure 3-1B**). Considering the enrichment of TPR lobe subcomplex proteins in our LC-MS/MS data, we focused our efforts on determining if CUL9 regulates the TPR-containing subunits. The most significantly and consistently enriched protein in all replicates of LC-MS/MS analysis was a component of the APC/C known as APC7 (**Figure 3-1B**; **Supplemental Figure 3-1A**). APC7 is solvent exposed, making it available for CUL9 binding. Additionally, APC7 is only expressed in vertebrates, just like CUL9 making it an attractive LC-MS/MS hit for downstream analysis. We validated the CUL9-APC7 interaction by co-immunoprecipitation in hPSCs and hNSCs (**Figure 3-1C-D**).

CUL9 deletion does not alter APC/C subunit levels or cell cycle profile

To determine if APC/C subunits were possibly targeted by CUL9 for ubiquitin mediated degradation, we examined if APC7 protein levels were enriched in CUL9 KO cells. Protein levels of APC7 were not significantly changed in either CUL9 KO clone as determined by Western blotting (**Figure 3-2**). We suspected that if CUL9 regulates APC7 or is involved in cell cycle progression, it may do so in a specific phase of the cycle. We synchronized WT and KO cells in mitosis by treating the cells with the microtubule destabilizing drug nocodazole at 100ng/mL for 16 hours. Then, we washed the drug off, collecting lysates every two hours for 12 hours to analyze protein expression as cell cycle progressed (Yiangou et al., 2019). Cyclin E and FZR1 were used to validate synchronization and determine what phase of cell cycle the cells were in at the time of collection. We used FZR1 peaks and Cyclin E as phase specific markers. Cyclin E levels gradually increase towards the end of G1-phase, peaking at S phase (Bloom and Cross, 2007). FZR1 levels peak at the end of mitosis, peak at early G1 phase, and are finally depleted as cells exit G1 and enter S-phase (Pines, 2011). CUL9 protein levels did not fluctuate significantly during cell cycle as previously reported (**Figure 3-2**)(Li et al., 2014; Yan et al., 2014). Additionally, expression of key phase specific proteins fluctuate as expected in CUL9 KO cells indicating that cell cycle progression is likely unaltered (**Figure 3-3**).

While ubiquitination canonically promotes proteasomal degradation of substrates, it can also result in a change in protein-protein interactions or protein localization and function. Based on our results, we postulated that CUL9 ubiquitination or interaction with the APC/C may play a role outside of protein stability. To determine if CUL9 affected APC/C function in cell cycle, we determined the cell cycle profile of CUL9 KO cells using flow cytometry analysis of DNA content. However, we did not see significant differences between control cells and CUL9 KO cells (**Figure 3-4A**). Together, these results suggest that CUL9 does not regulate a specific phase of cell cycle.

CUL9 protein levels increase when TPR subunit APC7 and adapter protein FZR1 are depleted

Since CUL9 does not appear to regulate the APC/C, we tested if APC/C regulates CUL9 stability. We noticed a moderate, but significant, increase in CUL9 protein levels when APC7 was depleted in hPSCs (**Figure 3-2B**). Since previous research reported that TPR domain subunits of the APC/C play an important role in recruitment of APC/C adapter proteins, we sought to determine if CUL9 protein levels were affected by inhibition of adapter protein recruitment (Vodermaier et al., 2003). Both APC/C-FZR1 and CDC20 recognize substrates by specific

degrons. One such degron is the D box motif. Canonical APC/C substrates like cyclin B and cyclin A contain D box motifs (Glotzer et al., 1991; He et al., 2013). We used the APC/C degron repository resource created through a collaboration between the Davey laboratory at The Institute of Cancer Research and the Morgan laboratory at the University of California, San Francisco to analyze the CUL9 protein sequence for potential APC/C degrons. The APC/C degron prediction tool employs ProViz to scan a protein of interest for regions like previously characterized degrons (Jehl et al., 2016). This resource identified a potential D-box motif sequence with a high consensus similarity to known motifs (RxxL) (TTRTILMMLLNR, amino acids 912-923) (Similarity score=0.83). This motif was also highly disordered (Disorder score=0.47), a common feature of degrons (Potenza et al., 2015; Wright and Dyson, 2015).

Since both APC/C complexes can recognize the D-box degron, we tested if inhibition of CDC20 or FZR1 association would affect CUL9 protein levels. We first investigated if chemical inhibition of APC/C-CDC20 affected CUL9 protein levels. To inhibit APC/C-CDC20, we treated the cells with two chemical inhibitors: ProTAME (tosyl-L-arginine methyl ester) and apcin (APC/C inhibitor). ProTAME blocks the APC/C-CDC20 interaction, and apcin binds to CDC20 and competitively inhibits ubiquitination of APC/C-CDC20 specific substrates (Sackton et al., 2014). Although we saw a consistent increase in the APC/C-CDC20 substrate Cyclin A2, CUL9 protein levels remained the same (**Figure 3-2C**). However, when we depleted FZR1 protein levels using siRNA, we saw a small, but significant increase in CUL9 protein levels that coincided with those observed in APC7 depleted cells (**Figure 3-2D**).

Considering depletion of APC7 or FZR1 results in increased CUL9 protein levels, we hypothesized that CUL9 overexpression would affect cell cycle progression. To test our hypothesis, we stably overexpressed FLAG tagged CUL9 using a CUL9-FLAG lentiviral construct. CUL9 was expressed 10-fold higher than in wild-type hPSCs (**Figure 3-4B**). We performed DNA content analysis by flow cytometry and determined that cells stably overexpressing CUL9 had a normal cell cycle profile as observed in the CUL9 KO cells (**Figure 3-4C**). This indicates that if CUL9 protein levels are negatively regulated by APC/C, it is likely independent of cell cycle progression.

Discussion

Our data showed CUL9 almost exclusively co-immunoprecipitated with APC/C subunits, specifically TPR subunits in hPSCs and differentiated NSCs. The most enriched subunit in our analysis was APC7. Like CUL9, APC7 is also a late evolutionary gene that is only present in vertebrates. Its function has been similarly elusive, as APC7 KO cells are viable with minimal observed phenotypes (Wild et al., 2018). Further characterization of the function of the CUL9-APC/C interaction could provide insight into the specific functions of both proteins. While APC7 KO cells do not show changes in cell cycle profile, they do show a slight decrease in ubiquitination of APC/C-FZR1 substrates which correlates with the small, but significant, increase we see in CUL9 protein levels (Vodermaier et al., 2003; Wild et al., 2018). Previous studies have demonstrated that APC7 preferentially binds to the IR-tail at the C-terminus of the FZR1 adapter protein explaining its relationship to APC/C-FZR1 ubiquitination activity (Vodermaier et al., 2003; Yamaguchi et al., 2015).

Depletion of APC7 and FZR1 both resulted in a small but significant increase in CUL9 protein levels. It is tempting to speculate that CUL9 is ubiquitinated by APC/C-FZR1 for proteasomal degradation, especially considering that CUL9 possesses a predicted APC/C degron. However, our methods do not directly test this hypothesis. An important first step would be validating the predicted D-box motif in CUL9. This could be done either by site directed mutations or in *vitro* experiments demonstrating direct binding and ubiquitination of CUL9 by APC/C-FZR1. CUL9 is a large protein (282 kDa) making its isolation or synthesis challenging. Additionally, the requirements for CUL9 activity and confirmation are not known. For example, the APC/C has many phosphorylation sites required for its activation (Qiao et al., 2016; Zhang et al., 2016). Without an understanding of CUL9 structure and regulation by post-translational modifications such as NEDD8, *in vitro* studies and site directed mutations could be difficult to interpret. A basic understanding of the biochemical properties of CUL9 are needed to truly characterize its regulation or function.

If we can produce recombinant CUL9, however, we could perform *in vitro* ubiquitination assays to determine if CUL9 is a substrate of APC/C-FZR1 – we could also isolate flag tagged CUL9 from our stable CUL9 overexpressing cells. We used immunoprecipitated FLAG-CUL9 to test its ability to ubiquitinate cytochrome c. Validated protocols to isolate APC/C-CDC20 could be modified to isolate APC/C-FZR1 (Qiao et al., 2016). Briefly, APC/C-FZR1 would be isolated from hPSCs synchronized in G1 phase using APC3-antibody cross-linked beads. Then, the elution would be re-immunoprecipitated using FZR1 antibody-coupled beads. Isolated APC/C-FZR1 and

recombinant/immunoprecipitated FLAG-CUL9 would be combined *in vitro* with recombinant E2, E1, ATP, and ubiquitin. Aliquots of the *in vitro* reaction would be collected and analyzed by immunoblotting for ubiquitin and CUL9. This experiment would determine if CUL9 is a substrate of APC/C, or if the interaction exists for another purpose.

The increase in CUL9 protein levels upon APC/C inactivation, though significant, are small. Additionally, increase or decrease in CUL9 protein levels do not affect cell cycle progression. We hypothesize that if APC/C-FZR1 targets CUL9 for proteasomal degradation it is likely specific to a phase of cell cycle and affects another process. This hypothesis is also supported by the CUL9-APC7 co-immunoprecipitation. Only a small amount of total endogenous CUL9 protein co-immunoprecipitate with APC7. If this interaction only occurs at a certain stage of cell cycle, not all cells in an asynchronous population would have the interaction at the time of sample collection. APC/C regulation is highly spatiotemporal, so a phase specific interaction is plausible. However, CUL9 protein levels do not fluctuate during cell cycle as we demonstrated, so if the interaction is phase specific it may be modulated by post-translational modification rather than by oscillations in protein levels of either protein. The APC/C has over 100 identified substrates, and is predicted to have nearly double as many. These substrates are involved in processes ranging from apoptosis to metabolism. For example, APC/C-FZR1 is active during G2 phase where it regulates DNA damage response rather than cell cycle (Bassermann et al., 2008). Future studies should address differential CUL9 regulation both throughout cell cycle and in different cell types. These studies could reveal novel CUL9 functions.

Analysis of this interaction and its role in neuronal differentiation deserves further exploration. Although we validated this interaction by LC-MS/MS and Western blot analysis of endogenous immunoprecipitation of CUL9 in neural stem cells, we did not perform further analysis. However, we have shown evidence that CUL9 deletion affects early neuronal differentiation, specifically neural rosette formation (**Chapter 1**). APC/C-FZR1 has a known role in neurodevelopment so this interaction could be important for neuronal differentiation (Almeida et al., 2005; Delgado-Esteban et al., 2013; Konishi, 2004; Li et al., 2008; Silies and Klämbt, 2010; Stegmüller et al., 2006). Interestingly, CUL9 and FZR1 levels increase during neuronal differentiation, but APC7 levels decrease (van de Leemput et al., 2014). Whether CUL9 protein levels increase following FZR1 and/or APC7 depletion or vice versa should be validated. This interaction and its outcomes could be dynamic as the protein levels change during differentiation. Additionally, deletion of FZR1 in the brain of mice does not produce an observable phenotype, but causes cognitive defects (Kuczera et al., 2011; Li et al., 2008). Further behavioral analysis of the phenotypically normal

CUL9 and APC7 KO mice should be done to determine if these mice have the same cognitive defects.

The exact role of CUL9 in stem cells remains unclear. While our results identify a novel interaction between CUL9 and the APC/C, the purpose of this interaction and potential regulation are impossible to interpret or explore without further characterization of CUL9. Identification of CUL9 adapter proteins is necessary to identify substrates and determine CUL9 function. Differences in CUL9 function between cell types may be a contributing factor to the historically challenging nature of identifying CUL9 adapters and substrates. Other CUL9 associated proteins identified by our mass spectrometric analysis of the endogenous CUL9 immunoprecipitation should be investigated as well. Most of these proteins are involved in transcriptional regulation. Some, like DDX39A, DDX3X, and DHX9, contain are DEAD box helicases which unwind RNA duplexes and regulate RNA processing and metabolism (Linder and Jankowsky, 2011; Song and Ji, 2019). Validation of these potential substrates could reveal a role for CUL9 in transcriptional regulation in early development. We hope that the CUL9 KO hPSC line we have created will be a useful tool in studying CUL9 function during differentiation to a variety of cell types. Once we identify true CUL9 substrates in hPSCs using biochemical and proteomics techniques the purpose of the CUL9-APC/C interaction and its potential role in CUL9 regulation could be better characterized.

Figures

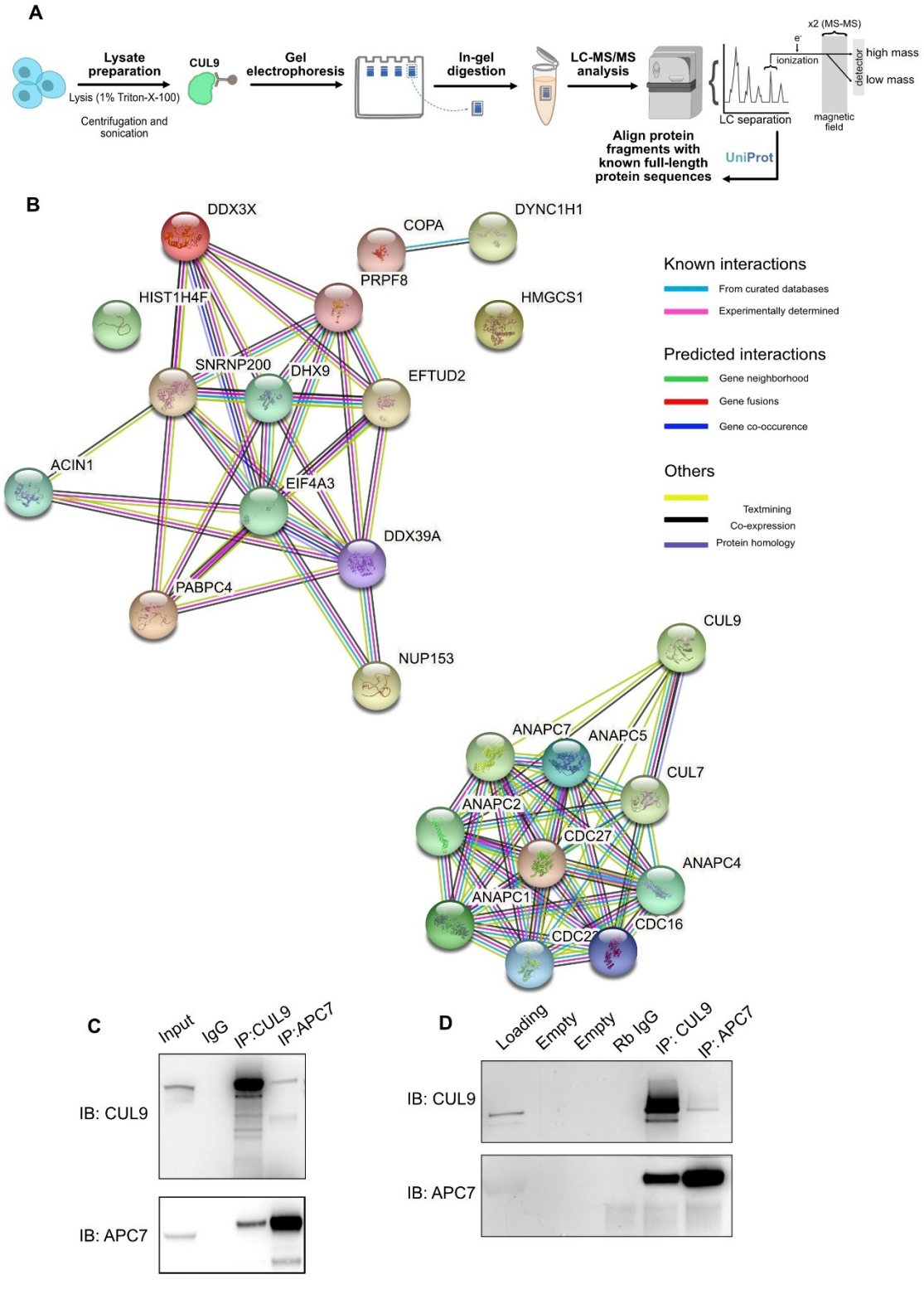
A
Lysate preparation
Lysis (1% Triton-X-100)
Centrifugation and sonication
CUL9
Gel electrophoresis
In-gel digestion
LC-MS/MS analysis
x2 (MS-MS)
ionization
high mass
low mass
detector
LC separation
magnetic field
Align protein fragments with known full-length protein sequences
UniProt
B
DDX3X
COPA
DYNC1H1
PRPF8
HIST1H4F
HMGCS1
SNRNP200
DHX9
EFTUD2
ACIN1
EIF4A3
DDX39A
PABPC4
NUP153
Known interactions
From curated databases
Experimentally determined
Predicted interactions
Gene neighborhood
Gene fusions
Gene co-occurence
Others
Textmining
Co-expression
Protein homology
CUL9
ANAPC7
ANAPC5
CUL7
ANAPC2
CDC27
ANAPC4
ANAPC1
CDC16
C
Input
IgG
IP:CUL9
IP:APC7
IB: CUL9
IB: APC7
D
Loading
Empty
Empty
Rb IgG
IP: CUL9
IP: APC7
IB: CUL9
IB: APC7

Figure 3-1: CUL9 interacts with several subunits of the APC/C.

(**A**) Workflow for LC-MS/MS analysis of endogenous CUL9 immunoprecipitation from hPSC lysates. (**B**) Results from query using Search Tool for the retrieval of Interacting Genes/Proteins (STRING) (Franceschini et al., 2012, 2016; Jensen et al., 2009; Mering, 2003; von Mering, 2004; Snel, 2000; Szklarczyk et al., 2011, 2015, 2017, 2019). Diagram depicts known and predicted direct and indirect protein-protein interactions amongst the significant proteins identified in the endogenous CUL9 immunoprecipitation. Significance of proteins determined by Fisher's exact test. Colored nodes represent queried proteins and the first shell of interactors. Clear nodes indicate second shell of interactors. Filled nodes show known, partial, or predicted structure. Empty nodes indicate structure information is not available for the given protein. All hits were statistically significant in one replicate (Fisher's exact test, a=0.05) and validated in at least two replicates. The CUL9 and APC7 interaction was validated by co-immunoprecipitation in hPSCs (**C**) and hNSCs (**D**). Input is 1.5% (30 μg) of total lysate used in immunoprecipitation (2mg); n=2.

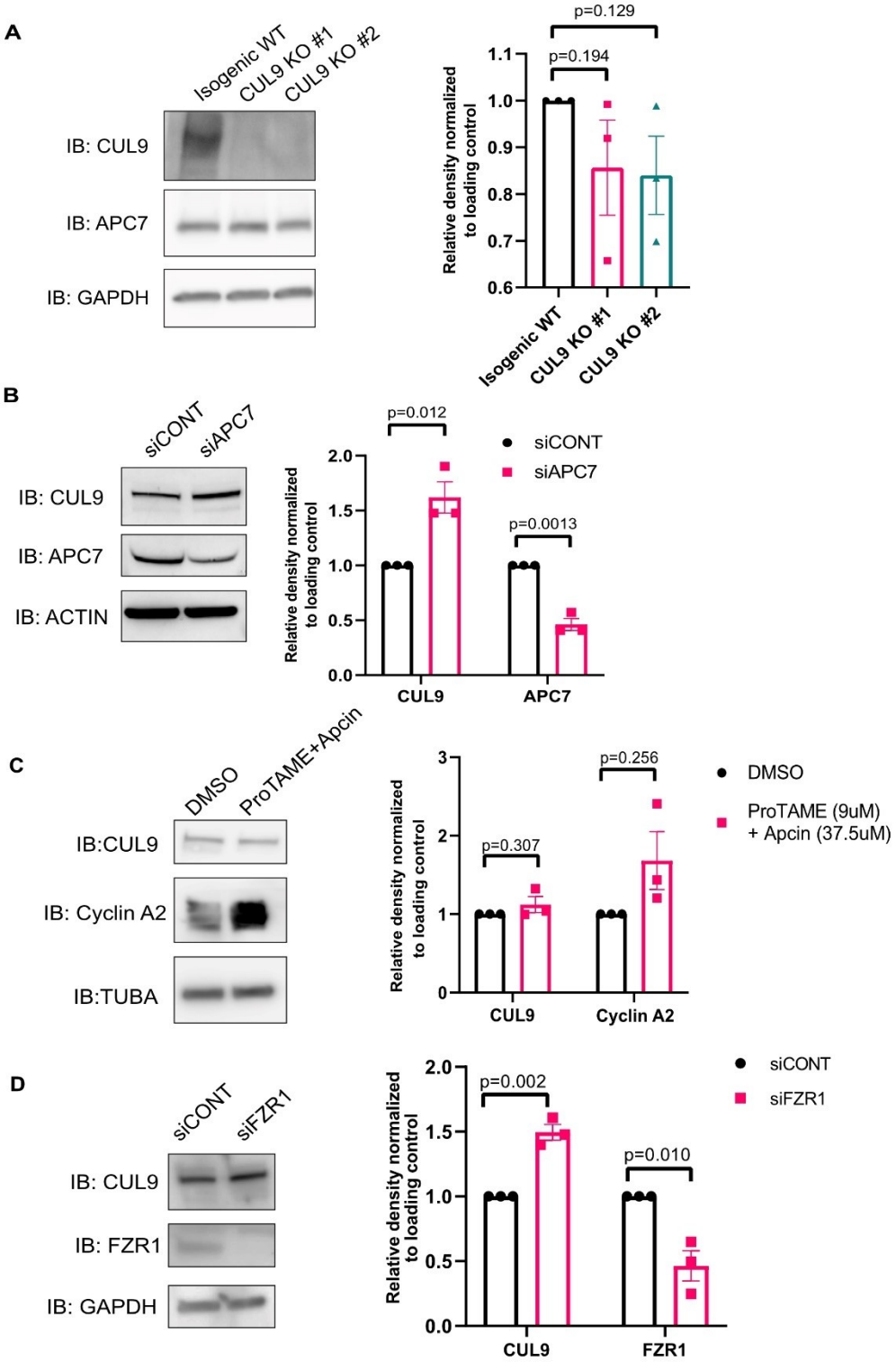
A
Isogenic WT
CUL9 KO #1
CUL9 KO #2
IB: CUL9
IB: APC7
IB: GAPDH
p=0.129
p=0.194
Relative density normalized to loading control
1.1
1.0
0.9
0.8
0.7
0.6
Isogenic WT
CUL9 KO #1
CUL9 KO #2
B
siCONT
siAPC7
IB: CUL9
IB: APC7
IB: ACTIN
p=0.012
p=0.0013
siCONT
siAPC7
Relative density normalized to loading control
2.0
1.5
1.0
0.5
0.0
CUL9
APC7
C
DMSO
ProTAME+Apcin
IB:CUL9
IB: Cyclin A2
IB:TUBA
p=0.307
p=0.256
DMSO
ProTAME (9uM)
+ Apcin (37.5uM)
Relative density normalized to loading control
3
2
1
0
CUL9
Cyclin A2
D
siCONT
siFZR1
IB: CUL9
IB: FZR1
IB: GAPDH
p=0.002
p=0.010
siCONT
siFZR1
Relative density normalized to loading control
2.0
1.5
1.0
0.5
0.0
CUL9
FZR1

Figure 3-2: CUL9 protein levels are altered by depletion of APC/C subunits in hPSCs
(**A**) CUL9 KO clones have equivalent protein levels of APC7 and FZR1 to control cells as determined by Western blotting. n=3; mean +/- SEM; Analysis done using student's t-test, α=0.05. Depletion of APC7 results in increased CUL9 levels in hPSCs (n=3) (**B**). Downregulation of APC7 results in significantly increased CUL9 levels as determined by Western blotting. mean +/- SEM; Analysis done using student's t-test, α=0.05. (**C**) Chemical inhibition of APC/C-CDC20 does not affect CUL9 protein levels. Cells were treated with either DMSO or both 9uM ProTAME (Tocris) and 37.5 uM Apcin (Tocris) for 24 hours. While APC/C-CDC20 substrate cyclin A2 is consistently increased in treated cells, CUL9 levels are unchanged. Analysis done using student's t-test, α=0.05 n=3. (**D**) siRNA mediated knockdown of FZR1 shows significant increase in CUL9 protein levels as determined by Western blotting. n=3; mean +/- SEM; Analysis done using student's t-test, α=0.05.

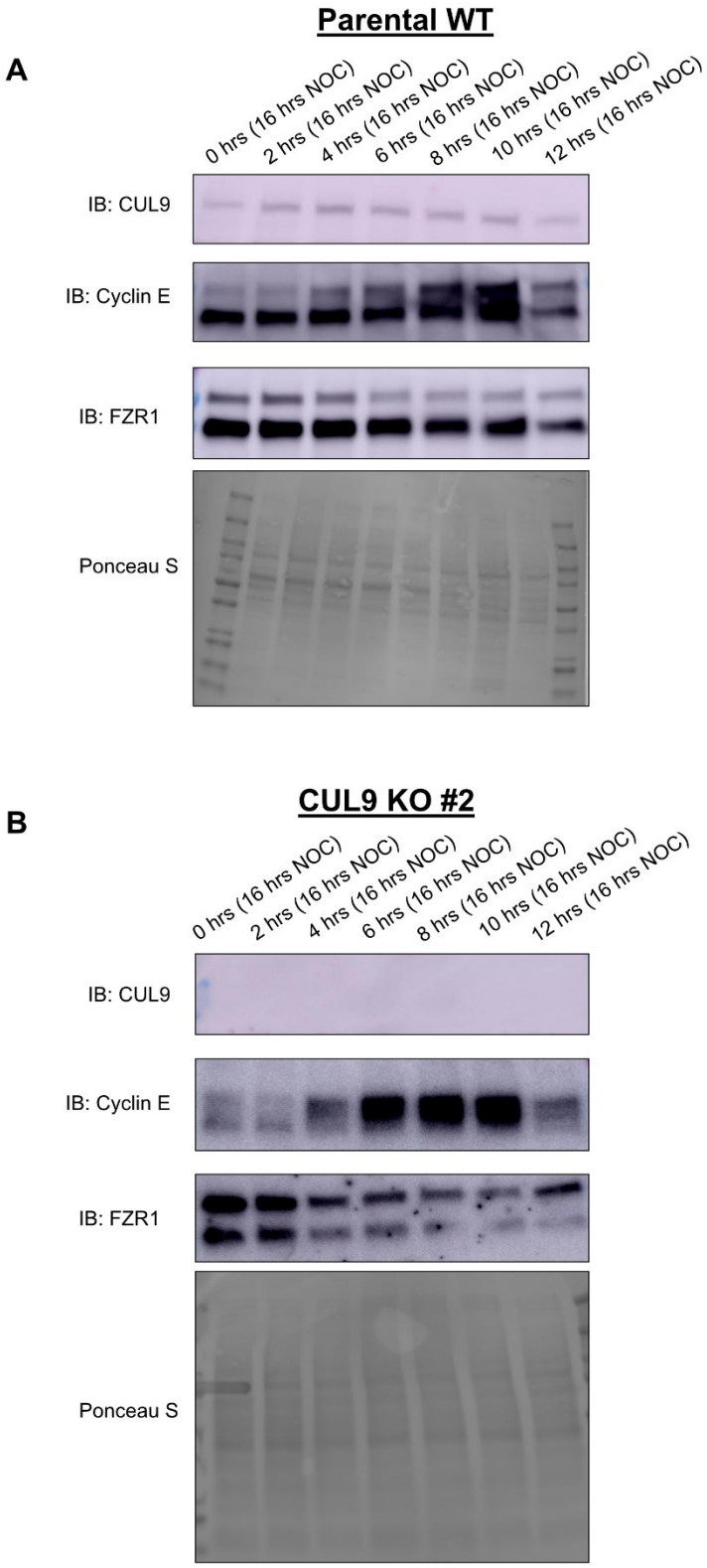
A
Parental WT
0 hrs (16 hrs NOC)
2 hrs (16 hrs NOC)
4 hrs (16 hrs NOC)
6 hrs (16 hrs NOC)
8 hrs (16 hrs NOC)
10 hrs (16 hrs NOC)
12 hrs (16 hrs NOC)
IB: CUL9
IB: Cyclin E
IB: FZR1
Ponceau S
B
CUL9 KO #2
0 hrs (16 hrs NOC)
2 hrs (16 hrs NOC)
4 hrs (16 hrs NOC)
6 hrs (16 hrs NOC)
8 hrs (16 hrs NOC)
10 hrs (16 hrs NOC)
12 hrs (16 hrs NOC)
IB: CUL9
IB: Cyclin E
IB: FZR1
Ponceau S

Figure 3-3: CUL9 levels do not significantly fluctuate during cell cycle progression.
Cell cycle synchronization was performed as described in (Yiangou et al., 2019). Briefly, hPSCs were treated with 100 ng/mL uM of nocodazole for 16 hours. Lysates were collected every 2 hours after release for 12 hours then analyzed by Western blot. Cyclin E and FZR1 were used to validate synchronization. FZR1 peaks at G1 phase and Cyclin E at S phase. Ponceau S staining before blotting was used for loading. (**A**) CUL9 protein levels remain constant despite changes in Cyclin E and FZR1 protein levels. n=3 (**B**) Cyclin E and FZR1 protein levels still fluctuate as expected during cell cycle progression in CUL9 KO cells. n=3.

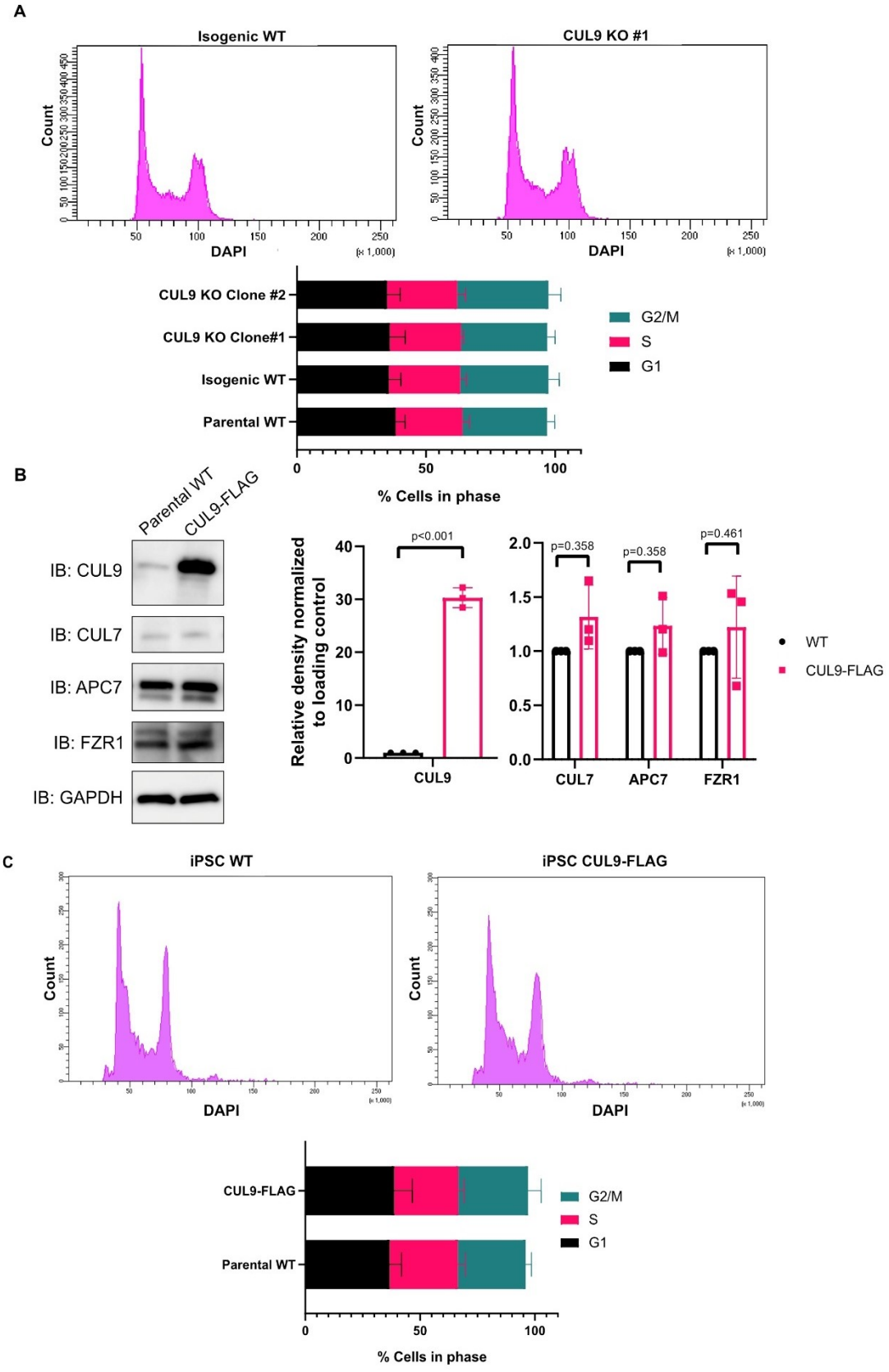
A
Isogenic WT
CUL9 KO #1
Count
DAPI
(× 1,000)
CUL9 KO Clone #2
CUL9 KO Clone#1
Isogenic WT
Parental WT
G2/M
S
G1
% Cells in phase
B
Parental WT
CUL9-FLAG
IB: CUL9
IB: CUL7
IB: APC7
IB: FZR1
IB: GAPDH
Relative density normalized to loading control
p<0.001
p=0.358
p=0.358
p=0.461
CUL9
CUL7
APC7
FZR1
WT
CUL9-FLAG
C
iPSC WT
iPSC CUL9-FLAG
Count
DAPI
CUL9-FLAG
Parental WT
G2/M
S
G1
% Cells in phase

Figure 3-4: CUL9 does not regulate cell cycle progression in hPSCs.
(**A**) CUL9 KO cells have a normal cell cycle profile. DNA content analysis by flow cytometry was done on CUL9 KO cells and control cells. Cell phases were determined by DNA content. <50 A.U. Pacific Blue, or <1N =sub-g1; 50-60 A.U Pacific blue, 1N, G1; 60-90 A.U. Pacific blue, 1<N<2, S; 90-120 A.U. Pacific blue, 2N, G2/M; >120 A.U. Pacific blue, >2N, Polyploidy. n=3; mean +/- SD. (**B**) Lentiviral stable CUL9-FLAG overexpression line shows 30-fold increase in CUL9 protein levels, but no changes in APC7 or FZR1 levels as determined by Western blotting. n=3; mean +/- SEM; Analysis done using student's t-test, α=0.05. (**C**) CUL9-FLAG expressing cells have normal cell cycle profile. DNA content analysis by flow cytometry was done on CUL9-FLAG expressing cell line and control cell line. Cell phases were determined by DNA content as described in A. n=3; mean +/- SD.

Tables

Accesion Number	Protein name	Total spectral counts IP:CUL9	Total spectral counts IgG	% Coverage IP:CUL9	% Coverage IgG	Fisher's Exact Test (p-value)	# of replicates
O75643	U5 small nuclear ribonucleoprotein 200 kDa helicase	38	14	25	9.3	0.009	2
Q08211	ATP-dependent RNA helicase A	34	15	31	16	0.044	3
Q9UJX3	Anaphase-promoting complex subunit 7	40	0	60	0	<0.0001	4
Q8IWT3	Cullin-9	29	0	17	0	<0.0001	4
Q9H1A4	Anaphase-promoting complex subunit 1	35	0	21	0	<0.0001	3
Q6P2Q9	Pre-mRNA-processing-splicing factor 8	24	5	14	4	0.005	2
P62805	Histone H4	26	8	44	34	0.013	3
Q9UJX4	Anaphase-promoting complex subunit 5	28	0	42	0	<0.0001	2
P38919	Eukaryotic initiation factor 4A-III	21	1	39	1.9	<0.0001	3
P30260	Cell division cycle protein 27 homolog	19	0	40	0	<0.0001	3
P49790	Nuclear pore complex protein Nup153	17	0	18	0	<0.0001	3
Q13042	Cell division cycle protein 16 homolog	21	0	30	0	<0.0001	3
Q14204	Cytoplasmic dynein 1 heavy chain 1	14	3	4.9	1.1	0.024	2

Q15029	116 kDa U5 small nuclear ribonucleoprotein component	38	14	16	3	0.014	2
Q9UJX2	Cell division cycle protein 23 homolog	15	0	29	0	0.00019	3
Q9UJX5	Anaphase-promoting complex subunit 4	17	0	26	0	<0.0001	3
Q9UJX6	Anaphase-promoting complex subunit 2	8	0	14	0	0.01	3
Q9UKV3	Apoptotic chromatin condensation inducer in the nucleus	8	0	8.1	0	0.01	2
Q01581	Hydroxymethylglutaryl-CoA synthase, cytoplasmic	6	0	13	0	0.032	2
Q14999	Cullin-7	8	0	6	0	0.01	3
O00148	ATP-dependent RNA helicase DDX39A	15	0	41	0	<0.0001	2
Q13310	Polyadenylate-binding protein 4	7	0	15	0	0.018	2
O00571	ATP-dependent RNA helicase DDX3X	4	0	7.4	0	0.05	2

Table 3-1: Proteins significantly enriched in endogenous CUL9 immunoprecipitation from hPSC lysate as determined by LC-MS/MS.

Protein significance was determined using a Fisher's exact test, $\alpha < 0.05$. All proteins were identified using a 95% protein probability or higher, a 1% FDR, and present in at least two hPSC LC-MS/MS replicates, n=4. Relevant LC-MS/MS information in table is from a representative LC-MS/MS run.

Accesion Number	Protein name	Total spectral counts IP:CUL9	Total spectral counts IgG	% Coverage IP:CUL9	% Coverage IgG
Q8IWT3	Cullin-9	3	0	2	2
Q9UJX3	Anaphase-promoting complex subunit 7	5	0	8	8
Q13042	Cell division cycle protein 16 homolog	3	0	4	4
P30260	Cell division cycle protein 27 homolog	2	0	3	3
Q9UJX2	Cell division cycle protein 23 homolog	1	0	2	0
Q9UJX6	Anaphase-promoting complex subunit 2	1	0	1	0

Table 3-2: Proteins present in endogenous CUL9 immunoprecipitation from hNPC lysate as determined by LC-MS/MS.

All proteins were absent in IgG, but not the CUL9 immunoprecipitation. Identified proteins were present only in CUL9 immunoprecipitation and not in IgG control, with a 95% protein probability or higher, and a 1% FDR, n=1.

Supplemental Figures

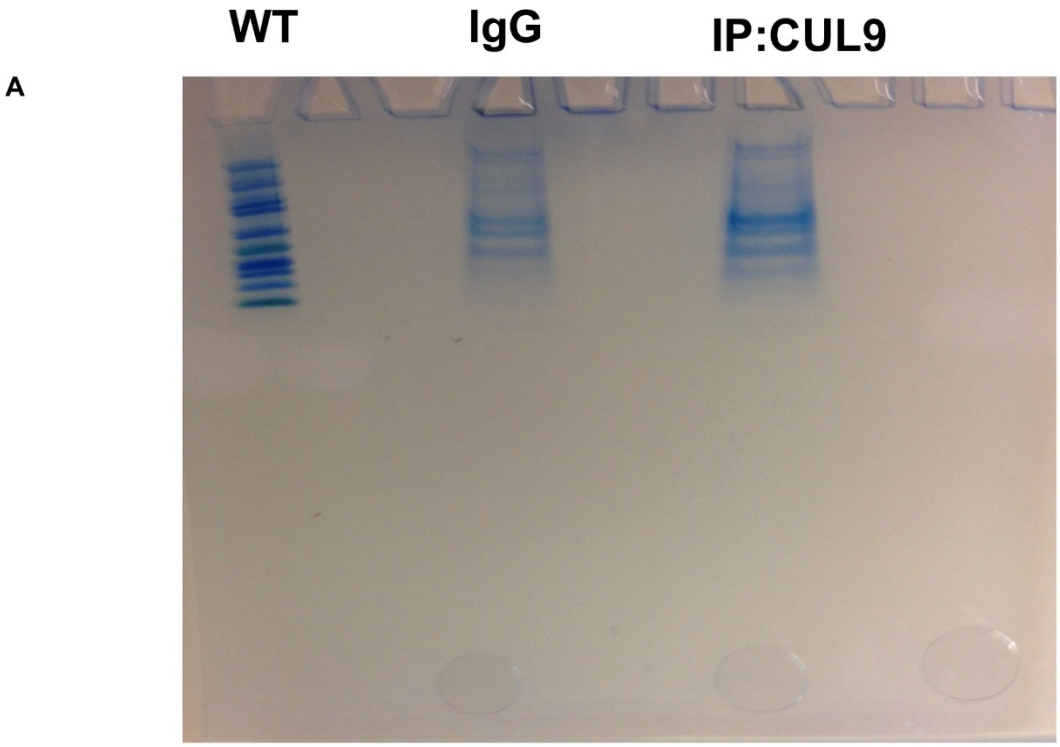

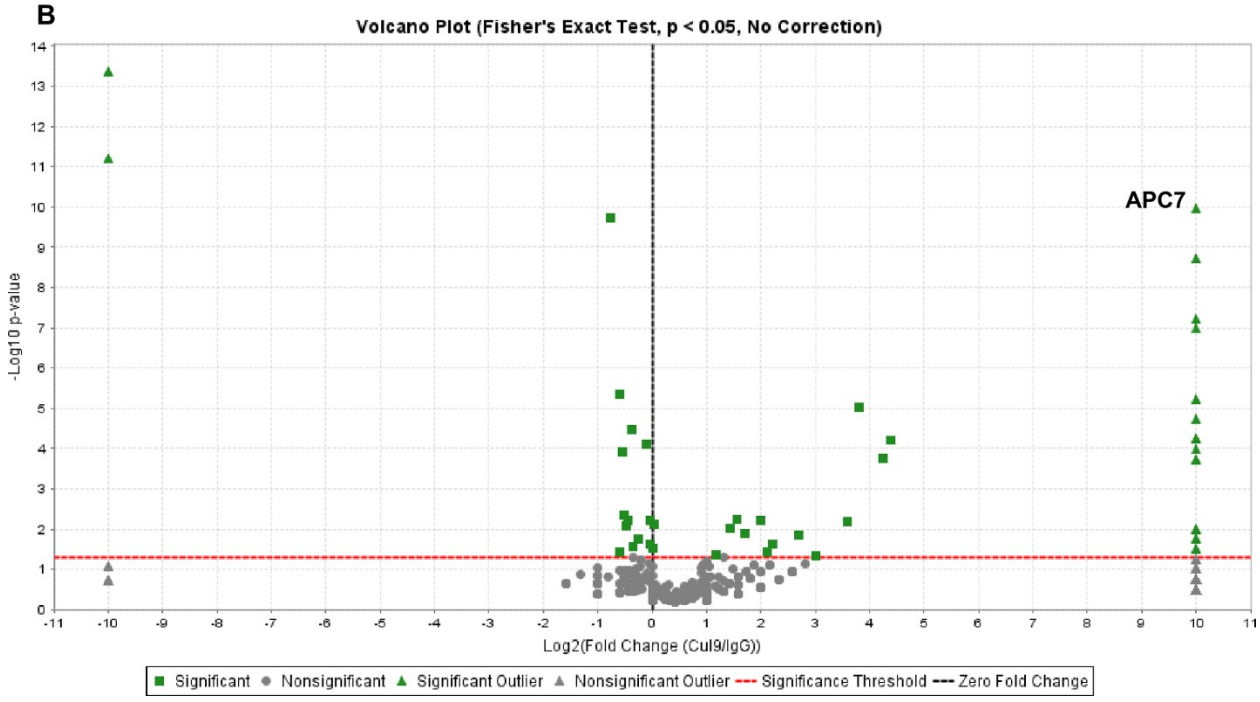

Supplemental Figure 3- 1

(**A**) Coomassie stained protein gel showing loading, IgG control, and CUL9 immunoprecipitation. All proteins from each lane were isolated from the gel. (**B**) Volcano plot showing significantly enriched hits in CUL9 immunoprecipitation. Plot made using Scaffold. Analysis performed on Scaffold using Fisher's exact test, $p<0.05$.

Chapter 4

QUANTITATIVE PROTEOMICS REVEALS CUL9 RELATED SIGNALING PATHWAYS IN CORTICAL DIFFERENTIATION

Parts of Chapter 4 have been adapted with permission from Ortolano, N.A., Romero-Morales, A.I., Rasmussen M.L., Bodnya, C., Kline, L.A., Joshi, P., Connelly, J.P., Rose K.L., Pruett-Miller, S., and Gama V. (2021). A proteomics approach for the identification of cullin-9 (CUL9) related signaling pathways in induced pluripotent stem cell models. PLoS One.

Summary

The cullin-ring ligase (CRL) family of E3 ubiquitin ligases plays a critical role in regulation of early developmental processes, including synapse formation and axon guidance. However, Cullin-9 (CUL9) has proven to be a unique CRL with an elusive function. CRLs generally form large complexes that ubiquitinate a set of specific substrates. CUL9 has not been shown to form large complexes and has only two identified substrates. We performed a quantitative proteomics screen using Isobaric Tags for Relative and Absolute Quantification (iTRAQ) in human induced pluripotent stem cell (hiPSCs), neural stem cell (hNSCs), and neural progenitor cell (hNPCs) CUL9 KO cells to identify proteins enriched or depleted in the absence of CUL9. We identified protein networks related to metabolic, ubiquitin degradation, and transcriptional regulation pathways that are disrupted by CUL9 deletion in both hPSCs. No significant changes in oxygen consumption rates or ATP production were detected in either cell type. We hope that this large-scale proteomics screen of potential CUL9 substrates will provide needed insight and direction for studying CUL9 function in neuronal differentiation.

Introduction

Proper protein turnover is required for the normal function of all cellular processes – ubiquitination accounts for 80% of all protein degradation. E3 ubiquitin ligases are the main effector enzymes, performing the final transfer of ubiquitin to a substrate generally marking it for proteasomal degradation. Aberrant E3 ubiquitin ligase or proteasome function often observed in aging individuals can produce unwelcome proteins to aggregate resulting in neurodegenerative disorders like Parkinson's disease (Ciechanover and Kwon, 2015). Accumulating evidence indicates that mutations resulting in abnormal E3 ligase function also contribute to neurodevelopmental disorders including patient susceptibility to Autism Spectrum Disorder (ASD) (Glessner et al., 2009; K et al., 2009; Yi et al., 2017).

Several members of the largest family of E3 ubiquitin ligases, the Cullin RING Ligase (CRL) family play a pivotal role in development (Arai et al., 2003; Dealy et al., 1999; Li et al., 2002; Singer et al., 1999; Wang et al., 1999), and have even been implicated in critical stages of early neurodevelopment such as axon guidance (Wang et al., 2013b), synapse formation (Simó and Cooper, 2013), and neuronal migration (Feng et al., 2007; Simó et al., 2010). Although mouse knockout (KO) models of most CRLs result in embryonic or neonatal lethality (Arai et al., 2003; Dealy et al., 1999; Li et al., 2002; Singer et al., 1999; Wang et al., 1999), CUL9 KO mice are viable. Various phenotypes have been reported in CUL9 KO mice, providing preliminary insight into its function in development (Li et al., 2014; Pei et al., 2011; Skaar et al., 2007). However, there are key differences between mouse and human cortical development. For example, the mouse brains do not have gyri and the outer subventricular zone is greatly expanded with increased cell diversity including higher amounts of outer radial glia cells (Molnár et al., 2019). Characterizing CUL9 function in a human derived system could reveal novel functions. In this study, we derived human neural stem cells and neural progenitors from hiPSCs to identify any potential phenotypes potentially overlooked or absent in the mouse KO model.

CUL9 is highly expressed in the brain, particularly in the cerebral cortex, based on RNA expression data obtained from human tissue samples and neuronal cells differentiated from human pluripotent stem cells (hPSCs) (Human Protein Atlas) (van de Leemput et al., 2014). CUL9 expression increases substantially during the neural induction phase when neural stem (hNSCs) and progenitor cells (hNPCs) form. Our previous data (**Chapter 1**) indicates that CUL9 is required for formation of neural rosettes, an *in vitro* structure akin to the neural tube, leading us to further investigate CUL9's function in hiPSC-derived NSCs and NPCs.

Maintenance of the precursor pool in the early stage of corticogenesis is crucial for appropriate production of mature neurons (Dwyer et al., 2016; Gage and Temple, 2013; Hitoshi et al., 2002). Overexpansion or exhaustion of the precursor pool can lead to aberrant organization and/or size of cortical layers ultimately altering brain size (Hong et al., 2017; Manzini and Walsh, 2011). Regulation of protein levels of neuronal transcription factors like PAX6 and SOX2 in neural precursor cells is key to maintaining self-renewal and proper differentiation. Despite this, there are few studies focused on characterizing post-translational regulation of neuronal transcription factors (Fang et al., 2014; Lim et al., 2017; Tuoc and Stoykova, 2008; Wang et al., 2016). In this study, we employed quantitative proteomics to identify any potential CUL9 substrates in iPSCs, NSCs, and NPCs to determine if CUL9 is involved in modulating neuronal differentiation.

While analysis of the proteome is easily accessible with the advent of mass spectrometry, determining the effect of different conditions or treatments on the proteome is more challenging. Quantitative proteomics techniques such as Stable Isotope Labeling with Amino Acids in Cell Culture (SILAC) and isobaric tag for relative and absolute quantification (iTRAQ) have emerged to allow comparison between the proteomes of two or more samples (Ordureau et al., 2015). For SILAC, cells are cultured long-term in media containing heavy isotopes or normal (“light”) isotopes, allowing quantitative comparison of protein levels between experimental conditions in one mass spectrometry analysis (Cao et al., 2012; Ong et al., 2002, 2003). Although SILAC is a powerful tool for proteome quantification, its applications are limited by several factors. Some cell lines are adversely affected from metabolic incorporation of heavy isotopes, including hPSCs (Scheerlinck et al., 2016). Additionally, production and maintenance of SILAC cell lines is time consuming and costly. These challenges were a motivating force for the development of strategies like iTRAQ (Rauniyar and Yates, 2014; Ting et al., 2011; Wenger et al., 2011; Wiese et al., 2007). iTRAQ simply requires the addition of an isobaric tag to the primary amine group of peptides after they have been isolated from cells (Rauniyar and Yates, 2014; Wiese et al., 2007). Additionally, it is effective across cell types since labeling takes place after lysate collection. In fact, it was used to successfully identify protein changes during iPSC astrocyte differentiation (Cao et al., 2012). We used iTRAQ to screen for novel CUL9 substrates in hiPSCs, hNSCs, and hNPCs due to its high sensitivity, reproducibility, and multiplexing capabilities.

We identified 124 proteins significantly increased or decreased in hiPSCs or hNPCs. Many of the proteins identified in iPSCs were involved in pathways involved in metabolism, specifically fatty acid metabolism. However, we saw no changes in the oxygen consumption or ATP production of hiPSC or hNPC CUL9 KO cells. We hope that our quantitative proteomics analysis

will guide future research aiming to characterize CUL9 and its function in the early stages of development using our newly developed CUL9 KO hiPSC line.

Results

iTRAQ identifies different sets of proteins altered in hiPSC and NPC CUL9 KO cells.

Quantitative proteomic approaches have emerged as an innovative way to quantify dynamic changes in protein levels and protein interactions during differentiation (Cao et al., 2012; Konze et al., 2017; Molina et al., 2009). To provide insight into CUL9 function during NSC differentiation, we performed an in-depth analysis of proteins significantly altered in CUL9 KO hPSCs and hNPCs compared to WT using Isobaric Tags for Relative and Absolute Quantification (iTRAQ). Briefly, protein lysate was isolated from four cell populations and simultaneously analyzed using tandem liquid chromatography mass spectrometry by covalent labeling of peptides from each cell population with unique stable isotope labeled molecules (Wiese et al., 2007). Using this method, we compared the proteomes of CUL9 KO cells and Parental WT cells (**Figure 4-1A**). Two four-plex iTRAQ experiments were performed: (1) iPSC WT, iPSC CUL9 KO, NSC WT, and NSC CUL9 KO. (2) NSC WT, NSC CUL9 KO, NPC WT, and NPC CUL9 KO. Each four-plex was completed once in each of the two isogenic KO clones, acting as replicates. Briefly, each of the protein samples were labeled with a unique iTRAQ reagent of equivalent mass. The iTRAQ reagents labeled all primary amine groups of the peptides. Once each sample had been labeled with its unique iTRAQ label (i.e. 114, 115, 116, or 117), the four samples were mixed at a 1:1 ratio (200ug total protein of each sample). The sample mixture was analyzed by LC-MS/MS for protein identification and quantification (**Figure 4-1A**; **Supplemental Figure 4-1**). WT iPSC and WT NPCs were compared to WT NSC samples to validate induction of key genes for each cell type (**Tables 4-1 and 4-2**). 54 total proteins were significantly altered in iPSC CUL9 KO clones and 72 in NPC CUL9 KO clones (**Figure 4-1A**; **Supplemental Tables 4-1 - 4-4**). Notably, only two proteins were significantly altered in both cell types: Glutaredoxin-1 (GLRX) and Protein kish-A (TMEM167A), both of which have been implicated in neurological disease and metabolic regulation (Akterin et al., 2006; Portela et al., 2019; Segura-Collar et al., 2020).

hiPSC CUL9 KO cells have altered protein levels of metabolic proteins.

We analyzed the direct and indirect interactions amongst the proteins significantly altered in hiPSC CUL9 KO clones using the Search Tool for the Retrieval of Interacting Genes/Proteins (STRING) (Franceschini et al., 2012, 2016; Jensen et al., 2009; von Mering, 2004; Snel, 2000; Szklarczyk et al., 2011, 2015, 2017, 2019). As described in **Chapter 3**, STRING is a database of known and predicted protein-protein interactions. These include physical interactions as well as

indirect interactions including shared functions or common signaling pathways. We identified an interesting cluster of interacting proteins within the CUL9 KO iPSC significantly altered hits: a group of enzymes involved in fatty acid metabolism (left-center) (**Figure 4-2A**). Additionally, we used the Database for Annotation, Visualization and Integrated Discovery (DAVID) bioinformatics resource to identify trends in our iTRAQ data using direct gene ontology (GO) classification (Huang et al., 2009b, 2009a). Many of the proteins were associated with GO terms reflecting their metabolic function like “oxidation reduction processes” and “cholesterol biosynthesis processes” (**Figure 4-2B**). Additionally, over 40% of the proteins identified were associated with subcellular localization at integral membranes including in the endoplasmic reticulum where lipids are synthesized (**Figure 4-2C**). They were also significantly associated with molecular function terms like “ATP binding,” a common function of metabolic enzymes (**Figure 4-2D**).

Based on the results of these analyses, we focused our efforts on characterizing the effects of CUL9 deletion and depletion on metabolic function, specifically related to fatty acid metabolism. Fatty acid synthesis has been implicated in promoting pluripotency and reprogramming through acetylation of key proteins involved in mitochondrial fission (Wang et al., 2017). Additionally, deficiencies in fatty acid oxidation can result in the loss of the NSC pool in the mammalian cortex through increased differentiation to NPCs. In fact, inborn deficiencies in fatty acid oxidation are associated with developmental neural disorders such as Autism Spectrum Disorder (Xie et al., 2016).

Stearoyl-coA desaturase (SCD1) is enriched in CUL9 KO iPSCs compared to parental iPSCs and catalyzes the rate limiting step in the synthesis of monounsaturated fatty acids which are incorporated into key cellular structures like lipid membranes (**Supplemental Table 4-1**) (Ariyama et al., 2010; Dobrzyn et al., 2004). Specifically, SCD1 converts palmitoyl-CoA and stearoyl-CoA, to palmitoleoyl-CoA and oleoyl-CoA, the most prevalent monounsaturated fatty acids present in key lipid populations such as phospholipids, triglycerides, and cholesterol esters (Dobrzyn et al., 2004; Miyazaki et al., 2001). SCD1 expression drastically increases during the first 30 days of cortical differentiation; after day 30 SCD1 mRNA levels decrease and stabilize (van de Leemput et al., 2014). Based on this, SCD1 function is potentially important for NSC and NPC production and therefore a promising potential CUL9 interacting protein. Another significantly increased protein, TM7SF2 (delta(14)-sterol reductase), is involved in a key reaction in cholesterol biosynthesis upstream of SCD1 (**Supplementary Table 4-1**) (Bennati et al., 2006). Like SCD1, it’s levels drastically increase during the first 30 days of cortical differentiation and continue to do so beyond day 70 (van de Leemput et al., 2014). Based on this, TM7SF2 may be

important not only for neural precursor production but the differentiation of post-mitotic cortical neurons. However, there were no significant differences in protein levels of either proteins in CUL9 KO clones (**Figure 4-3A and B**) or CUL9 KD cells (**Supplemental Figure 4-2A and B**) as determined by Western blotting.

However, we considered that since the fold changes were below 2-fold, the increased protein levels of SCD1 and TM7SF2 may not be detectable by Western blotting. To determine if CUL9 could still affect the function of these proteins, we analyzed CUL9 KO and KD cells metabolic function using Seahorse analysis of oxygen consumption rate and ATP production. We saw no changes in the oxygen consumption rate or ATP production in KO and KD hPSCs (**Figure 4-3C-F**; **Supplemental Figure 4-2C-F**) or hNPCs (**Figure 4-3G-J**; **Supplemental Figure 4-2C-F**) although specific analysis of fatty acid metabolism is needed to confirm SCD1 and TM7SF2 function is not altered in CUL9 KO or KD cells.

iTRAQ identified altered levels of key neuronal transcription factors.

When we searched the significantly altered (increased and decreased) NPC hits against the STRING database we did not see large cluster of interacting proteins (**Figure 4-4A**). However, GO analysis revealed many of the proteins associated with biological processes terms relevant to neuronal development like “positive regulation of synaptic transmission” (**Figure 4-4B**). More significantly, we noticed that the subcellular localization of the proteins was associated with the nucleoplasm, and many were associated with poly (A) RNA binding (**Figure 4-4C and D**). Based on this, we decided to focus on validating neuronal transcription factors with altered protein levels in the NPC CUL9 KO based on our iTRAQ analysis. We previously observed that both CUL9 KO clones have decreased levels of TUBB3 at the hNPC stage (**Chapter 2**). As TUBB3 expression is critical for neuronal maturation and synapse formation (Poirier et al., 2010), we suspected a neuronal transcription factor upstream of TUBB3 may be involved in the observed abnormalities during neural rosette formation. iTRAQ revealed that the transcription factors SRY-box transcription factor 3 (SOX3) and Homeobox cut-like 1 (CUX1) were significantly increased in CUL9 KO hNPCs (**Supplemental Tables 4-3 and 4-4**).

The SOX family of proteins consists of transcription factors known to coordinate the transcriptional programs of precursors during developmental processes, most notably neurodevelopment (Sarkar and Hochedlinger, 2013). SOX family member SOX3 was significantly upregulated in CUL9 KO NPCs (Table 3). SOX3 is highly expressed in NSCs and NPCs. As NPCs

differentiate to early born neurons, SOX3 levels are reduced, and SOX11 levels increase. Despite this, SOX3 binds to both NSC and neuronal genes though the neuronal genes are not expressed in the presence of SOX3. SOX3 binds to bivalent neuronal genes to mark them for SOX11 binding and neuronal transcription (Bergsland et al., 2011). Bivalent gene domains contain both H3 lysine 27 methylation and H3 lysine 4 methylation, which simultaneously prevents their transcription while poising them for activation (Bernstein et al., 2006). Bivalent domains are common in progenitor cells, especially embryonic stem cells. In fact, SOX2 binds NSC genes containing bivalent domains in embryonic stem cells to mark them for SOX3 binding (Bergsland et al., 2011). While SOX3 is highly expressed at the NPC stage, CUX1, is a transcription factor generally expressed in upper layer neurons (LII-IV) of the cortex (Nieto et al., 2004). CUX1 transcriptional activity regulates neuronal maturation processes such as dendritic branching and synapse formation (Cubelos et al., 2010). However, expression of CUX1 has been reported at extremely low levels in the ventricular zone and sub-ventricular zones where NSCs and NPCs reside, respectively (Nieto et al., 2004; Zimmer et al., 2004). The role for CUX1 at this stage remains elusive. Although these transcription factors seemed like promising hits, we did not observe altered levels of either protein by Western blotting, although, we did observe variable expression of these proteins between biological replicates (**Figure 4-5**).

Discussion

The function of CUL9 has always been elusive, and its characterization is seemingly resistant to common biochemical approaches used to identify ubiquitin substrates, including mass spectrometric analysis (Gama et al., 2014; Li et al., 2014). We applied quantitative proteomics approaches to try and reveal CUL9 interacting proteins and gain insight into its function in early neuronal differentiation. By analyzing the proteome of human CUL9 KO iPSCs, NSCs, and NPCs we identified over 100 proteins that were significantly altered in iPSC and NPC CUL9 KO cells, but only two were significantly altered in both cell types. Overall, most of the hits were involved in fatty acid metabolism based on STRING and DAVID GO term analysis.

We sought to validate two proteins significantly increased in iPSCs, SCD1 and TM7SF2, involved in fatty acid desaturation and cholesterol biosynthesis. However, we did not detect a significant increase in these proteins by immunoblotting or detect any significant changes in oxygen consumption rate or ATP production. There were several other proteins involved in fatty acid synthesis we identified by iTRAQ like Fatty acid desaturase 2 (FADS2) and the delta-isomerase IDI1 that should be validated. Specific fatty acid metabolic assays using Seahorse analysis and metabolomics may also provide greater insight into any metabolic defects in CUL9 KO or KD cells.

The small changes we observe in CUL9 KO and KD proteins by iTRAQ could be because CUL9 regulates mRNA transcription through interaction or regulation with mRNA processing proteins rather than directly with the proteins identified by iTRAQ. For example, neuronal transcription factors CUX1 and SOX3 were significantly upregulated in CUL9 KO NPCs. However, this was not validated by immunoblotting, though, we did see great variation between biological replicates in both KO clones, indicating this is not just an effect of clonal variability. We also observed this variability when quantifying levels of pluripotency factors and neuronal markers (**Chapter 2**). Interestingly, our LC-MS/MS analysis of CUL9 immunoprecipitation revealed CUL9 interaction with several proteins involved in mRNA processing and transcription like spliceosome component Small nuclear ribonucleoprotein U5 subunit 200 (SNRNP200) or RNA helicases DDX39A and DHX9 (**Chapter 3**). CUL9's interactions with these proteins, direct or indirect, should be elucidated to explore if CUL9 plays a role in RNA processing. Regulation at the mRNA processing level could explain why CUL9 substrates remain elusive and so much variability was observed in the expression of key cell marker proteins in the CUL9 KO cell lines.

CUL9 interaction with other E3 ubiquitin ligases outside of CUL7 should also be investigated. CUL9 interaction with CUL1 and its F-Box associated protein FBXW2 should be explored, as FBXW2 was significantly increased in iPSCs – FBXW2 could even act as a substrate adapter for CUL9 as it does for CUL1 as no F-box proteins are currently known to associate with CUL9. Additionally, ubiquitin ligases outside of the CRL family may interact with CUL9. HERC5 was significantly increased in CUL9 KO hPSCS and HERC1 was significantly decreased in CUL9 KO hNPCs. Compensation by these E3 ubiquitin ligases should also be considered. Depletion and deletion of ligases often results in compensation by another. Compensation by one or both ligases could also explain why phenotypes have been absent or subtle in mouse and cellular models. A more sensitive proteomics approach focused on screening differences in ubiquitinated protein populations rather than protein levels would allow identification of substrates ubiquitinated for purposes other than proteasomal degradation. A di-gly quantitative proteomics approach would allow for unbiased quantification of differentially ubiquitinated proteins in CUL9 KO cells (Ordureau et al., 2015).

Alternatively, the small changes we observed in protein levels in the CUL9 KO cells compared to WT cells could be because CUL9 is autoinhibited in the WT cells. CUL9 has an Ariadne domain present at it's C-terminus. Ariadne domains generally inhibit the activity of RBR and their association with CRLs activates their enzymatic activity (Duda et al., 2013; Marín and Ferrús, 2002; Smit and Sixma, 2014). It is not known if CUL9's predicted Ariadne domain is functional and if it interacts with either its cullin or RBR domain. The inter-molecular interactions of CUL9 structure likely complicate its characterization. Additionally, CUL9 may need to form a homodimer or heterodimerize with another CRL, like CUL1 mentioned above, to initiate it enzymatic activity. Cells may need to be analyzed under certain conditions or exposed to cellular stress to promote CUL9 activity in WT cells. Truncations or point mutations of CUL9's RBR, cullin, and Ariadne domains should be performed to see how it affects CUL9 activity. If a structural change is required to induce CUL9 activity, quantitative proteomics comparing a CRISPR knock-in cell line expressing constitutively active CUL9 and WT cells may provide better insight into CUL9 substrates across various cell types. Our study identifies CUL9 related pathways, but further analysis of CUL9 ubiquitination, function, and regulation during a variety cell transitions is required to understand where CUL9 fits into the crosstalk between these pathways and its potential contribution to early development.

Figures

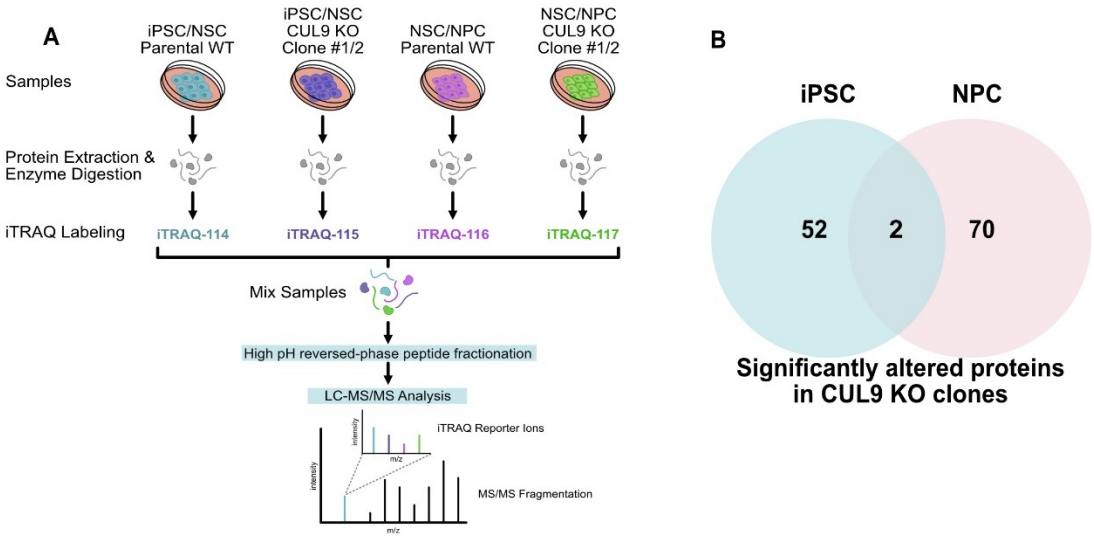

Figure 4-1: Analysis of CUL9 KO iPSCs and NPCs

(**A**) Protocol for iTRAQ labeling of samples. Two comparisons were done: (1) iPSC WT, iPSC CUL9 KO, NSC WT, and NSC CUL9 KO. (2) NSC WT, NSC CUL9 KO, NPC WT, and NPC CUL9 KO. Each comparison was done for CUL9 KO #1 (n=1) and #2 (n=1). (**B**) Venn diagram showing number of significantly altered proteins in iPSC iTRAQ data and hNPC data. Two proteins were significantly altered in both datasets.

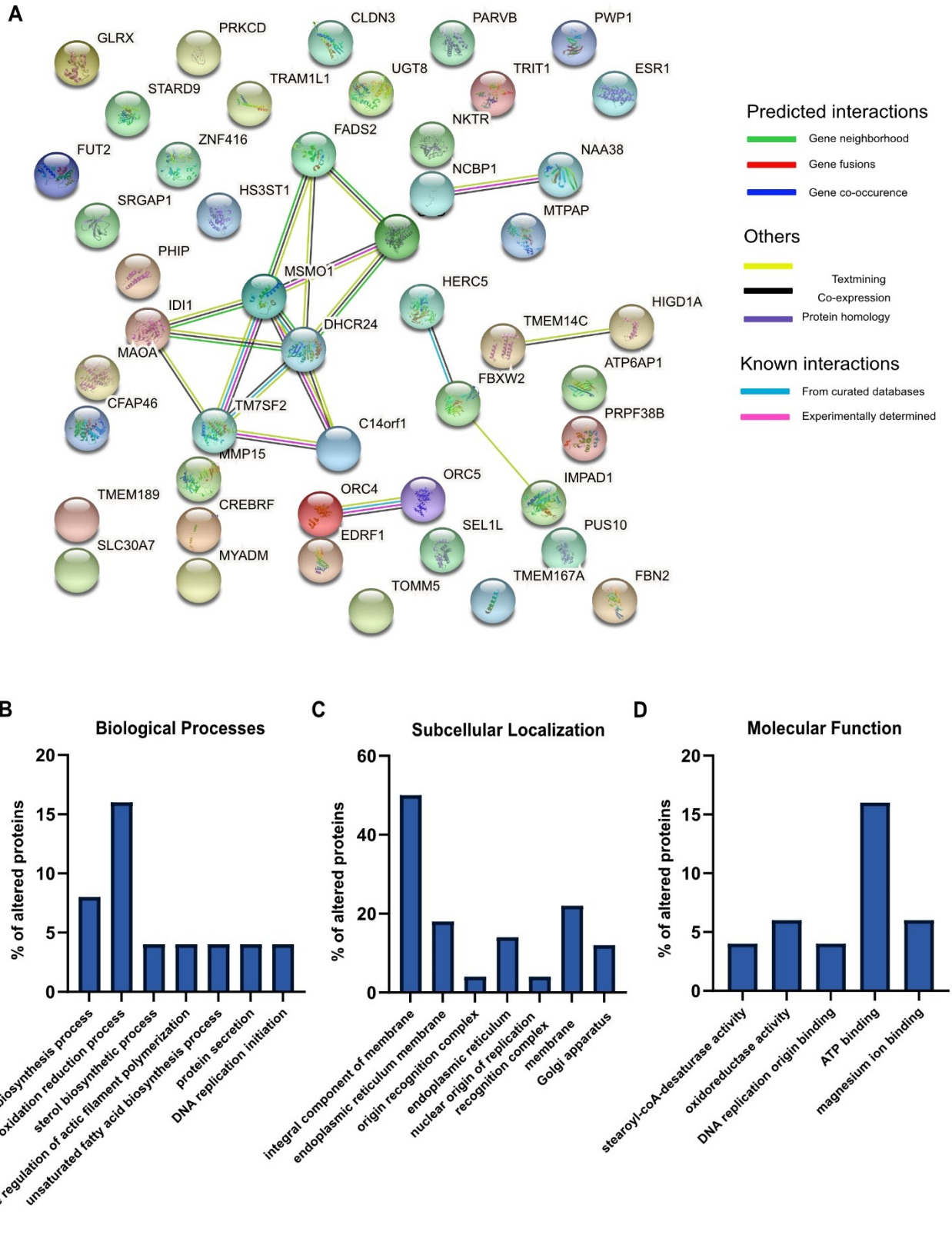
A
GLRX
PRKCD
CLDN3
PARVB
PWP1
STARD9
TRAM1L1
UGT8
TRIT1
ESR1
NKTR
FADS2
ZNF416
FUT2
NAA38
NCBP1
HS3ST1
SRGAP1
MTPAP
PHIP
MSMO1
HERC5
HIGD1A
IDI1
DHCR24
TMEM14C
MAOA
ATP6AP1
FBXW2
CFAP46
TM7SF2
PRPF38B
C14orf1
MMP15
IMPAD1
ORC5
TMEM189
ORC4
CREBRF
SEL1L
PUS10
EDRF1
SLC30A7
MYADM
TMEM167A
FBN2
TOMM5
Predicted interactions
Gene neighborhood
Gene fusions
Gene co-occurence
Others
Textmining
Co-expression
Protein homology
Known interactions
From curated databases
Experimentally determined
B
Biological Processes
% of altered proteins
cholesterol biosynthesis process
oxidation reduction process
sterol biosynthetic process
negative regulation of actic filament polymerization
unsaturated fatty acid biosynthesis process
protein secretion
DNA replication initiation
C
Subcellular Localization
% of altered proteins
integral component of membrane
endoplasmic reticulum membrane
origin recognition complex
endoplasmic reticulum
nuclear origin of replication
recognition complex
membrane
Golgi apparatus
D
Molecular Function
% of altered proteins
stearoyl-coA-desaturase activity
oxidoreductase activity
DNA replication origin binding
ATP binding
magnesium ion binding

Figure 4-2: CUL9 KO iPSCs have significantly altered levels of key proteins in metabolism as determined by iTRAQ.

(**A**) Results from query using Search Tool for the retrieval of Interacting Genes/Proteins (STRING). Diagram depicts known and predicted direct and indirect protein-protein interactions amongst the significant proteins identified in CUL9 KO hPSCs and NPCs. Proteins displayed are significantly (B-H method) altered in one clone and have an average normalized fold change of $\geq$1.2 or $\leq$ 0.8 in the other. Colored nodes represent queried proteins and the first shell of interactors. Clear nodes indicate second shell of interactors. Filled nodes show known, partial, or predicted structure. Empty nodes indicate non known or predicted structure is available for the given protein. DAVID functional annotation of significantly altered proteins was used to identify significantly enriched gene ontology (GO) terms. Significantly altered proteins were identified in Clone #1 or Clone #2 iPSC or hNPC datasets compared to WT iPSC. Significance was determined by the Benjamini-Hochberg method. Proteins significantly (B-H method) altered in one clone with an average normalized fold change of $\geq$1.2 or $\leq$ 0.8 were included in GO analysis. (**B**) GO biological processes direct classifications enriched in full dataset. (**C**) GO cellular compartment direct (CC) classifications enriched in full dataset. (**D**) GO molecular function direct (MF) classifications enriched in full dataset.

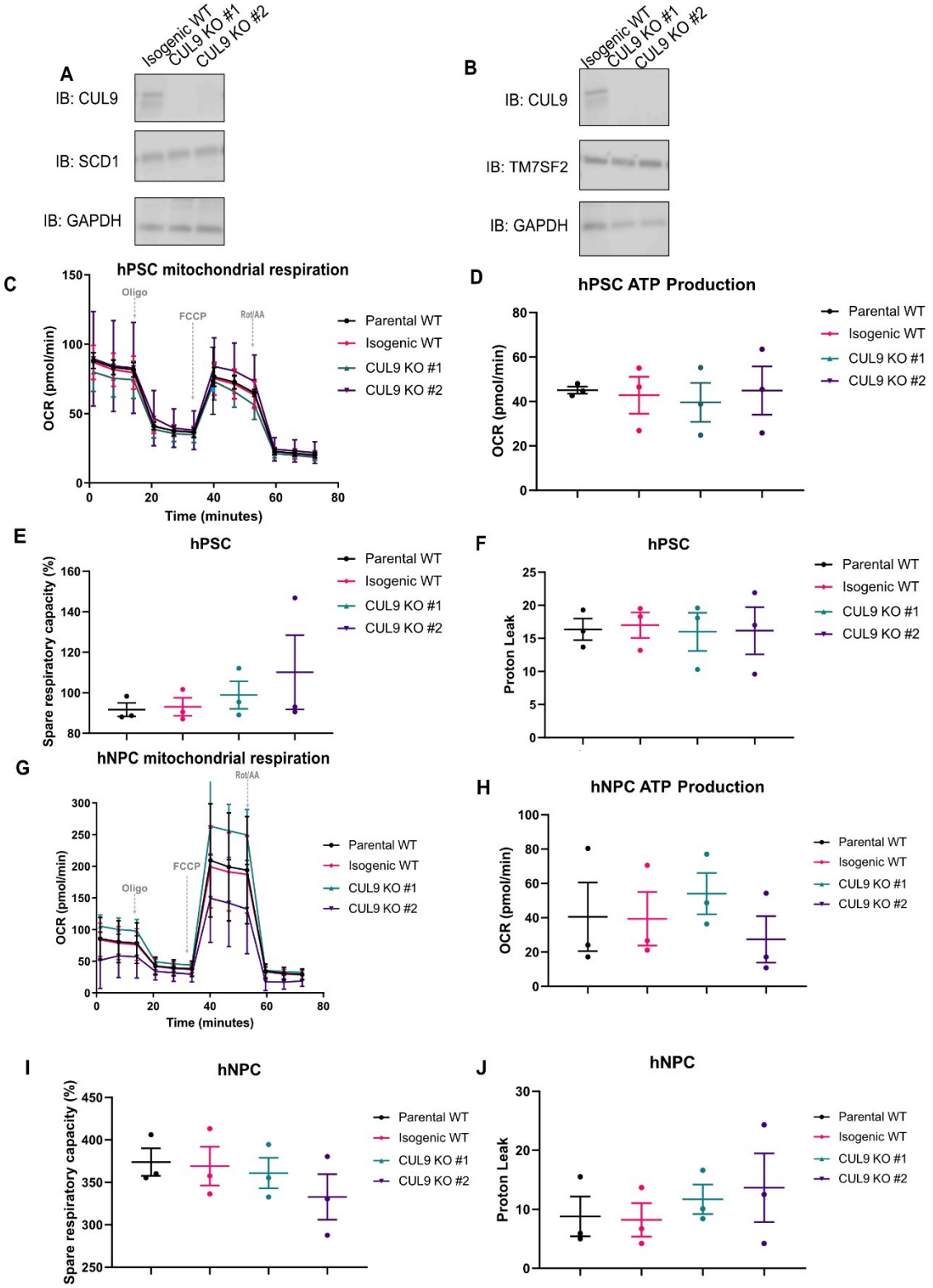
A
Isogenic WT
CUL9 KO #1
CUL9 KO #2
IB: CUL9
IB: SCD1
IB: GAPDH
B
Isogenic WT
CUL9 KO #1
CUL9 KO #2
IB: CUL9
IB: TM7SF2
IB: GAPDH
C
hPSC mitochondrial respiration
Oligo
FCCP
Rot/AA
OCR (pmol/min)
Time (minutes)
Parental WT
Isogenic WT
CUL9 KO #1
CUL9 KO #2
D
hPSC ATP Production
OCR (pmol/min)
Parental WT
Isogenic WT
CUL9 KO #1
CUL9 KO #2
E
hPSC
Spare respiratory capacity (%)
Parental WT
Isogenic WT
CUL9 KO #1
CUL9 KO #2
F
hPSC
Proton Leak
Parental WT
Isogenic WT
CUL9 KO #1
CUL9 KO #2
G
hNPC mitochondrial respiration
Rot/AA
FCCP
Oligo
OCR (pmol/min)
Time (minutes)
Parental WT
Isogenic WT
CUL9 KO #1
CUL9 KO #2
H
hNPC ATP Production
OCR (pmol/min)
Parental WT
Isogenic WT
CUL9 KO #1
CUL9 KO #2
I
hNPC
Spare respiratory capacity (%)
Parental WT
Isogenic WT
CUL9 KO #1
CUL9 KO #2
J
hNPC
Proton Leak
Parental WT
Isogenic WT
CUL9 KO #1
CUL9 KO #2

Figure 4-3: CUL9 KO hPSCs and hNPCs display normal metabolic profile.

CUL9 KO express normal levels of key fatty acid metabolism enzymes SCD1 (**A**) and DHCR24 (**B**) n-3; mean +/- SEM; Analysis done using student's t-test, α=0.05. CUL9 KO hPSCs have the same oxygen consumption rate (OCR) (**C**), ATP production (**D**), spare respiratory capacity (**E**), and levels of proton leak (**F**) as parental and isogenic WT hPSCs. CUL9 KO hNPCs also display no abnormalities (**G-J**). n = 3 independent experiments done in triplicate, error bars are +/- SEM. (OCR) was measured using the Seahorse Biosciences Mito Stress Test on an XFe96 analyzer. ATP production was calculated from the corresponding OCR traces in panels A and C for each condition. Spare respiratory capacity is the difference between maximal respiration or basal respiration. Oligomycin inhibits ATP synthase interrupting the electron transport chain ultimately disrupting mitochondrial respiration and ATP production. FCCP is an uncoupler, uncoupling ATP production from the electron transport chain. Rotenone (complex I inhibitor) and antimycin A (complex III inhibitor) completely inhibit mitochondrial respiration, only permitting nonmitochondrial respiration to persist.

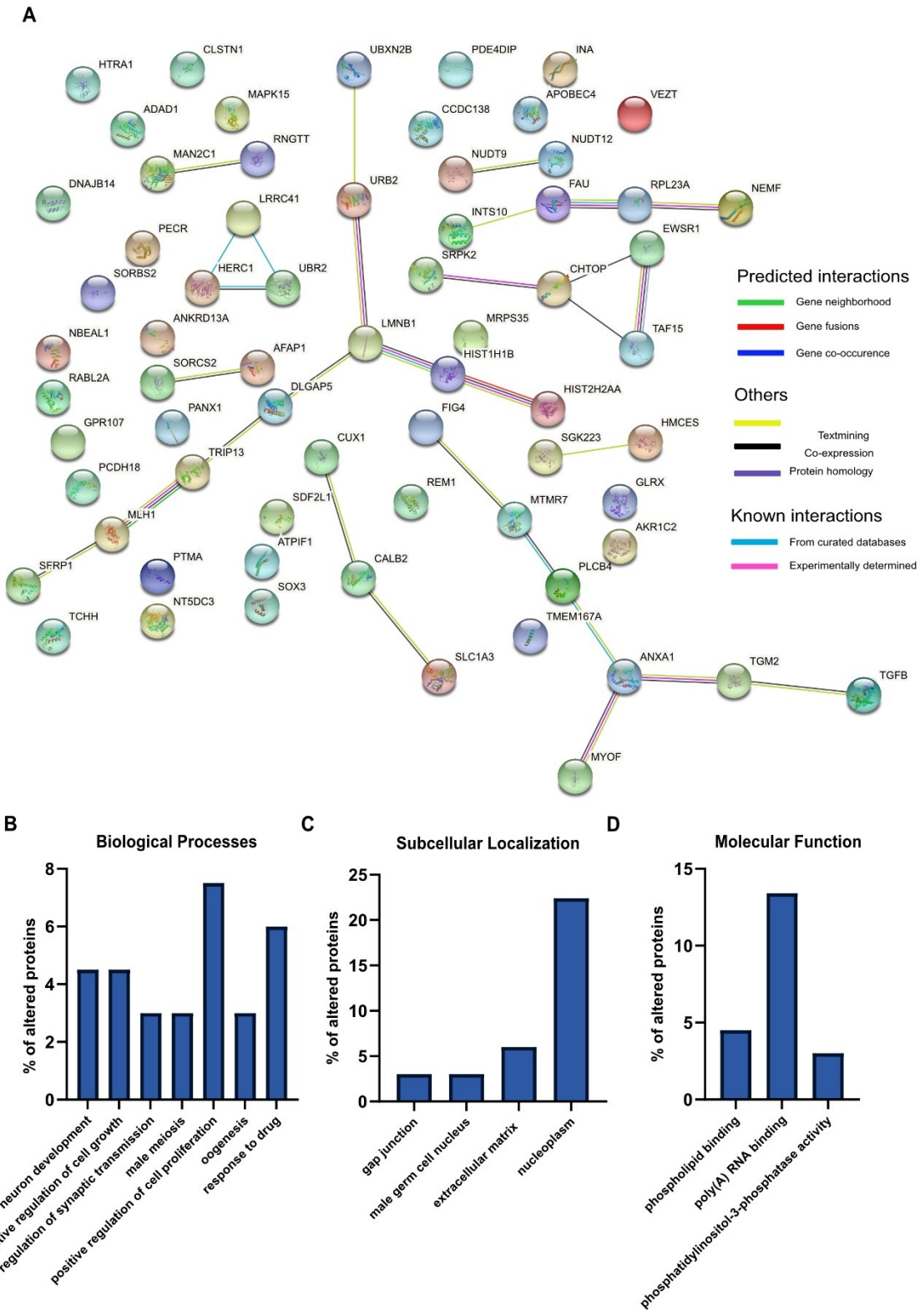
A
HTRA1
CLSTN1
ADAD1
MAPK15
RNGTT
MAN2C1
DNAJB14
LRRC41
PECR
SORBS2
HERC1
UBR2
ANKRD13A
NBEAL1
AFAP1
SORCS2
RABL2A
DLGAP5
PANX1
GPR107
TRIP13
PCDH18
MLH1
SFRP1
PTMA
NT5DC3
TCHH
ATPIF1
SDF2L1
SOX3
CUX1
CALB2
SLC1A3
UBXN2B
URB2
LMNB1
PDE4DIP
INA
APOBEC4
VEZT
CCDC138
NUDT12
NUDT9
FAU
RPL23A
NEMF
INTS10
EWSR1
SRPK2
CHTOP
TAF15
MRPS35
HIST1H1B
HIST2H2AA
FIG4
HMCES
SGK223
REM1
GLRX
MTMR7
AKR1C2
PLCB4
TMEM167A
ANXA1
TGM2
TGFB
MYOF
Predicted interactions
Gene neighborhood
Gene fusions
Gene co-occurence
Others
Textmining
Co-expression
Protein homology
Known interactions
From curated databases
Experimentally determined
B
Biological Processes
% of altered proteins
0
2
4
6
8
neuron development
positive regulation of cell growth
positive regulation of synaptic transmission
male meiosis
positive regulation of cell proliferation
oogenesis
response to drug
C
Subcellular Localization
% of altered proteins
0
5
10
15
20
25
gap junction
male germ cell nucleus
extracellular matrix
nucleoplasm
D
Molecular Function
% of altered proteins
0
5
10
15
phospholipid binding
poly(A) RNA binding
phosphatidylinositol-3-phosphatase activity

Figure 4- 4: iTRAQ analysis of CUL9 KO NPCs show altered levels of proteins involved in neuronal processes.

(**A**) Results from query using Search Tool for the retrieval of Interacting Genes/Proteins (STRING). Diagram depicts known and predicted direct and indirect protein-protein interactions amongst the significant proteins identified in CUL9 KO hPSCs and NPCs. Proteins displayed are significantly (B-H method) altered in one clone and have an average normalized fold change of $\geq$1.2 or $\leq$ 0.8 in the other. Colored nodes represent queried proteins and the first shell of interactors. Clear nodes indicate second shell of interactors. Filled nodes show known, partial, or predicted structure. Empty nodes indicate non known or predicted structure is available for the given protein. DAVID functional annotation of significantly altered proteins was used to identify significantly enriched gene ontology (GO) terms. Significantly altered proteins were identified in Clone #1 or Clone #2 iPSC or hNPC datasets compared to WT iPSC. Significance was determined by the Benjamini-Hochberg method. Proteins significantly (B-H method) altered in one clone with an average normalized fold change of $\geq$1.2 or $\leq$ 0.8 were included in GO analysis. (**B**) GO biological processes direct classifications enriched in full dataset. (**C**) GO cellular compartment direct (CC) classifications enriched in full dataset. (**D**) GO molecular function direct (MF) classifications enriched in full dataset.

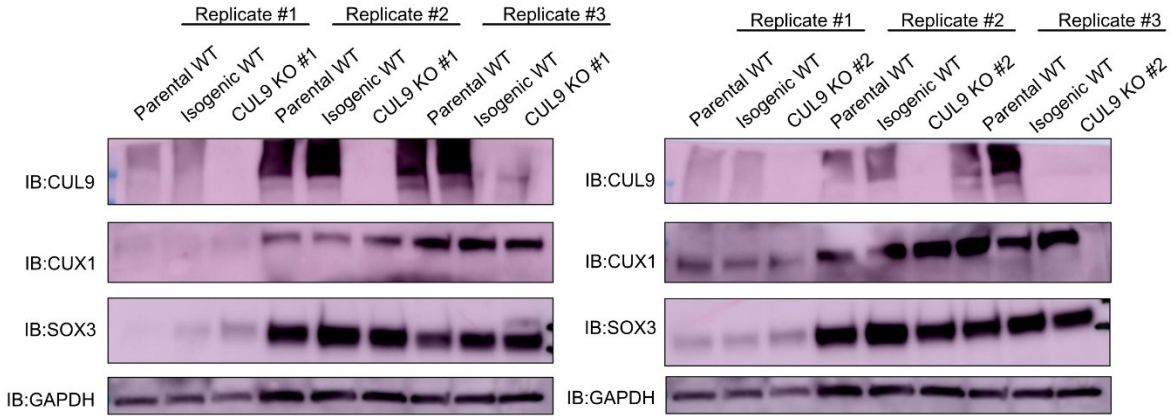

Figure 4-5: CUL9 KO hNPCs have expected levels of key neuronal transcription factors. CUL9 KO cells express normal levels of transcription factors CUX1 (**A**) and SOX3 (**B**) n=3, all independent, biological replicates shown in single blot to demonstrate variability between replicates.

Tables

Accesion Number	Protein name	Fold change
P61601	Neurocalcin-delta (NCLAD)	2.337549
P08670	Vimentin (VIM)	2.208392
P48681	Nestin (NES)	1.416172
Q7L190	Developmental pluripotency-associated protein 4 (DPPA4)	0.514056
P16422	Epithelial cell adhesion molecule (ECAM)	0.197921

Table 4-1: Markers of differentiation are increased in NSCs and markers of pluripotency are decreased.

Normalized fold change of WT NSCs compared to WT iPSCs is shown. Listed proteins are significantly (B-H method) altered in WT NSCs. More information is included in the raw data available at Zenodo at 10.5281/zenodo.4340970.

Accesion Number	Protein name	Fold change
Q6PUV4	Complexin-2 (CPLX2)	14.86192
O43602	Neuronal migration protein doublecortin (DCX)	2.861057
Q13509	Tubulin beta-3 chain (TUBB3)	2.564271
Q16650	T-box brain protein 1 (TBR1)	2.306249
P11137	Microtubule-associated protein 2 (MAP2)	2.168276

Table 4-2: Markers of differentiation are increased in NPCs as determined by iTRAQ analysis.

Normalized fold change of WT NPCs compared to WT iPSCs is shown. Listed proteins are significantly (B-H method) altered in WT NPCs. More information is included in the raw data available at Zenodo at 10.5281/zenodo.4340970.

Supplemental Figures

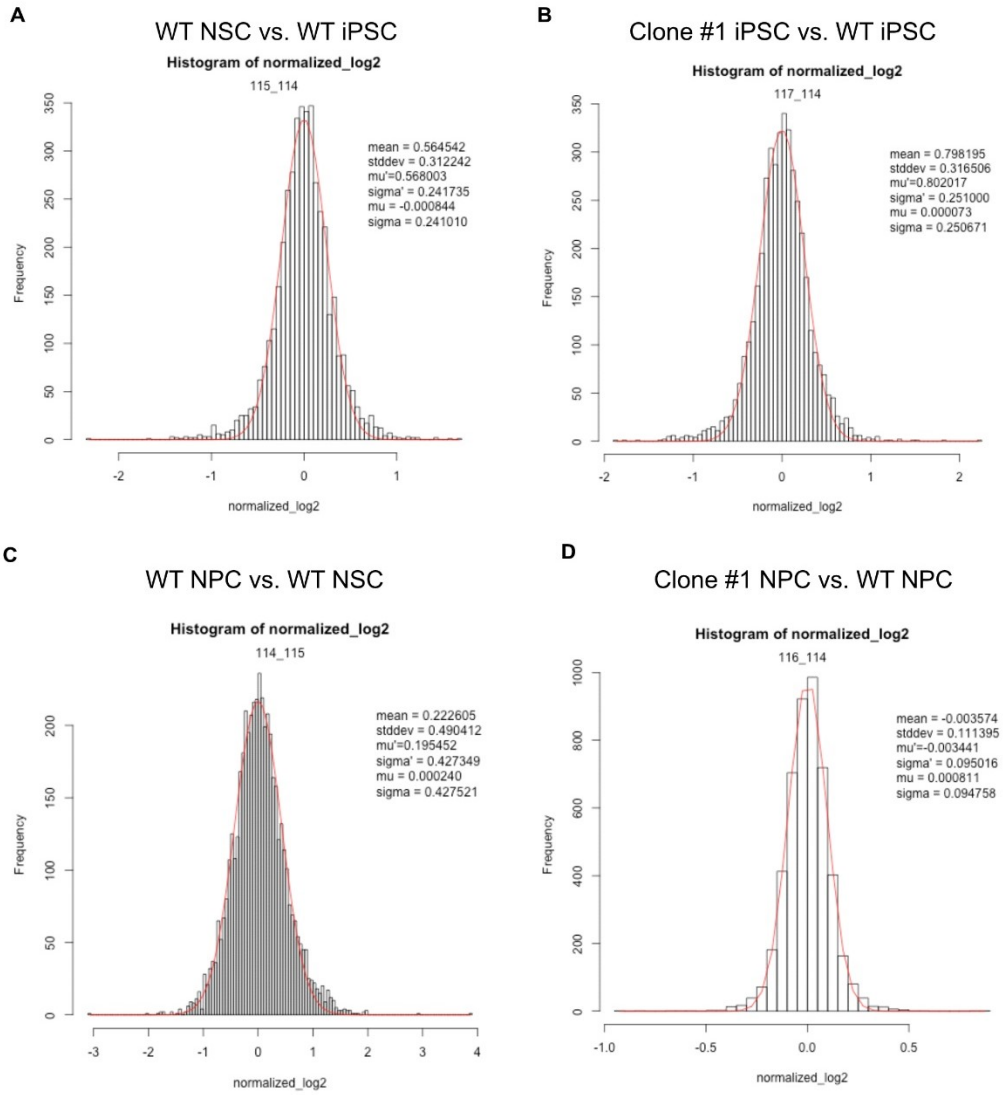

Supplemental Figure 4-1: Representative histograms showing normalized distribution of (log) quantification protein ratios

Ratios are (**A**) WT NSC vs. WT iPSC, (**B**) Clone #1 vs. WT iPSC, (**C**) WT NPC vs. WT NSC, and (**D**) Clone #1 NPC vs. WT NPC. More information is included in the raw data available at Zenodo at 10.5281/zenodo.4340970.

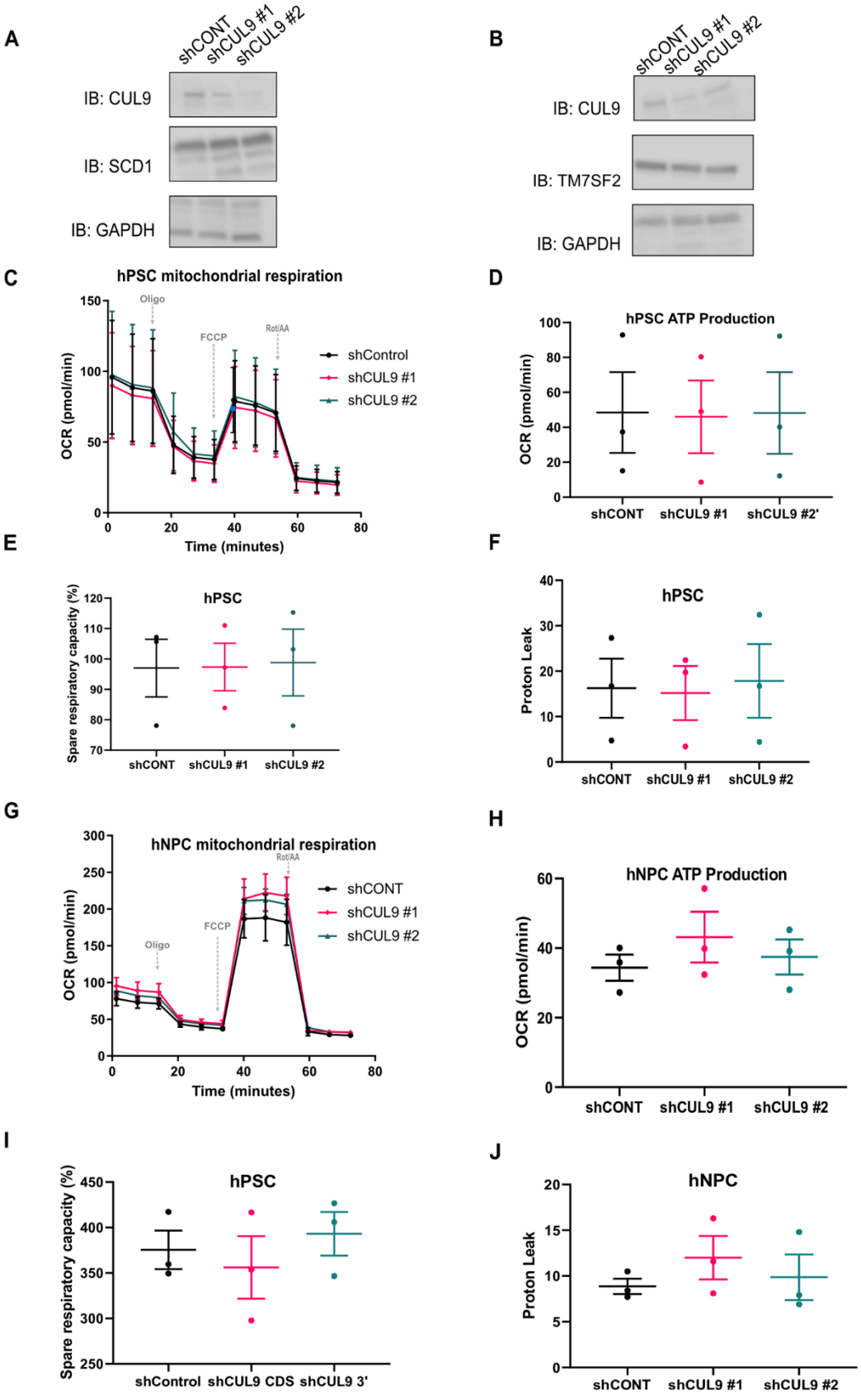
A
shCONT
shCUL9 #1
shCUL9 #2
IB: CUL9
IB: SCD1
IB: GAPDH
B
shCONT
shCUL9 #1
shCUL9 #2
IB: CUL9
IB: TM7SF2
IB: GAPDH
C
hPSC mitochondrial respiration
Oligo
FCCP
Rot/AA
shControl
shCUL9 #1
shCUL9 #2
OCR (pmol/min)
Time (minutes)
D
hPSC ATP Production
OCR (pmol/min)
shCONT
shCUL9 #1
shCUL9 #2'
E
hPSC
Spare respiratory capacity (%)
shCONT
shCUL9 #1
shCUL9 #2
F
hPSC
Proton Leak
shCONT
shCUL9 #1
shCUL9 #2
G
hNPC mitochondrial respiration
Rot/AA
FCCP
Oligo
shCONT
shCUL9 #1
shCUL9 #2
OCR (pmol/min)
Time (minutes)
H
hNPC ATP Production
OCR (pmol/min)
shCONT
shCUL9 #1
shCUL9 #2
I
hPSC
Spare respiratory capacity (%)
shControl
shCUL9 CDS
shCUL9 3'
J
hNPC
Proton Leak
shCONT
shCUL9 #1
shCUL9 #2

Supplemental Figure 4- 2: CUL9 KD hPSCs and hNPCs have expected levels of key metabolic proteins and display normal metabolic profile.

CUL9 KD cells express normal levels of key fatty acid metabolism enzymes SCD1 (**A**) and DHCR24 (**B**) n=3; mean +/- SEM; Analysis done using student's t-test, α=0.05. CUL9 KO hPSCs have the same oxygen consumption rate (OCR) (**C**), ATP production (**D**), spare respiratory capacity (**E**), and levels of proton leak (**F**) as parental and shCONT hPSCs. CUL9 KD hNPCs also display no abnormalities (**G-J**). n = 3 independent experiments done in triplicate, error bars are +/- SEM. (OCR) was measured using the Seahorse Biosciences Mito Stress Test on an XFe96 analyzer. ATP production was calculated from the corresponding OCR traces in panels A and C for each condition. Spare respiratory capacity is the difference between maximal respiration or basal respiration. Oligomycin inhibits ATP synthase interrupting the electron transport chain ultimately disrupting mitochondrial respiration and ATP production. FCCP is an uncoupler, uncoupling ATP production from the electron transport chain. Rotenone (complex I inhibitor) and antimycin A (complex III inhibitor) completely inhibit mitochondrial respiration, only permitting nonmitochondrial respiration to persist.

Supplemental Tables

Accesion Number	Protein name	Average Fold change
Q9UKR5	Probable ergosterol biosynthetic protein 28	1.73124362
Q13907	Isopentenyl-diphosphate Delta-isomerase 1	1.43603743
Q05655	Protein kinase C delta type	1.43894964
Q9P2P6	StAR-related lipid transfer protein 9	1.36846482
Q5BKU6	Putative uncharacterized protein LOC641298	1.65583073
O00767	Acyl-CoA desaturase	1.52906982
O95864	Fatty acid desaturase 2	1.45157253
Q8TBQ9	Protein kish-A	1.60943599
Q5VTL8	Pre-mRNA-splicing factor 38B	1.49114395
Q9HBI1	Beta-parvin	1.58617857
Q8N4H5	Mitochondrial import receptor subunit TOM5 homolog	1.52365713
Q96S97	Myeloid-associated differentiation marker	1.35557214
Q15629	Translocating chain-associated membrane protein 1	1.54173542
A5PLL7	Transmembrane protein 189	1.51629998
Q8WWQ0	PH-interacting protein	1.30767666
O76062	Delta(14)-sterol reductase	1.99376933
Q3MIT2	Putative tRNA pseudouridine synthase Pus10	1.89802436
P03372	Estrogen receptor	1.70822558

O43929	Origin recognition complex subunit 4	1.49477837
Q15800	Methylsterol monooxygenase 1	1.68470794
P21397	Amine oxidase [flavin-containing] A	1.68237405
Q9Y241	HIG1 domain family member 1A	1.55562951
Q15904	V-type proton ATPase subunit S1	1.3252173
Q8NEW0	Zinc transporter 7	1.52678668
Q3B7T1	Erythroid differentiation-related factor 1	1.30583798
Q10981	Galactoside 2-alpha-L-fucosyltransferase 2	1.49225957
Q9NVV4	Poly(A) RNA polymerase, mitochondrial	1.40702841
Q13362	Serine/threonine-protein phosphatase 2A 56 kDa regulatory subunit gamma isoform	1.45966722
O43913	Origin recognition complex subunit 5	1.3459856
Q15392	Delta(24)-sterol reductase	1.45814413
O15551	Claudin-3	1.43943087
Q13610	Periodic tryptophan protein 1 homolog	1.43047919
Q9UKT8	F-box/WD repeat-containing protein 2	1.42849749
P51511	Matrix metalloproteinase-15	1.33742358
O14792	Heparan sulfate glucosamine 3-O-sulfotransferase 1	1.39813
Q9UII4	E3 ISG15--protein ligase HERC5	1.39813
Q7Z6B7	SLIT-ROBO Rho GTPase-activating protein 1	1.38847241
Q16880	2-hydroxyacylsphingosine 1-beta-galactosyltransferase	1.38751032

Q9NX62	Inositol monophosphatase 3	1.3387713
Q9BWM5	Zinc finger protein 416	1.38558816
Q9P0S9	Transmembrane protein 14C	1.36895257
Q8IYW2	Tetratricopeptide repeat protein 40	1.37983763
Q09161	Nuclear cap-binding protein subunit 1	1.32853936

Supplemental Table 4-1: iTRAQ hits significantly upregulated in CUL9 KO hPSCs. Average normalized fold change of Clone #1 and Clone #2 is shown for significantly altered hits in iPSC and NPC datasets. Listed proteins are significantly (B-H method) altered in one clone and have an average normalized fold change of $\geq$1.2 or $\leq$ 0.8. More information is included in the raw data available at Zenodo at 10.5281/zenodo.4340970.

Accesion Number	Protein name	Average Fold change
P46013	Antigen KI-67	0.769131844
P35556	Fibrillin-2	0.750413642
Q9BRA0	LSM domain-containing protein 1	0.716728439
Q8IUR6	CREB3 regulatory factor	0.677596583
P35754	Glutaredoxin-1	0.763702051
P30414	NK-tumor recognition protein	0.610261087
Q9H3H1	tRNA dimethylallyltransferase, mitochondrial	0.531631504
Q9UBV2	Protein sel-1 homolog 1	0.51423457

Supplemental Table 4-2: iTRAQ hits significantly downregulated in CUL9 KO hPSCs. Average normalized fold change of Clone #1 and Clone #2 is shown for significantly altered hits in iPSC and NPC datasets. Listed proteins are significantly (B-H method) altered in one clone and have an average normalized fold change of $\geq$1.2 or $\leq$ 0.8. More information is included in the raw data available at Zenodo at 10.5281/zenodo.4340970.

Accesion Number	Protein name	Average fold change
P06454	Prothymosin alpha	1.865343387
P22676	Calretinin	1.533276108
Q96FZ2	UPF0361 protein C3orf37	1.480866141
P04083	Annexin A1	1.213559203
Q9HBM0	Vezatin	1.253546028
Q9UII2	ATPase inhibitor, mitochondrial	1.276662668
Q15645	Pachytene checkpoint protein 2 homolog	1.204796874
P41225	Transcription factor SOX-3	1.33740947
Q9NVR2	Integrator complex subunit 10	1.321742589
P40692	DNA mismatch repair protein Mlh1	1.318996958
Q86UY8	5'-nucleotidase domain-containing protein 3	1.206290249
Q9HCN8	Stromal cell-derived factor 2-like protein 1	1.29454152
Q8N474	Secreted frizzled-related protein 1	1.276719184
O94985	Calsyntenin-1	1.27406708
Q8TD08	Mitogen-activated protein kinase 15	1.267021704
Q9BY49	Peroxisomal trans-2-enoyl-CoA reductase	1.253916463
Q96M93	Adenosine deaminase domain-containing protein 1	2.624976566
Q15345	Leucine-rich repeat-containing protein 41	2.255276848
P21980	Protein-glutamine gamma-glutamyltransferase 2	2.076716876
Q9BW91	ADP-ribose pyrophosphatase, mitochondrial	1.487771001

Q15398	Disks large-associated protein 5	1.638419219
P39880	Homeobox protein cut-like 1	1.581512045
Q9HCL0	Protocadherin-18	1.512887324
Q9NZM1	Myoferlin	1.306401551
Q96PQ0	VPS10 domain-containing receptor SorCS2	1.408641551
Q6ZS30	Neurobeachin-like protein 1	1.407665493
Q14CS0	UBX domain-containing protein 2B	1.379652127
P20700	Lamin-B1	1.236894044
Q8IWV8	E3 ubiquitin-protein ligase UBR2	1.327125259

Supplemental Table 4-3: iTRAQ hits significantly upregulated in CUL9 KO NPCs. Average normalized fold change of Clone #1 and Clone #2 is shown for significantly altered hits in iPSC and NPC datasets. Listed proteins are significantly altered (B-H method) in one clone and have an average normalized fold change of $\geq$1.2 or $\leq$ 0.8. More information is included in the raw data available at Zenodo at 10.5281/zenodo.4340970.

Accesion Number	Protein name	Average fold change
Q8N556	Actin filament-associated protein 1	0.795228428
O60524	Nuclear export mediator factor NEMF	0.78373685
Q15147	1-phosphatidylinositol 4,5-bisphosphate phosphodiesterase beta-4	0.783193794
Q86YV5	Tyrosine-protein kinase SgK223	0.780484149
O94875	Sorbin and SH3 domain-containing protein 2	0.762834098
Q9Y3Y2	Chromatin target of PRMT1 protein	0.771906013
Q8TBM8	DnaJ homolog subfamily B member 14	0.758615754
P35754	Glutaredoxin-1	0.662818451
Q16352	Alpha-internexin	0.727653838
P61812	Transforming growth factor beta-2	0.534937125
Q9Y216	Myotubularin-related protein 7	0.756968171
O75628	GTP-binding protein REM 1	0.741904062
Q9UBK7	Rab-like protein 2A	0.735248858
Q6FI13	Histone H2A type 2-A	0.734230293
P62750	60S ribosomal protein L23a	0.805924043
P82673	28S ribosomal protein S35, mitochondrial	0.722117016
Q9NTJ4	Alpha-mannosidase 2C1	0.721616656
Q5VW38	Protein GPR107	0.710696029
Q92804	TATA-binding protein-associated factor 2N	0.707746465
Q01844	RNA-binding protein EWS	0.791573732
P43003	Excitatory amino acid transporter 1	0.700426

Q92743	Serine protease HTRA1	0.699455676
O60942	mRNA-capping enzyme	0.698971019
Q5VU43	Myomegalin	0.772895589
Q07283	Trichohyalin	0.766397027
P52895	Aldo-keto reductase family 1 member C2	0.684112048
Q14146	Unhealthy ribosome biogenesis protein 2 homolog	0.679857619
Q92562	Polyphosphoinositide phosphatase	0.676098121
P78362	SRSF protein kinase 2	0.754539616
Q96RD7	Pannexin-1	0.630821853
Q8IZ07	Ankyrin repeat domain-containing protein 13A	0.603449331
P16401	Histone H1.5	0.747703307
P62861	40S ribosomal protein S30	0.690847608
Q96M89	Coiled-coil domain-containing protein 138	0.547262362
Q8WW27	Putative C->U-editing enzyme APOBEC-4	0.476419557
Q15751	Probable E3 ubiquitin-protein ligase HERC1	0.439917392
Q9BQG2	Peroxisomal NADH pyrophosphatase NUDT12	0.365085062
Q8TBQ9	Protein kish-A	0.285844917

Supplemental Table 4-4: iTRAQ hits significantly downregulated in CUL9 KO NPCs. Average normalized fold change of Clone #1 and Clone #2 is shown for significantly altered hits in iPSC and NPC datasets. Listed proteins are significantly (B-H method) altered in one clone and have an average normalized fold change of $\geq$1.2 or $\leq$ 0.8. More information is included in the raw data available at Zenodo at 10.5281/zenodo.4340970.

Chapter 5

FINAL DISCUSSION, CONCLUSION, AND FUTURE DIRECTIONS

Introduction

Post-translational modifications (PTMs) critically regulate protein function and turnover and are required for normal function of all cellular processes (Conibear, 2020). Ubiquitination is a well-studied PTM that canonically signals for proteasomal degradation (Hershko and Ciechanover, 1998; Swatek and Komander, 2016). However, ubiquitin can signal for more than just proteasomal degradation (Akutsu et al., 2016; French et al., 2021). One ubiquitin moiety contains seven lysine residues and each can be used to link another moiety forming a polyubiquitin chain. How moieties within a polyubiquitin chain are linked determine their effect on the substrate's outcome. For example, K63-linked ubiquitin chains signal for DNA repair (Akutsu et al., 2016; French et al., 2021). Ubiquitin moieties are added to a substrate through the sequential reactions of three key enzymes (Ye and Rape, 2009). An activating enzyme, known as the E1, forms a high energy thioester bond with ubiquitin in an ATP dependent manner. The E2 enzyme "attacks" this high energy bond promoting ubiquitin transfer to this conjugating enzyme. Finally, an E3 ligase directly or indirectly transfers ubiquitin to the targeted substrate.

Cullin Ring Ligases (CRLs) are the largest family of E3 ubiquitin ligases and their activity accounts for 20% of all ubiquitin-mediated proteasomal degradation (Baek et al., 2020b; Duda et al., 2011; Petroski and Deshaies, 2005; Zimmerman et al., 2010). There are eight cullin scaffolds, and each can form multiple complexes through recruitment of adapter proteins, substrate receptors and E2 enzymes (Lydeard et al., 2013; Zimmerman et al., 2010). The versatility of CRLs is what makes them so important – their activity caters to the everchanging needs of the cell. This adaptability is put the test during cell cycle where nearly 100,000 proteins need to be degraded at the right time in the right place for proper cell division to occur (Jang et al., 2020). Deletion of five of the eight cullins in mice is embryonic or neonatal lethal primarily due to cell cycle defects (Arai et al., 2003; Dealy et al., 1999; Liu et al., 2012; Singer et al., 1999; Wang et al., 1999; Zhu et al., 2016). However, embryonic deletion of CUL9, a non-canonical and poorly characterized cullin scaffold, produces viable pups and most studies report they have no apparent phenotype (Gama et al., 2014; Skaar et al., 2005, 2007). However, the effect of CUL9 deletion on mice remains inconclusive as one study reports that the mice develop widespread tumors throughout their body (Li et al., 2014; Pei et al., 2011). Despite this, there have not been reports of any

developmental defects related to CUL9 function. As I explored in **Chapter 1**, the combined challenges of characterizing the CUL9 KO mouse model and its unique and virtually uncharacterized biochemical structure and regulation have made its function, particularly during development, elusive.

Our laboratory identified the first CUL9 substrate, cytosolic cytochrome c (Gama et al., 2014). Following DNA damage, cytochrome c is released from the mitochondria into the cytosol to initiate the caspase cascade that ultimately executes apoptosis. We determined that CUL9 targets cytochrome c after its release from the mitochondria in post-mitotic neurons and neuroblastoma cells ultimately promoting their survival. We became interested in the role of CUL9 in developing neurons due to its high expression in the mammalian brain as well as its significant induction during hiPSC differentiation to neural progenitor cells and cortical neurons (Gama et al., 2014; Hollville et al., 2020; van de Leemput et al., 2014). Our lab also demonstrated that hiPSCs and hNPCs are more sensitive to apoptosis than their differentiated counterparts, so we suspected that CUL9 would have a unique role in these more undifferentiated cell types (Crowther et al., 2013; Dumitru et al., 2012). Additionally, we thought that a non-transformed human-cell derived model may provide greater insight into the function of this late evolutionary gene only present in vertebrates. Indeed, the work detailed in **Chapter 2** demonstrates that CUL9 deletion does not affect apoptotic sensitivity in hiPSCs nor the degradation of cytochrome c, however, it does affect neuronal differentiation of the cells, specifically the formation of neural rosettes, an *in vitro* model of neurulation. These results suggest that a human-cell derived model may be more suited to study CUL9 function during early development.

Although proteomics approaches have been unsuccessful in the past by our laboratory and others (Li et al., 2014; Skaar et al., 2005, 2007), we successfully employed proteomics approaches to identify CUL9 direct and indirect interacting proteins and substrates to understand the mechanism of this differentiation defect. In **Chapter 3**, I determined that CUL9 interacts with several subunits of the major cell cycle regulator APC/C in hiPSCs and hNPCs through LC-MS/MS analysis of immunoprecipitation of endogenous CUL9. I provided evidence that the CUL9-APC/C interaction may negatively regulate CUL9 protein levels in hiPSCs. While this provides insight into CUL9 regulation, it did not provide direct insight into CUL9 function as deletion and overexpression of CUL9 did not affect cell cycle progression in hiPSCs. In **Chapter 4**, I used quantitative proteomics to compare the proteome of CUL9 KO hiPSCs and hNPCs to that of WT cells to identify proteins significantly increased in CUL9 KO cells in hopes of finding a substrate. Although I did not identify a substrate, I found significantly altered levels of clusters of proteins

involved in fatty acid metabolism. However, I saw no changes in basal oxidative phosphorylation or ATP production. Interestingly though, clusters of proteins involved in mRNA regulation and processing were also identified in both proteomics analyses providing a promising future direction. In this chapter, I will discuss the open questions in the field my data has addressed, new questions based on my results, and our plans to address these gaps in knowledge about CUL9 function and its role in neurodevelopment and beyond.

Evolutionary insight into CUL9 function

The aim of my dissertation work was to determine if a human-cell derived model of early cell fate decisions during development could reveal the role of CUL9 in early development, and particularly neurodevelopment. We thought that a human model of CUL9 was critical in revealing its function as CUL9 is a late evolutionary gene and its characterization in mouse models has been particularly challenging. Cullins are ancient and their presence can be traced all the way back to the emergence of the first eukaryotes nearly 3 billion years ago (Marín, 2009). An evolutionary analysis revealed that there were three ancient cullins before the divergence of the first eukaryotes, unikonts (ancestors of animals and fungi) and bikonts (ancestors of plants) (Marín, 2009). These three cullins were dubbed *Cul*α, *Cul*β, and *Cul*γ. *Cul*α appears to the be the ancient ancestor of the mammalian *Cul1*, *Cul2*, *Cul5*, *Cul7*, and *Cul9* while *Cul3* is derived from *Cul*β and *Cul4a/b* from *Cul*γ. The researchers note that each of these groups often share common adapter proteins. CUL1 and CUL7 have been shown to associate with FBOX proteins, CUL3 canonically associates with BTB proteins, and CUL4 with DDB proteins (Lydeard et al., 2013). They suggest that though CUL2 and CUL5 do not associate with FBOX proteins, evidence of the emergence of these genes indicates they may have not have appeared until later evolutionarily (Marín, 2009). Critically, the researchers hypothesize that *Cul9* is a gene fusion between *Cul7* and an Ariadne containing ligase (Marín and Ferrús, 2002). *Cul7* is only about 250 base pairs away from the *Cul9* gene in both mice and humans, further supporting this hypothesis.

The evolutionary relationship between *Cul9*, *Cul7*, and *Cul1* should be further explored. Research efforts exploring the relationship between CUL9 and CUL7 have been done with varying results. One study demonstrates that though CUL9 and CUL7 heterodimerize, it is not required for their activity (Skaar et al., 2005, 2007). Another demonstrated that CUL9 and CUL7 regulate one another to mediate the degradation of SURVIVIN in cancer cells, functionally connecting the two proteins (Li et al., 2014; Pei et al., 2011). However, there is no evidence of a connection

between CUL1 and CUL9 enzymatic function. Both CUL1 and CUL7 complex with FBOX proteins. In our own proteomics analysis, we identified altered levels of F-box and WD-repeat domain-containing 2 (FBXW2) in CUL9 KO hiPSCs. FBXW2 acts as a substrate receptor for CUL1 containing SCF complexes (Miura et al., 1999; Wang et al., 2013a; Yang et al., 2005, 2019). Determining if this is protein acts as a substrate receptor for CUL9 could prove helpful in identifying its substrates. Additionally, CUL1 and CUL7 form a functional heterodimer through association with FBXW8 that is required for embryonic development in mice (Tsunematsu et al., 2006). Heterodimerization of CUL1 and CUL9 though FBOX binding is also plausible. It is possible that CUL9 function is difficult to identify because evolutionarily related cullins can compensate for its function, however, this would be an uncommon phenomenon. CRLs have been shown to have surprisingly little overlap in function, each seeming to have evolved to fulfill a specific cellular need (Emanuele et al., 2011). CUL9 seemingly has emerged to combine the functions of Cullin, RBR, and even HECT ligases, making its compensation challenging to reconcile. Both CUL7 and CUL9 contain a CPH domain (**Table 5-1**), also present in HERC2 connecting it to yet another ligase family. Our quantitative proteomics data also revealed the altered levels of two HECT E3 ligases, HERC2 and HERC5, in hiPSCs and hNPCs, respectively. The potential functional relationship between these ligases should be explored. CUL9 contains structural homology to several ligases and ligase subunits and its functional relationship to these ligases should be clarified. CUL9 has evolved to incorporate elements of all known ligase families, so a more holistic approach to its characterization and its relationship to other homologous ligases is needed.

We also identified that CUL9 interacts with several subunits of the E3 ubiquitin ligase complex APC/C, most specifically its subunit APC7 by LC-MS/MS analysis of immunoprecipitation of endogenous CUL9 protein. Like CUL9, APC7 is also a late evolutionary protein only present in vertebrates with a similarly elusive function. It's thought to be a duplication of another APC/C subunit, APC3 (Thornton et al., 2006). Both subunits contain the only common domain between some subunits in the APC/C: the tetratricopeptide repeat domain (TPR) (Chang et al., 2015, 2014; Vodermaier et al., 2003). The TPR domain of APC7 and APC3 bind to the IR tail of FZR1, CDC20, and APC10 (Vodermaier et al., 2003; Wendt et al., 2001). Specifically, deletion of the C-terminus IR-tail of APC10 prevents incorporation of APC3 into the complex (Wendt et al., 2001). Recent studies determined that APC7 is critical for interaction and recruitment of FZR1 specifically, while APC3 recruits CDC20 (Wild et al., 2018). APC7 and FZR1 knockdown caused a small, but significant increase in CUL9 protein levels, indicating that APC/C-FZR1 may target CUL9 through proteasomal mediated degradation. However, controversial studies claim that some APC/C

subunits can act independently of their association with the complex (Wang et al., 2019). It would be interesting to explore if APC7 and/or FZR1 could act as a substrate receptor for CUL9. CUL9 contains an APC10/DOC domain which, theoretically, APC7 should be able to interact with via its TPR domain. Additionally, Parkin, an RBR ligase highly homologous to CUL9, complexes with CDC20 and FZR1 independently of APC/C via its RBR domain – a specific point mutation in a serine residue whose phosphorylation is required for its activity prevents formation of the complex (Lee et al., 2015; Meza-Gutierrez et al., 2015). Site-directed point mutations of the APC10/DOC domain and RBR domain based on previous studies characterizing their protein-protein interactions should be performed in the homologous CUL9 domains to determine if APC7 and FZR1 could form a CUL9 containing CRL (**Table 5-1**). The simultaneous emergence of CUL9 and APC7 evolutionarily combined with our data demonstrating their interaction via immunoprecipitation and co-regulation via siRNA depletion suggests they may functionally interact. Overall, we believe that our newly developed hiPSC CUL9 KO model will be a key tool for understanding the evolutionary factors driving the emergence of the *Cul9* gene in vertebrates.

CUL9 in early neurodevelopment

hiPSCs are also an attractive model for studying CUL9 function during early mammalian development due to their pluripotency or ability to differentiate into virtually any cell type (De Los Angeles et al., 2015). Reports of tissue specific expression of CUL9 in mouse and human samples are conflicting. One of the very first reports on CUL9 (previously H7-AP1) performed a Northern blot analysis measuring the RNA levels of CUL9 in various tissues in the mouse (Moynihan et al., 1999). They determined that CUL9 RNA expression is highest in the brain and the testis. A recent analysis of mRNA and protein levels of CUL9 in mouse tissues demonstrates that CUL9 is specifically enriched in the cerebral cortex and cerebellum (**Figure 5-1**). RNA levels of CUL9 also increase during hiPSC cortical differentiation as determined by RNA-seq (van de Leemput et al., 2014), and we demonstrated that CUL9 protein levels drastically increase as well. Our study suggests that CUL9 is required for human neuronal differentiation, a phenotype that has not been reported in CUL9 KO mice (Ortolano et al., 2021). However, no studies have thoroughly analyzed neurodevelopment in CUL9 KO mice since they have no obvious physical neurological deformities (Gama et al., 2014; Hollville et al., 2020; Li et al., 2014; Pei et al., 2011; Skaar et al., 2005, 2007). Subtle neurodevelopmental defects can cause cognitive defects though (Dong et al., 2020; Kuczera et al., 2011; Li et al., 2008; Pick et al., 2013). The altered neural rosette formation we observed in CUL9 KO and KD cells was subtle and even differences between neuronal markers

like TUBB3 were only slightly decreased (Ortolano et al., 2021). In-depth analysis of neurobehavioral deficits like increased anxiety, altered social interactions, and fear-extinction should be done to clarify the mice truly have no neurodevelopmental defects.

Conversely, APC7 levels decrease over the course of hiPSC cortical differentiation (van de Leemput et al., 2014). It would be exciting to investigate the potential role of the CUL9-APC7 interaction over the course of neuronal induction. Although CUL9 and APC7 co-immunoprecipitate in NSCs as demonstrated by immunoblotting and LC-MS/MS analysis, our preliminary data indicates that depletion of APC7 does not cause a significant increase in CUL9 protein levels (**Figure 5-2**). Could CUL9 regulate APC7 in NPCs? How does the change in expression of these proteins affect the potential formation and function of a CUL9-APC7 complex? Additionally, heterozygote FZR1 KO mice display defective fear extinction further emphasizing the importance of characterizing CUL9 KO mouse behavior (Kuczera et al., 2011; Li et al., 2008). APC7 KO mice have no apparent phenotypes and cell cycle is unaltered in these mice (Wild et al., 2018). Behavioral characterization of these mice could also provide insight into the importance of the CUL9-APC7 interaction during cortical differentiation.

Examination of other specialized neuronal cell types in CUL9 KO hiPSCs should be conducted as well. The behavioral phenotypes observed in heterozygote FZR1 KO mice are not the result of altered cortical differentiation, but disorganization in the hypothalamus. Protocols for differentiation of hypothalamic like neurons are available (Wang et al., 2015). Differentiation to this specific neuronal lineage and others may provide further insight into CUL9 function during neuronal development. An excellent start would be to determine the multipotent capacity of CUL9 KO NSCs by differentiation to astrocytes, neurons, and oligodendrocytes. Additionally, our study analyzes a non-specific population of neural precursor cells. A recent study determined that there are at least nine genetically distinct progenitor populations within the human cortex (Eze et al., 2021). Sorting the hiPSC-derived precursor population by genetic signature to isolate specific progenitor populations may identify more substantial neuronal differentiation defects in CUL9 KO cells. This experiment could be complemented by performing single cell sequencing from the CUL9 KO mouse at different stages of development to determine if there are significant changes in the expression or functionality of a specific precursor or neuronal population in the mouse brain to determine if a specific subset of neurons or neural precursors are affected. Additionally, this could address the role of CUL9 in human-specific cortical development, which is more complex than that of mice (Arlotta and Paşca, 2019; Molnár et al., 2019). For example, humans have an additional radial glia population known as outer radial glia which have been characterized using

human brain organoids (Liu et al., 2017a; Pollen et al., 2015). Developing CUL9 KO human brain organoids would allow us to isolate these specific cell populations and examine the holistic effect of CUL9 deletion on human brain development. It would be exciting to perform these differentiations alongside iPSCs reprogrammed from fibroblasts obtained from patients with neurodevelopmental disorders like autism, especially considering the role of other CRLs in these diseases. (Fischer et al., 2020; Liu et al., 2020)

If CUL9 function has a greater impact on aging neuronal cells, or even the later stages of development, our CUL9 KO hiPSC model would be ineffective at identifying CUL9 function in the brain. CUL9 mRNA and protein expression continue to increase for more than 70 days during hiPSC cortical differentiation and its levels increase over time in mouse brains, specifically in parasympathetic neurons (Gama et al., 2014; Hollville et al., 2020; van de Leemput et al., 2014). An organoid cultured for 60 days is only representative of a developing brain at about four months post-conception (Kelava and Lancaster, 2016). Although longer time in culture could promote further development (Gordon et al., 2021), this is still limited by the lack of vascularization, which is still in its infancy (Cakir et al., 2019). Some have successfully modeled neurodegenerative disorders in human brain organoids . One group developed a 3D neuronal cell culture model by overexpressing two key proteins involved in Alzheimer's disease progression. This model recapitulated protein aggregation in the neurons and increased levels of tangled hyperphosphorylated tau protein observed in patients more closely than mouse models (Kim et al., 2015). Mouse models of neurodegenerative disease have limitations. Deletion of the most mutated gene in Parkinson's patients, *Parkin*, in mice does not elicit a Parkinson's-like behavioral phenotype or the loss of dopaminergic neurons characteristic of the disease unless the mice are exposed to mitotic stress (Dawson et al., 2010; Hollville et al., 2020). A recent study demonstrated that though CUL9 is highly homologous to Parkin, co-deletion in mice does not exacerbate the phenotype (Hollville et al., 2020). However, the authors suggest that mitotic stress or another form of stress may need to be applied to observe a behavioral phenotype in CUL9 KO mice. Regardless, if a human-derived model of aging or late-stage development is needed to reveal CUL9 function in the brain, we will have to wait for more effective tools to emerge.

CUL9 function likely varies across cell types

All currently reported CUL9 substrates seem cell-type specific. Both identified substrates, cytochrome c and SURVIVIN, promote survival in cancer cells and post-mitotic neurons, both of

which have increased resistance to apoptosis (Gama et al., 2014; Li et al., 2014). Less differentiated cells like hESCs and hNSCs, however, are more sensitive to apoptosis (Crowther et al., 2013; Dumitru et al., 2012). We did not identify cytochrome c or SURVIVIN as CUL9 interacting proteins in either our LC-MS/MS analysis of immunoprecipitation of endogenous CUL9 or their altered levels in CUL9 KO hiPSCs, hNSCs, or hNPCs by quantitative proteomic analysis (Ortolano et al., 2021). Moreover, cytochrome c degradation in the cytosol is not affected as would be expected in CUL9 KO hiPSCs treated with the DNA damaging agent Etoposide and the proteasome inhibitor Bortezomib, further indicating that if CUL9 plays a role in regulating survival of these cells, it is unique from its previously described functions. In fact, our data suggests that cytochrome c degradation may be differentially regulated all together. Etoposide treatment in WT hiPSCs also treated with a caspase inhibitor show accumulation of cytochrome c in the cytosol. Although the addition of bortezomib results in increased levels of cytochrome c in the cytosol, there are also increased levels of cytochrome c still localized to the mitochondria indicating that proteasomal degradation may be required for its release from the mitochondria during apoptosis. In CUL9 KO cells, we observed no significant change in cytosolic cytochrome c levels following etoposide treatment, but we did see decreased levels of cytochrome c localized to the mitochondria and the cytosol following additional treatment with bortezomib. This suggests that cytochrome c protein levels in and outside of mitochondria may be regulated in a non-proteasomal dependent manner like autophagy (Dikic and Elazar, 2018). Additionally, CUL9 may inhibit this degradation rather than promote it as observed in more differentiated cell types. Whether this holds true in other progenitor cell types should be tested.

We plan to leverage our hiPSC KO model to characterize CUL9 function in a variety of tissues and their progenitors. Outside of the mouse KO model, most CUL9 functional studies have been conducted in transformed or cancer cell lines due to its reported role in regulating p53 localization in cancer cells (Li and Xiong, 2017a; Li et al., 2014; Nikolaev et al., 2003). While others have reported that CUL9 affects cell proliferation and cell cycle progression, CUL9 KO and overexpression hiPSCs had a normal cell cycle profile indicating CUL9 likely has a cell cycle independent role. We can examine the effect of CUL9 deletion and overexpression in a variety of cell types and determine any effect it may have on early human development. Determining if our KO and overexpression lines are capable of differentiation to the endoderm, ectoderm, and mesoderm lineages (trilineage differentiation) is an important first step. We could also examine the effect of CUL9 deletion or overexpression on a 3D model of gastrulation known as a “gastruloid” which models a human embryo around 18 to 21 days old complete with distinct

development of the three lineages (Beccari et al., 2018; Brink et al., 2014; Moris et al., 2020). It would also be exciting to leverage the newly developed “blastoid” model which recapitulates early human blastocyst development in a dish (Liu et al., 2021; Yu et al., 2021). Because CUL9 KO mice are viable, detailed analysis of embryo histology has never been conducted. Additionally, mouse and human blastocyst development have major differences (Rossant and Tam, 2017), so the effect of CUL9 deletion on this early stage of development may provide insight not only into the holistic function CUL9 has in early development in general, but direct future studies on the specific cell types or tissues altered CUL9 function may affect.

CUL9 mRNA and protein levels are highly expressed in the testis of mice and humans (Moynihan et al., 1999; Uhlén et al., 2015). Additionally, the highest rate of CUL9 mutation in cancer, over 60%, is in human testicular cancer samples or cell lines (Tate et al., 2019). Despite this, there were no reported reproductive issues in CUL9 KO mice and mice were born at the expected mendelian ratios. Additionally, the study reporting widespread tumor formation in CUL9 KO mice did not report tumors in the testis (Pei et al., 2011). This, again, could indicate a distinction between CUL9 function in mice and humans. Researchers have found that human testicular development, especially during puberty is distinct from that of mice (Guo et al., 2020). Although we cannot model late stages of development that occur during puberty, we can model the early stages using hiPSC-derived models. Protocols for differentiation to male germ cells including spermatids, a cell type where CUL9 is highly expressed (Uhlén et al., 2015), are readily available (Easley et al., 2012). Additionally, testicular organoid based models have been developed which could be used to examine the effects of CUL9 deletion on testis organ development. It would be exciting to do these experiments alongside a hiPSC KO model of a member of the MAGE family of E3 ubiquitin ligases (Gee et al., 2020). This family of ligases has well-defined roles in testicular development and emerging roles in cell development making them an attractive complement and positive control for our experiments (Gee et al., 2020). To examine the role of CUL9 in testicular cancer, we could develop CUL9 KO and overexpression models in testicular cancer cell lines to determine their effect. Additionally, we could analyze immunoprecipitation of CUL9 endogenous protein using LC-MS/MS as we did in hiPSCs and hNSCs to identify novel CUL9 interacting proteins. A genome wide association study of CUL9 mutations may also provide insight into the effect of CUL9 mutation on the testis as well as other organisms – this would be well complemented by a phenotype wide association study.

However, one caveat to using our CUL9 KO iPSC line is the variability between our CUL9 KO clones. Although both clones had altered lumen size compared to control, one was

significantly increased and the other decreased. Additionally, there were significant differences in the proteins identified by iTRAQ between the clones. The source of this variability should be identified before moving forward with analyzing differentiation efficiency in these clones. We are currently performing whole exome sequencing in these lines to determine if there are non-specific mutations contributing to these effects. Additionally, compensation by other ligases like CUL7 should be investigated. The HERC ligases HERC2 and HERC5 were also identified in iTRAQ and should therefore also be investigated. Alternatively, this variability could be indicative that a consistent phenotype in these cells requires exposure to a stress like DNA damage. Proteomic and phenotypic analysis of these clones in different environmental conditions could be key to finding a consistent phenotype in CUL9 KO cells and mice.

CUL9 as a dynamic regulator of gene expression during differentiation

The cell-specific roles of CUL9 indicates that CUL9 may have a more dynamic role during cellular differentiation than we realized. The combined hits from our LC-MS/MS analysis and proteomics analysis indicate that CUL9 interacts with proteins involved every stage of gene expression including transcription, mRNA processing and export, and translation in hiPSCs and hNPCs (**Table 5-2**) (Ortolano et al., 2021). Genes involved in transcription and RNA processing are upregulated in CUL9 KO hiPSCs, however, they are downregulated in hNPCs (**Table 5-2**). This trend further supports the idea that CUL9 plays specific roles in different cell types and that it may play a dynamic role during cellular differentiation. In fact, this “transcriptional switch” falls in line with previous observations about the genomic and transcriptional changes during hiPSC differentiation to hNPCs (Bax et al., 2019; Bi et al., 2019; Chanarat and Mishra, 2018; Saez et al., 2018; Tee and Reinberg, 2014). Pluripotent stem cells are constantly balancing their self-renewal capacity with their dynamic ability to respond to external cues and differentiate to a new cell type with a different transcriptional landscape. Stem cells are in a constant hypertranscriptional state – their total RNA and mRNA content is double that of NSCs (Efroni et al., 2008; Kim et al., 2017; Tee and Reinberg, 2014). Chromatin is also less condensed, loosely binding chromatin bound proteins like histones, a binding state unique to pluripotent cells known as “hyperdynamic binding” (Meshorer et al., 2006). As hPSCs differentiate to NPCs, their chromatin condenses and binding to associated proteins becomes stronger (Meshorer et al., 2006). Stem cells also have unique histone modifications, the most distinctive is bivalent genes. These contain both H3 lysine 27 methylation and H3 lysine 4 methylation, which simultaneously prevents gene transcription while

poising them for activation upon differentiation (Bernstein et al., 2006). These bivalent modifications are also present in progenitor cells, including NPCs.

Nucleosomes are composed of four histones: H2A, H2B, H3, and H4 (Cutter and Hayes, 2015). Two of each of the core histones come together to form an octamer that DNA wraps around, compacting it. Each octamer is then connected by a linker histone known as H1. Our LC-MS/MS analysis of CUL9 immunoprecipitation in hESCs identified a subunit of H4 as a CUL9 interacting protein (**Table 5-2**). Interestingly, we identified a subunit of H2A and the linker H1 decreased in CUL9 KO hNPCs as determined by iTRAQ (**Table 5-2**). We could analyze the histone modifications present in CUL9 KO hiPSCs and hNPCs using mass spectrometry (Völker-Albert et al., 2018). This would be an important experiment to do also considering the number of fatty acid metabolic proteins significantly altered in CUL9 KO cells (**Chapter 4**). The rates of fatty acid synthesis and fatty acid oxidation impact acetylation of proteins in other pathways. This contributes to transcriptional regulation, particularly in relationship to histone acetylation levels (Galdieri and Vancura, 2012; McDonnell et al., 2016; Morrish et al., 2010). Chromatin immunoprecipitation sequencing (ChIPSeq) analysis of pluripotent and differentiation specific transcription factors in CUL9 KO cells would also be interesting (Furey, 2012). Although we did not see consistent differences in expression of neuronal or pluripotent markers, we did see more variable protein expression in CUL9 KO cells. ChIPSeq analysis of chromatin bound OCT4 or PAX6 may provide insight into CUL9 interaction with histones and provide a mechanistic explanation for the variability in gene expression we observed in CUL9 KO cells.

We identified several components of the spliceosome and related RNA helicases in our mass spectrometric analysis of hiPSC CUL9 immunoprecipitation (**Table 5-2**). The spliceosome is a large molecular machine composed of nearly 100 proteins and five small nuclear RNAs that remove introns from mRNA precursors (Wilkinson et al., 2020). The small nuclear RNAs complex with proteins to form the small nuclear ribonucleoproteins (snRPs) U1, U2, U4, U5, and U6. The spliceosome assembles on mRNA precursors through the recognition of specific sequences marking the 5’ and 3’ ends of introns and intron excision is ultimately catalyzed by the U6/U2 snRNP complex (Matera and Wang, 2014). RNA helicases are required for spliceosome function and critically alter the structure of snRNP complexes throughout the process. Interestingly, spliceosome function is elevated in pluripotent stem cells, and some components are overexpressed indicating the complex has a unique assembly (Kim et al., 2017). There are even specific subunits of the complex that are required for proper splicing of the mRNA transcripts of key pluripotency genes like *Oct4* (Lu et al., 2013). Characterization of CUL9 interaction with the

spliceosome should be explored. Specifically, it would be interesting to determine if CUL9 ubiquitinates any of the components identified in the immunoprecipitation. The addition of K63-linked ubiquitin chains to snRNPs can affect alternative splicing and has even been shown to regulate stem cell self-renewal (Chanarat and Mishra, 2018). One of the RNA helicases we identified, DDX39A, has been shown to be ubiquitinated in human cells, but the mechanism is not known (Chanarat and Mishra, 2018; Sugiura et al., 2007). *De novo* mutations of another identified RNA helicase, DDX3X, result in cortical malformations that cause symptoms like intellectual disabilities and seizures (Lennox et al., 2020). Exploring the dynamic regulation of the spliceosome by CUL9 during cortical differentiation could provide insight into the mechanism behind the abnormalities in neural rosette formation we observed.

We also identified a variety of RNA binding proteins through quantitative proteomics analysis of CUL9 KO iPSC and NPCs (**Table 5-2**). Notably, RNA binding proteins identified in CUL9 KO NPCs were all decreased compared to WT. Characterizing the connecting between CUL9 and the variety of RNA binding proteins we identified could provide insight into CUL9 function during cortical differentiation, and specifically in NPCs. Studies have demonstrated that RPBs are highly expressed in embryonic stem cells to support hyperactive transcription observed in the highly proliferative cell type (Bi et al., 2019; Ye and Blelloch, 2014). Expression of several RBPs decreases during differentiation, and depletion of RBPs promotes expression of differentiation associated genes (Ye and Blelloch, 2014). Additionally, the altered levels of fatty acid metabolic enzymes we observed in hiPSCs (**Chapter 4**) could contribute to regulation of RNA processing. Metabolic enzymes often moonlight as RNA binding proteins (RBPs) (Castello et al., 2015). In fact, the extensively studied glycolytic enzyme GAPDH has been shown to directly bind RNA (Rodríguez-Pascual et al., 2008; Singh and Green, 1993). As PSCs are highly transcriptionally active to support their rapid proliferation, it comes as no surprise that RBPs are highly expressed in PSCs; one study demonstrated that significant upregulation of RPB expression is observed within three days of MEF reprogramming (Kwon et al., 2013). Considering the metabolic switches engaged during stem cell differentiation, it is no surprise crosstalk between RPB function and fatty acid metabolism has been observed. Fatty acid synthase (FASN) has even been identified as a RBP by RNA interactome studies (Castello et al., 2015). Crosstalk has also been demonstrated in neural progenitors. For example, the RPB Musashi-1 (MSI1), a common marker of neural progenitor cells, is inhibited by monounsaturated fatty acids (Clingman et al., 2014). Outside of exploring the connection between RNA processing regulation and fatty acid metabolism, it will be important to determine if fatty acid metabolism specifically is altered in the

KO cells via Seahorse since we only analyzed oxidative phosphorylation and ATP production in these cells. We also identified two mitochondrial specific proteins, one which is a component of the mitochondrial proteasome (**Table 5-2**). It would be interesting to investigate CUL9's role in mitochondrial transcription as well.

Revealing CUL9 structure and function requires in-depth biochemical characterization

A major challenge to identifying CUL9 substrates is that its structure and the functionality of its domains are unknown. Ideally, CUL9 protein would be purified, crystalized, and imaged via cryogenic electron microscopy to determine its protein structure. Structural analysis of CUL9 could provide insight into its ubiquitination mechanism if CUL9 could be isolated in complex with its adapter proteins and substrate. There are major questions as to how CUL9 domains interact with one another not only to position a substrate for ubiquitination, but how its catalytic domains (CULLIN and RBR) are activated. Since CUL9 is a member of the Ariadne family of RBR ligases, it could, theoretically, promote ubiquitination activity via its CULLIN domain through interaction between the CULLIN and RBR domain. Additionally, the CTD, where an Ariadne domain would likely be present based on homology with other Ariadne RBRs, could bind to and inhibit the RBR domain. How these domains interact with one another and regulate ubiquitination of CUL9 substrates and its autoubiquitination can only be addressed by detailed structural studies. In fact, some of suggested that analysis of CUL9 structure could reveal an entirely new family of ligases (Baek, 2016). However, CUL9 is an extremely large protein (over 250 kDa) and it has not been successfully isolated from cells with enough purity to analyze its structure (Gama et al., 2014; Li et al., 2014; Skaar et al., 2005, 2007). Another strategy for analyzing CUL9 structure is to biochemically characterize its domains by validating their predicted functions by introducing truncations and site directed mutations via CRISPR knock-in protocols or expression of lentiviral CUL9-FLAG constructs utilized to analyze CUL9's role in cell cycle in **Chapter 3** (**Table 5-1**).

The first challenge to characterizing CUL9 ubiquitin activity is the limited number of identified substrate and their cell specificity. Therefore, characterization of CUL9 domains would need to be conducted by measuring ubiquitination levels of a known substrate in a relevant cell type. Measuring cytochrome c ubiquitination levels in the glioblastoma U87-MG cell line via Western blotting as a readout would likely be the best option (Gama et al., 2014). U87-MG cells are transfectable and amenable to CRISPR directed knock-in mutations. Although deletions of CUL9 domains may be a good preliminary strategy, large deletions can affect protein structure

and affect its function beyond the contribution of the domain, so site-directed mutagenesis, if possible, would be the best strategy. The first goal of site directed mutation would be to generate a mutant version of CUL9 without ligase activity. As CUL9 has two domains with potential ubiquitin ligase activity, the RBR and CULLIN domain, I would make a construct with an alanine mutation to key residues in each. The catalytic cysteine in the RING2 domain of the RBR that is required for ubiquitin transfer should be mutated to an alanine. Since the catalytic cysteine is not known, performing an RBR truncation initially, and then mutating all cysteines in the RING2 domain would be the best strategy (**Table 5-1**). In the CULLIN domain, the conserved lysine residue that is modified by the ubiquitin-like protein NEDD8 should be mutated to an arginine – mutation to arginine better conserves the structure of the cullin than mutation to alanine (Sui et al., 2015). K1886 is the predicted neddylation site of CUL9 based on homology with other cullins, however, a truncation, followed by site-directed mutations of all lysine residues to delineate which is modified by NEDD8 would be the best approach. Deletion of the CTD, where an Ariadne domain is likely present, could also provide insight into CUL9 ubiquitination activity (**Table 5-1**). The Ariadne domain can inhibit the RBR domain by blocking the catalytic cysteine in RBR2. However, it can also activate the Cullin domain, so how the CTD regulates CUL9 activity is important. Measuring levels of CUL9 ubiquitination as a readout of autoubiquitination may provide a good readout for its activity as well.

Mutations in the NTDs, where CUL9 is most likely to recruit adapters and substrate receptors, could provide insight into the composition of CRL complexes. Alanine mutation of Q417 and F419 have already been shown to prevent CUL9 association with p53 (Li and Xiong, 2017b; Pei et al., 2011). Determining if these mutations prevent co-immunoprecipitation of cytochrome c and CUL9 or levels of ubiquitinated cytochrome c would determine if the CRL complex targeting cytochrome c recruits its substrate receptor to this domain. Site directed mutagenesis in the serine residues of APC10/DOC domain should also be done – mutation of a conserved serine residue in all APC10/DOC domains renders the APC10 subunit inactive in yeast (Grossberger et al., 1999). Quantitative proteomic analysis comparing CUL9 endogenous immunoprecipitation between WT CUL9 and a mutant form of CUL9 that reduces cytochrome c ubiquitination or CUL9 autoubiquitination could reveal CUL9 adapter proteins and help elucidate the first CRL complex.

Although we were able to identify common sets of proteins that were significantly altered by CUL9 deletion in KO hiPSCs and hNPCs, the fold change differences between CUL9 KO and WT were small and we were unable to validate the changes in several identified proteins by Western blot. More sensitive quantitative proteomic approaches may be more effective at

identifying a CUL9 substrate. SILAC has emerged as a powerful application of quantitative proteomics (Chen et al., 2015; Ong et al., 2002, 2003). By simply culturing cells in media containing labeled amino acids containing heavy isotopes or normal (“light”) isotopes, one can quantitatively compare levels of various proteins between experimental conditions in one mass spectrometry analysis (Ong et al., 2002). Not only does this significantly limit the time spent on analysis and experiments, it almost eliminates nonspecific background often observed in protein interaction studies, increasing detection sensitivity (Chen et al., 2015). Using SILAC to compare the proteomes of CUL9 KO and WT cells may provide the sensitivity needed to identify true substrates. To further increase the sensitivity of this analysis, di-gly immunoprecipitation could be performed (Fulzele and Bennett, 2018). Briefly, after trypsinization, ubiquitin polypeptides bound to substrates will leave a characteristic diglycine (diGLY)-modified lysine residue that can be recognized by an antibody. Immunoprecipitation with this specific antibody enriches the number of ubiquitin modified proteins for analysis increasing the specificity of the analysis for analyzing true substrates and not just proteins with altered levels.

There are other effective tools that could be used to identify CUL9 substrates. It can be challenging to identify substrates since the interaction between a substrate and a ligase is transient and unstable. Researchers developed tools to stabilize these interactions improving the chances of catching a ligase bound to its substrate (Kliza and Husnjak, 2020). One method known as proximity-dependent biotin labeling (BioID) could be useful for identifying CUL9 substrates since information about adapter proteins and the type of ubiquitin chains the ligase catalyzes is not needed (Coyaud et al., 2015; Roux et al., 2012). This method was successfully used to identify nearly 50 new substrates of an SCF complex (Coyaud et al., 2015). CUL9 would be fused to a biotin ligase, BirA, which would biotinylate all proteins within 10nm of CUL9. Biotinylated proteins would then be purified and analyzed by mass spectrometry. In the end, understanding CUL9 function requires a greater understanding of its biochemical properties to provide direction in identifying substrates.

Figures

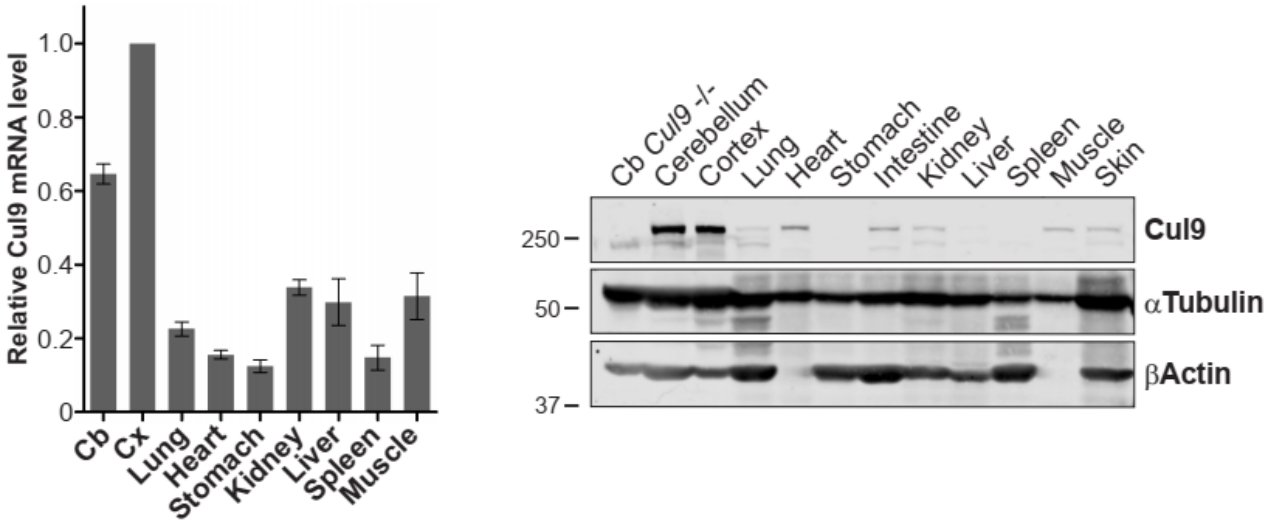

Figure 5-1. CUL9 mRNA and protein expression in mouse tissues.

Data provided by Mohanish Deshmukh laboratory at the University of North Carolina, Chapel Hill Neuroscience Center. Samples were collected from indicated tissues of a wild-type mouse. RNA and protein lysate were extracted and mRNA and protein levels of CUL9 were measured by RT-qPCR and Western blot, respectively.

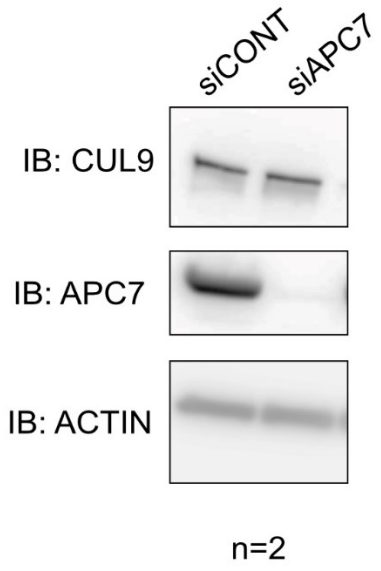

Figure 5-2. APC7 depletion in hPSC-derived hNSCs does not affect CUL9 protein levels.

siRNA mediated knockdown of APC7 does not alter CUL9 protein levels in hNSCs levels as determined by Western blotting. n=2

Tables

Mutant	Amino Acids	Point mutations	Domain's Reported Function	References
FL CUL9	---	---	Promotes survival in post-mitotic neurons and cancer cells	*Gama et al. (2014). Sci. Signal.; Li et al. (2014). Mol. Cell.*
CUL9ΔCPH	363-469	**Q417A**, **F419A**	Mediates interaction of CUL9 and p53 in the cytoplasm of unstressed human cells	*Nikolaev et al. (2003). Cell; Kaustov et al. (2007). J. of Biol. Chem.; Pei et al. (2011) Cancer Res.*
CUL9ΔAPC10/ DOC	1167-1297	S1176F, S1177F, S1183F, S1196F, S1199F, S1202F, S1224F, S1227F, S1228F, S1241F, S1243F, S1257F, S1259F	Homologous to single domain protein APC10; found in proteins containing ubiquitination domains such as RING and HECT	*Grossberger et al. (1999). J. of Biol. Chem.; Hwang et al. 1997; Grossberger et al. (1999)*
CUL9ΔRBR	1953-2236	C2154A, C2160A, C2166A, C2171A, C2177A, C2181A, C2184A, C2189A, C2192A	Mediates protein interactions and ubiquitin ligase activity	*Eisenhaber et al. (2007). Genome Biol.*
CUL9ΔAriadne	2300-2517	---	Present in other RBR ligases like TRIAD1 and HHARI; Ubiquitin activity of domain containing proteins is activated by binding to neddylated CRL; Domain autoinhibits activity of RBR ligase domain	*Duda et al. (2013) Structure; Dove et al (2018) J. Mol. Biol; Marine and Ferris (2002) Molecular Biology and Evolution*
CUL9ΔCULLIN	1697-1785	K1881R, K1868R, K1859R, **K1886R**, K1795, K1790R, K1766R	Scaffolding domain common among all CRLs; associates with catalytic RING subunit; modified by ubiquitin like molecule NEDD8 at conserved lysine residue	*Duda et al. (2011). Curr. Opinion in Struc. Biol.; Sakata et al. (2007). Nat Struct.*

Table 5-1. Planned CUL9 truncations and point mutations

Detailed information about the known and predicted functions of each CUL9 domain and the associated references are listed. Additionally, proposed truncations and point mutations to analyze the function of each domain are included. Bolded point mutations indicate these are predicted to or demonstrated to render the domain non-functional. Specifically, the K1886R mutation is the predicted lysine modified by NEDD8 based on homology with the neddylation recognition sites on other cullins (Skaar et al., 2007). Q417A and F419A in the CPH domain disrupt CUL9-p53 binding in mice (Pei et al., 2011).

Gene		Description	Present in hESC CUL9 IP	iTRAQ: iPSC fold change	iTRAQ: NPC fold change
DDX3X	DEAD-Box Helicase 3 X-Linked	Member of DEAD-Box domain containing family of RNA helicases	Yes	-	-
DDX39A	DEAD-Box Helicase 39A	Member of DEAD-Box domain containing family of RNA helicases	Yes	-	-
EIF4A3	Eukaryotic Translation Initiation Factor 4A3; DEAD-Box protein 48	Member of DEAD-Box domain containing family of RNA helicases	Yes	-	-
PRPF8	Pre-MRNA Processing Factor 8	Component of the splicesome	Yes	-	-
SNRNP200	Small Nuclear Ribonucleoprotein U5 Subunit 200	Component of the splicesome; Member of DEXH-box family RNA helicases	Yes	-	-
DHX9	DExH-Box Helicase 9	Member of DEXH-box family RNA helicases	Yes	-	-
EFTUD2	Elongation Factor Tu GTP Binding Domain Containing 2	GTPase component of the splicesome	Yes	-	-

NUP153	Nuclear Pore Complex Protein Nup153	Contains an RNA binding domain; regulates transport of macromolecules between nucleus and cytosol	Yes	-	-
PABPC4	Poly(A) Binding Protein Cytoplasmic 4	Binds to mRNA poly(A) tail; regulates protein stability	Yes	-	-
PUS10	TRNA Pseudouridine Synthase Pus10	Post-transcriptionally modifies mRNA; RNA chaperone; splicesome biogenesis	No	1.8980244	-
NCBP1	Nuclear cap binding protein subunit 1	Component of cap-binding complex that binds 5' cap of pre-mRNA in the nucleus	No	1.3285394	-
TAF15	TATA binding protein association factor 2N	Component of the transcription initiation factor complex involved in RNA polymerase II mediated transcription	No	-	0.707746
EWSR1	EWS RNA binding protein 1	RNA binding protein involved in many cellular processes	No	-	0.791574

		including pre-mRNA processing			
RNGTT	mRNA capping enxyme	Catalyzes the formation of the mRNA 5' cap	No	-	0.698971
H4C6	H4 clustered histone 6	Histone component	Yes	-	-
H2AC18	H2A clustered histone 18	Histone component	No	-	0.73423
H1-5	H1.5 Linker Histone, Cluster Member	Histone component	No	-	0.747703
ORC4	Origin recognition complex subunit 4	Origin of recognition complex comonent that initiates DNA replication	No	1.4947784	-
ORC5	Origin recognition complex subunit 5	Origin of recognition complex comonent that initiates DNA replication	No	1.3459856	-
DNAJB14	DnaJ Heat Shock Protein Family (Hsp40) Member B14	Protein chaperone that promotes protein folding	No	-	0.758616
RPL23A	60S ribosomal protein L23a	Component of the 60S subunit of the ribosome	No	-	0.805924

FAU	FAU Ubiquitin Like And Ribosomal Protein S30 Fusion	Fusion protein consisting of the ubiquitin-like protein FUBI at the N-terminus and ribosomal protein S30 at the C-terminus	No	-	0.690848
TRIT1	tRNA mitochondria dimethyltransferase	Critically modifies cytoplasmic and mitochondrial tRNAs for translation	No	0.5316315	-
MRPS28	Mitochondrial Ribosomal Protein S28	28S subunit of the mitochondrial ribosome	No	-	0.722117

Table 5 1. LC-MS/MS and iTRAQ hits related to gene expression.

Select proteins of interest identified by LC-MS/MS analysis of CUL9 immunoprecipitation from hESCs and iTRAQ analysis of CUL9 KO hiPSCs and hNPCs. All proteins are involved in transcription, mRNA processing, translation, or DNA replication. Brief description of function and fold change of CUL9 KO cells compared to WT are included.

Appendix

METHODS

Cell culture

Human embryonic stem cell lines H9 (WA09) were obtained from WiCell Research Institute (Wisconsin). Human induced pluripotent stem cell line (GM25256) was obtained from Coriell. Cells were seeded as undifferentiated colonies on plates coated with Matrigel (Corning), maintained at 37°C and 5% CO2, and passaged as needed using Gentle Cell Dissociation Reagent (Stem Cell technologies). H9s were fed daily with mTeSR (Stem Cell Technologies), and iPSCs were fed daily with E8 (see supplemental information for E8 preparation). Methods for neuronal and neural rosette differentiation included in supplemental information.

E8 Media Preparation

Large-batch preparation of basal media E4 consists of 48 L of DMEM/F12 HEPES (Thermo, Cat. 11330057), 3.072 g of L-Ascorbic acid 2-phosphate sesquimagnesium salt hydrate (Sigma, Cat. A8960), 930.86 μL of sodium selenite solution (0.7mg/mL in PBS) (Sigma, Cat. 214485), 26.04 g of sodium bicarbonate (Sigma, Cat S3817), and sodium chloride (Sigma, S7653). Final pH was adjusted to 7.4. E4 is then filtered, and 100 μL of insulin solution (Sigma Cat. I9278), 500 μL of transferrin solution (R&D Systems, Cat. 2914-HT-001G), 50 μg of FGF2 (Peprotech, Cat. 100-18B), and 1 μg of TGFB1 (Peprotech, Cat. 100-21) were added to make E8.

Cell treatments

Cell treatments were performed on 2-3 day old hPSC colonies. Cells were treated with proteasome inhibitor Bortezomib at a concentration of 0.5 μM. Pan-caspase inhibitor Q-VD-OPh (SM Biochemicals) was added to cells at a concentration of 25 μM. The DNA damaging agent etoposide was added to cells at a concentration of 1 μM or 20 μM for 3 or 24 hours, respectively. Cells were treated with both 9uM ProTAME (Tocris) and 37.5 μM Apcin (Tocris) for 24 hours. Nocadozole was added to cell media at 100 ng/mL for 16 hours then cells were washed with fresh media three times. Lysate was collected every two hours for 24 hours. All stock solutions were

prepared in DMSO and chemicals were added directly to the media alongside an equivalent DMSO only control.

Neuronal Differentiation

Differentiation of hESCs into neural stem cells was performed using the STEMdiff Neural Induction Medium (Stem Cell Technologies). NPCs were split every seven to nine days and fed daily. Following the third split, cells were maintained in STEMdiff Neural Progenitor Medium (Stem Cell Technologies). This method was employed for cells analyzed in Figure 5C.

Cortical neuron induction of iPSCs was performed following the dual SMAD protocol published by Chambers et al. 2009, except that 0.4 μM LDN193189 (Stemgent Cat. 04-0074) was substituted for Noggin (Chambers et al., 2009; Di Pardo et al., 2017; Neely et al., 2012). Neural induction media consists of 410 mL of Knockout DMEM/F12 (Invitrogen #12660), 75 mL Knockout Serum (Invitrogen #10828), 5 μL of B-mercaptoethanol (Sigma #M3148), and N2 medium. N2 medium consists of DMEM/F12 (Invitrogen #10565-018, + glutamax), 0.775 g D-glucose, and 5mL N2 supplement (Thermo Fisher Scientific #17502048). After 10 days of neural induction, neural differentiation was initiated as reported by (Shi et al., 2012). Details and validation of this differentiation method have been previously reported (Di Pardo et al., 2017; Joshi et al., 2019; Neely et al., 2012). Schematic outlining method is in Figure 2A.

Neural rosette differentiation

Cells were dissociated into single cell suspension and seeded $3.0*10^6$ cells/well of an AggrewellTM 800 (STEM CELL Technologies) in dual SMAD inhibitor media to form neutralized EBs. EBs were incubated at 37°C with 5% CO2 for 48 hours. 50% of total media volume was changed every two days to minimize disruption. On day five, EB diameter was measured using ImageJ, and EBs were harvested according to the manufacturer's protocol (STEM CELL Technologies) and transferred to a 35mm imaging plate (Cellvis, cat # D35-14-1.5-N) coated with Matrigel (Corning). Media was changed daily through day nine. Cells were fixed with 100% ice-cold methanol (Fisher Scientific, cat # A454-4). Images were acquired using an Andor DU-897 EMCCD camera mounted on a Nikon Spinning Disk microscope equipped with a 0.45 NA 10X and 0.75 NA 20X objectives.

A neural rosette quantification macro was developed using NIS elements to quantify the rosette lumenal area based on ZO-1 staining. Max projections were generated per ROI, followed by advanced denoise of the image. Binary mask intensity thresholding for the ZO-1 was done using control images. Measured data was exported to an Excel file. Data was analyzed in GraphPad Prism using a one-way ANOVA. Outliers were removed prior to ANOVA analysis using ROUT outlier identification method (Q=1%).

RNAi transfection

Commercially available siRNA (Thermo Fisher Scientific) was used to generate transient knockdowns of CUL9 and APC7 in hPSCs. hPSCs were seeded at 100,000 cells per well in a 6-well dish coated with Matrigel on d0. hNPCs were split 1:3 seven to nine days following neural induction on d0. Cells were transfected as per the manufacturer protocol using Lipofectamine RNAiMax (Thermo Fisher Scientific) in mTeSR on d1 and d2. Cells were left to recover for an additional 24 hours in fresh mTeSR or STEMDiff neural induction media, respectively. Cells were collected or fixed for analysis by Western blot on d4. Silencer Select Negative Control No. 1 (Thermo Fisher Scientific) was used as a control. The siRNA oligo sequences are as follows: CUL9 (s23061) 5'-GCUCGUCUACUUCACAAAtt-3'; APC7 (s229369) 5'-GCUGAACAGUAAUAGUGUUtt-3'; FZR1 (s27991) 5'-GGAUUAACGAGAAUGAGAAtt-3'; APC2 (s29882) 5'-CACUGGAUGUAUCUACAAtt-3'; APC10 (s20327) 5'-GAGCUCCAUUGGUAAAUUUtt-3'.

CRISPR gene editing

hCUL9-/- GM25256 iPSCs were generated using CRISPR-Cas9. Briefly, a sgRNA was designed to target an early, conserved exon with at least 3bp of mismatch to any other site in the human genome to mitigate the risk of off-target editing (Supp Figure 1A). GM25256 iPSCs were pretreated with mTeSR1 (Stem Cell Technologies) supplemented with 1X RevitaCell (Thermo Fisher Scientific) for 2 hours. Then, approximately 1X106 cells were transiently co-transfecting with precomplexed ribonuclear proteins (RNPs) consisting of 500 pmol of chemically modified sgRNA (hCUL9.sgRNA - 5'- ugcucaugaccaagcacgag -3', Synthego), 140 pmol of spCas9 protein (St. Jude Protein Production Core), and 500ng of pMaxGFP (Lonza). The transfection was performed via nucleofection (Lonza, 4D-Nucleofector™ X-unit) using solution P3 and program CA-137 in a large (100ul) cuvette according to the manufacturer's recommended protocol. Cells

were then plated onto Matrigel (Corning) coated plates into prewarmed (37C) mTeSR1 media supplemented with 1X RevitaCell. Several days post nucleofection, cells were single cell sorted on viability by flow cytometry and clonally selected as previously described (Chen and Pruett-Miller, 2018). Clones were screened and verified for the desired out-of-frame indel modifications via targeted deep sequencing using gene specific primers with partial Illumina adapter overhangs (hCUL9.F – 5'- gacggtgccatggctgggaggtcag-3' and hCUL9.R – 5'-aatgtactcaccgccagcccagcct-3', overhangs not shown) on a Miseq Illumina sequencer. NGS analysis of clones was performed using CRIS.py (Connelly and Pruett-Miller, 2019). Normal karyotypes were validated using metaphase spread analysis (Genomic Associates) and pluripotency was validated using PluriTest microarray analysis (Thermo) (Müller et al., 2011).

Western blotting

Cultured cells were lysed in 1% Triton buffer containing PMSF, PhosStop (Roche), and protease inhibitor cocktail. Protein concentrations were determined using the bicinchoninic acid method (Thermo Scientific), and 30-50 μg of protein was run on 4-20% Mini-Protean TGX precast protein gels (BioRad) in Tris-Gly-SDS buffer. Gels were then transferred onto polyvinylidene difluoride membranes at 4ºC overnight to ensure sufficient transfer of large proteins. Membranes were blocked in 5% milk in 0.1% Tween prior to primary antibody incubation. We used antibodies against OCT4 (Cell Signaling Technology, Cat. 75463S), NANOG (Cell Signaling Technology, Cat. 4903S), SOX2 (Cell Signaling Technology, Cat. 5049S), Cleaved Caspase-3 (Cell Signaling Technology, Cat. 9661S), CUL9 (Bethyl Laboratories, Cat. A300-98A), CUL7 (Bethyl Laboratories, Cat. A300-223A), ANAPC7 (Bethyl Laboratories, Cat. A302-551), FZR1 (Abcam, Cat. ab3242), and Cyclin-A2 (Cell Signaling Technology, Cat. 4656T), PAX6 (Cell Signaling Technology Cat. 60433), Nestin (STEMCELL Technologies, Cat. 60091), TUBB3 (Cell Signaling Technology, Cat. 4466S), MAP2 (Thermo Fisher Scientific, Cat. 131500), beta-Actin (Sigma, Cat. A1978), alpha-Tubulin (Sigma, Cat. T9026), and GAPDH (Cell Signaling Technology, Cat. 5147S), SOX3 (Thermo Fisher, Cat. PA5-35983), TM7SF2 (Thermo Scientific, Cat. 12033-1-AP), CUX1 (Abcam, Cat. ab54583), and SCD1 (Bethyl, Laboratories, Cat. A305-259A-T). HRP-conjugated secondary antibodies against mouse or rabbit IgG were purchased from Jackson Laboratories, and blots were developed with ECL Plus reagent (Amersham Biosciences). Clean-Blot IP detection reagent (HRP) (Life Technologies) was used in place of mouse or rabbit IgG

secondaries for immunoprecipitation samples. Band density was determined using Image Studio Lite v5.2. Data was analyzed using unpaired Student's t-test.

Immunofluorescence and microscopy

Cells were seeded on 35 mm glass bottom plates (Cellvis). Cells were fixed with 4% paraformaldehyde for 30 min at 4ºC and permeabilized during blocking in 2% BSA containing 0.3% Triton X-100 for 1 hr at room temperature. After blocking, cells were treated with primary and secondary antibodies using standard methods. The following primary antibodies were used: OCT4 (Cell Signaling Technology, Cat. 75463S), NANOG (Cell Signaling Technology, Cat. 4903S), PAX6 (Cell Signaling Technology Cat. 60433), NESTIN (STEMCELL Technologies, Cat. 60091), TUBB3 (Cell Signaling Technology, Cat. 4466S), MAP2 (Thermo Fisher Scientific, Cat. 131500), Cytochrome *c* (BD Pharmingen, Cat. 556433). All secondary antibodies were conjugated to Alexa fluorophore derivatives (Thermo). See detailed information about antibodies in Supplemental table 6. Nuclei were stained with Hoechst 3342 (Thermo). Fixed and stained cells were mounted with Fluoromount-G slide mounting medium (Electron Microscopy Sciences). Images were acquired using an Andor DU-897 camera mounted on a Nikon Spinning Disk. The software used for image acquisition and producing representative images was Nikon Elements.

Real-Time Quantitative PCR

Total RNA was extracted using Tri Reagent Solution (Thermo). cDNA was prepared per the manufacturer's protocol using the high capacity cDNA reverse transcription kit (Thermo). RT-qPCR was performed using a SYBR Green PCR Master Mix (Thermo) on a QuantStudio 3 Real-Time PCR System (Thermo) using the manufacturer provided standard curve protocol. mRNA levels and fold change were calculated using the comparative Ct method (Schmittgen and Livak, 2008). Glucose-6-phosphate isomerase (GPI) was used as a loading control for calculation of relative mRNA levels. Significance was determined using an unpaired Student's t-test. The following primer sets were used: GPI: FW: 5'- GTGTACCTTCTAGTCCCGCC -3' RV: 5'-GGTCAAGCTGAAGTGGTTGAAGC-3'; CUL9: FW: 5'-GAAGAACTCATTCGACAGAGGC-3' RV: 5'-CAGTTGGCGTAGACCTCAGG-3'; OCT4: FW: 5'-GGGCTCTCCCATGCATTCAAAC-3' RV: 5'-CACCTTCCCTCCAACCAGTTGC-3'; NANOG: FW: 5'-TGGGATTTACAGGCGTGAGCCAC-3' RV: 5'-AAGCAAAGCCTCCCAATCCCAAAC-3'; MAP2: FW: 5'-CTCAGCACCGCTAACAGAGGE-3' RV: 5'-CATTGGCGCTTCGGACAAG-3'; TUBB3: FW: 5'-

GGCCAAGGGTCACTACACG-3' RV: 5'-GCAGTCGCAGTTTTCACACTC-3'; TBR1: FW: 5'-GCAGCAGCTACCCACATTCA-3' RV: 5'-AGGTTGTCAGTGGTCGAGATA-3'; EMX2: FW: 5'-CGGCACTCAGCTACGCTAAC-3' RV: 5'-CAAGTCCGGGTTGGAGTAGAC-3' Efficiency of primer sets were between 90-110% as determined by standard curve.

Agilent Seahorse XF Cell Mito Stress Test

iPSCs were plated in E8 media on Matrigel-coated Seahorse XF96 V3 PS cell culture microplates 2 days before the assay at 8 x 104 cells per well. One hour prior to the assay, media was switched to XF DMEM media containing 1 mM pyruvate, 2 mM glutamine, and 10 mM glucose. Oxygen consumption rate (OCR) was measured sequentially after addition of 1.0 µM oligomycin, 1.5 µM FCCP, and 0.5 µM rotenone/antimycin A. To obtain cortical neurons, iPSCs were differentiated and maintained as described in the Neuronal Differentiation section for 25 days as reported by Shi et al., 2012. Cortical neurons were plated in maintenance media on Matrigel-coated Seahorse XF96 V3 PS cell culture microplates 2 days before the assay at 8 x 104 cells per well. One hour prior to the assay, media was switched to XF DMEM media containing 1 mM pyruvate, 2 mM glutamine, and 10 mM glucose. Oxygen consumption rate (OCR) was measured sequentially after addition of 1.5 µM oligomycin, 1.5 µM FCCP, and 0.5 µM rotenone/antimycin A.

Cell cycle analysis by flow cytometry

Cells were dissociated to a single cell concentration when they were 70-80% confluent using Gentle Cell Dissociation. Cells were washed 3X with PBS, then fixed in 70% EtOH at -20 ºC for at least 2 hours. 1*106 cells were stained in 1mL of 1µg/mL of DAPI in a 0.1% Triton solution containing RNase overnight in the dark. Stained cells were analyzed using a 405nm (6-paramaters) laser of a 3-laser BD Fortessa. Forward and side scatter parameters were used to exclude doublets and debris. DAPI staining intensity was used to determine DNA content of cells. Gates for sub-G1, G1, S, G2/M, and polyploidy were determined based on DNA content.

Immunoprecipitation

Immunoprecipitation experiments were performed by incubating 2mg of whole-cell lysates with 2 µg of PARC/H7AP1 (Bethyl, Cat. A300-98A), ANAPC7 (Bethyl, Cat. A302-551A) or FZR1

(Abcam, Cat. ab3242) for 1 hr at 4ºC. 40 μL of 50/50 slurry of Dynabeads (Invitrogen) was added to sample and left to incubate for 1 hr at 4ºC. Beads were separated by magnet and washed in 1% Triton. Protein was eluted and incubated with Elution Buffer (Invitrogen) and LDS/BME sample buffer at 95ºC for 5 min. Immunoprecipitations were analyzed by Western blot or LC-MS/MS.

LC-MS/MS analysis

For in-gel digestion, the samples were solubilized in lithium dodecyl sulfate (LDS) sample buffer (Invitrogen, Carlsbad,CA, USA). The samples were loaded onto 4–12% NuPAGE Novex Bis-Tris gel and MOPs running buffer was used for separation (Invitrogen). The samples were allowed to run into the gel for 1.5–2 cm. The gel was fixed and stained with Colloidal Blue Staining kit (Invitrogen) then washed and the stained area was excised and diced to 1 mm cubes. Proteins were reduced with 45 mM DTT for 20 min at 551C, followed by alkylation with 100 mM iodoacetamide for 30 min at room temperature in the dark. The volume of iodoacetamide added was the same as the volume of DTT added. After reduction and alkylation, gel pieces were destained with three consecutive washes with a 50:50 mixture of 50 mM ammonium bicarbonate and ACN for 10 min, dehydrated with 100% ACN for 10 min, and dried in a SpeedVac. The gel pieces were rehydrated in a 50 mL of solution containing 10 ng/mL trypsin (Promega, Madison, WI, USA) in 25 mM ammonium bicarbonate (pH 8.0) for 15 min. 100 mL of 25 mM ammonium bicarbonate buffer was added to each sample and the samples were incubated at 371C for 18 h.

Peptides were extracted using 60% ACN/0.1% TFA twice. The extracted samples were pooled and dried in a SpeedVac and reconstituted in 0.1% formic acid for subsequent analysis. An analytical column was packed with 20cm of C18 reverse phase material (Jupiter, 3 μm beads, 300Å, Phenomenox) directly into a laser-pulled emitter tip. The peptide solutions were loaded on the capillary reverse phase analytical column (360 μm O.D. x 100 μm I.D.) using a Dionex Ultimate 3000 nanoLC and autosampler. The mobile phase solvents consisted of 0.1% formic acid, 99.9% water (solvent A) and 0.1% formic acid, 99.9% acetonitrile (solvent B). Peptides were gradient eluted at a flow rate of 350 nL/min. The 95 minute gradient consisted of the following: 1-98 min, 2-45% B; 98-105 min, 45-90% B; 105-107 min, 90% B; 107-110 min, 90-2% B; 110-120 min (column equilibration), 2% B. A Q Exactive Plus mass spectrometer (Thermo Scientific), equipped with a nanoelectrospray ionization source, was used to mass analyze the eluting peptides. The instrument method consisted of MS1 using an MS AGC target value of 3e6, followed by up to 15 MS/MS scans of the most abundant ions detected in the preceding MS scan.

A maximum MS/MS ion time of 40 ms was used with a MS2 AGC target of 1e5, a 3% underfill ratio and an intensity threshold of 7.5e4. Dynamic exclusion was set to 20s, HCD collision energy was set to 27 and peptide match and isotope exclusion were enabled. For identification of peptides, tandem mass spectra were searched with Sequest (Thermo Fisher Scientific) against a human subset database created from the UniprotKB protein database (www.uniprot.org). Variable modifications of +57.0214 on Cys (carbamidomethylation) and +15.9949 on Met (oxidation) were included for database searching. Search results were assembled using Scaffold 4.3.4. (Proteome Software) and significance was determined using a Fisher's exact test. More details on the analyses can be found in the publically available raw data at Zenodo at 10.5281/zenodo.4340970.

Quantitative proteomics analysis

Samples were diluted with 100mM TEAB, reduced with 5uL of 200mM TCEP at 55°C for one hour, and available Cys residues were carbamidomethylated with 5mL of 375mM Iodoacetamide for 30 minutes in the dark at room temperature. Protein samples were precipitated with acetone at -20°C. A volume of ice-cold acetone six times the sample volume was added to each sample, and precipitation was carried out overnight. After precipitation, samples were centrifuged at 18,000xg at 4°C, protein pellets were washed with ice-cold acetone, centrifuged, and precipitates were allowed to dry. Proteins were then reconstituted in 100 mM TEAB (pH 8.0) and digested with Promega Gold trypsin overnight at 37°C. Quantitative proteomics analysis was performed using isobaric tags for relative and absolute quantification (iTRAQ). Peptides were labeled with iTRAQ reagents according to the manufacturer's instructions (SCIEX). After labeling was complete, labeled peptides were combined and fractionation was performed using the Thermo Scientific Pierce High pH Reversed-Phase Peptide Fractionation Kit (Product No. 84868) similar to the manufacturer's recommended protocol. After loading peptides onto the reverse phase resin, a wash was performed with 5% acetonitrile, 0.1% triethylamine. Elution steps consisted of the following: 7.5%, 10%, 12.5%, 15%, 17.5%, 20%, 22.5%, 25%, 27.55, 30%, 35%, 60%, and 80% acetonitrile with 0.1% triethylamine. Fractions were dried via vacuum centrifugation in SpeedVac concentrator, and peptides were reconstituted in 0.1% formic acid for analysis by LC-coupled tandem mass spectrometry (LC-MS/MS). An analytical column was packed with 35cm of C18 reverse phase material (Jupiter, 3 µm beads, 300Å, Phenomenox) directly into a laser-pulled emitter tip. Peptides were loaded on the capillary reverse phase analytical column (360 µm O.D. x 100 µm I.D.) using a Dionex Ultimate 3000 nanoLC and autosampler. The mobile phase solvents consisted of 0.1% formic acid, 99.9% water (solvent A)

and 0.1% formic acid, 99.9% acetonitrile (solvent B). For the first ten fractions, peptides were gradient-eluted at a flow rate of 350 nL/min, using a 180-minute gradient. The gradient consisted of the following: 5-30 %B in 140 min, 30-50 %B in 10 min, 50-70 %B in 5 min, 70 %B in 5 min; 70-5 %B in 4 min, followed by column equilibration for the next sample. A Q Exactive Plus mass spectrometer (Thermo Scientific), equipped with a nanoelectrospray ionization source, was used to mass analyze the eluting peptides. The Q Exactive instrument was operated in data-dependent mode acquiring HCD MS/MS scans (R = 17,500) after each MS1 scan on the 15 most abundant ions using an MS1 ion target of 3 × 106 ions and an MS2 target of 1 × 105 ions. The HCD-normalized collision energy was set to 30, dynamic exclusion was set to 30 s, and peptide match and isotope exclusion were enabled. For the final three fractions, the peptides were combined for LC-MS/MS analysis. This final combined pool of peptides and the 5% acetonitrile wash were analyzed using a similar data acquisition method with a gradient that consisted of 5-50 %B in 105 min, followed by 50-98 %B in 50 min, 98 %B for 5 min, 98-5 %B in 3 min, and column re-equilibration.

Peptide/protein identifications and quantitative analysis were performed using Spectrum Mill (Agilent) as previously described (Noto et al., 2019). MS/MS spectra were searched against a subset of the UniProt KB protein database containing human proteins. Auto-validation procedures in Spectrum Mill were used to filter the data to <1% false discovery rates at the protein and peptide level. After peptides were identified and proteins were quantified, the results were then filtered to include those proteins for which a minimum of two unique peptides were identified. Log2 protein ratios were fit to a normal distribution using non-linear (least squares) regression. The calculated mean derived from the Gaussian fit was used to normalize individual log2 ratios for each quantified protein. The normalized log2 ratios were then fit to a normal distribution, and the mean and standard deviation values derived from the Gaussian fit of the normalized ratios were used to calculate p values. Subsequently, p values were corrected for multiple comparisons by the Benjamini-Hochberg method (Noto et al., 2019). More details on the analyses can be found in the publically available raw data at Zenodo at 10.5281/zenodo.4340970.

Lentiviral transduction

To generate lentiviral-mediated CUL9 overexpression of iPSC, iPSC colonies at 50-70% confluency were transduced with pLVX-EF1alpha-IRES-mcherry vector (Takara) containing a CUL9-FLAG sequence (1MOI). Cells were fed with mTESR 24 hours later. 48 hours after initial

transduction, m-Cherry positive cells were selected for and plated in StemFlex (Thermo) plus CloneR (StemCell Technologies) in 96-well plates using flow activated cell sorting. After 72 hours, cells were fed again with StemFlex plus CloneR. Until colonies were apparent, cells were fed every other day with StemFlex only. Transduction efficiency was validated by Western blot analysis of recovered colonies. Lentivirus was prepared per manufacturer protocol using Lenti-X packaging single shots (VSV-G) (Takara). Lentiviral concentration was determined using Lenti-X GoStix Plus (Takara). Lentiviral particles obtained from Sigma Aldrich (SHCLNV-NM_015089) were used to produce lentiviral stable KD cells. shRNA #1 (TRCN0000004448) targeted the 3' sequence: 5'-CCGGTCTGTAGTGCTTCCTGTTTGCCTCGAGGCAAACAGGAAGCACTACAGATTTTT-3' and shRNA #2 (TRCN0000424584) targeted the CDS sequence: 5'-CCGGGATCTCTGTGTCCGTGGAAATCTCGAGATTTCCACGGACACAGAGATCTTTTTTG -3'. Titer provided by Sigma was used to calculate MOI. Cells transduced at 1 MOI.

CaspaseGlo 3/7 Assay

Cells were plated onto Matrigel (Corning) white round-bottomed 96-well plates at 10,000 cells/well. Triplicate wells were used per condition. After 24 hrs, media was removed and CaspaseGlo 3/7 reagent (Promega #8091) and fresh media was added at a 1:1 ratio. The samples were incubated at room temperature in the dark for one hour. Samples were then analyzed in a Promega GloMax luminometer according to manufacturer instructions.

Statistical Analysis

All experiments were performed with a minimum of 3 biological replicates. Statistical significance was determined by unpaired, two-tailed Student's t-test or by one- or two-way ANOVA as appropriate for each experiment. GraphPad Prism v8.1.2 was used for all statistical analysis and data visualization. Statistical analysis of quantitative proteomics and LC-MS/MS experiments was conducted by the Vanderbilt Proteomics core – details about these analyses can be found in their respective methods sections and corresponding references (Noto et al., 2019) and in the publicly available data sets at Zenodo at 10.5281/zenodo.4340970.

Error bars in all bar graphs and scatter plots represent standard error of the mean or standard deviation as described for each figure. No outliers were removed from the analyses

except in the neural rosette analyses. We employed the ROUT method to exclude outliers in our analysis of neural rosette lumen size. Briefly, the ROUT method identifies outliners from non-linear regression using the false-discovery rate (Motulsky and Brown, 2006). This method is more effective than other common outlier exclusion methods like Grubb's at identifying more than one outlier making it the ideal method for our dataset. In each biological replicate (5 ROI), we often measure the lumen size of 600 or more rosettes. When the data points of all three replicates are combined, we have as many as 2500 data points. We use ROUT to remove outliers prior to our one-way ANOVA analysis (Q=1%).

DATA AVAILABILITY STATEMENT

All proteomics datasets are publicly available at Zenodo at 10.5281/zenodo.4340970.

REFERENCES

Akterin, S., Cowburn, R.F., Miranda-Vizuete, A., Jiménez, A., Bogdanovic, N., Winblad, B., and Cedazo-Minguez, A. (2006). Involvement of glutaredoxin-1 and thioredoxin-1 in beta-amyloid toxicity and Alzheimer's disease. Cell Death Differ. *13*, 1454–1465.

Akutsu, M., Dikic, I., and Bremm, A. (2016). Ubiquitin chain diversity at a glance. J. Cell Sci. *129*, 875–880.

Almeida, A., Bolaños, J.P., and Moreno, S. (2005). Cdh1/Hct1-APC Is Essential for the Survival of Postmitotic Neurons. J. Neurosci. *25*, 8115–8121.

Altieri, D.C. (2006). The case for survivin as a regulator of microtubule dynamics and cell-death decisions. Curr. Opin. Cell Biol. *18*, 609–615.

Ando, H., Sato, T., Ito, T., Yamamoto, J., Sakamoto, S., Nitta, N., Asatsuma-Okumura, T., Shimizu, N., Mizushima, R., Aoki, I., et al. (2019). Cereblon Control of Zebrafish Brain Size by Regulation of Neural Stem Cell Proliferation. IScience *15*, 95–108.

Andrews, P., He, Y.J., and Xiong, Y. (2006). Cytoplasmic localized ubiquitin ligase cullin 7 binds to p53 and promotes cell growth by antagonizing p53 function. Oncogene *25*, 4534–4548.

Arai, T., Kasper, J.S., Skaar, J.R., Ali, S.H., Takahashi, C., and DeCaprio, J.A. (2003). Targeted disruption of p185/Cul7 gene results in abnormal vascular morphogenesis. Proc. Natl. Acad. Sci. *100*, 9855–9860.

Ariyama, H., Kono, N., Matsuda, S., Inoue, T., and Arai, H. (2010). Decrease in Membrane Phospholipid Unsaturation Induces Unfolded Protein Response. J. Biol. Chem. *285*, 22027–22035.

Arlotta, P., and Paşca, S.P. (2019). Cell diversity in the human cerebral cortex: from the embryo to brain organoids. Curr. Opin. Neurobiol. *56*, 194–198.

Badura-Stronka, M., Jamsheer, A., Materna-Kiryluk, A., Sowińska, A., Kiryluk, K., Budny, B., and Latos-Bieleńska, A. (2010). A novel nonsense mutation in CUL4B gene in three brothers with X-linked mental retardation syndrome. Clin. Genet. *77*, 141–144.

Baek, K. (2016). Interaction Between Two E3 ligases, NEDD8ylated Cullin and HHARI. Master of Science. University of Tennessee Health Science Center.

Baek, K., Krist, D.T., Prabu, J.R., Hill, S., Klügel, M., Neumaier, L.-M., von Gronau, S., Kleiger, G., and Schulman, B.A. (2020a). NEDD8 nucleates a multivalent cullin–RING–UBE2D ubiquitin ligation assembly. Nature *578*, 461–466.

Baek, K., Scott, D.C., and Schulman, B.A. (2020b). NEDD8 and ubiquitin ligation by cullin-RING E3 ligases. Curr. Opin. Struct. Biol. *67*, 101–109.

Bai, C., Sen, P., Hofmann, K., Ma, L., Goebl, M., Harper, J.W., and Elledge, S.J. (1996). SKP1 Connects Cell Cycle Regulators to the Ubiquitin Proteolysis Machinery through a Novel Motif, the F-Box. Cell *86*, 263–274.

Ballabeni, A., Park, I.-H., Zhao, R., Wang, W., Lerou, P.H., Daley, G.Q., and Kirschner, M.W. (2011). Cell cycle adaptations of embryonic stem cells. Proc. Natl. Acad. Sci. *108*, 19252–19257.

Barford, D., Hu, S.H., and Johnson, L.N. (1991). Structural mechanism for glycogen phosphorylase control by phosphorylation and AMP. J. Mol. Biol. *218*, 233–260.

Bar-On, O., Shapira, M., Skorecki, K., Hershko, A., and Hershko, D.D. (2010). Regulation of APC/CCdh1 ubiquitin ligase in differentiation of human embryonic stem cells. Cell Cycle *9*, 5.

Bassermann, F., Frescas, D., Guardavaccaro, D., Busino, L., Peschiaroli, A., and Pagano, M. (2008). The Cdc14B-Cdh1-Plk1 Axis Controls the G2 DNA-Damage-Response Checkpoint. Cell *134*, 256–267.

Baum, T., and Gama, V. (2021). Dynamic properties of mitochondria during human corticogenesis. Development *148*.

Bax, M., McKenna, J., Do-Ha, D., Stevens, C.H., Higginbottom, S., Balez, R., Cabral-da-Silva, M. e C., Farrawell, N.E., Engel, M., Poronnik, P., et al. (2019). The Ubiquitin Proteasome System Is a Key Regulator of Pluripotent Stem Cell Survival and Motor Neuron Differentiation. Cells *8*, 581.

Beal, R., Deveraux, Q., Xia, G., Rechsteiner, M., and Pickart, C. (1996). Surface hydrophobic residues of multiubiquitin chains essential for proteolytic targeting. Proc. Natl. Acad. Sci. U. S. A. *93*, 861–866.

Beccari, L., Moris, N., Girgin, M., Turner, D.A., Baillie-Johnson, P., Cossy, A.-C., Lutolf, M.P., Duboule, D., and Arias, A.M. (2018). Multi-axial self-organization properties of mouse embryonic stem cells into gastruloids. Nature *562*, 272–276.

Becker, K.A., Ghule, P.N., Therrien, J.A., Lian, J.B., Stein, J.L., van Wijnen, A.J., and Stein, G.S. (2006). Self-renewal of human embryonic stem cells is supported by a shortened G1 cell cycle phase. J. Cell. Physiol. *209*, 883–893.

Bennati, A.M., Castelli, M., Della Fazia, M.A., Beccari, T., Caruso, D., Servillo, G., and Roberti, R. (2006). Sterol dependent regulation of human TM7SF2 gene expression: Role of the encoded 3β-hydroxysterol Δ14-reductase in human cholesterol biosynthesis. Biochim. Biophys. Acta BBA - Mol. Cell Biol. Lipids *1761*, 677–685.

Bergsland, M., Ramsköld, D., Zaouter, C., Klum, S., Sandberg, R., and Muhr, J. (2011). Sequentially acting Sox transcription factors in neural lineage development. Genes Dev. *25*, 2453–2464.

Bernstein, B.E., Mikkelsen, T.S., Xie, X., Kamal, M., Huebert, D.J., Cuff, J., Fry, B., Meissner, A., Wernig, M., Plath, K., et al. (2006). A Bivalent Chromatin Structure Marks Key Developmental Genes in Embryonic Stem Cells. Cell *125*, 315–326.

Bi, X., Xu, Y., Li, T., Li, X., Li, W., Shao, W., Wang, K., Zhan, G., Wu, Z., Liu, W., et al. (2019). RNA Targets Ribogenesis Factor WDR43 to Chromatin for Transcription and Pluripotency Control. Mol. Cell *75*, 102-116.e9.

Bloom, J., and Cross, F.R. (2007). Multiple levels of cyclin specificity in cell-cycle control. Nat. Rev. Mol. Cell Biol. *8*, 149–160.

Boughton, A.J., Krueger, S., and Fushman, D. (2020). Branching via K11 and K48 Bestows Ubiquitin Chains with a Unique Interdomain Interface and Enhanced Affinity for Proteasomal Subunit Rpn1. Struct. Lond. Engl. 1993 *28*, 29-43.e6.

Boward, B., Wu, T., and Dalton, S. (2017). Control of cell fate through cell cycle and pluripotency networks. 21.

Brink, S.C. van den, Baillie-Johnson, P., Balayo, T., Hadjantonakis, A.-K., Nowotschin, S., Turner, D.A., and Arias, A.M. (2014). Symmetry breaking, germ layer specification and axial organisation in aggregates of mouse embryonic stem cells. Development *141*, 4231–4242.

Bryson, S.E., Rogers, S.J., and Fombonne, E. (2003). Autism spectrum disorders: early detection, intervention, education, and psychopharmacological management. Can. J. Psychiatry Rev. Can. Psychiatr. *48*, 506–516.

Buchsbaum, I.Y., and Cappello, S. (2019). Neuronal migration in the CNS during development and disease: insights from in vivo and in vitro models. Development *146*.

Bullock, A.N., Debreczeni, J.É., Edwards, A.M., Sundström, M., and Knapp, S. (2006). Crystal structure of the SOCS2–elongin C–elongin B complex defines a prototypical SOCS box ubiquitin ligase. Proc. Natl. Acad. Sci. *103*, 7637–7642.

Cakir, B., Xiang, Y., Tanaka, Y., Kural, M.H., Parent, M., Kang, Y.-J., Chapeton, K., Patterson, B., Yuan, Y., He, C.-S., et al. (2019). Engineering of human brain organoids with a functional vascular-like system. Nat. Methods *16*, 1169–1175.

Calder, A., Roth-Albin, I., Bhatia, S., Pilquil, C., Lee, J.H., Bhatia, M., Levadoux-Martin, M., McNicol, J., Russell, J., Collins, T., et al. (2013). Lengthened G1 Phase Indicates Differentiation Status in Human Embryonic Stem Cells. Stem Cells Dev. *22*, 279–295.

Cao, R., Chen, K., Song, Q., Zang, Y., Li, J., Wang, X., Chen, P., and Liang, S. (2012). Quantitative proteomic analysis of membrane proteins involved in astroglial differentiation of neural stem cells by SILAC labeling coupled with LC-MS/MS. J. Proteome Res. *11*, 829–838.

Cardote, T.A.F., Gadd, M.S., and Ciulli, A. (2017). Crystal Structure of the Cul2-Rbx1-EloBC-VHL Ubiquitin Ligase Complex. Structure *25*, 901-911.e3.

Cardozo, T., and Pagano, M. (2004). The SCF ubiquitin ligase: insights into a molecular machine. Nat. Rev. Mol. Cell Biol. *5*, 739–751.

Carper, R.A., Moses, P., Tigue, Z.D., and Courchesne, E. (2002). Cerebral lobes in autism: early hyperplasia and abnormal age effects. NeuroImage *16*, 1038–1051.

Carroll, C.W., and Morgan, D.O. (2002). The Doc1 subunit is a processivity factor for the anaphase-promoting complex. Nat. Cell Biol. *4*, 880–887.

Carroll, C.W., Enquist-Newman, M., and Morgan, D.O. (2005). The APC subunit Doc1 promotes recognition of the substrate destruction box. Curr. Biol. CB *15*, 11–18.

Castello, A., Hentze, M.W., and Preiss, T. (2015). Metabolic Enzymes Enjoying New Partnerships as RNA-Binding Proteins. Trends Endocrinol. Metab. *26*, 746–757.

Cavallaro, M., Mariani, J., Lancini, C., Latorre, E., Caccia, R., Gullo, F., Valotta, M., DeBiasi, S., Spinardi, L., Ronchi, A., et al. (2008). Impaired generation of mature neurons by neural stem cells from hypomorphic Sox2 mutants. Development *135*, 541–557.

Caviness, V.S., and Sidman, R.L. (1973). Time of origin or corresponding cell classes in the cerebral cortex of normal and reeler mutant mice: an autoradiographic analysis. J. Comp. Neurol. *148*, 141–151.

Chambers, S.M., Fasano, C.A., Papapetrou, E.P., Tomishima, M., Sadelain, M., and Studer, L. (2009). Highly efficient neural conversion of human ES and iPS cells by dual inhibition of SMAD signaling. Nat. Biotechnol. *27*, 275–280.

Chanarat, S., and Mishra, S.K. (2018). Emerging Roles of Ubiquitin-like Proteins in Pre-mRNA Splicing. Trends Biochem. Sci. *43*, 896–907.

Chandrasekaran, A., Avci, H.X., Ochalek, A., Rösingh, L.N., Molnár, K., László, L., Bellák, T., Téglási, A., Pesti, K., Mike, A., et al. (2017). Comparison of 2D and 3D neural induction methods for the generation of neural progenitor cells from human induced pluripotent stem cells. Stem Cell Res. *25*, 139–151.

Chang, L., Zhang, Z., Yang, J., McLaughlin, S.H., and Barford, D. (2015). Atomic structure of the APC/C and its mechanism of protein ubiquitination. Nature *522*, 450–454.

Chang, L.-F., Zhang, Z., Yang, J., McLaughlin, S.H., and Barford, D. (2014). Molecular architecture and mechanism of the anaphase-promoting complex. Nature *513*, 388–393.

Chen, Y.-H., and Pruett-Miller, S.M. (2018). Improving single-cell cloning workflow for gene editing in human pluripotent stem cells. Stem Cell Res. *31*, 186–192.

Chen, X., Wei, S., Ji, Y., Guo, X., and Yang, F. (2015). Quantitative proteomics using SILAC: Principles, applications, and developments. Proteomics *15*, 3175–3192.

Ciechanover, A., and Kwon, Y.T. (2015). Degradation of misfolded proteins in neurodegenerative diseases: therapeutic targets and strategies. Exp. Mol. Med. *47*, e147–e147.

Ciechanover, A., Heller, H., Elias, S., Haas, A.L., and Hershko, A. (1980). ATP-dependent conjugation of reticulocyte proteins with the polypeptide required for protein degradation. Proc. Natl. Acad. Sci. U. S. A. *77*, 1365–1368.

Citri, A., and Malenka, R.C. (2008). Synaptic Plasticity: Multiple Forms, Functions, and Mechanisms. Neuropsychopharmacology *33*, 18–41.

Clingman, C.C., Deveau, L.M., Hay, S.A., Genga, R.M., Shandilya, S.M., Massi, F., and Ryder, S.P. (2014). Allosteric inhibition of a stem cell RNA-binding protein by an intermediary metabolite. ELife *3*.

Coghlan, S., Horder, J., Inkster, B., Mendez, M.A., Murphy, D.G., and Nutt, D.J. (2012). GABA system dysfunction in autism and related disorders: from synapse to symptoms. Neurosci. Biobehav. Rev. *36*, 2044–2055.

Conibear, A.C. (2020). Deciphering protein post-translational modifications using chemical biology tools. Nat. Rev. Chem. *4*, 674–695.

Connelly, J.P., and Pruett-Miller, S.M. (2019). CRIS.py: A Versatile and High-throughput Analysis Program for CRISPR-based Genome Editing. Sci. Rep. *9*, 4194.

Cope, G.A., and Deshaies, R.J. (2006). Targeted silencing of Jab1/Csn5 in human cells downregulates SCF activity through reduction of F-box protein levels. BMC Biochem. *7*, 1.

Cope, G.A., Suh, G.S.B., Aravind, L., Schwarz, S.E., Zipursky, S.L., Koonin, E.V., and Deshaies, R.J. (2002). Role of Predicted Metalloprotease Motif of Jab1/Csn5 in Cleavage of Nedd8 from Cul1. Science *298*, 608–611.

Courtheoux, T., Enchev, R.I., Lampert, F., Gerez, J., Beck, J., Picotti, P., Sumara, I., and Peter, M. (2016). Cortical dynamics during cell motility are regulated by CRL3 KLHL21 E3 ubiquitin ligase. Nat. Commun. *7*, 12810.

Coyaud, E., Mis, M., Laurent, E.M.N., Dunham, W.H., Couzens, A.L., Robitaille, M., Gingras, A.-C., Angers, S., and Raught, B. (2015). BioID-based Identification of Skp Cullin F-box (SCF)β-TrCP1/2 E3 Ligase Substrates. Mol. Cell. Proteomics MCP *14*, 1781–1795.

Craney, A., and Rape, M. (2013). Dynamic regulation of ubiquitin-dependent cell cycle control. Curr. Opin. Cell Biol. *25*, 704–710.

Crowther, A.J., Gama, V., Bevilacqua, A., Chang, S.X., Yuan, H., Deshmukh, M., and Gershon, T.R. (2013). Tonic Activation of Bax Primes Neural Progenitors for Rapid Apoptosis through a Mechanism Preserved in Medulloblastoma. J. Neurosci. *33*, 18098–18108.

Cubelos, B., Sebastián-Serrano, A., Beccari, L., Calcagnotto, M.E., Cisneros, E., Kim, S., Dopazo, A., Alvarez-Dolado, M., Redondo, J.M., Bovolenta, P., et al. (2010). Cux1 and Cux2 Regulate Dendritic Branching, Spine Morphology, and Synapses of the Upper Layer Neurons of the Cortex. Neuron *66*, 523–535.

Cubillos-Rojas, M., Amair-Pinedo, F., Peiró-Jordán, R., Bartrons, R., Ventura, F., and Rosa, J.L. (2014). The E3 Ubiquitin Protein Ligase HERC2 Modulates the Activity of Tumor Protein p53 by Regulating Its Oligomerization. J. Biol. Chem. *289*, 14782–14795.

Cui, C.-P., Zhang, Y., Wang, C., Yuan, F., Li, H., Yao, Y., Chen, Y., Li, C., Wei, W., Liu, C.H., et al. (2018). Dynamic ubiquitylation of Sox2 regulates proteostasis and governs neural progenitor cell differentiation. Nat. Commun. *9*, 4648.

Cunningham, C.N., Schmidt, C.A., Schramm, N.J., Gaylord, M.R., and Resendes, K.K. (2014). Human TREX2 components PCID2 and centrin 2, but not ENY2, have distinct functions in protein export and co-localize to the centrosome. Exp. Cell Res. *320*, 209–218.

Cutter, A.R., and Hayes, J.J. (2015). A brief review of nucleosome structure. FEBS Lett. *589*, 2914–2922.

Dawson, T.M., Ko, H.S., and Dawson, V.L. (2010). Genetic Animal Models of Parkinson's Disease. Neuron *66*, 646–661.

De Los Angeles, A., Ferrari, F., Xi, R., Fujiwara, Y., Benvenisty, N., Deng, H., Hochedlinger, K., Jaenisch, R., Lee, S., Leitch, H.G., et al. (2015). Hallmarks of pluripotency. Nature *525*, 469–478.

De Rubeis, S., He, X., Goldberg, A.P., Poultney, C.S., Samocha, K., Ercument Cicek, A., Kou, Y., Liu, L., Fromer, M., Walker, S., et al. (2014). Synaptic, transcriptional and chromatin genes disrupted in autism. Nature *515*, 209–215.

Dealy, M.J., Nguyen, K.V.T., Lo, J., Gstaiger, M., Krek, W., Elson, D., Arbeit, J., Kipreos, E.T., and Johnson, R.S. (1999). Loss of Cul1 results in early embryonic lethality and dysregulation of cyclin E. Nat. Genet. *23*, 245–248.

Delgado-Esteban, M., García-Higuera, I., Maestre, C., Moreno, S., and Almeida, A. (2013). APC/C-Cdh1 coordinates neurogenesis and cortical size during development. Nat. Commun. *4*, 2879.

Deng, L., Wang, C., Spencer, E., Yang, L., Braun, A., You, J., Slaughter, C., Pickart, C., and Chen, Z.J. (2000). Activation of the IkappaB kinase complex by TRAF6 requires a dimeric ubiquitin-conjugating enzyme complex and a unique polyubiquitin chain. Cell *103*, 351–361.

Denti, S., Fernandez-Sanchez, M.E., Rogge, L., and Bianchi, E. (2006). The COP9 signalosome regulates Skp2 levels and proliferation of human cells. J. Biol. Chem. *281*, 32188–32196.

Deveraux, Q., Ustrell, V., Pickart, C., and Rechsteiner, M. (1994). A 26 S protease subunit that binds ubiquitin conjugates. J. Biol. Chem. *269*, 7059–7061.

Di Pardo, A., Amico, E., Basit, A., Armirotti, A., Joshi, P., Neely, M.D., Vuono, R., Castaldo, S., Digilio, A.F., Scalabrì, F., et al. (2017). Defective Sphingosine-1-phosphate metabolism is a druggable target in Huntington's disease. Sci. Rep. *7*, 5280.

Dias, D.C., Dolios, G., Wang, R., and Pan, Z.-Q. (2002). CUL7: A DOC domain-containing cullin selectively binds Skp1·Fbx29 to form an SCF-like complex. Proc. Natl. Acad. Sci. *99*, 16601–16606.

Dikic, I., and Elazar, Z. (2018). Mechanism and medical implications of mammalian autophagy. Nat. Rev. Mol. Cell Biol. *19*, 349–364.

Dobrzyn, P., Dobrzyn, A., Miyazaki, M., Cohen, P., Asilmaz, E., Hardie, D.G., Friedman, J.M., and Ntambi, J.M. (2004). Stearoyl-CoA desaturase 1 deficiency increases fatty acid oxidation by activating AMP-activated protein kinase in liver. Proc. Natl. Acad. Sci. *101*, 6409–6414.

Dong, Z., Chen, W., Chen, C., Wang, H., Cui, W., Tan, Z., Robinson, H., Gao, N., Luo, B., Zhang, L., et al. (2020). CUL3 Deficiency Causes Social Deficits and Anxiety-like Behaviors by Impairing Excitation-Inhibition Balance through the Promotion of Cap-Dependent Translation. Neuron *105*, 475-490.e6.

Dove, K.K., and Klevit, R.E. (2017). RING-Between-RING E3s ligases: Emerging themes amid the variations. J. Mol. Biol. *429*, 3363–3375.

Duda, D.M., Borg, L.A., Scott, D.C., Hunt, H.W., Hammel, M., and Schulman, B.A. (2008). Structural Insights into NEDD8 Activation of Cullin-RING Ligases: Conformational Control of Conjugation. Cell *134*, 995–1006.

Duda, D.M., Scott, D.C., Calabrese, M.F., Zimmerman, E.S., Zheng, N., and Schulman, B.A. (2011). Structural regulation of cullin-RING ubiquitin ligase complexes. Curr. Opin. Struct. Biol. *21*, 257–264.

Duda, D.M., Olszewski, J.L., Schuermann, J.P., Kurinov, I., Miller, D.J., Nourse, A., Alpi, A.F., and Schulman, B.A. (2013). Structure of HHARI, a RING-IBR-RING Ubiquitin Ligase: Autoinhibition of an Ariadne-Family E3 and Insights into Ligation Mechanism. Structure *21*, 1030–1041.

Dumitru, R., Gama, V., Fagan, B.M., Bower, J.J., Swahari, V., Pevny, L.H., and Deshmukh, M. (2012). Human Embryonic Stem Cells Have Constitutively Active Bax at the Golgi and Are Primed to Undergo Rapid Apoptosis. Mol. Cell *46*, 573–583.

Dwyer, N.D., Chen, B., Chou, S.-J., Hippenmeyer, S., Nguyen, L., and Ghashghaei, H.T. (2016). Neural Stem Cells to Cerebral Cortex: Emerging Mechanisms Regulating Progenitor Behavior and Productivity. J. Neurosci. *36*, 11394–11401.

Easley, C.A., Phillips, B.T., McGuire, M.M., Barringer, J.M., Valli, H., Hermann, B.P., Simerly, C.R., Rajkovic, A., Miki, T., Orwig, K.E., et al. (2012). Direct Differentiation of Human Pluripotent Stem Cells into Haploid Spermatogenic Cells. Cell Rep. *2*, 440–446.

Efroni, S., Duttagupta, R., Cheng, J., Dehghani, H., Hoeppner, D.J., Dash, C., Bazett-Jones, D.P., Le Grice, S., McKay, R.D.G., Buetow, K.H., et al. (2008). Global Transcription in Pluripotent Embryonic Stem Cells. Cell Stem Cell *2*, 437–447.

Elkabetz, Y., Panagiotakos, G., Shamy, G.A., Socci, N.D., Tabar, V., and Studer, L. (2008). Human ES cell-derived neural rosettes reveal a functionally distinct early neural stem cell stage. Genes Dev. *22*, 152–165.

Emanuele, M.J., Elia, A.E.H., Xu, Q., Thoma, C.R., Izhar, L., Leng, Y., Guo, A., Chen, Y.-N., Rush, J., Hsu, P.W.-C., et al. (2011). Global Identification of Modular Cullin-RING Ligase Substrates. Cell *147*, 459–474.

Englund, C. (2005). Pax6, Tbr2, and Tbr1 Are Expressed Sequentially by Radial Glia, Intermediate Progenitor Cells, and Postmitotic Neurons in Developing Neocortex. J. Neurosci. *25*, 247–251.

Etlinger, J.D., and Goldberg, A.L. (1977). A soluble ATP-dependent proteolytic system responsible for the degradation of abnormal proteins in reticulocytes. Proc. Natl. Acad. Sci. *74*, 54–58.

Eze, U.C., Bhaduri, A., Haeussler, M., Nowakowski, T.J., and Kriegstein, A.R. (2021). Single-cell atlas of early human brain development highlights heterogeneity of human neuroepithelial cells and early radial glia. Nat. Neurosci. 1–11.

Faast, R., White, J., Cartwright, P., Crocker, L., Sarcevic, B., and Dalton, S. (2004). Cdk6–cyclin D3 activity in murine ES cells is resistant to inhibition by p16INK4a. Oncogene *23*, 491–502.

Fang, L., Zhang, L., Wei, W., Jin, X., Wang, P., Tong, Y., Li, J., Du, J.X., and Wong, J. (2014). A Methylation-Phosphorylation Switch Determines Sox2 Stability and Function in ESC Maintenance or Differentiation. Mol. Cell *55*, 537–551.

Feldman, R.M.R., Correll, C.C., Kaplan, K.B., and Deshaies, R.J. (1997). A Complex of Cdc4p, Skp1p, and Cdc53p/Cullin Catalyzes Ubiquitination of the Phosphorylated CDK Inhibitor Sic1p. Cell *91*, 221–230.

Feng, L., Allen, N.S., Simo, S., and Cooper, J.A. (2007). Cullin 5 regulates Dab1 protein levels and neuron positioning during cortical development. Genes Dev. *21*, 2717–2730.

Fero, M.L., Rivkin, M., Tasch, M., Porter, P., Carow, C.E., Firpo, E., Polyak, K., Tsai, L.H., Broudy, V., Perlmutter, R.M., et al. (1996). A syndrome of multiorgan hyperplasia with features of gigantism, tumorigenesis, and female sterility in p27(Kip1)-deficient mice. Cell *85*, 733–744.

Ferri, A.L.M., Cavallaro, M., Braida, D., Cristofano, A.D., Canta, A., Vezzani, A., Ottolenghi, S., Pandolfi, P.P., Sala, M., DeBiasi, S., et al. (2004). Sox2 deficiency causes neurodegeneration and impaired neurogenesis in the adult mouse brain. Development *131*, 3805–3819.

Filipczyk, A.A., Laslett, A.L., Mummery, C., and Pera, M.F. (2007). Differentiation is coupled to changes in the cell cycle regulatory apparatus of human embryonic stem cells. Stem Cell Res. *1*, 45–60.

Fischer, S., Schlotthauer, I., Kizner, V., Macartney, T., Dorner-Ciossek, C., and Gillardon, F. (2020). Loss-of-function Mutations of CUL3, a High Confidence Gene for Psychiatric Disorders, Lead to Aberrant Neurodevelopment In Human Induced Pluripotent Stem Cells. Neuroscience *448*, 234–254.

Franceschini, A., Szklarczyk, D., Frankild, S., Kuhn, M., Simonovic, M., Roth, A., Lin, J., Minguez, P., Bork, P., von Mering, C., et al. (2012). STRING v9.1: protein-protein interaction networks, with increased coverage and integration. Nucleic Acids Res. *41*, D808–D815.

Franceschini, A., Lin, J., von Mering, C., and Jensen, L.J. (2016). SVD-phy: improved prediction of protein functional associations through singular value decomposition of phylogenetic profiles. Bioinformatics *32*, 1085–1087.

French, M.E., Koehler, C.F., and Hunter, T. (2021). Emerging functions of branched ubiquitin chains. Cell Discov. *7*, 1–10.

Fu, A.K., and Ip, N.Y. (2015). Neddylation is needed for synapse maturation. Nat. Neurosci. *18*, 164–166.

Fulzele, A., and Bennett, E.J. (2018). Ubiquitin diGLY Proteomics as an Approach to Identify and Quantify the Ubiquitin-Modified Proteome. Methods Mol. Biol. Clifton NJ *1844*, 363–384.

Furey, T.S. (2012). ChIP–seq and beyond: new and improved methodologies to detect and characterize protein–DNA interactions. Nat. Rev. Genet. *13*, 840–852.

Füzesi-Levi, M.G., Ben-Nissan, G., Bianchi, E., Zhou, H., Deery, M.J., Lilley, K.S., Levin, Y., and Sharon, M. (2014). Dynamic Regulation of the COP9 Signalosome in Response to DNA Damage. Mol. Cell. Biol. *34*, 1066–1076.

Gage, F.H., and Temple, S. (2013). Neural stem cells: generating and regenerating the brain. Neuron *80*, 588–601.

Galdieri, L., and Vancura, A. (2012). Acetyl-CoA Carboxylase Regulates Global Histone Acetylation. J. Biol. Chem. *287*, 23865–23876.

Gama, V., Swahari, V., Schafer, J., Kole, A.J., Evans, A., Huang, Y., Cliffe, A., Golitz, B., Sciaky, N., Pei, X.-H., et al. (2014). The E3 ligase PARC mediates the degradation of cytosolic cytochrome c to promote survival in neurons and cancer cells. Sci. Signal. *7*, ra67–ra67.

Gee, R.R.F., Chen, H., Lee, A.K., Daly, C.A., Wilander, B.A., Tacer, K.F., and Potts, P.R. (2020). Emerging roles of the MAGE protein family in stress response pathways. J. Biol. Chem. *295*, 16121–16155.

Gieffers, C., Peters, B.H., Kramer, E.R., Dotti, C.G., and Peters, J.-M. (1999). Expression of the CDH1-associated form of the anaphase-promoting complex in postmitotic neurons. Proc. Natl. Acad. Sci. *96*, 11317–11322.

Gillott, A., Furniss, F., and Walter, A. (2001). Anxiety in high-functioning children with autism. Autism Int. J. Res. Pract. *5*, 277–286.

Glessner, J.T., Wang, K., Cai, G., Korvatska, O., Kim, C.E., Wood, S., Zhang, H., Estes, A., Brune, C.W., Bradfield, J.P., et al. (2009). Autism genome-wide copy number variation reveals ubiquitin and neuronal genes. Nature *459*, 569–573.

Glotzer, M. (2009). The 3Ms of central spindle assembly: microtubules, motors and MAPs. Nat. Rev. Mol. Cell Biol. *10*, 9–20.

Glotzer, M., Murray, A.W., and Kirschner, M.W. (1991). Cyclin is degraded by the ubiquitin pathway. Nature *349*, 132–138.

Goldenberg, S.J., Cascio, T.C., Shumway, S.D., Garbutt, K.C., Liu, J., Xiong, Y., and Zheng, N. (2004). Structure of the Cand1-Cul1-Roc1 Complex Reveals Regulatory Mechanisms for the Assembly of the Multisubunit Cullin-Dependent Ubiquitin Ligases. Cell *119*, 517–528.

Goldstein, G., Scheid, M., Hammerling, U., Schlesinger, D.H., Niall, H.D., and Boyse, E.A. (1975). Isolation of a polypeptide that has lymphocyte-differentiating properties and is probably represented universally in living cells. Proc. Natl. Acad. Sci. U. S. A. *72*, 11–15.

Gordon, A., Yoon, S.-J., Tran, S.S., Makinson, C.D., Park, J.Y., Andersen, J., Valencia, A.M., Horvath, S., Xiao, X., Huguenard, J.R., et al. (2021). Long-term maturation of human cortical organoids matches key early postnatal transitions. Nat. Neurosci. *24*, 331–342.

Graham, V., Khudyakov, J., Ellis, P., and Pevny, L. (2003). SOX2 Functions to Maintain Neural Progenitor Identity. Neuron *39*, 749–765.

Groisman, R., Polanowska, J., Kuraoka, I., Sawada, J., Saijo, M., Drapkin, R., Kisselev, A.F., Tanaka, K., and Nakatani, Y. (2003). The Ubiquitin Ligase Activity in the DDB2 and CSA Complexes Is Differentially Regulated by the COP9 Signalosome in Response to DNA Damage. Cell *113*, 357–367.

Grossberger, R., Gieffers, C., Zachariae, W., Podtelejnikov, A.V., Schleiffer, A., Nasmyth, K., Mann, M., and Peters, J.-M. (1999). Characterization of the DOC1/APC10 Subunit of the Yeast and the Human Anaphase-promoting Complex *. J. Biol. Chem. *274*, 14500–14507.

Guo, J., Nie, X., Giebler, M., Mlcochova, H., Wang, Y., Grow, E.J., Kim, R., Tharmalingam, M., Matilionyte, G., Lindskog, C., et al. (2020). The Dynamic Transcriptional Cell Atlas of Testis Development during Human Puberty. Cell Stem Cell *26*, 262-276.e4.

Gusmaroli, G., Figueroa, P., Serino, G., and Deng, X.W. (2007). Role of the MPN subunits in COP9 signalosome assembly and activity, and their regulatory interaction with Arabidopsis Cullin3-based E3 ligases. Plant Cell *19*, 564–581.

Hamasaki, T., Leingärtner, A., Ringstedt, T., and O'Leary, D.D.M. (2004). EMX2 Regulates Sizes and Positioning of the Primary Sensory and Motor Areas in Neocortex by Direct Specification of Cortical Progenitors. Neuron *43*, 359–372.

Haremaki, T., Metzger, J.J., Rito, T., Ozair, M.Z., Etoc, F., and Brivanlou, A.H. (2019). Self-organizing neuruloids model developmental aspects of Huntington's disease in the ectodermal compartment. Nat. Biotechnol. *37*, 1198–1208.

Hazlett, H.C., Gu, H., Munsell, B.C., Kim, S.H., Styner, M., Wolff, J.J., Elison, J.T., Swanson, M.R., Zhu, H., Botteron, K.N., et al. (2017). Early brain development in infants at high risk for autism spectrum disorder. Nature *542*, 348–351.

He, J., Chao, W.C.H., Zhang, Z., Yang, J., Cronin, N., and Barford, D. (2013). Insights into Degron Recognition by APC/C Coactivators from the Structure of an Acm1-Cdh1 Complex. Mol. Cell *50*, 649–660.

Herrero-Mendez, A., Almeida, A., Fernández, E., Maestre, C., Moncada, S., and Bolaños, J.P. (2009). The bioenergetic and antioxidant status of neurons is controlled by continuous degradation of a key glycolytic enzyme by APC/C-Cdh1. Nat. Cell Biol. *11*, 747–752.

Hershko, A., and Ciechanover, A. (1998). The ubiquitin system. Annu. Rev. Biochem. *67*, 425–479.

Hershko, A., Ciechanover, A., and Rose, I.A. (1979). Resolution of the ATP-dependent proteolytic system from reticulocytes: a component that interacts with ATP. Proc. Natl. Acad. Sci. U. S. A. *76*, 3107–3110.

Hershko, A., Ciechanover, A., Heller, H., Haas, A.L., and Rose, I.A. (1980). Proposed role of ATP in protein breakdown: conjugation of protein with multiple chains of the polypeptide of ATP-dependent proteolysis. Proc. Natl. Acad. Sci. U. S. A. *77*, 1783–1786.

Hershko, A., Heller, H., Elias, S., and Ciechanover, A. (1983). Components of ubiquitin-protein ligase system. Resolution, affinity purification, and role in protein breakdown. J. Biol. Chem. *258*, 8206–8214.

Hitoshi, S., Alexson, T., Tropepe, V., Donoviel, D., Elia, A.J., Nye, J.S., Conlon, R.A., Mak, T.W., Bernstein, A., and Kooy, D. van der (2002). Notch pathway molecules are essential for the maintenance, but not the generation, of mammalian neural stem cells. Genes Dev. *16*, 846–858.

Hofmann, K., and Bucher, P. (1998). The PCI domain: a common theme in three multiprotein complexes. Trends Biochem. Sci. *23*, 204–205.

Hofmann, R.M., and Pickart, C.M. (1999). Noncanonical MMS2-Encoded Ubiquitin-Conjugating Enzyme Functions in Assembly of Novel Polyubiquitin Chains for DNA Repair. Cell *96*, 645–653.

Hollville, E., Joers, V., Nakamura, A., Swahari, V., Tansey, M.G., Moy, S.S., and Deshmukh, M. (2020). Characterization of a Cul9-Parkin double knockout mouse model for Parkinson's disease. Sci. Rep. *10*, 16886.

Honda, T., Kobayashi, K., Mikoshiba, K., and Nakajima, K. (2011). Regulation of cortical neuron migration by the Reelin signaling pathway. Neurochem. Res. *36*, 1270–1279.

Hong, S.-J., Bernhardt, B.C., Gill, R.S., Bernasconi, N., and Bernasconi, A. (2017). The spectrum of structural and functional network alterations in malformations of cortical development. Brain J. Neurol. *140*, 2133–2143.

Hori, T., Osaka, F., Chiba, T., Miyamoto, C., Okabayashi, K., Shimbara, N., Kato, S., and Tanaka, K. (1999). Covalent modification of all members of human cullin family proteins by NEDD8. Oncogene *18*, 6829–6834.

Horton, A.C., Rácz, B., Monson, E.E., Lin, A.L., Weinberg, R.J., and Ehlers, M.D. (2005). Polarized secretory trafficking directs cargo for asymmetric dendrite growth and morphogenesis. Neuron *48*, 757–771.

Huang, D.T., Hunt, H.W., Zhuang, M., Ohi, M.D., Holton, J.M., and Schulman, B.A. (2007). Basis for a ubiquitin-like protein thioester switch toggling E1–E2 affinity. Nature *445*, 394–398.

Huang, D.W., Sherman, B.T., and Lempicki, R.A. (2009a). Systematic and integrative analysis of large gene lists using DAVID bioinformatics resources. Nat. Protoc. *4*, 44–57.

Huang, D.W., Sherman, B.T., and Lempicki, R.A. (2009b). Bioinformatics enrichment tools: paths toward the comprehensive functional analysis of large gene lists. Nucleic Acids Res. *37*, 1–13.

Huang, J., Ikeuchi, Y., Malumbres, M., and Bonni, A. (2015). A Cdh1-APC/FMRP Ubiquitin Signaling Link Drives mGluR-Dependent Synaptic Plasticity in the Mammalian Brain. Neuron *86*, 726–739.

Huber, C., Dias-Santagata, D., Glaser, A., O'Sullivan, J., Brauner, R., Wu, K., Xu, X., Pearce, K., Wang, R., Uzielli, M.L.G., et al. (2005). Identification of mutations in CUL7 in 3-M syndrome. Nat. Genet. *37*, 1119–1124.

Huber, C., Delezoide, A.-L., Guimiot, F., Baumann, C., Malan, V., Le Merrer, M., Da Silva, D.B., Bonneau, D., Chatelain, P., Chu, C., et al. (2009). A large-scale mutation search reveals genetic heterogeneity in 3M syndrome. Eur. J. Hum. Genet. *17*, 395–400.

Husnjak, K., Elsasser, S., Zhang, N., Chen, X., Randles, L., Shi, Y., Hofmann, K., Walters, K.J., Finley, D., and Dikic, I. (2008). Proteasome subunit Rpn13 is a novel ubiquitin receptor. Nature *453*, 481–488.

Isidor, B., Pichon, O., Baron, S., David, A., and Caignec, C.L. (2010). Deletion of the CUL4B gene in a boy with mental retardation, minor facial anomalies, short stature, hypogonadism, and ataxia. Am. J. Med. Genet. A. *152A*, 175–180.

Jang, S.-M., Redon, C.E., Thakur, B.L., Bahta, M.K., and Aladjem, M.I. (2020). Regulation of cell cycle drivers by Cullin-RING ubiquitin ligases. Exp. Mol. Med. *52*, 1637–1651.

Jehl, P., Manguy, J., Shields, D.C., Higgins, D.G., and Davey, N.E. (2016). ProViz—a web-based visualization tool to investigate the functional and evolutionary features of protein sequences. Nucleic Acids Res. *44*, W11–W15.

Jensen, L.J., Kuhn, M., Stark, M., Chaffron, S., Creevey, C., Muller, J., Doerks, T., Julien, P., Roth, A., Simonovic, M., et al. (2009). STRING 8--a global view on proteins and their functional interactions in 630 organisms. Nucleic Acids Res. *37*, D412–D416.

Jin, J., Ang, X.L., Shirogane, T., and Wade Harper, J. (2005). Identification of Substrates for F-Box Proteins. In Methods in Enzymology, (Elsevier), pp. 287–309.

Jin, L., Williamson, A., Banerjee, S., Philipp, I., and Rape, M. (2008). Mechanism of ubiquitin-chain formation by the human anaphase-promoting complex. Cell *133*, 653–665.

Jones, D., and Candido, E.P. (2000). The NED-8 conjugating system in Caenorhabditis elegans is required for embryogenesis and terminal differentiation of the hypodermis. Dev. Biol. *226*, 152–165.

Joshi, P., Bodnya, C., Ilieva, I., Neely, M.D., Aschner, M., and Bowman, A.B. (2019). Huntington's disease associated resistance to Mn neurotoxicity is neurodevelopmental stage and neuronal lineage dependent. Neurotoxicology *75*, 148–157.

Juo, P., and Kaplan, J.M. (2004). The anaphase-promoting complex regulates the abundance of GLR-1 glutamate receptors in the ventral nerve cord of C. elegans. Curr. Biol. CB *14*, 2057–2062.

K, Y., Tt, R., Kh, C., Ac, R., Dr, B., R, P., Rj, W., Md, E., and Bd, P. (2009). Ube3a is required for experience-dependent maturation of the neocortex. Nat. Neurosci. *12*, 777–783.

Kamura, T., Koepp, D.M., Conrad, M.N., Skowyra, D., Moreland, R.J., Iliopoulos, O., Lane, W.S., Kaelin, W.G., Elledge, S.J., Conaway, R.C., et al. (1999). Rbx1, a Component of the VHL Tumor Suppressor Complex and SCF Ubiquitin Ligase. Science *284*, 657–661.

Kannan, M., Lee, S.-J., Schwedhelm-Domeyer, N., and Stegmüller, J. (2012). The E3 ligase Cdh1-anaphase promoting complex operates upstream of the E3 ligase Smurf1 in the control of axon growth. Development *139*, 3600–3612.

Kaustov, L., Lukin, J., Lemak, A., Duan, S., Ho, M., Doherty, R., Penn, L.Z., and Arrowsmith, C.H. (2007). The Conserved CPH Domains of Cul7 and PARC Are Protein-Protein Interaction Modules That Bind the Tetramerization Domain of p53. J. Biol. Chem. *282*, 11300–11307.

Kelava, I., and Lancaster, M.A. (2016). Dishing out mini-brains: Current progress and future prospects in brain organoid research. Dev. Biol. *420*, 199–209.

Kelsall, I.R., Duda, D.M., Olszewski, J.L., Hofmann, K., Knebel, A., Langevin, F., Wood, N., Wightman, M., Schulman, B.A., and Alpi, A.F. (2013). TRIAD1 and HHARI bind to and are activated by distinct neddylated Cullin-RING ligase complexes. EMBO J. *32*, 2848–2860.

Kim, Y.-D., Lee, J., Kim, H.-S., Lee, M.-O., Son, M.-Y., Yoo, C.H., Choi, J.-K., Lee, S.C., and Cho, Y.S. (2017). The unique spliceosome signature of human pluripotent stem cells is mediated by SNRPA1, SNRPD1, and PNN. Stem Cell Res. *22*, 43–53.

Kim, Y.H., Choi, S.H., D'Avanzo, C., Hebisch, M., Sliwinski, C., Bylykbashi, E., Washicosky, K.J., Klee, J.B., Brüstle, O., Tanzi, R.E., et al. (2015). A 3D human neural cell culture system for modeling Alzheimer's disease. Nat. Protoc. *10*, 985–1006.

Kipreos, E.T., Lander, L.E., Wing, J.P., He, W.W., and Hedgecock, E.M. (1996). cul-1 Is Required for Cell Cycle Exit in C. elegans and Identifies a Novel Gene Family. Cell *85*, 829–839.

Kliza, K., and Husnjak, K. (2020). Resolving the Complexity of Ubiquitin Networks. Front. Mol. Biosci. *7*.

Kominami, K., Seth-Smith, H., and Toda, T. (1998). Apc10 and Ste9/Srw1, two regulators of the APC-cyclosome, as well as the CDK inhibitor Rum1 are required for G1 cell-cycle arrest in fission yeast. EMBO J. *17*, 5388–5399.

Kong, A., Frigge, M.L., Masson, G., Besenbacher, S., Sulem, P., Magnusson, G., Gudjonsson, S.A., Sigurdsson, A., Jonasdottir, A., Jonasdottir, A., et al. (2012). Rate of de novo mutations and the importance of father's age to disease risk. Nature *488*, 471–475.

Konishi, Y. (2004). Cdh1-APC Controls Axonal Growth and Patterning in the Mammalian Brain. Science *303*, 1026–1030.

Konze, S.A., Werneburg, S., Oberbeck, A., Olmer, R., Kempf, H., Jara-Avaca, M., Pich, A., Zweigerdt, R., and Buettner, F.F.R. (2017). Proteomic Analysis of Human Pluripotent Stem Cell Cardiomyogenesis Revealed Altered Expression of Metabolic Enzymes and PDLIM5 Isoforms. J. Proteome Res. *16*, 1133–1149.

Kuczera, T., Stilling, R.M., Hsia, H.-E., Bahari-Javan, S., Irniger, S., Nasmyth, K., Sananbenesi, F., and Fischer, A. (2011). The anaphase promoting complex is required for memory function in mice. Learn. Mem. *18*, 49–57.

Kumar, S., Tomooka, Y., and Noda, M. (1992). Identification of a set of genes with developmentally down-regulated expression in the mouse brain. Biochem. Biophys. Res. Commun. *185*, 1155–1161.

Kumar, S., Yoshida, Y., and Noda, M. (1993). Cloning of a cDNA which encodes a novel ubiquitin-like protein. Biochem. Biophys. Res. Commun. *195*, 393–399.

Kurasawa, Y., and Todokoro, K. (1999). Identification of human APC10/Doc1 as a subunit of anaphase promoting complex. Oncogene *18*, 5131–5137.

Kwon, S.C., Yi, H., Eichelbaum, K., Föhr, S., Fischer, B., You, K.T., Castello, A., Krijgsveld, J., Hentze, M.W., and Kim, V.N. (2013). The RNA-binding protein repertoire of embryonic stem cells. Nat. Struct. Mol. Biol. *20*, 1122–1130.

Lange, C., Huttner, W.B., and Calegari, F. (2009). Cdk4/CyclinD1 Overexpression in Neural Stem Cells Shortens G1, Delays Neurogenesis, and Promotes the Generation and Expansion of Basal Progenitors. Cell Stem Cell *5*, 320–331.

Lasorella, A., Stegmüller, J., Guardavaccaro, D., Liu, G., Carro, M.S., Rothschild, G., de la Torre-Ubieta, L., Pagano, M., Bonni, A., and Iavarone, A. (2006). Degradation of Id2 by the anaphase-promoting complex couples cell cycle exit and axonal growth. Nature *442*, 471–474.

Lee, S.B., Kim, J.J., Nam, H.-J., Gao, B., Yin, P., Qin, B., Yi, S.-Y., Ham, H., Evans, D., Kim, S.-H., et al. (2015). Parkin Regulates Mitosis and Genomic Stability through Cdc20/Cdh1. Mol. Cell *60*, 21–34.

Lee, S.-H., Choi, J.-H., Lee, N., Lee, H.-R., Kim, J.-I., Yu, N.-K., Choi, S.-L., Lee, S.-H., Kim, H., and Kaang, B.-K. (2008). Synaptic Protein Degradation Underlies Destabilization of Retrieved Fear Memory. Science *319*, 1253–1256.

Lennox, A.L., Hoye, M.L., Jiang, R., Johnson-Kerner, B.L., Suit, L.A., Venkataramanan, S., Sheehan, C.J., Alsina, F.C., Fregeau, B., Aldinger, K.A., et al. (2020). Pathogenic DDX3X Mutations Impair RNA Metabolism and Neurogenesis during Fetal Cortical Development. Neuron *106*, 404-420.e8.

Lever, A.G., and Geurts, H.M. (2016). Psychiatric Co-occurring Symptoms and Disorders in Young, Middle-Aged, and Older Adults with Autism Spectrum Disorder. J. Autism Dev. Disord. *46*, 1916–1930.

Li, V.C., and Kirschner, M.W. (2014). Molecular ties between the cell cycle and differentiation in embryonic stem cells. Proc. Natl. Acad. Sci. *111*, 9503–9508.

Li, Z., and Xiong, Y. (2017a). Cytoplasmic E3 ubiquitin ligase CUL9 controls cell proliferation, senescence, apoptosis and genome integrity through p53. Oncogene *36*, 5212–5218.

Li, Z., and Xiong, Y. (2017b). Cytoplasmic E3 ubiquitin ligase CUL9 controls cell proliferation, senescence, apoptosis and genome integrity through p53. Oncogene *36*, 5212–5218.

Li, B., Ruiz, J.C., and Chun, K.T. (2002). CUL-4A Is Critical for Early Embryonic Development. Mol. Cell. Biol. *22*, 4997–5005.

Li, H., Collado, M., Villasante, A., Matheu, A., Lynch, C.J., Cañamero, M., Rizzoti, K., Carneiro, C., Martínez, G., Vidal, A., et al. (2012). p27(Kip1) directly represses Sox2 during embryonic stem cell differentiation. Cell Stem Cell *11*, 845–852.

Li, M., Shin, Y.-H., Hou, L., Huang, X., Wei, Z., Klann, E., and Zhang, P. (2008). The adaptor protein of the anaphase promoting complex Cdh1 is essential in maintaining replicative lifespan and in learning and memory. Nat. Cell Biol. *10*, 1083–1089.

Li, Z., Pei, X.-H., Yan, J., Yan, F., Cappell, K.M., Whitehurst, A.W., and Xiong, Y. (2014). CUL9 Mediates the Functions of the 3M Complex and Ubiquitylates Survivin to Maintain Genome Integrity. Mol. Cell *54*, 805–819.

Lim, S., Bhinge, A., Alonso, S.B., Aksoy, I., Aprea, J., Cheok, C.F., Calegari, F., Stanton, L.W., and Kaldis, P. (2017). Cyclin-Dependent Kinase-Dependent Phosphorylation of Sox2 at Serine 39 Regulates Neurogenesis. Mol. Cell. Biol. *37*.

Linder, P., and Jankowsky, E. (2011). From unwinding to clamping — the DEAD box RNA helicase family. Nat. Rev. Mol. Cell Biol. *12*, 505–516.

Litterman, N., Ikeuchi, Y., Gallardo, G., O'Connell, B.C., Sowa, M.E., Gygi, S.P., Harper, J.W., and Bonni, A. (2011). An OBSL1-Cul7Fbxw8 ubiquitin ligase signaling mechanism regulates Golgi morphology and dendrite patterning. PLoS Biol. *9*, e1001060.

Liu, J., Furukawa, M., Matsumoto, T., and Xiong, Y. (2002). NEDD8 modification of CUL1 dissociates p120(CAND1), an inhibitor of CUL1-SKP1 binding and SCF ligases. Mol. Cell *10*, 1511–1518.

Liu, J., Liu, W., Yang, L., Wu, Q., Zhang, H., Fang, A., Li, L., Xu, X., Sun, L., Zhang, J., et al. (2017a). The Primate-Specific Gene TMEM14B Marks Outer Radial Glia Cells and Promotes Cortical Expansion and Folding. Cell Stem Cell *21*, 635-649.e8.

Liu, L., Lee, S., Zhang, J., Peters, S.B., Hannah, J., Zhang, Y., Yin, Y., Koff, A., Ma, L., and Zhou, P. (2009). CUL4A Abrogation Augments DNA Damage Response and Protection against Skin Carcinogenesis. Mol. Cell *34*, 451–460.

Liu, L., Yin, Y., Li, Y., Prevedel, L., Lacy, E.H., Ma, L., and Zhou, P. (2012). Essential role of the CUL4B ubiquitin ligase in extra-embryonic tissue development during mouse embryogenesis. Cell Res. *22*, 1258–1269.

Liu, L., Michowski, W., Inuzuka, H., Shimizu, K., Nihira, N.T., Chick, J.M., Li, N., Geng, Y., Meng, A.Y., Ordureau, A., et al. (2017b). G1 cyclins link proliferation, pluripotency and differentiation of embryonic stem cells. Nat. Cell Biol. *19*, 177–188.

Liu, L., Wong, C.C., Gong, B., and Yu, J. (2018). Functional significance and therapeutic implication of ring-type E3 ligases in colorectal cancer. Oncogene *37*, 148–159.

Liu, T., Zhang, L., Joo, D., and Sun, S.-C. (2017c). NF-κB signaling in inflammation. Signal Transduct. Target. Ther. *2*, 1–9.

Liu, X., Yang, X., Li, Y., Wang, X., Ma, J., Jiang, W., Liu, Y., Sun, W., and Gong, Y. (2020). Generation of patient-specific pluripotent induced stem cell line SDUBMSI002-A from a patient with X-linked mental retardation syndrome. Stem Cell Res. *43*, 101724.

Liu, X., Tan, J.P., Schröder, J., Aberkane, A., Ouyang, J.F., Mohenska, M., Lim, S.M., Sun, Y.B.Y., Chen, J., Sun, G., et al. (2021). Modelling human blastocysts by reprogramming fibroblasts into iBlastoids. Nature 1–6.

Lu, X., Göke, J., Sachs, F., Jacques, P.-É., Liang, H., Feng, B., Bourque, G., Bubulya, P.A., and Ng, H.-H. (2013). SON connects the splicing-regulatory network with pluripotency in human embryonic stem cells. Nat. Cell Biol. *15*, 1141–1152.

Lukaszewicz, A., Savatier, P., Cortay, V., Giroud, P., Huissoud, C., Berland, M., Kennedy, H., and Dehay, C. (2005). G1 Phase Regulation, Area-Specific Cell Cycle Control, and Cytoarchitectonics in the Primate Cortex. Neuron *47*, 353–364.

Ly, P.T., Tan, Y.S., Koe, C.T., Zhang, Y., Xie, G., Endow, S., Deng, W.-M., Yu, F., and Wang, H. (2019). CRL4Mahj E3 ubiquitin ligase promotes neural stem cell reactivation. PLOS Biol. *17*, e3000276.

Lydeard, J.R., Schulman, B.A., and Harper, J.W. (2013). Building and remodelling Cullin–RING E3 ubiquitin ligases. EMBO Rep. *14*, 1050–1061.

Lykke-Andersen, K., Schaefer, L., Menon, S., Deng, X.-W., Miller, J.B., and Wei, N. (2003). Disruption of the COP9 Signalosome Csn2 Subunit in Mice Causes Deficient Cell Proliferation, Accumulation of p53 and Cyclin E, and Early Embryonic Death. Mol. Cell. Biol. *23*, 6790–6797.

Mahrour, N., Redwine, W.B., Florens, L., Swanson, S.K., Martin-Brown, S., Bradford, W.D., Staehling-Hampton, K., Washburn, M.P., Conaway, R.C., and Conaway, J.W. (2008). Characterization of Cullin-box Sequences That Direct Recruitment of Cul2-Rbx1 and Cul5-Rbx2 Modules to Elongin BC-based Ubiquitin Ligases *. J. Biol. Chem. *283*, 8005–8013.

Manzini, M.C., and Walsh, C.A. (2011). What disorders of cortical development tell us about the cortex: one plus one doesn't always make two. 11.

Margottin-Goguet, F., Hsu, J.Y., Loktev, A., Hsieh, H.M., Reimann, J.D.R., and Jackson, P.K. (2003). Prophase destruction of Emi1 by the SCF(betaTrCP/Slimb) ubiquitin ligase activates the anaphase promoting complex to allow progression beyond prometaphase. Dev. Cell *4*, 813–826.

Marín, I. (2009). Diversification of the cullin family. BMC Evol. Biol. *9*, 267.

Marín, I., and Ferrús, A. (2002). Comparative Genomics of the RBR Family, Including the Parkinson's Disease–Related Gene Parkin and the Genes of the Ariadne Subfamily. Mol. Biol. Evol. *19*, 2039–2050.

Marín, I., Lucas, J.I., Gradilla, A.-C., and Ferrús, A. (2004). Parkin and relatives: the RBR family of ubiquitin ligases. Physiol. Genomics *17*, 253–263.

Masui, S., Nakatake, Y., Toyooka, Y., Shimosato, D., Yagi, R., Takahashi, K., Okochi, H., Okuda, A., Matoba, R., Sharov, A.A., et al. (2007). Pluripotency governed by Sox2 via regulation of Oct3/4 expression in mouse embryonic stem cells. Nat. Cell Biol. *9*, 625–635.

Matera, A.G., and Wang, Z. (2014). A day in the life of the spliceosome. Nat. Rev. Mol. Cell Biol. *15*, 108–121.

Mathias, N., Johnson, S.L., Winey, M., Adams, A.E., Goetsch, L., Pringle, J.R., Byers, B., and Goebl, M.G. (1996). Cdc53p acts in concert with Cdc4p and Cdc34p to control the G1-to-S-phase transition and identifies a conserved family of proteins. Mol. Cell. Biol. *16*, 6634–6643.

Matsumoto, M.L., Wickliffe, K.E., Dong, K.C., Yu, C., Bosanac, I., Bustos, D., Phu, L., Kirkpatrick, D.S., Hymowitz, S.G., Rape, M., et al. (2010). K11-Linked Polyubiquitination in Cell Cycle Control Revealed by a K11 Linkage-Specific Antibody. Mol. Cell *39*, 477–484.

McDonnell, E., Crown, S.B., Fox, D.B., Kitir, B., Ilkayeva, O.R., Olsen, C.A., Grimsrud, P.A., and Hirschey, M.D. (2016). Lipids Reprogram Metabolism to Become a Major Carbon Source for Histone Acetylation. Cell Rep. *17*, 1463–1472.

Menon, S., Chi, H., Zhang, H., Deng, X.W., Flavell, R.A., and Wei, N. (2007). COP9 signalosome subunit 8 is essential for peripheral T cell homeostasis and antigen receptor-induced entry into the cell cycle from quiescence. Nat. Immunol. *8*, 1236–1245.

Mering, C. v. (2003). STRING: a database of predicted functional associations between proteins. Nucleic Acids Res. *31*, 258–261.

von Mering, C. (2004). STRING: known and predicted protein-protein associations, integrated and transferred across organisms. Nucleic Acids Res. *33*, D433–D437.

Meshorer, E., Yellajoshula, D., George, E., Scambler, P.J., Brown, D.T., and Misteli, T. (2006). Hyperdynamic Plasticity of Chromatin Proteins in Pluripotent Embryonic Stem Cells. Dev. Cell *10*, 105–116.

Mevissen, T.E.T., and Komander, D. (2017). Mechanisms of Deubiquitinase Specificity and Regulation. Annu. Rev. Biochem. *86*, 159–192.

Meyer, H.-J., and Rape, M. (2014). Enhanced Protein Degradation by Branched Ubiquitin Chains. Cell *157*, 910–921.

Meza-Gutierrez, F., Hundley, F.V., and Toczyski, D.P. (2015). Parallel Parkin: Cdc20 Takes a New Partner. Mol. Cell *60*, 3–4.

Miura, M., Hatakeyama, S., Hattori, K., and Nakayama, K. (1999). Structure and Expression of the Gene Encoding Mouse F-Box Protein, Fwd2. Genomics *62*, 50–58.

Miyazaki, M., Man, W.C., and Ntambi, J.M. (2001). Targeted Disruption of Stearoyl-CoA Desaturase1 Gene in Mice Causes Atrophy of Sebaceous and Meibomian Glands and Depletion of Wax Esters in the Eyelid. J. Nutr. *131*, 2260–2268.

Molina, H., Yang, Y., Ruch, T., Kim, J.-W., Mortensen, P., Otto, T., Nalli, A., Tang, Q.-Q., Lane, M.D., Chaerkady, R., et al. (2009). Temporal profiling of the adipocyte proteome during differentiation using a five-plex SILAC based strategy. J. Proteome Res. *8*, 48–58.

Molnár, Z., Clowry, G.J., Šestan, N., Alzu'bi, A., Bakken, T., Hevner, R.F., Hüppi, P.S., Kostović, I., Rakic, P., Anton, E.S., et al. (2019). New insights into the development of the human cerebral cortex. J. Anat. *235*, 432–451.

Moris, N., Anlas, K., van den Brink, S.C., Alemany, A., Schröder, J., Ghimire, S., Balayo, T., van Oudenaarden, A., and Martinez Arias, A. (2020). An in vitro model of early anteroposterior organization during human development. Nature *582*, 410–415.

Morrish, F., Noonan, J., Perez-Olsen, C., Gafken, P.R., Fitzgibbon, M., Kelleher, J., VanGilst, M., and Hockenbery, D. (2010). Myc-dependent Mitochondrial Generation of Acetyl-CoA Contributes to Fatty Acid Biosynthesis and Histone Acetylation during Cell Cycle Entry. J. Biol. Chem. *285*, 36267–36274.

Motulsky, H.J., and Brown, R.E. (2006). Detecting outliers when fitting data with nonlinear regression – a new method based on robust nonlinear regression and the false discovery rate. BMC Bioinformatics *7*, 123.

Moynihan, T.P., Ardley, H.C., Nuber, U., Rose, S.A., Jones, P.F., Markham, A.F., Scheffner, M., and Robinson, P.A. (1999). The Ubiquitin-conjugating Enzymes UbcH7 and UbcH8 Interact with RING Finger/IBR Motif-containing Domains of HHARI and H7-AP1. J. Biol. Chem. *274*, 30963–30968.

Müller, F.-J., Schuldt, B.M., Williams, R., Mason, D., Altun, G., Papapetrou, E.P., Danner, S., Goldmann, J.E., Herbst, A., Schmidt, N.O., et al. (2011). A bioinformatic assay for pluripotency in human cells. Nat. Methods *8*, 315–317.

Nalepa, G., Rolfe, M., and Harper, J.W. (2006). Drug discovery in the ubiquitin–proteasome system. Nat. Rev. Drug Discov. *5*, 596–613.

Neely, M.D., Litt, M.J., Tidball, A.M., Li, G.G., Aboud, A.A., Hopkins, C.R., Chamberlin, R., Hong, C.C., Ess, K.C., and Bowman, A.B. (2012). DMH1, a Highly Selective Small Molecule BMP Inhibitor Promotes Neurogenesis of hiPSCs: Comparison of PAX6 and SOX1 Expression during Neural Induction. ACS Chem. Neurosci. *3*, 482–491.

Neganova, I., Zhang, X., Atkinson, S., and Lako, M. (2009). Expression and functional analysis of G1 to S regulatory components reveals an important role for CDK2 in cell cycle regulation in human embryonic stem cells. Oncogene *28*, 20–30.

Nieto, M., Monuki, E.S., Tang, H., Imitola, J., Haubst, N., Khoury, S.J., Cunningham, J., Gotz, M., and Walsh, C.A. (2004). Expression of Cux-1 and Cux-2 in the subventricular zone and upper layers II–IV of the cerebral cortex. J. Comp. Neurol. *479*, 168–180.

Nikolaev, A.Y., and Gu, W. (2003). PARC: A Potential Target for Cancer Therapy. Cell Cycle *2*, 168–170.

Nikolaev, A.Y., Li, M., Puskas, N., Qin, J., and Gu, W. (2003). Parc: a cytoplasmic anchor for p53. Cell *112*, 29–40.

Noto, J.M., Rose, K.L., Hachey, A.J., Delgado, A.G., Romero-Gallo, J., Wroblewski, L.E., Schneider, B.G., Shah, S.C., Cover, T.L., Wilson, K.T., et al. (2019). Carcinogenic Helicobacter pylori Strains Selectively Dysregulate the In Vivo Gastric Proteome, Which May Be Associated with Stomach Cancer Progression. Mol. Cell. Proteomics MCP *18*, 352–371.

Ohta, T., Michel, J.J., Schottelius, A.J., and Xiong, Y. (1999). ROC1, a Homolog of APC11, Represents a Family of Cullin Partners with an Associated Ubiquitin Ligase Activity. Mol. Cell *3*, 535–541.

Ohtake, F., Saeki, Y., Ishido, S., Kanno, J., and Tanaka, K. (2016). The K48-K63 Branched Ubiquitin Chain Regulates NF-κB Signaling. Mol. Cell *64*, 251–266.

Ohtake, F., Tsuchiya, H., Saeki, Y., and Tanaka, K. (2018). K63 ubiquitylation triggers proteasomal degradation by seeding branched ubiquitin chains. Proc. Natl. Acad. Sci. U. S. A. *115*, E1401–E1408.

Ong, S.-E., Blagoev, B., Kratchmarova, I., Kristensen, D.B., Steen, H., Pandey, A., and Mann, M. (2002). Stable Isotope Labeling by Amino Acids in Cell Culture, SILAC, as a Simple and Accurate Approach to Expression Proteomics. Mol. Cell. Proteomics *1*, 376–386.

Ong, S.-E., Kratchmarova, I., and Mann, M. (2003). Properties of ^{13}C-Substituted Arginine in Stable Isotope Labeling by Amino Acids in Cell Culture (SILAC). J. Proteome Res. *2*, 173–181.

Ordureau, A., Münch, C., and Harper, J.W. (2015). Quantifying Ubiquitin Signaling. Mol. Cell *58*, 660–676.

O'Roak, B.J., Vives, L., Girirajan, S., Karakoc, E., Krumm, N., Coe, B.P., Levy, R., Ko, A., Lee, C., Smith, J.D., et al. (2012). Sporadic autism exomes reveal a highly interconnected protein network of de novo mutations. Nature *485*, 246–250.

Ortolano, N.A., Romero-Morales, A.I., Rasmussen, M.L., Bodnya, C., Kline, L.A., Joshi, P., Connelly, J.P., Rose, K.L., Pruett-Miller, S.M., and Gama, V. (2021). A proteomics approach for the identification of cullin-9 (CUL9) related signaling pathways in induced pluripotent stem cell models. PLOS ONE *16*, e0248000.

Ou, C.-Y., Lin, Y.-F., Chen, Y.-J., and Chien, C.-T. (2002). Distinct protein degradation mechanisms mediated by Cul1 and Cul3 controlling Ci stability in Drosophila eye development. Genes Dev. *16*, 2403–2414.

Passmore, L.A., McCormack, E.A., Au, S.W.N., Paul, A., Willison, K.R., Harper, J.W., and Barford, D. (2003). Doc1 mediates the activity of the anaphase-promoting complex by contributing to substrate recognition. EMBO J. *22*, 786–796.

Patmanidi, A.L., Champeris Tsaniras, S., Karamitros, D., Kyrousi, C., Lygerou, Z., and Taraviras, S. (2017). Concise Review: Geminin-A Tale of Two Tails: DNA Replication and Transcriptional/Epigenetic Regulation in Stem Cells: Geminin in Stem Cell Self-Renewal and Differentiation. STEM CELLS *35*, 299–310.

Paylor, R., Tracy, R., Wehner, J., and Rudy, J.W. (1994). DBA/2 and C57BL/6 mice differ in contextual fear but not auditory fear conditioning. Behav. Neurosci. *108*, 810–817.

Pei, X.-H., Bai, F., Li, Z., Smith, M.D., Whitewolf, G., Jin, R., and Xiong, Y. (2011). Cytoplasmic CUL9/PARC Ubiquitin Ligase Is a Tumor Suppressor and Promotes p53-Dependent Apoptosis. Cancer Res. *71*, 2969–2977.

Peters, J.-M. (2006). The anaphase promoting complex/cyclosome: a machine designed to destroy. Nat. Rev. Mol. Cell Biol. *7*, 644–656.

Peth, A., Berndt, C., Henke, W., and Dubiel, W. (2007). Downregulation of COP9 signalosome subunits differentially affects the CSN complex and target protein stability. BMC Biochem. *8*, 27.

Petroski, M.D., and Deshaies, R.J. (2005). Function and regulation of cullin–RING ubiquitin ligases. Nat. Rev. Mol. Cell Biol. *6*, 9–20.

Pick, J.E., Wang, L., Mayfield, J.E., and Klann, E. (2013). Neuronal expression of the ubiquitin E3 ligase APC/C-Cdh1 during development is required for long-term potentiation, behavioral flexibility, and extinction. Neurobiol. Learn. Mem. *100*, 25–31.

Pickart, C.M., and Rose, I.A. (1985). Functional heterogeneity of ubiquitin carrier proteins. J. Biol. Chem. *260*, 1573–1581.

Pilaz, L.-J., Patti, D., Marcy, G., Ollier, E., Pfister, S., Douglas, R.J., Betizeau, M., Gautier, E., Cortay, V., Doerflinger, N., et al. (2009). Forced G1-phase reduction alters mode of division, neuron number, and laminar phenotype in the cerebral cortex. Proc. Natl. Acad. Sci. *106*, 21924–21929.

Pines, J. (2011). Cubism and the cell cycle: the many faces of the APC/C. Nat. Rev. Mol. Cell Biol. *12*, 427–438.

Poirier, K., Saillour, Y., Bahi-Buisson, N., Jaglin, X.H., Fallet-Bianco, C., Nabbout, R., Castelnau-Ptakhine, L., Roubertie, A., Attie-Bitach, T., Desguerre, I., et al. (2010). Mutations in the neuronal β-tubulin subunit TUBB3 result in malformation of cortical development and neuronal migration defects. Hum. Mol. Genet. *19*, 4462–4473.

Pollen, A.A., Nowakowski, T.J., Chen, J., Retallack, H., Sandoval-Espinosa, C., Nicholas, C.R., Shuga, J., Liu, S.J., Oldham, M.C., Diaz, A., et al. (2015). Molecular Identity of Human Outer Radial Glia During Cortical Development. Cell *163*, 55–67.

Ponti, G., Obernier, K., Guinto, C., Jose, L., Bonfanti, L., and Alvarez-Buylla, A. (2013). Cell cycle and lineage progression of neural progenitors in the ventricular-subventricular zones of adult mice. Proc. Natl. Acad. Sci. *110*, E1045–E1054.

Portela, M., Segura-Collar, B., Argudo, I., Sáiz, A., Gargini, R., Sánchez-Gómez, P., and Casas-Tintó, S. (2019). Oncogenic dependence of glioma cells on kish/TMEM167A regulation of vesicular trafficking. Glia *67*, 404–417.

Potenza, E., Domenico, T.D., Walsh, I., and Tosatto, S.C.E. (2015). MobiDB 2.0: an improved database of intrinsically disordered and mobile proteins. Nucleic Acids Res. *43*, D315–D320.

Qiao, R., Weissmann, F., Yamaguchi, M., Brown, N.G., VanderLinden, R., Imre, R., Jarvis, M.A., Brunner, M.R., Davidson, I.F., Litos, G., et al. (2016). Mechanism of APC/CCDC20 activation by mitotic phosphorylation. Proc. Natl. Acad. Sci. U. S. A. *113*, E2570-2578.

Rajalingam, K., and Dikic, I. (2016). SnapShot: Expanding the Ubiquitin Code. Cell *164*, 1074-1074.e1.

Rana, A.S.J.B., Ge, Y., and Strieter, E.R. (2017). Ubiquitin Chain Enrichment Middle-Down Mass Spectrometry (UbiChEM-MS) Reveals Cell-Cycle Dependent Formation of Lys11/Lys48 Branched Ubiquitin Chains. J. Proteome Res. *16*, 3363–3369.

Rape, M. (2018). Ubiquitylation at the crossroads of development and disease. Nat. Rev. Mol. Cell Biol. *19*, 59–70.

Rauniyar, N., and Yates, J.R. (2014). Isobaric Labeling-Based Relative Quantification in Shotgun Proteomics. J. Proteome Res. *13*, 5293–5309.

Ripke, S., Neale, B.M., Corvin, A., Walters, J.T.R., Farh, K.-H., Holmans, P.A., Lee, P., Bulik-Sullivan, B., Collier, D.A., Huang, H., et al. (2014). Biological insights from 108 schizophrenia-associated genetic loci. Nature *511*, 421–427.

Roccio, M., Schmitter, D., Knobloch, M., Okawa, Y., Sage, D., and Lutolf, M.P. (2013). Predicting stem cell fate changes by differential cell cycle progression patterns. Development *140*, 459–470.

Rodríguez-Pascual, F., Redondo-Horcajo, M., Magán-Marchal, N., Lagares, D., Martínez-Ruiz, A., Kleinert, H., and Lamas, S. (2008). Glyceraldehyde-3-phosphate dehydrogenase regulates endothelin-1 expression by a novel, redox-sensitive mechanism involving mRNA stability. Mol. Cell. Biol. *28*, 7139–7155.

van Roessel, P., Elliott, D.A., Robinson, I.M., Prokop, A., and Brand, A.H. (2004). Independent regulation of synaptic size and activity by the anaphase-promoting complex. Cell *119*, 707–718.

Ropers, H.-H., and Hamel, B.C.J. (2005). X-linked mental retardation. Nat. Rev. Genet. *6*, 46–57.

Rossant, J., and Tam, P.P.L. (2017). New Insights into Early Human Development: Lessons for Stem Cell Derivation and Differentiation. Cell Stem Cell *20*, 18–28.

Roux, K.J., Kim, D.I., Raida, M., and Burke, B. (2012). A promiscuous biotin ligase fusion protein identifies proximal and interacting proteins in mammalian cells. J. Cell Biol. *196*, 801–810.

Sackton, K.L., Dimova, N., Zeng, X., Tian, W., Zhang, M., Sackton, T.B., Meaders, J., Pfaff, K.L., Sigoillot, F., Yu, H., et al. (2014). Synergistic blockade of mitotic exit by two chemical inhibitors of the APC/C. Nature *514*, 646–649.

Saez, I., Koyuncu, S., Gutierrez-Garcia, R., Dieterich, C., and Vilchez, D. (2018). Insights into the ubiquitin-proteasome system of human embryonic stem cells. Sci. Rep. *8*, 4092.

Saha, A., and Deshaies, R.J. (2008). Multimodal activation of the ubiquitin ligase SCF by Nedd8 conjugation. Mol. Cell *32*, 21–31.

Salomoni, P., and Calegari, F. (2010). Cell cycle control of mammalian neural stem cells: putting a speed limit on G1. Trends Cell Biol. *20*, 233–243.

Sarkar, A., and Hochedlinger, K. (2013). The Sox Family of Transcription Factors: Versatile Regulators of Stem and Progenitor Cell Fate. Cell Stem Cell *12*, 15–30.

Scheerlinck, E., Van Steendam, K., Daled, S., Govaert, E., Vossaert, L., Meert, P., Van Nieuwerburgh, F., Van Soom, A., Peelman, L., De Sutter, P., et al. (2016). Assessing the impact of minimizing arginine conversion in fully defined SILAC culture medium in human embryonic stem cells. Proteomics *16*, 2605–2614.

Schmittgen, T.D., and Livak, K.J. (2008). Analyzing real-time PCR data by the comparative CT method. Nat. Protoc. *3*, 1101–1108.

Schulman, B.A., and Wade Harper, J. (2009). Ubiquitin-like protein activation by E1 enzymes: the apex for downstream signalling pathways. Nat. Rev. Mol. Cell Biol. *10*, 319–331.

Schulman, B.A., Carrano, A.C., Jeffrey, P.D., Bowen, Z., Kinnucan, E.R.E., Finnin, M.S., Elledge, S.J., Harper, J.W., Pagano, M., and Pavletich, N.P. (2000). Insights into SCF ubiquitin ligases from the structure of the Skp1–Skp2 complex. Nature *408*, 381–386.

Schumann, C.M., Bloss, C.S., Barnes, C.C., Wideman, G.M., Carper, R.A., Akshoomoff, N., Pierce, K., Hagler, D., Schork, N., Lord, C., et al. (2010). Longitudinal magnetic resonance imaging study of cortical development through early childhood in autism. J. Neurosci. Off. J. Soc. Neurosci. *30*, 4419–4427.

Segura-Collar, B., Gargini, R., Tovar-Ambel, E., Hernández-SanMiguel, E., Epifano, C., Pérez de Castro, I., Hernández-Laín, A., Casas-Tintó, S., and Sánchez-Gómez, P. (2020). The EGFR-TMEM167A-p53 Axis Defines the Aggressiveness of Gliomas. Cancers *12*.

Seol, J.H., Feldman, R.M.R., Zachariae, W., Shevchenko, A., Correll, C.C., Lyapina, S., Chi, Y., Galova, M., Claypool, J., Sandmeyer, S., et al. (1999). Cdc53/cullin and the essential Hrt1 RING–H2 subunit of SCF define a ubiquitin ligase module that activates the E2 enzyme Cdc34. Genes Dev. *13*, 1614–1626.

Shi, Y., Kirwan, P., and Livesey, F.J. (2012). Directed differentiation of human pluripotent stem cells to cerebral cortex neurons and neural networks. Nat. Protoc. *7*, 1836–1846.

Shi, Y., Chen, X., Elsasser, S., Stocks, B.B., Tian, G., Lee, B.-H., Shi, Y., Zhang, N., de Poot, S.A.H., Tuebing, F., et al. (2016). Rpn1 provides adjacent receptor sites for substrate binding and deubiquitination by the proteasome. Science *351*.

Sidorov, M.S., Auerbach, B.D., and Bear, M.F. (2013). Fragile X mental retardation protein and synaptic plasticity. Mol. Brain *6*, 15.

Silies, M., and Klämbt, C. (2010). APC/C(Fzr/Cdh1)-dependent regulation of cell adhesion controls glial migration in the Drosophila PNS. Nat. Neurosci. *13*, 1357–1364.

Simó, S., and Cooper, J.A. (2013). Rbx2 regulates neuronal migration through different cullin 5-RING ligase adaptors. Dev. Cell *27*, 399–411.

Simó, S., Jossin, Y., and Cooper, J.A. (2010). Cullin 5 regulates cortical layering by modulating the speed and duration of Dab1-dependent neuronal migration. J. Neurosci. Off. J. Soc. Neurosci. *30*, 5668–5676.

Singer, J.D., Gurian-West, M., Clurman, B., and Roberts, J.M. (1999). Cullin-3 targets cyclin E for ubiquitination and controls S phase in mammalian cells. Genes Dev. *13*, 2375–2387.

Singh, R., and Green, M.R. (1993). Sequence-specific binding of transfer RNA by glyceraldehyde-3-phosphate dehydrogenase. Science *259*, 365–368.

Singh, R., Letai, A., and Sarosiek, K. (2019). Regulation of apoptosis in health and disease: the balancing act of BCL-2 family proteins. Nat. Rev. Mol. Cell Biol. *20*, 175–193.

Sivakumar, S., and Gorbsky, G.J. (2015). Spatiotemporal regulation of the anaphase-promoting complex in mitosis. Nat. Rev. Mol. Cell Biol. *16*, 82–94.

Skaar, J.R., Arai, T., and DeCaprio, J.A. (2005). Dimerization of CUL7 and PARC Is Not Required for All CUL7 Functions and Mouse Development. Mol. Cell. Biol. *25*, 5579–5589.

Skaar, J.R., Florens, L., Tsutsumi, T., Arai, T., Tron, A., Swanson, S.K., Washburn, M.P., and DeCaprio, J.A. (2007). PARC and CUL7 Form Atypical Cullin RING Ligase Complexes. Cancer Res. *67*, 2006–2014.

Skowyra, D., Craig, K.L., Tyers, M., Elledge, S.J., and Harper, J.W. (1997). F-box proteins are receptors that recruit phosphorylated substrates to the SCF ubiquitin-ligase complex. Cell *91*, 209–219.

Skowyra, D., Koepp, D.M., Kamura, T., Conrad, M.N., Conaway, R.C., Conaway, J.W., Elledge, S.J., and Harper, J.W. (1999). Reconstitution of G1 Cyclin Ubiquitination with Complexes Containing SCFGrr1 and Rbx1. Science *284*, 662–665.

Smit, J.J., and Sixma, T.K. (2014). RBR E3-ligases at work. EMBO Rep. *15*, 142–154.

Snel, B. (2000). STRING: a web-server to retrieve and display the repeatedly occurring neighbourhood of a gene. Nucleic Acids Res. *28*, 3442–3444.

Song, H., and Ji, X. (2019). The mechanism of RNA duplex recognition and unwinding by DEAD-box helicase DDX3X. Nat. Commun. *10*, 3085.

Stegmüller, J., Konishi, Y., Huynh, M.A., Yuan, Z., DiBacco, S., and Bonni, A. (2006). Cell-Intrinsic Regulation of Axonal Morphogenesis by the Cdh1-APC Target SnoN. Neuron *50*, 389–400.

Stewart, M.D., Ritterhoff, T., Klevit, R.E., and Brzovic, P.S. (2016). E2 enzymes: more than just middle men. Cell Res. *26*, 423–440.

Sugiura, T., Sakurai, K., and Nagano, Y. (2007). Intracellular characterization of DDX39, a novel growth-associated RNA helicase. Exp. Cell Res. *313*, 782–790.

Sui, Y., Liu, Y., and Xu, G. (2015). A lysine-to-arginine mutation on NEDD8 markedly reduces the activity of cullin RING E3 ligase through the impairment of neddylation cascades. Biochem. Biophys. Res. Commun. *461*, 653–658.

Sullivan, J.M., Havrda, M.C., Kettenbach, A.N., Paolella, B.R., Zhang, Z., Gerber, S.A., and Israel, M.A. (2016). Phosphorylation Regulates Id2 Degradation and Mediates the Proliferation of Neural Precursor Cells. STEM CELLS *34*, 1321–1331.

Swatek, K.N., and Komander, D. (2016). Ubiquitin modifications. Cell Res. *26*, 399–422.

Szklarczyk, D., Franceschini, A., Kuhn, M., Simonovic, M., Roth, A., Minguez, P., Doerks, T., Stark, M., Muller, J., Bork, P., et al. (2011). The STRING database in 2011: functional interaction networks of proteins, globally integrated and scored. Nucleic Acids Res. *39*, D561–D568.

Szklarczyk, D., Franceschini, A., Wyder, S., Forslund, K., Heller, D., Huerta-Cepas, J., Simonovic, M., Roth, A., Santos, A., Tsafou, K.P., et al. (2015). STRING v10: protein–protein interaction networks, integrated over the tree of life. Nucleic Acids Res. *43*, D447–D452.

Szklarczyk, D., Morris, J.H., Cook, H., Kuhn, M., Wyder, S., Simonovic, M., Santos, A., Doncheva, N.T., Roth, A., Bork, P., et al. (2017). The STRING database in 2017: quality-controlled protein–protein association networks, made broadly accessible. Nucleic Acids Res. *45*, D362–D368.

Szklarczyk, D., Gable, A.L., Lyon, D., Junge, A., Wyder, S., Huerta-Cepas, J., Simonovic, M., Doncheva, N.T., Morris, J.H., Bork, P., et al. (2019). STRING v11: protein–protein association networks with increased coverage, supporting functional discovery in genome-wide experimental datasets. Nucleic Acids Res. *47*, D607–D613.

Takahashi, K., and Yamanaka, S. (2006). Induction of Pluripotent Stem Cells from Mouse Embryonic and Adult Fibroblast Cultures by Defined Factors. Cell *126*, 663–676.

Takahashi, T., Nowakowski, R., and Caviness, V. (1995). The cell cycle of the pseudostratified ventricular epithelium of the embryonic murine cerebral wall. J. Neurosci. *15*, 6046–6057.

Tarpey, P.S., Raymond, F.L., O'Meara, S., Edkins, S., Teague, J., Butler, A., Dicks, E., Stevens, C., Tofts, C., Avis, T., et al. (2007). Mutations in CUL4B, Which Encodes a Ubiquitin E3 Ligase Subunit, Cause an X-linked Mental Retardation Syndrome Associated with Aggressive Outbursts, Seizures, Relative Macrocephaly, Central Obesity, Hypogonadism, Pes Cavus, and Tremor. Am. J. Hum. Genet. *80*, 345–352.

Tate, J.G., Bamford, S., Jubb, H.C., Sondka, Z., Beare, D.M., Bindal, N., Boutselakis, H., Cole, C.G., Creatore, C., Dawson, E., et al. (2019). COSMIC: the Catalogue Of Somatic Mutations In Cancer. Nucleic Acids Res. *47*, D941–D947.

Tateishi, K., Omata, M., Tanaka, K., and Chiba, T. (2001). The NEDD8 system is essential for cell cycle progression and morphogenetic pathway in mice. J. Cell Biol. *155*, 571–580.

Tee, W.-W., and Reinberg, D. (2014). Chromatin features and the epigenetic regulation of pluripotency states in ESCs. Development *141*, 2376–2390.

Teng, J., Takei, Y., Harada, A., Nakata, T., Chen, J., and Hirokawa, N. (2001). Synergistic effects of MAP2 and MAP1B knockout in neuronal migration, dendritic outgrowth, and microtubule organization. J. Cell Biol. *155*, 65–76.

Thornton, B.R., Ng, T.M., Matyskiela, M.E., Carroll, C.W., Morgan, D.O., and Toczyski, D.P. (2006). An architectural map of the anaphase-promoting complex. Genes Dev. *20*, 449–460.

Ting, L., Rad, R., Gygi, S.P., and Haas, W. (2011). MS3 eliminates ratio distortion in isobaric multiplexed quantitative proteomics. Nat. Methods *8*, 937–940.

Tomoda, K., Yoneda-Kato, N., Fukumoto, A., Yamanaka, S., and Kato, J.-Y. (2004). Multiple functions of Jab1 are required for early embryonic development and growth potential in mice. J. Biol. Chem. *279*, 43013–43018.

Tsunematsu, R., Nishiyama, M., Kotoshiba, S., Saiga, T., Kamura, T., and Nakayama, K.I. (2006). Fbxw8 is essential for Cul1-Cul7 complex formation and for placental development. Mol. Cell. Biol. *26*, 6157–6169.

Tuoc, T.C., and Stoykova, A. (2008). Trim11 modulates the function of neurogenic transcription factor Pax6 through ubiquitin–proteosome system. Genes Dev. *22*, 1972–1986.

Uhlén, M., Fagerberg, L., Hallström, B.M., Lindskog, C., Oksvold, P., Mardinoglu, A., Sivertsson, Å., Kampf, C., Sjöstedt, E., Asplund, A., et al. (2015). Proteomics. Tissue-based map of the human proteome. Science *347*, 1260419.

Vallier, L. (2015). Cell Cycle Rules Pluripotency. Cell Stem Cell *17*, 131–132.

van de Leemput, J., Boles, N.C., Kiehl, T.R., Corneo, B., Lederman, P., Menon, V., Lee, C., Martinez, R.A., Levi, B.P., Thompson, C.L., et al. (2014). CORTECON: A Temporal Transcriptome Analysis of In Vitro Human Cerebral Cortex Development from Human Embryonic Stem Cells. Neuron *83*, 51–68.

Vaughn, A.E., and Deshmukh, M. (2008). Glucose metabolism inhibits apoptosis in neurons and cancer cells by redox inactivation of cytochrome c. *10*, 19.

Vodermaier, H.C. (2004). APC/C and SCF: Controlling Each Other and the Cell Cycle. Curr. Biol. *14*, R787–R796.

Vodermaier, H.C., Gieffers, C., Maurer-Stroh, S., Eisenhaber, F., and Peters, J.-M. (2003). TPR Subunits of the Anaphase-Promoting Complex Mediate Binding to the Activator Protein CDH1. Curr. Biol. *13*, 1459–1468.

Vogl, A.M., Brockmann, M.M., Giusti, S.A., Maccarrone, G., Vercelli, C.A., Bauder, C.A., Richter, J.S., Roselli, F., Hafner, A.-S., Dedic, N., et al. (2015). Neddylation inhibition impairs spine development, destabilizes synapses and deteriorates cognition. Nat. Neurosci. *18*, 239–251.

Vogl, A.M., Phu, L., Becerra, R., Giusti, S.A., Verschueren, E., Hinkle, T.B., Bordenave, M.D., Adrian, M., Heidersbach, A., Yankilevich, P., et al. (2020). Global site-specific neddylation profiling reveals that NEDDylated cofilin regulates actin dynamics. Nat. Struct. Mol. Biol. *27*, 210–220.

Völker-Albert, M.C., Schmidt, A., Forne, I., and Imhof, A. (2018). Analysis of Histone Modifications by Mass Spectrometry. Curr. Protoc. Protein Sci. *92*, e54.

Volpato, V., Smith, J., Sandor, C., Ried, J.S., Baud, A., Handel, A., Newey, S.E., Wessely, F., Attar, M., Whiteley, E., et al. (2018). Reproducibility of Molecular Phenotypes after Long-Term Differentiation to Human iPSC-Derived Neurons: A Multi-Site Omics Study. Stem Cell Rep. *11*, 897–911.

Vousden, K.H., and Lane, D.P. (2007). p53 in health and disease. Nat. Rev. Mol. Cell Biol. *8*, 275–283.

Vulto-van Silfhout, A.T., Nakagawa, T., Bahi-Buisson, N., Haas, S.A., Hu, H., Bienek, M., Vissers, L.E.L.M., Gilissen, C., Tzschach, A., Busche, A., et al. (2015). Variants in CUL4B are associated with cerebral malformations. Hum. Mutat. *36*, 106–117.

Wang, C., Deng, L., Hong, M., Akkaraju, G.R., Inoue, J., and Chen, Z.J. (2001). TAK1 is a ubiquitin-dependent kinase of MKK and IKK. Nature *412*, 346–351.

Wang, C.-C., Lo, H.-F., Lin, S.-Y., and Chen, H. (2013a). RACK1 (receptor for activated C-kinase 1) interacts with FBW2 (F-box and WD-repeat domain-containing 2) to up-regulate GCM1 (glial cell missing 1) stability and placental cell migration and invasion. Biochem. J. *453*, 201–208.

Wang, J., Zhang, Y., Hou, J., Qian, X., Zhang, H., Zhang, Z., Li, M., Wang, R., Liao, K., Wang, Y., et al. (2016). Ube2s regulates Sox2 stability and mouse ES cell maintenance. Cell Death Differ. *23*, 393–404.

Wang, L., Meece, K., Williams, D.J., Lo, K.A., Zimmer, M., Heinrich, G., Martin Carli, J., Leduc, C.A., Sun, L., Zeltser, L.M., et al. (2015). Differentiation of hypothalamic-like neurons from human pluripotent stem cells. J. Clin. Invest. *125*, 796–808.

Wang, L., Zhang, T., Wang, L., Cai, Y., Zhong, X., He, X., Hu, L., Tian, S., Wu, M., Hui, L., et al. (2017). Fatty acid synthesis is critical for stem cell pluripotency via promoting mitochondrial fission. EMBO J. *36*, 1330–1347.

Wang, Y., Penfold, S., Tang, X., Hattori, N., Riley, P., Harper, J.W., Cross, J.C., and Tyers, M. (1999). Deletion of the Cul1 gene in mice causes arrest in early embryogenesis and accumulation of cyclin E. Curr. Biol. *9*, 1191-S2.

Wang, Y., Han, T., Gan, M., Guo, M., Xie, C., Jin, J., Zhang, S., Wang, P., Cao, J., and Wang, J.-B. (2019). A novel function of anaphase promoting complex subunit 10 in tumor progression in non-small cell lung cancer. Cell Cycle Georget. Tex *18*, 1019–1032.

Wang, Y., Argiles-Castillo, D., Kane, E.I., Zhou, A., and Spratt, D.E. (2020). HECT E3 ubiquitin ligases – emerging insights into their biological roles and disease relevance. J. Cell Sci. *133*.

Wang, Z., Hou, Y., Guo, X., van der Voet, M., Boxem, M., Dixon, J.E., Chisholm, A.D., and Jin, Y. (2013b). The EBAX-type Cullin-RING E3 ligase and Hsp90 guard the protein quality of the SAX-3/Robo receptor in developing neurons. Neuron *79*, 903–916.

Wegiel, J., Flory, M., Kuchna, I., Nowicki, K., Ma, S.Y., Imaki, H., Wegiel, J., Cohen, I.L., London, E., Wisniewski, T., et al. (2014). Stereological study of the neuronal number and volume of 38 brain subdivisions of subjects diagnosed with autism reveals significant alterations restricted to the striatum, amygdala and cerebellum. Acta Neuropathol. Commun. *2*, 141.

Wei, N., Serino, G., and Deng, X. (2008). The COP9 signalosome: more than a protease. Trends Biochem. Sci. *33*, 592–600.

Wei, W., Ayad, N.G., Wan, Y., Zhang, G.-J., Kirschner, M.W., and Kaelin, W.G. (2004). Degradation of the SCF component Skp2 in cell-cycle phase G1 by the anaphase-promoting complex. Nature *428*, 194–198.

Wendt, K.S., Vodermaier, H.C., Jacob, U., Gieffers, C., Gmachl, M., Peters, J.M., Huber, R., and Sondermann, P. (2001). Crystal structure of the APC10/DOC1 subunit of the human anaphase-promoting complex. Nat. Struct. Biol. *8*, 784–788.

Wenger, C.D., Lee, M.V., Hebert, A.S., McAlister, G.C., Phanstiel, D.H., Westphall, M.S., and Coon, J.J. (2011). Gas-phase purification enables accurate, multiplexed proteome quantification with isobaric tagging. Nat. Methods *8*, 933–935.

Whitby, F.G., Xia, G., Pickart, C.M., and Hill, C.P. (1998). Crystal structure of the human ubiquitin-like protein NEDD8 and interactions with ubiquitin pathway enzymes. J. Biol. Chem. *273*, 34983–34991.

White, J., Stead, E., Faast, R., Conn, S., Cartwright, P., and Dalton, S. (2005). Developmental Activation of the Rb–E2F Pathway and Establishment of Cell Cycle-regulated Cyclin-dependent Kinase Activity during Embryonic Stem Cell Differentiation. Mol. Biol. Cell *16*, 2018–2027.

Wiese, S., Reidegeld, K.A., Meyer, H.E., and Warscheid, B. (2007). Protein labeling by iTRAQ: a new tool for quantitative mass spectrometry in proteome research. Proteomics *7*, 340–350.

Wild, T., Budzowska, M., Hellmuth, S., Eibes, S., Karemore, G., Barisic, M., Stemmann, O., and Choudhary, C. (2018). Deletion of APC7 or APC16 Allows Proliferation of Human Cells without the Spindle Assembly Checkpoint. Cell Rep. *25*, 2317-2328.e5.

Wilkinson, M.E., Charenton, C., and Nagai, K. (2020). RNA Splicing by the Spliceosome. Annu. Rev. Biochem. *89*, 359–388.

Wilson, P.G., and Stice, S.S. (2006). Development and differentiation of neural rosettes derived from human embryonic stem cells. Stem Cell Rev. *2*, 67–77.

Wright, P.E., and Dyson, H.J. (2015). Intrinsically disordered proteins in cellular signalling and regulation. Nat. Rev. Mol. Cell Biol. *16*, 18–29.

Wu, K., Yamoah, K., Dolios, G., Gan-Erdene, T., Tan, P., Chen, A., Lee, C.-G., Wei, N., Wilkinson, K.D., Wang, R., et al. (2003). DEN1 is a dual function protease capable of processing the C terminus of Nedd8 and deconjugating hyper-neddylated CUL1. J. Biol. Chem. *278*, 28882–28891.

Xie, Z., Jones, A., Deeney, J.T., Hur, S.K., and Bankaitis, V.A. (2016). Inborn Errors of Long-Chain Fatty Acid β-Oxidation Link Neural Stem Cell Self-Renewal to Autism. Cell Rep. *14*, 991–999.

Xu, P., Duong, D.M., Seyfried, N.T., Cheng, D., Xie, Y., Robert, J., Rush, J., Hochstrasser, M., Finley, D., and Peng, J. (2009). Quantitative proteomics reveals the function of unconventional ubiquitin chains in proteasomal degradation. Cell *137*, 133–145.

Yamaguchi, M., Yu, S., Qiao, R., Weissmann, F., Miller, D.J., VanderLinden, R., Brown, N.G., Frye, J.J., Peters, J.-M., and Schulman, B.A. (2015). Structure of an APC3-APC16 complex: Insights into assembly of the Anaphase Promoting Complex/Cyclosome. J. Mol. Biol. *427*, 1748–1764.

Yamoah, K., Oashi, T., Sarikas, A., Gazdoiu, S., Osman, R., and Pan, Z.-Q. (2008). Autoinhibitory regulation of SCF-mediated ubiquitination by human cullin 1's C-terminal tail. Proc. Natl. Acad. Sci. *105*, 12230–12235.

Yan, J., Walz, K., Nakamura, H., Carattini-Rivera, S., Zhao, Q., Vogel, H., Wei, N., Justice, M.J., Bradley, A., and Lupski, J.R. (2003). COP9 Signalosome Subunit 3 Is Essential for Maintenance of Cell Proliferation in the Mouse Embryonic Epiblast. Mol. Cell. Biol. *23*, 6798–6808.

Yan, J., Yan, F., Li, Z., Sinnott, B., Cappell, K.M., Yu, Y., Mo, J., Duncan, J.A., Chen, X., Cormier-Daire, V., et al. (2014). The 3M Complex Maintains Microtubule and Genome Integrity. Mol. Cell *54*, 791–804.

Yang, C.-S., Yu, C., Chuang, H.-C., Chang, C.-W., Chang, G.-D., Yao, T.-P., and Chen, H. (2005). FBW2 Targets GCMa to the Ubiquitin-Proteasome Degradation System *. J. Biol. Chem. *280*, 10083–10090.

Yang, F., Xu, J., Li, H., Tan, M., Xiong, X., and Sun, Y. (2019). FBXW2 suppresses migration and invasion of lung cancer cells via promoting β-catenin ubiquitylation and degradation. Nat. Commun. *10*, 1382.

Yang, V.S., Carter, S.A., Hyland, S.J., Tachibana-Konwalski, K., Laskey, R.A., and Gonzalez, M.A. (2011). Geminin Escapes Degradation in G1 of Mouse Pluripotent Cells and Mediates the Expression of Oct4, Sox2, and Nanog. Curr. Biol. *21*, 692–699.

Yang, X., Menon, S., Lykke-Andersen, K., Tsuge, T., Di Xiao, null, Wang, X., Rodriguez-Suarez, R.J., Zhang, H., and Wei, N. (2002). The COP9 signalosome inhibits p27(kip1) degradation and impedes G1-S phase progression via deneddylation of SCF Cul1. Curr. Biol. CB *12*, 667–672.

Yau, R., and Rape, M. (2016). The increasing complexity of the ubiquitin code. Nat. Cell Biol. *18*, 579–586.

Ye, J., and Blelloch, R. (2014). Regulation of Pluripotency by RNA Binding Proteins. Cell Stem Cell *15*, 271–280.

Ye, Y., and Rape, M. (2009). Building ubiquitin chains: E2 enzymes at work. Nat. Rev. Mol. Cell Biol. *10*, 755–764.

Yi, J.J., Paranjape, S.R., Walker, M.P., Choudhury, R., Wolter, J.M., Fragola, G., Emanuele, M.J., Major, M.B., and Zylka, M.J. (2017). The autism-linked UBE3A T485A mutant E3 ubiquitin ligase activates the Wnt/β-catenin pathway by inhibiting the proteasome. J. Biol. Chem. *292*, 12503–12515.

Yiangou, L., Grandy, R.A., Morell, C.M., Tomaz, R.A., Osnato, A., Kadiwala, J., Muraro, D., Garcia-Bernardo, J., Nakanoh, S., Bernard, W.G., et al. (2019). Method to Synchronize Cell Cycle of Human Pluripotent Stem Cells without Affecting Their Fundamental Characteristics. Stem Cell Rep. *12*, 165–179.

Yu, H., Peters, J.M., King, R.W., Page, A.M., Hieter, P., and Kirschner, M.W. (1998). Identification of a cullin homology region in a subunit of the anaphase-promoting complex. Science *279*, 1219–1222.

Yu, L., Wei, Y., Duan, J., Schmitz, D.A., Sakurai, M., Wang, L., Wang, K., Zhao, S., Hon, G.C., and Wu, J. (2021). Blastocyst-like structures generated from human pluripotent stem cells. Nature 1–7.

Zhang, C., Leng, F., Saxena, L., Hoang, N., Yu, J., Alejo, S., Lee, L., Qi, D., Lu, F., Sun, H., et al. (2019). Proteolysis of methylated SOX2 protein is regulated by L3MBTL3 and CRL4DCAF5 ubiquitin ligase. J. Biol. Chem. *294*, 476–489.

Zhang, S., Chang, L., Alfieri, C., Zhang, Z., Yang, J., Maslen, S., Skehel, M., and Barford, D. (2016). Molecular mechanism of APC/C activation by mitotic phosphorylation. Nature *533*, 260–264.

Zhang, X., Neganova, I., Przyborski, S., Yang, C., Cooke, M., Atkinson, S.P., Anyfantis, G., Fenyk, S., Keith, W.N., Hoare, S.F., et al. (2009). A role for NANOG in G1 to S transition in human embryonic stem cells through direct binding of CDK6 and CDC25A. J. Cell Biol. *184*, 67–82.

Zhao, Y., and Sun, Y. (2012). CUL4B ubiquitin ligase in mouse development: a model for human X-linked mental retardation syndrome? Cell Res. *22*, 1224–1226.

Zhao, R., Deibler, R.W., Lerou, P.H., Ballabeni, A., Heffner, G.C., Cahan, P., Unternaehrer, J.J., Kirschner, M.W., and Daley, G.Q. (2014). A nontranscriptional role for Oct4 in the regulation of mitotic entry. Proc. Natl. Acad. Sci. *111*, 15768–15773.

Zheng, J., Yang, X., Harrell, J.M., Ryzhikov, S., Shim, E.H., Lykke-Andersen, K., Wei, N., Sun, H., Kobayashi, R., and Zhang, H. (2002a). CAND1 binds to unneddylated CUL1 and regulates the formation of SCF ubiquitin E3 ligase complex. Mol. Cell *10*, 1519–1526.

Zheng, N., Schulman, B.A., Song, L., Miller, J.J., Jeffrey, P.D., Wang, P., Chu, C., Koepp, D.M., Elledge, S.J., and Pagano, M. (2002b). Structure of the Cul1–Rbx1–Skp1–F boxSkp2 SCF ubiquitin ligase complex. *416*, 7.

Zhu, Z., Wang, L., Hao, R., Zhao, B., Sun, L., and Ye, R.D. (2016). Cutting Edge: A Cullin-5-TRAF6 Interaction Promotes TRAF6 Polyubiquitination and Lipopolysaccharide Signaling. J. Immunol. Baltim. Md 1950 *197*, 21–26.

Zimmer, C., Tiveron, M.-C., Bodmer, R., and Cremer, H. (2004). Dynamics of Cux2 expression suggests that an early pool of SVZ precursors is fated to become upper cortical layer neurons. Cereb. Cortex N. Y. N 1991 *14*, 1408–1420.

Zimmerman, E.S., Schulman, B.A., and Zheng, N. (2010). Structural assembly of cullin-RING ubiquitin ligase complexes. Curr. Opin. Struct. Biol. *20*, 714–721.